MOLECULAR FUNCTIONS OF THE RAD9A-RAD1-HUS1 DNA DAMAGE CHECKPOINT CLAMP IN GENOME MAINTENANCE AND TUMORIGENESIS

A Dissertation

Presented to the Faculty of the Graduate School

of Cornell University

In Partial Fulfillment of the Requirements for the Degree of

Doctor of Philosophy

by

Darshil R Patel

August 2018

© 2018 Darshil R Patel

MOLECULAR FUNCTIONS OF THE RAD9A-RAD1-HUS1 DNA DAMAGE CHECKPOINT CLAMP IN GENOME MAINTENANCE AND TUMORIGENESIS

Darshil R Patel, Ph.D.

Cornell University 2018

DNA damage checkpoint pathways are part of the broader cellular DNA damage response (DDR) that promotes genome maintenance when cells experience DNA damage. The RAD9A-HUS1-RAD1 (9-1-1) complex is a DDR component that functions as a heterotrimeric DNA binding clamp that promotes checkpoint signaling and DNA repair. Loss of 9-1-1 function has severe consequences, including embryonic lethality, genomic instability, subfertility and hypersensitivity to replication stress.

To fully understand the role of the 9-1-1 complex in DNA repair, we first utilized a targeted mutation approach to identify functionally important residues of HUS1 that drive clamp formation, DNA interactions, and downstream effector functions. These studies revealed that both checkpoint signaling and DNA repair by the 9-1-1 complex separably promote genome maintenance. Next, a proteome-wide screen identified novel HUS1interactors and uncovered a new role for the 9-1-1 complex in regulating protein neddylation.

As *Hus1* loss results in radial chromosome formation and hypersensitivity to inter-strand crosslinking (ICL) agents, phenotypes also seen in the genome instability syndrome Fanconi Anemia (FA), we investigated the relationship between the 9-1-1

complex and the FA DNA repair pathway. Our studies suggested that the 9-1-1 complex was essential for recruitment of several FA proteins during ICL repair. Furthermore, the 9-1-1 complex also protected stalled replication forks against MRE11-dependent fork degradation. Overall, these data suggest a role for the 9-1-1 complex in coordinating multiple signaling and repair proteins required for accurate ICL repair.

DDR proteins are known to protect against cancer-initiating mutations in normal cells; however they also support tumor growth at later stages, allowing cancers to tolerate elevated stress levels associated with malignant transformation. We explored the role of HUS1 in cancer, and discovered that *Hus1* deficiency decreased cell transformation in cultured cells and decreased tumorigenesis in mouse models of lung and skin cancer. Expression analysis in multiple cancer cell lines revealed that HUS1 levels in cancer can increase through a mechanism involving alternative polyadenylation.

In sum, this dissertation decodes distinct functions for the 9-1-1 complex in DNA repair and tumorigenesis, and identifies novel interactions between HUS1 and effectors important for genomic integrity and cell survival.

BIOGRAPHICAL SKETCH

Darshil Patel was born on March 26, 1990 in Vadodara, India. In 2008, he received his high school diploma from Corona High School in California. Thereafter, he enrolled into Riverside community college to continue his education. During his time at the community college, he was awarded Beckman Coulter summer internship in 2009, which allowed him to work as a research intern at Ambryx Biotechnology Incorporation, a cancer research-based company. He continued working at Ambryx Biotechnology until 2011. In 2010, after completing two years of general education at the community college, he transferred to the University of California Los Angeles (UCLA) in California. At UCLA, he majored in Molecular, Cell and Developmental Biology (MCDB) and minored in Anthropology. During his first year, he worked in Dr. Elaine Tobin's Lab to understand the regulatory functions of the circadian clock proteins, CCA1 and LYH in *Arabidopsis Thaliana.* Thereafter, he joined Dr. Samuel French Lab in the department of Pathology at UCLA, where his research was focused at developing a proteomic based program to study the development of liver cancer induced by hepatitis C viral infection. He also actively volunteered at UCLA Santa Clarita Cancer Center in Valencia, California as a student intern. During his tenure at both labs, he learnt essential skills in basic molecular and biochemistry techniques, as well as exposed him to basic and translational research. After completing his B.S. degree in 2012, Darshil decided to join the Biochemistry, Molecular and Cell Biology (BMCB) program at Cornell University for his doctorate. He completed his dissertation work with Dr. Robert Weiss, where he focused on understanding the distinct roles for the DNA damage checkpoint clamp subunit HUS1 in genome maintenance.

I would like to dedicate this thesis to my lovely and ever-supporting parents,
Renu & Rohit

ACKNOWLEDGMENTS

It would not have been possible to complete my doctoral dissertation work without the support of several individuals, who stood by me throughout this time, supporting and encouraging my work.

I would like to start by thanking my advisor, Dr. Robert Weiss for his unqualified support and assistance during my stay in his laboratory. As a student, I could not have asked for a better mentor. He provided me with all the guidance as well as the freedom to successfully complete my work. From him, I have learnt several important technical and intellectual skills needed to be an independent researcher. I feel my great privilege and honor to have worked under him, as he has prepared me for the next phase of my scientific life.

Along with Dr. Weiss, I would like to thank the members of the Weiss lab for their support and guidance. Dr. Pei Xin Lim provided great support and guidance during my early days in the lab. I was able to work with him and learn a great deal about the scientific tenacity required in research. I would also like to thank former members of the lab, Dr. Amy Lyndaker, Dr. Tim Pierpont, Dr. Yashira Abril Negron, and Dr. April Blong for providing a collaborative and healthy lab environment. I also had the privilege to work with excellent lab members and co-authors, Dr. Joanna Mleczko, and Catalina Pereira, who made substantial contribution to my dissertation work. Finally, I would like to thank the other current members of the Weiss lab, Dr. Elizabeth Moore, and Irma Fernandez for their continued support, guidance and their friendship; it was a great pleasure working with you all. I would also like to thank undergraduate mentees that I work with Ellen Hong, Charlton Tsai, Brenna Remick, and Cindy Luan for their contribution to my work.

My committee members, Dr. John Schimenti and Dr. Marcus Smolka were

also instrumental for my success as they continuously provided great scientific input and suggestions for shaping my work. I would like to thank my collaborators for their help with the project, Dr. Marcus Smolka, Dr. John Schimenti, Dr. Andrew White, Dr. Jeff Pleiss, members of the Smolka Lab, and several members of the R3 group. I also appreciate the support and guidance that I received from my class members and my funding sources.

Finally, I would like to thank my friends and family, especially my wife, Bhumika, for showering me with selfless love, encouragement and support throughout my journey.

TABLE OF CONTENTS

CHAPTER 1: Literature review 1

1.1. DNA damage 1

1.2. DNA damage response (DDR) 4

1.3. Checkpoint signaling: DDR Kinases 7
1.3.1. ATM: Master regulator of DSBs 8
1.3.2. ATR: Mediator of DNA replication stress 11

1.4. DNA Repair 14
1.4.1. Direct reversal of DNA damage 15
1.4.2. Mismatch repair (MMR) 15
1.4.3. Base excision repair (BER) 16
1.4.4. Nucleotide excision repair (NER) 20
1.4.5. Translesion synthesis (TLS) 21
1.4.6. DSB repair – Non homologous end joining (NHEJ) and homologous recombination (HR) 22
1.4.6.1. Non-homologous end-joining 22
1.4.6.2. Homologous recombination 23
1.4.6.3. Relationship between BRCA1 and 53BP1 in repair choice 25
1.4.6.4. Other DSB repair pathways 27
1.4.7. Fanconi anemia pathway mediated DNA ICL repair 27

1.5. The RAD9A-HUS1-RAD1 (9-1-1) complex 29
1.5.1. Identification of the 9-1-1 complex 30
1.5.2. Structure and loading of the 9-1-1 complex 30
1.5.3. Role for the 9-1-1 complex in checkpoint signaling and DNA repair 32
1.5.4. Physiological relevance of the 9-1-1 complex 35

1.6. Crosstalk between replication fork stability and DNA repair machinery for genome maintenance 39

1.7. Role of DDR proteins in tumorigenesis and anti-cancer therapeutics 49

1.8. Summary 52

CHAPTER 2: Genome protection by the 9-1-1 complex subunit HUS1 requires clamp formation, DNA contacts, and ATR signaling-independent effector functions 55

2.1 Abstract 55
2.2 Introduction 56
2.3 Materials and methods 58
2.4 Results 72
2.5 Discussion 93

2.6. Acknowledgement 97

CHAPTER 3: The 9-1-1 DNA damage response complex acts upstream of BRCA1, FANCD2, and RAD51 during DNA interstrand crosslink repair to maintain genomic stability 98

3.1 Abstract 98
3.2 Introduction 99
3.3 Materials and methods 102
3.4 Results 111
3.5 Discussion 155
3.6. Acknowledgement 162

CHAPTER 4: A novel role for the 9-1-1 complex in regulating neddylation for genome maintenance 164

4.1 Abstract 164
4.2 Introduction 165
4.3 Materials and methods 168
4.4 Results 175
4.5 Discussion 188
4.6. Acknowledgement 195

CHAPTER 5: Tumor promoting functions for the DNA damage response protein HUS1 196

5.1 Abstract 196
5.2 Introduction 197
5.3 Materials and methods 199
5.4 Results 206
5.5 Discussion 240
5.6. Acknowledgement 247

CHAPTER 6: Summary and future directions 249

REFERENCES 259

LIST OF FIGURES

Figure 1.1.	Illustration of the DNA damage and its physiological consequences	3
Figure 1.2.	Role of ATM and ATR in DDR signaling in response to DNA damage	6
Figure 1.3.	Model depicting the mechanism of mammalian DNA repair pathways	18
Figure 1.4.	Simplified model depicting the distinct role for the 9-1-1 complex in response to replication stress	33
Figure 1.5.	Therapeutic targeting of DDR genes for treatment against oncogenic-induced replication stress in cancer cells	53
Figure 2.1.	mHUS1 residue is critical for 9-1-1 clamp formation	76
Figure 2.2.	Multiple positively-charged residues on the HUS1 inner ring are synergistically important for genotoxic stress responses	79
Figure 2.3.	Certain configurations of positively charged residues in the inner ring of HUS1 are dispensable for genotoxic stress responses	81
Figure 2.4.	The identification of a novel conserved hydrophobic pocket in the outer ring of HUS1	82
Figure 2.5.	Two hydrophobic pockets on the outer surface of HUS1 are required for genotoxic stress responses.	85
Figure 2.6.	DNA damage-induced HUS1 localization is defective in HUS1 clamp forming and DNA interacting mutants, but not in HUS1 pocket mutants	88
Figure 2.7.	9-1-1-dependent checkpoint signaling requires clamp formation and DNA associations but not HUS1 outer surface pocket function, which is necessary for effector interactions	91
Figure 3.1.	9-1-1 complex dysfunction causes cellular hypersensitivity to DNA crosslinking agents and leads to ICL-induced radial chromosome formation	112
Figure 3.2.	The 9-1-1 complex is required for suppressing radial chromosome formation upon MMC treatment	114
Figure 3.3.	HUS1 is required for FANCD2 focus formation and chromatin loading in response to ICL	117
Figure 3.4.	*Hus1* deficiency leads to loss of MMC-induced FANCD2 but not γH2AX focus formation	119
Figure 3.5.	9-1-1 subunits directly interact with multiple Fanconi anemia pathway components	122

Figure 3.6. The 9-1-1 complex promotes RAD51 localization to the DNA in response to MMC-induced replication stress 126

Figure 3.7. HUS1 is required for RAD51 function in response to replication stress 128

Figure 3.8. RAD51 defects observed upon *Hus1* loss are replication stress specific 130

Figure 3.9. RAD51 loading fails to occur in Hus1-deficient cells despite the presence of RPA-coated ssDNA after MMC 133

Figure 3.10. HUS1 regulates the pRPA32 and RAD51 loading during ICL repair 135

Figure 3.11. The 9-1-1 complex protects stalled replication forks against MRE11-dependent fork degradation 136

Figure 3.12. The 9-1-1 complex promotes BRCA1 loading following ICL induction 138

Figure 3.13. The HUS1 outer surface is important for repair protein recruitment in response to MMC-induced ICLs 142

Figure 3.14. Outer surface of HUS1 is important for recruitment of FANCD2 and RAD51 144

Figure 3.15. Outer surface of HUS1 is not essential for suppressing radial chromosome formation 145

Figure 3.16. 9-1-1 mediated checkpoint signaling is essential for MMC-induced BRCA1 recruitment, replication fork protection, and the prevention of chromosomal instability 149

Figure 3.17. 9-1-1 mediated checkpoint signaling is critical for recruitment of BRCA1 151

Figure 3.18. 9-1-1 mediated checkpoint signaling is essential for replication fork protection and the prevention of chromosomal instability 153

Figure 3.19. CHK1 inhibition phenocopies *Rad9a*$^{SA/SA}$ mutant cells 154

Figure 4.1. Proteomics screen identified novel 9-1-1 complex interacting proteins 177

Figure 4.2. HUS1 physically interacts with neddylation proteins 181

Figure 4.3. HUS1 regulates the expression and recruitment of neddylation proteins 182

Figure 4.4. HUS1 regulates UV-induced DNA damage repair 185

Figure 4.5. Auxin-inducible degron (AID) tagging of HUS1 allowed rapid depletion of endogenous HUS1 in human cells 189

Figure 5.1. Enhanced oncogene-induced checkpoint activation and chromosomal aberrations following conditional *Hus1* inactivation 208

Figure 5.2.	Decreased proliferation, checkpoint activation, and chromosomal aberrations following simultaneous conditional *K-ras* activation and *Hus1* inactivation	209
Figure 5.3.	Decreased cell transformation associated with increased checkpoint activation following oncogene activation in *Hus1*-deficient cells	212
Figure 5.4.	Suppression of *KrasG12D*-driven lung tumorigenesis by conditional *Hus1* inactivation	213
Figure 5.5:	Effect of *Hus1* loss on *K-ras* induced lung tumors	215
Figure 5.6.	Decreased immortalization and malignant transformation in MEFs with reduced *Hus1* expression	217
Figure 5.7.	Effects of partial *Hus1* impairment on cell immortalization	219
Figure 5.8.	Decreased tumorigenesis following two-step chemical carcinogenesis in mice with partial *Hus1* impairment	223
Figure 5.9.	Decreased carcinogen-induced skin tumor development in mice with an intermediate degree of *Hus1* impairment	225
Figure 5.10:	Lack of acute DMBA hypersensitivity in cells and mice with partial *Hus1* impairment	227
Figure 5.11:	Lack of acute TPA hypersensitivity in cells and mice with partial *Hus1* impairment	229
Figure 5.12.	*HUS1* expression is elevated in cancer cells	233
Figure 5.13.	APA is responsible for upregulating *HUS1* expression in cancer cells	237
Figure 5.14.	Non-mediated Decay (NMD) actively degrades intron-spliced *Hus1* mRNA transcript	241

LIST OF TABLES

Table 1.1. A list of DNA repair proteins that interact with the 9-1-1 complex 34

Table 2.1. Primers used for site-directed mutagenesis of *mHus1* 60

Table 2.2. List of UniProtKB accession numbers of the PCNA, RAD9A, HUS1 and RAD1 sequences used for evolutionary conservation analysis 65

Table 2.3. Summary of clonogenic survival and short-term viability assay results for all mHUS1 mutants analyzed 73

Table 3.1. Key resources table 104

Table 3.2. Chromosomal aberrations in *Hus1*$^{-/-}$ *p21*$^{-/-}$ and *Hus1*$^{+/+}$ *p21*$^{-/-}$ control cells following MMC treatment 115

Table 3.3. Chromosomal aberrations in *Hus1*$^{-/-}$ +HUS1, *Hus1*$^{-/-}$ +vec and *Hus1*$^{-/-}$ +PM4 cells following MMC treatment 145

Table 4.1. Oligonucleotide sequences for mAID cloning 174

Table 4.2. List of 9-1-1-interacting DDR proteins identified in the proteomic screen 178

Table 5.1. Oligonucleotide sequences for qPCR and cloning 205

CHAPTER 1

LITERATURE REVIEW

1.1. DNA Damage

Faithful transmission of genetic material from a mother cell into daughter cells is essential for survival at the cellular and organismal level. Interestingly, DNA bases are extremely vulnerable to spontaneous chemical modifications that result in cells undergoing approximately 100,000 modifications daily through exogenous and endogenous insults (Lindahl, 1993; Lindahl and Wood, 1999). DNA modifications and damage involve covalent and non-covalent changes to the DNA structure, such as base pair mismatch, pyrimidine dimers, and bulky DNA adduct formation (Hoeijmakers, 2009). One of the simplest forms of DNA damage occurs through spontaneous hydrolysis of nucleotide residues, resulting in the formation of abasic sites and deaminated bases such as uracil and xanthine (Krokan and Bjørås, 2013; Lindahl, 1974). Reactive oxygen species (ROS) and alkylated products are endogenous DNA damage–causing agents that account for single-stranded DNA (ssDNA) breaks and that generate complex oxidative bases in DNA (Hoeijmakers, 2009). As a protective measure, cells synthesize antioxidants and low–molecular weight scavengers to break down ROS and metabolic derivatives. In a similar fashion, extensive repair pathways, such as base excision repair (BER) and mismatch repair (MMR), have evolved to repair abasic sites and deaminated bases (Hoeijmakers, 2009; Lindahl, 1993; Sancar et al., 2004). However, exogenous DNA–damaging agents, such as ionizing radiation (IR) and chemical genotoxins, often result in the formation

of more toxic and harmful DNA lesions (Gensler and Bernstein, 1981; Kelner, 1949; Lindahl and Wood, 1999). Evidence implicating exogenous agents as potential modifiers of "genetic material" emerged in the late 1930s, way ahead of the discovery of the structure of DNA (Dulbecco, 1949; Hollaender and Duggar, 1938; Kelner, 1949). For example, ultraviolet (UV) light from the sun induces the formation of bulky DNA adducts such as cyclobutane pyrimidine dimers and (6-4) photoproducts (Hoeijmakers, 2009). Chemical agents such as cisplatin, mitomycin C (MMC), and psoralen are known to form covalent links between two bases of the same or different DNA strands (Auerbach and Kilbey, 1971; Bernstein et al., 1985; Jackson and Loeb, 2001). Other environmental factors, such as cigarette smoke and asbestos, also induce DNA lesions, resulting in the formation of oxidative species and DNA adducts (Jackson, 2009). Finally, IR and chemical toxins promote the generation of double-stranded DNA breaks (DSBs) (Jackson and Bartek, 2009b). DSBs are rare compared to other kinds of DNA lesions; however, they are extremely toxic to cells. DSB repair requires an elaborate protein machinery, and faulty DSB repair (erroneous rejoining of broken DNA ends) results in deletion, amplification, or translocation of chromosomal regions (Haber, 2000; Richardson and Jasin, 2000). Nevertheless, any form of DNA damage compromises the integrity of the cellular genome, and genomic instability predisposes the organism to neurological defects, immunodeficiency, cell death, and cancer (Jackson and Bartek, 2009b).

The consequences of DNA damage depend on various factors, such as the type of damage, extent of damage, and stage of the cell cycle (Hoeijmakers, 2009). Figure

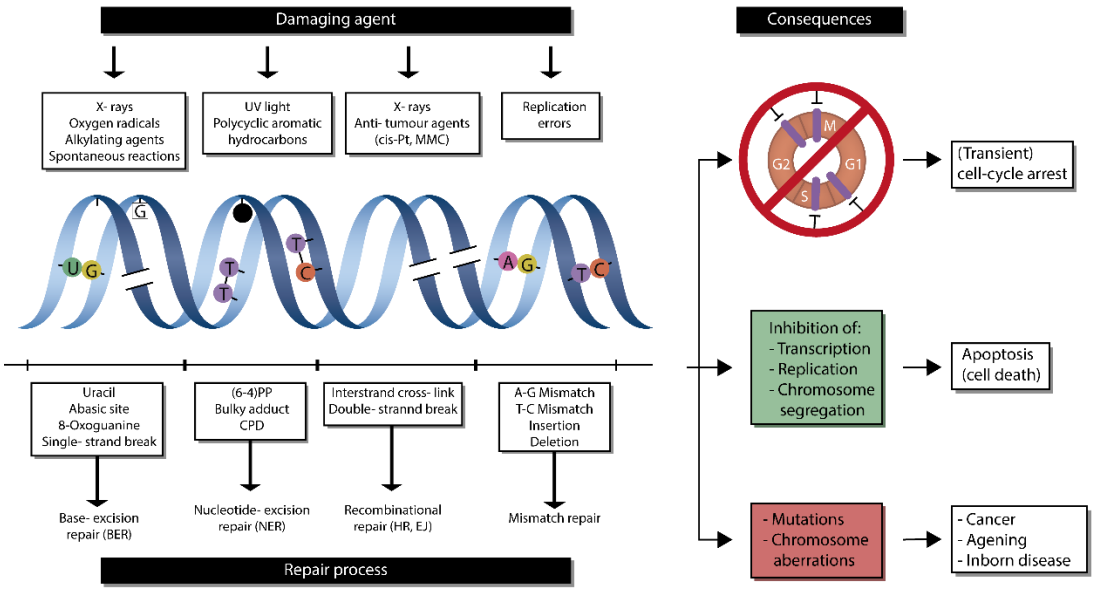

Figure 1.1. Illustration of the DNA damage and its physiological consequences: There are variety of exogenous and endogenous sources that can induce DNA. In response to DNA damage, cell activation of a cell cycle checkpoint, regulate transcriptional programs, execute DNA repair depending on the DNA lesion or in cases of severe damage, initiate apoptosis. Failure to monitor the DNA damage can result in accumulation of mutations and chromosomal aberrations.

1 outlines various types of DNA damage and their outcomes. For example, short-term acute DNA damage induces cell cycle arrest, altered DNA metabolism, blockage of replication and transcription, or cell death (Zhou and Elledge, 2000). However, prolonged DNA damage can result in genomic instability and the onset of tumorigenesis (Bartkova et al., 2005; Gorgoulis et al., 2005; Halazonetis et al., 2008). In addition, cells also deliberately induce DNA damage to regulate various cellular processes. For example, during meiosis, cells deliberately generate DSBs to initiate recombination between homologous chromosomes to promote accurate chromosome segregation (Murakami and Keeney, 2008). Similarly, DSBs are generated to stimulate immunoglobulin class switch recombination and V(D)J (variable, diversity, joining gene segments) recombination for lymphocyte production (Khanna and Jackson, 2001). Thus, proper monitoring and repair of DNA lesions is critical for maintaining genome integrity within the cell.

1.2. DNA Damage Response (DDR)

To ensure genomic integrity, cells have evolved a surveillance mechanism that monitors and manages DNA damage and that is known as the DDR. It is a set of complex regulatory mechanisms that can detect and respond to DNA damage, including checkpoint signaling (Zhou and Elledge, 2000). The DNA damage checkpoint governs three important stages of the cell cycle: G1/S transition, S phase progression, and G2/M transition. In response to DNA damage, checkpoint signaling promotes cell cycle arrest to ensure that cells with unrepaired DNA does not undergo cell division (Paulovich et al., 1997; Zhou and Elledge, 2000). Rao and Johnson were

the first to propose the idea of DNA damage checkpoints in 1970 (Rao and Johnson, 1970). However, the first experimental evidence demonstrating the functional importance of DNA checkpoints was presented by Weinert and Hartwell in 1989 (Hartwell and Weinert, 1989; Paulovich et al., 1997). Initial studies suggested an extensive role for DNA damage checkpoints in regulating the pace of the cell cycle to monitor cell growth and cell mass accumulation (Weinert et al., 1994). Further studies have implicated DNA damage checkpoints in regulating DNA repair, transcription, chromatin remodeling, and apoptosis pathways (Bartek and Lukas, 2003; Zhou and Elledge, 2000). With the diverse roles DNA damage checkpoints play, their malfunction results in the accumulation of DNA mutations, genomic instability, developmental defects, and predisposition to various genetic disorders, including cancer (Barlow et al., 1996; Bartkova et al., 2005; Brown and Baltimore, 2000; Tibbetts et al., 1999).

The checkpoint pathway is composed of three main groups of proteins: sensors, transducers, and effectors. The sensor proteins monitor and recognize DNA lesions and initiate a signaling cascade. Following sensor signaling, the transducer proteins, typically protein kinases, are activated and can further amplify the damage signal through their phosphorylation activity. At this point, the effector proteins execute the function of the DDR, e.g., halting cell cycle progression (Bartek et al., 2004; Zhou and Elledge, 2000). Given the importance of DNA damage checkpoints, most of the proteins in the pathway are highly conserved across eukaryotes, which has enabled the identification and detailed analysis of the checkpoint network and signaling (Sancar et al., 2004).

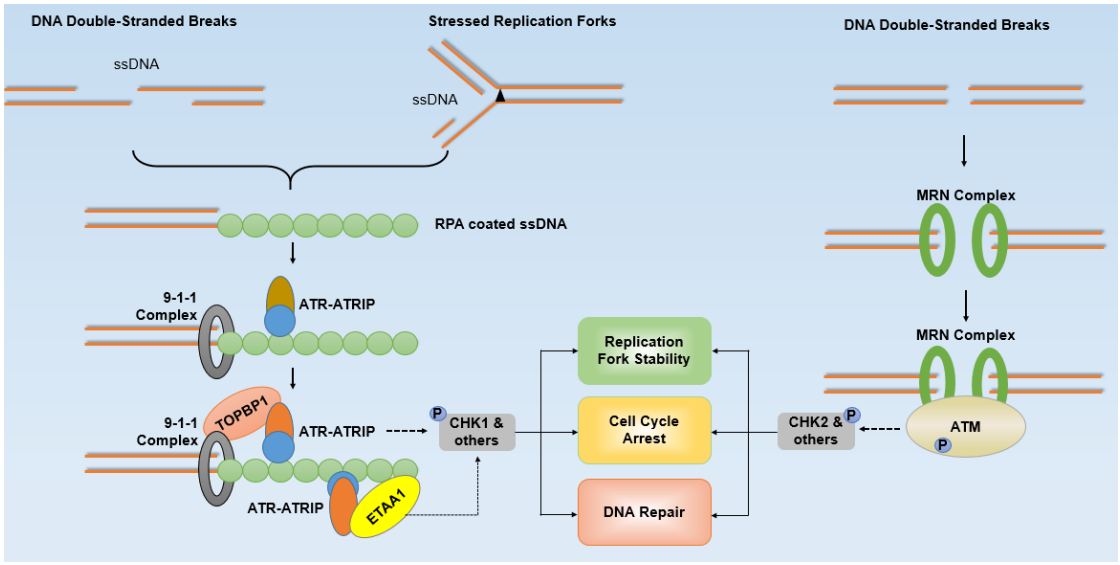

Fig. 1.2. Roles of ATM and ATR in DDR signaling in response to DNA damage: In response to replication stress or exposed single stranded DNA, the ATR kinase is activated with the help of TOPBP1 and 9-1-1 complex. Activated ATR phosphorylates various downstream effectors proteins, including CHK1, which mediates cell cycle arrest, and other substrates that regulate DNA repair and fork stability. Apart from the TOPBP1-9-1-1 complex axis, ETAA1 has been recently implicated in activating ATR. However, in response to DSBs, MRN complex binds the broken ends of the DNA and promotes the recruitment and activation of ATM**.** Like ATR, activated ATM phosphorylates various downstream effectors proteins, including CHK2, which mediates cell cycle arrest, and other substrates that regulate DNA repair and fork stability.

3. Checkpoint Signaling: DDR Kinases

In mammalian systems, the primary checkpoint response to DNA damage is led by the members of protein serine/threonine (S/T) kinases family that contain a catalytic domain belonging to PIKK–ATM (phosphoinositide 3-kinase–related kinases–ataxia-telangiectasia mutated) and ATR (ATM and RAD3-related) (Fig. 2) (Abraham, 2001). Both ATM and ATR are large protein kinases with a predicted molecular weight of over 300 kDa. Both kinases contain a large helical solenoid HEAT repeat domain of variable length, followed by a FAT (FRAP [mechanistic target of rapamycin kinase]–ATM–TRRAP [transformation/transcription domain-associated protein]) domain and a C-terminal kinase domain (Blackford and Jackson, 2017; Sibanda et al., 2017). The HEAT repeat domain mediates protein–protein interactions (Perry and Kleckner, 2003). Similarly, a few studies have identified a role for the ATM FAT domain in regulating ATM interaction with Tip60; however, other structural evidence points to the importance of the FAT domains in conserving kinase activity (Jiang et al., 2006; Mordes et al., 2008). Given the size of these kinases, there is limited information regarding their crystal structure (Rao et al., 2017; Wang et al., 2017).

Regarding substrate specificity, most phosphorylation targets of ATM and ATR contain an acidic or hydrophobic residue next to the S/T phosphorylation site (S/T-Q motif) (Jette and Lees-Miller, 2015). Several S/T-Q motifs are also present in ATM and ATR, subjecting them to autophosphorylation; however, the roles of autophosphorylation remain controversial. In both cases, conflicting evidence argues a role for autophosphorylation at S1981 (in ATM) and T1989 (in ATR) in their respective activation. However, structural and in vivo studies have disproved the

importance of S1981 in ATM activation (Blackford and Jackson, 2017; Lau et al., 2016). Although T1989 in ATR can be used as a marker of ATR activation, the site itself is not well conserved among eukaryotes (Liu et al., 2011). Even though both protein complexes regulate aspects of DNA damage, knockout of *Atr* in mice is embryonically lethal; in contrast, the loss of *Atm* produces viable offspring (Barlow et al., 1996; Brown and Baltimore, 2000). However, *Atm*-deficient mice exhibit various defects such as growth retardation, neurologic dysfunction, infertility, defects in lymphocyte maturation, and extreme sensitivity to IR (Barlow et al., 1996). Both ATM and ATR activation is regulated by DNA damage; ATR responds to replication stress, while ATM plays an analogous role during DSB formation (Abraham, 2001).

1.3.1. ATM: Master regulator of DSBs

The *ATM* gene was initially identified in the 1970s, when several patients with ataxia-telangiectasia (AT) developed severe complications following cancer radiotherapy (Taylor et al., 1976). AT is a rare inherited genetic disorder, where patients exhibit cerebellar ataxia, oculocutaneous telangiectasia, dilated blood vessels, immunodeficiency, predisposition to lymphoid tumors, and hypersensitivity to IR (Barlow et al., 1996). In the next decade, several groups observed that cells from patients with AT exhibited checkpoint defects and p53 inactivation in response to IR (Blackford and Jackson, 2017). Eventually, Shiloh's group identified and partially cloned the *ATM* gene in 1995 (Savitsky et al., 1995).

ATM recruitment to the DNA is facilitated by the presence of DSBs. In response to DSBs, the MRE11–RAD50–NBS1 (MRE11 homolog, DSB repair

nuclease–RAD50 DSB repair protein–nibrin [MRN]) complex binds the broken ends of the DNA, enabling the recruitment of ATM to the damage site (Abraham, 2001; Perry and Kleckner, 2003; Trenz et al., 2006). MRE11 is a highly conserved DNA-binding protein and serves as an endonuclease and exonuclease against a variety of ssDNA or dsDNA substrates (Lee and Paull, 2005). MRE11 nuclease activity also plays a crucial role in regulating fork stability and repair pathway choice (Schlacher et al., 2011; Trenz et al., 2006). RAD50 is a large DNA-binding protein that helps tether the two ends of the DNA while interacting with MRE11 and NBS1 (Lamarche et al., 2010). Finally, the C-terminal tail of NBS1 mediates the interaction with ATM; however, the underlying mechanism of the role of the MRN complex in activating ATM remains unclear (Dupre et al., 2006). Studies using purified enzymes have suggested that the MRN complex promotes conformational changes of inactive ATM dimers to active monomers in the absence of DNA (Paull, 2015). However, in *Xenopus* egg extract, ATM dimer monomerization requires the presence of DNA (Dupre et al., 2006). ATM also has weak DNA end-binding affinity, so in the case of extensive DNA damage or oxidative stress, ATM can monomerize via MRN-independent mechanisms (Dupre et al., 2006; Guo et al., 2010). Upon monomerization and localization to the damage site, ATM autophosphorylation and other cellular stimuli promote ATM activation, promoting the phosphorylation of ATM targets (Blackford and Jackson, 2017). There is significant overlap among the ATM substrates and ATR targets, such as H2AX (H2A histone family member X); however, the signaling cascades differ between the two (Matsuoka et al., 2007). The primary target of ATM upon DSB is CHK2 (checkpoint kinase 2), which in turn

phosphorylates a plethora of targets unknown to ATR signaling (Bartek and Lukas, 2003; Lee and Paull, 2005). ATM recruitment and activation triggers a series of phosphorylation and acetylation events by ATM as well as on ATM. A positive feedback loop sustains ATM phosphorylation, where ATM phosphorylates c-ABL, allowing c-ABL to phosphorylate Tip60, which in turn acetylates ATM at the C-terminal FAT (FATC) motif at K3016 (Jiang et al., 2011; Shafman et al., 1997).

In response to DSBs, the activated ATM phosphorylates H2AX, and the phosphorylated H2AX (γH2AX) serves a marker of DNA damage (Lee and Paull, 2005). γH2AX is also recognized by another key DDR protein: MDC1 (mediator of DNA damage checkpoint 1). Upon recognizing the γH2AX–MDC1 interaction, ATM phosphorylates MDC1 to stabilize its interaction with γH2AX (Stucki et al., 2005). MDC1 is further constitutively phosphorylated by CK2 (Casein Kinase 2) at several sites, facilitating MDC1 interaction with the MRN complex and their retention at the damaged DNA containing γH2AX mark (Chapman and Jackson, 2008; Wu et al., 2008). This ATM–MDC1–MRN interaction enables amplification of the DDR signal along the chromatin.

ATM also plays a significant role in DSB repair. In part, it promotes both the error-free homologous recombination (HR) and error-prone non-homologous end-joining (NHEJ) pathways for repairing DSBs. Phosphorylated MDC1 also interacts with and promotes the retention of the RNF8 (ring finger protein 8)–RNF168 ubiquitination cascade that facilitates the recruitment of 53BP1 (p53-binding protein) to the damage site (Kolas et al., 2007). 53BP1 is a DSB repair protein that promotes NHEJ and serves as an antagonist to HR (Bunting et al., 2010). ATM phosphorylates

53BP1 at several sites, mediating its interaction with other NHEJ proteins such as RIF1 (replication timing regulatory factor 1) and PTIP (PAX-interacting protein 1) (Escribano-Díaz et al., 2013; Hustedt and Durocher, 2016). Interestingly, ATM also phosphorylates the MRN-binding resection factor CtIP (CtBP-interacting protein), as well as BRCA1 (breast cancer early onset gene 1) to promote HR (Cortez et al., 1999; Wang et al., 2013a). However, the mechanism regulating the interplay between ATM and the DSB repair pathways remains unclear and is an active area of research.

1.3.2. ATR: Mediator of DNA replication stress

Unlike ATM, ATR activation occurs in response replication stress induced by endogenous factors, UV, or chemical agents such as aphidicolin and HU (Abraham, 2001). Several groups initially identified it in 1994 using genetic screens in *Saccharomyces cerevisiae* (Allen et al., 1994; Weinert et al., 1994). Later, the respective groups of Carr and Schreiber labs attempted to clone the human *ATR* gene (Blackford and Jackson, 2017). Unlike ATM, ATR is essential for cell viability, and *ATR* mutations are linked with several genetic disorders similar to AT (Brown and Baltimore, 2000; Heikkinen et al., 2005). In humans, *ATR* (A2101G) mutation has been reported in patients with Seckel syndrome. Often, such patients experience growth retardation, dental malocclusion, microcephaly, and physical and skeletal abnormalities (Friedel et al., 2009). The loss of ATR has also been implicated in loss of tissue homeostasis resulting in premature aging (Brown and Baltimore, 2000; de Klein et al., 2000; Ruzankina et al., 2007).

ATR is activated in response to replication stress induced by exogenous or

endogenous sources. Upon experiencing replication stress, single-stranded regions of DNA accumulate and become coated with replication protein A (RPA), which then recruits ATRIP (ATR-interacting protein) and ATR (Zou and Elledge, 2003). ATRIP acts as an obligatory partner to ATR, as it facilitates direct interaction with RPA using an acidic alpha-helix domain, enabling stable localization of ATR at the damage site (Ball et al., 2007). Subsequently, a heterotrimeric ring-shaped DNA-binding clamp, the RAD9A–HUS1–RAD1 (9-1-1) complex is loaded at the 5′ primer junction by the DNA clamp loader RAD17RFC2-5 (Parrilla-Castellar et al., 2004; Sancar et al., 2004). Recruitment of the 9-1-1 complex promotes interaction between the phosphorylated C-terminal tail of RAD9A with TopBP1 (topoisomerase-binding protein 1), which enables the activation domain of TopBP1 to bind and stimulate the ATR checkpoint kinase (Lee et al., 2007; Majka et al., 2006b; Mordes et al., 2008). TopBP1 interaction with ATR is facilitated by the ATR-activating domain in BRCT (BRCA1 C- terminal) domains VI and VII in TopBP1 (Delacroix et al., 2007; Lee et al., 2007). It is also important to note that TopBP1 recruitment is not solely dependent on the 9-1-1 complex. Other protein complexes such as MRN and BLM (Bloom syndrome protein) have been implicated in regulating TopBP1 recruitment to the DNA, suggesting an independent role of TopBP1 outside ATR activation (Blackford et al., 2015; Duursma et al., 2013; Liu et al., 2017). However, interaction between these proteins, e.g., the ATR–TopBP1–9-1-1 complex, is quintessential for ATR activation and cell viability, as the loss of any of the above proteins can result in embryonic lethality.

Until recently, 9-1-1-TopBP1 axis was the only known activator of ATR;

however, proteomic studies from three independent groups have shown that ETAA1 (Ewing's tumor associated antigen 1) can also activate ATR (Bass et al., 2016; Feng et al., 2016; Haahr et al., 2016). Collectively, these reports suggest that ETAA1 interacts directly with RPA using two RPA-binding domains. Once localized to the damaged DNA, ETAA1 can interact with ATR and promote ATR activation. ETAA1 loss results in hypersensitivity to replication stress and reduced fork progression consistent with loss of ATR activation responses. However, the authors claim that both TopBP1 and ETAA1 function independently but in parallel in ATR activation. How these two proteins fine tune their ATR pathway regulation and their importance in functional contexts remains unclear.

Upon activation, ATR phosphorylates various downstream substrates, including CHK1 and p53 (Tibbetts et al., 1999; Zhao and Piwnica-Worms, 2001) . CHK1 is another protein kinase in the signaling cascade that is activated upon phosphorylation by ATR; in turn, it phosphorylates various targets, including CDC25 and p53 (Blasius et al., 2011). CDC25 phosphorylation by CHK1 promotes rapid degradation of CDC25, resulting in sustained phosphorylation and inhibition of cyclin-dependent kinase 2 (CDK2), leading to cell cycle arrest (Donzelli and Draetta, 2003). Furthermore, ATR–CHK1 signaling also promotes the stabilization of stalled replication forks (RF) and inhibits origin firing (Ciccia and Elledge, 2010). In addition to regulating checkpoint signaling, ATR also plays a crucial role in RF stabilization and DNA repair pathway promotion, such as the Fanconi anemia (FA) pathway (Andreassen et al., 2004; Friedel et al., 2009).

In the last few decades, a considerable amount of work from several groups

has laid a solid foundation for understanding the significance of the DDR and checkpoint signaling. At the core of the DDR, ATM and ATR orchestrate complex signaling cascades to promote cell viability and DNA damage tolerance (DDT). Some of the outstanding questions commonly proposed in the field relate to understanding of the significance of these kinases in regulating cancer initiation or progression. Both kinases have several known, well-characterized targets; however, the functional importance of the majority of other targets remains unclear. With continued research, we will be able to tease apart the molecular details and identify other important factors that contribute to this signaling network.

1.4. DNA Repair

In response to genotoxic stress, cells initiate checkpoint signaling to halt cell cycle progression and prevent the duplication of damaged DNA. Cell cycle arrest provides time for cells to assess the damage to initiate apoptosis in response to extensive DNA damage or initiate DNA repair based on the lesion. In any mammalian system, at least eight repair pathways can be initiated to repair damaged DNA (Hoeijmakers, 2009). The seven classic repair pathways are direct reversal, MMR, BER, nucleotide excision repair (NER), translesion synthesis (TLS), HR, and NHEJ (Fig 3.). Besides the above classic DNA repair pathways, a newly characterized repair pathway, mediated by FA genes to repair DNA inter/intrastrand crosslinks, has been identified (Dietlein et al., 2014). In the following chapter, I will briefly discuss the functional importance of each pathway.

1.4.1. Direct reversal of DNA damage

Unlike other repair pathways, direct reversal does not require a multi-step process. For example, alkylating agents in the cell can modify the guanine base by methylating it, forming an O-6-methylguanine, which disrupts guanine–cytosine interaction. To restore the base, O-6-methylguanine–DNA methyltransferase (MGMT) transfers the alkyl group from guanine to a cytosine residue, restoring the base (Hakem, 2008). *Mgmt* loss in mice does not manifest any developmental or meiotic defects; however, *Mgmt*$^{-/-}$ mice display increased tumorigenesis in response to alkylating carcinogens, indicating the importance of the direct reversal pathway in cancer (Sakumi et al., 1997).

1.4.2. Mismatch repair (MMR)

The MMR pathway is responsible for identifying and repairing erroneous insertions, deletions, and misincorporations of DNA bases that were bypassed by proofreading machinery (Li, 2007). MMR is a highly conserved repair pathway, as it plays an essential role in both prokaryotic and eukaryotic organisms. In humans, MSH2 (mutS homolog 2), MSH3, and MSH6 play key roles in detecting lesions and initiating repair (Li, 2007). MSH2 heterodimerizes with MSH6 or MSH3 to form a MutSα or MutSβ complex, respectively, where the former MutSα complex detects small mismatches, whereas the latter complex identifies large mismatches and insertion loops (Kunkel and Erie, 2005). Along with the MutSα and MutSβ complexes, MLH1 (mutL homolog 1) and PMS2 (PMS1 homolog 2, MMR system component) form the MutLα complex to coordinate multiple steps in MMR (Constantin et al.,

2005). Once the tertiary complex between the MutSα, MutSβ, and MutLα complexes is formed, the MutLα complex facilitates the interaction between RFC (replication factor C)–PCNA and the MutSα complex. PMS2 nicks the lesion in an adenosine triphosphate (ATP)-dependent manner, enabling EXO1 (exonuclease 1) recruitment. EXO1 resects the DNA, leaving behind ssDNA to be coated by RPA. Finally, the replicative POLD is recruited to the DNA to resynthesize the DNA, followed by ligase activity to restore duplex integrity (Fig. 3) (Hsieh and Yamane, 2008; Kunkel and Erie, 2005).

As MMR proteins are highly conserved, several disorders are associated with MMR gene mutations. Approximately 70–80% of germline mutations identified in patients with Lynch syndrome that is characterized by early onset of colorectal cancers, involve *MLH1* or *MSH2* (Peltomaki and Vasen, 2004). Other than that, mutations in several MMR genes promote fertility defects and spontaneous tumorigenesis, especially lymphomas and gastrointestinal cancers (Hakem, 2008; Mukherjee et al., 2010).

1.4.3. Base excision repair (BER)

The BER pathway restores non-helix–distorting base modifications. DNA base modifications often arise from deamination, methylation, or oxidation of bases (David et al., 2007). Tomas Lindahl identified the first BER protein, uracil–DNA glycosylase (UNG) in 1974, observing that the enzyme cleaved the bond between uracil and deoxyribose (Lindahl, 1974). The term DNA glycosylase was coined for the enzyme that cleaves a mismatch or modified DNA base from deoxyribose (Krokan et al.,

1997). Since then, several DNA glycosylases, such as mutY–DNA glycosylase (MUTYH, *Myh*) and 8-oxoguanine–DNA glycosylase (OGG1), have been identified and they promote the removal of damaged DNA bases. Once the DNA glycosylase acts, an abasic site is generated, which meets the requirement for APE1 (apyrimidinic endonuclease 1) recruitment, along with Polβ to the abasic site. APE1 makes two cuts in the backbone and Polβ promotes for the removal of 5'sugar phosphate group, facilitating PCNA (proliferating cell nuclear antigen) and DNA polymerase δ/ε (POLD and POLE, respectively) recruitment to the damage site. The polymerase displaces and resynthesizes the nucleotides from the damaged sites. Lastly, XRCC1 (X-ray repair cross-complementing 1)/ LIGI (DNA Ligase I) performs strand ligation (Krokan and Bjørås, 2013). Analogous to base modification restoration, single-stranded breaks are also repaired by a set of BER proteins. PARP (Poly ADP-ribose polymerase) 1/2 sense SSBs and facilitate the recruitment of FEN1 (flap structure–specific endonuclease 1) and XRCC1 for DNA synthesis–ligation (Fig. 3) (Dietlein et al., 2014). It is also important to note that PARP proteins are not essential for BER, and PARP has been implicated in HR and alt-NHEJ repair and fork stability (Ray Chaudhuri et al., 2016; Schultz et al., 2003; Wang et al., 2006a).

Given the importance of the BER pathway, loss-of-function gene mutations can affect cell survival. Mice display grossly normal phenotypes with the loss of one of DNA glycosylase (*Myh*, *Ogg1*, *Ung*); however, the loss of two or more DNA glycosylases predisposes mice to several tumor types (Hakem, 2008). Interestingly, targeting the downstream BER pathway proteins such as LIG1, APE1, XRCC1, and FEN1 results in embryonic lethality in mice (Sancar et al., 2004).

Figure 1.3. Model depicting the mechanism of mammalian DNA repair pathways.

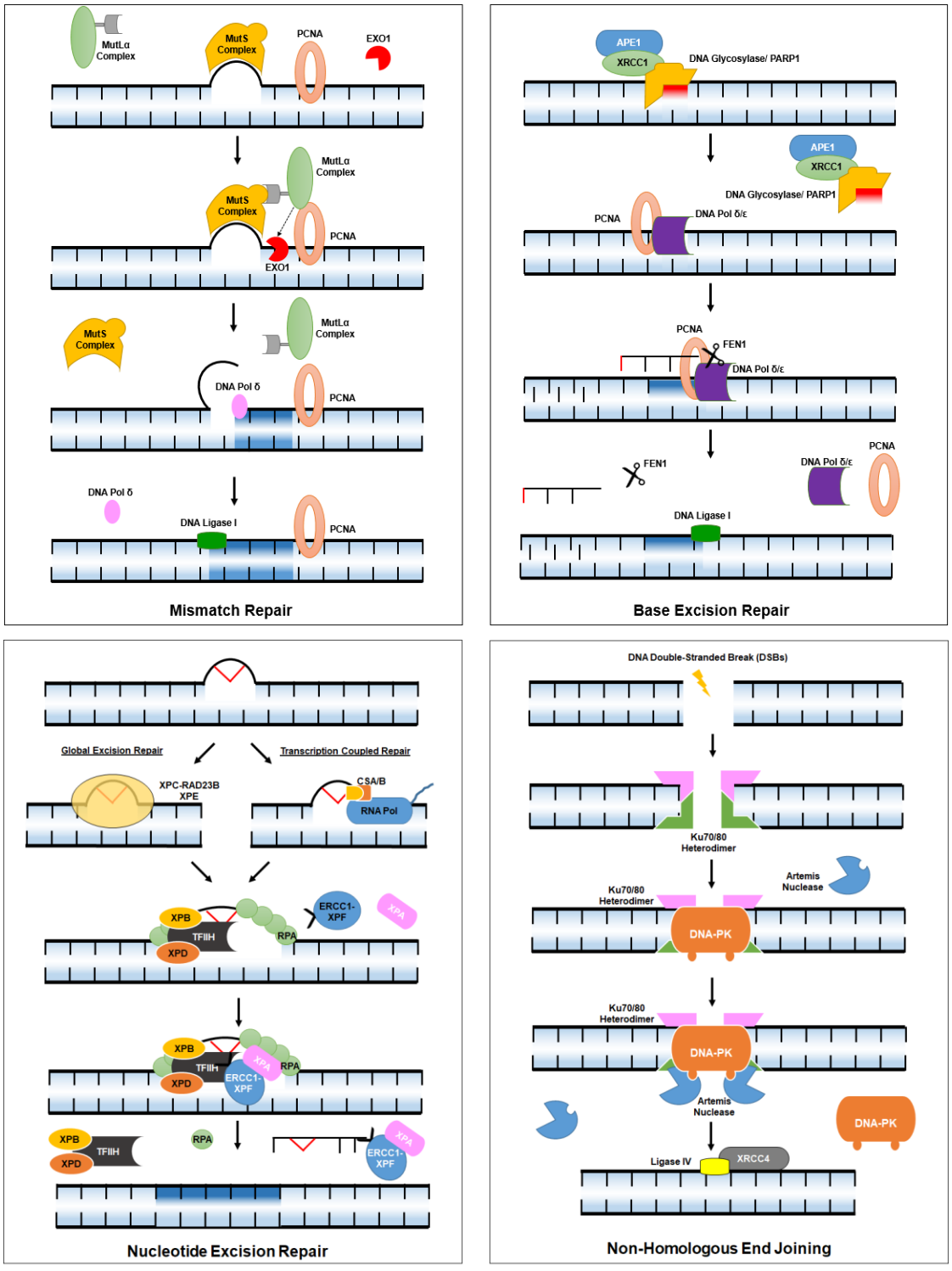

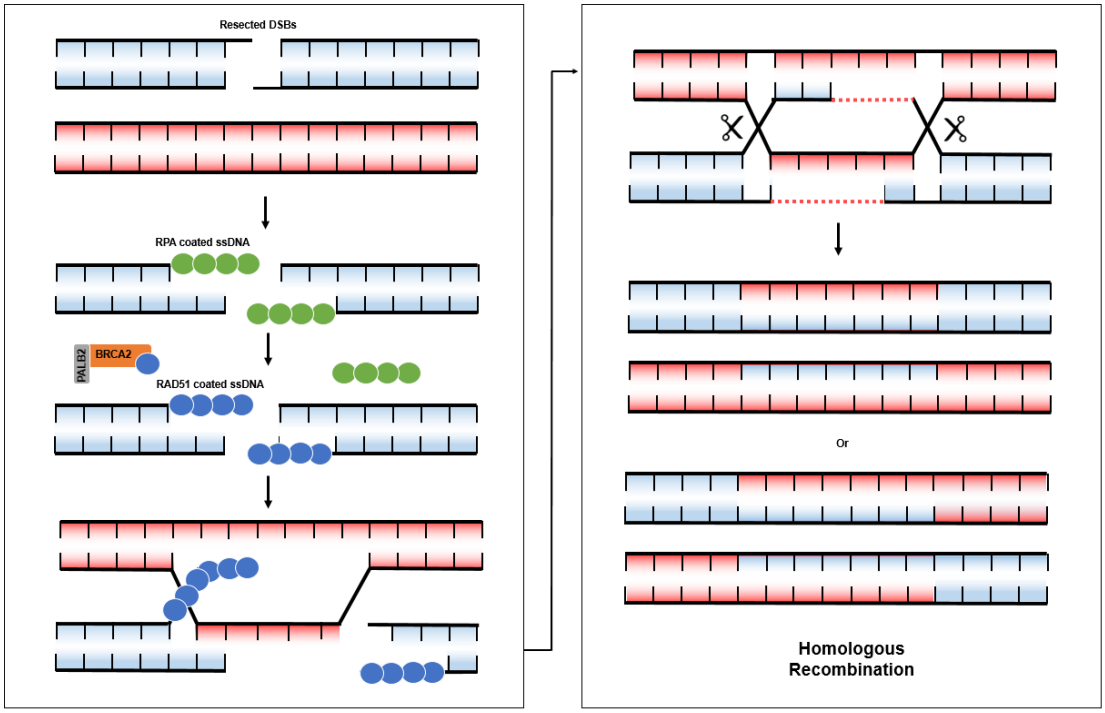
Resected DSBs
RPA coated ssDNA
PALB2
BRCA2
RAD51 coated ssDNA
Or
Homologous
Recombination

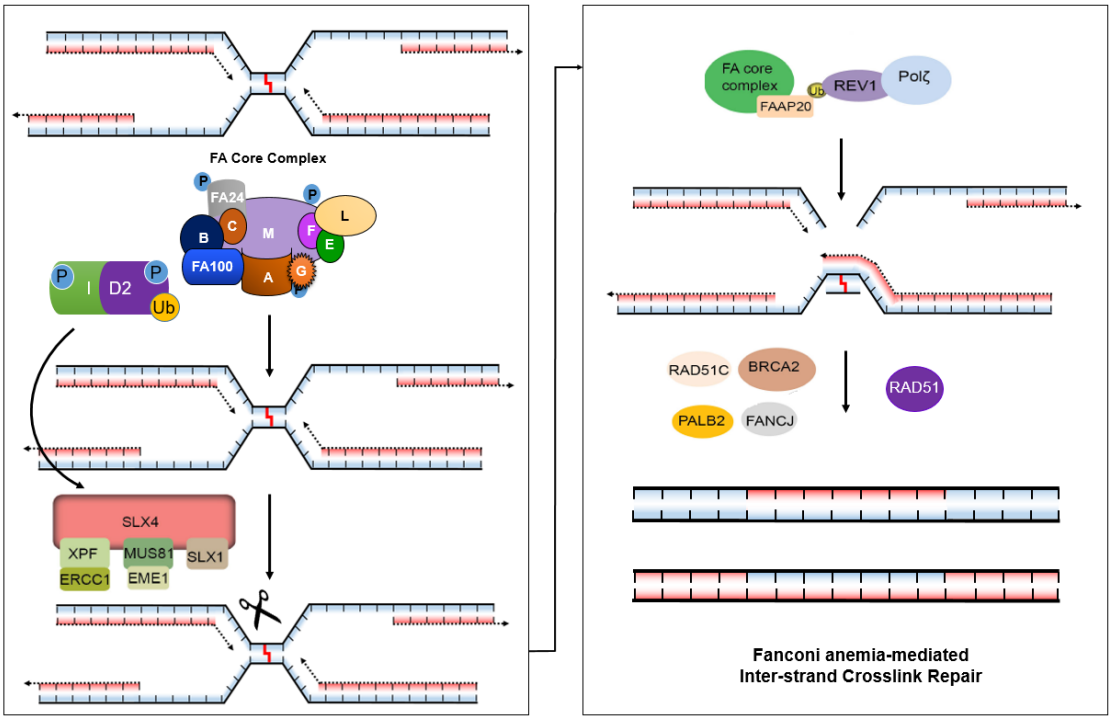
FA Core Complex
P
FA24
C
M
F
L
B
E
FA100
A
G
P
I
D2
P
Ub
SLX4
XPF
MUS81
SLX1
ERCC1
EME1
FA core
complex
Ub
FAAP20
REV1
Polζ
RAD51C
BRCA2
RAD51
PALB2
FANCJ
Fanconi anemia-mediated
Inter-strand Crosslink Repair

1.4.4. Nucleotide excision repair (NER)

NER is the major repair system for removing bulky DNA adducts and helix-distorting lesions often induced by UV exposure or chemical carcinogens. NER has two distinct mechanisms that identify and repair DNA lesions: global genome NER (GG-NER) and transcription coupled NER (TC-NER) (Wienholz et al., 2017). GG-NER can identify and repair lesions throughout the genome; in contrast, TC-NER repairs lesions in actively transcribed genes. Except for the lesion recognition proteins, both pathways involve the same proteins. In GG-NER, the XPC–RAD23B and UV–DDB (damage-specific DNA-binding protein) proteins identify the lesion, but in TC-NER, the CSA, CSB (Cockayne Syndrome A and B), and XAB2 proteins sense transcriptional stalling and initiate lesion repair. Once the damage is recognized, both pathways recruit TFIIH (transcription factor IIH) to unwind the DNA, aided by the XPB (xeroderma pigmentosum B) and XPD helicases. Stalling of XPD at the lesion promotes XPF/ERCC1 and XPG recruitment, which in turn initiates the 5′ incision at the damage site. POLΔ/δ resynthesizes the damaged DNA aided by PCNA or XRCC1. Finally, ligase I or III seals the nick (Fig. 3) (Schärer, 2013).

In humans, NER gene mutations contribute to various disorders, including cancer, neurological abnormalities, and skin diseases (Hakem, 2008). Some of the widely known diseases include xeroderma pigmentosum (XP), Cockayne syndrome (CS), and trichothiodystrophy (TTD) (Garfinkel and Bailis, 2002). Growth retardation is a commonly observed phenotype in NER mutant mice. In addition, people with mutations in most of their NER genes are extremely sensitive to UV exposure and are predisposed to UV-induced skin cancer (Forment and O'Connor, 2018).

1.4.5. Translesion synthesis (TLS)

TLS repair is a part of the DNA damage tolerance mechanism, where a TLS polymerase replaces a stalled replicative POL to bypass the DNA lesion. In mammalian systems, at least seven known polymerases can perform DNA lesion bypass. In response to stalling of the replicative POL, cells experience replication stress that promotes ssDNA generation (Ghosal and Chen, 2013). RPA coats the ssDNA, enabling ATR–CHK1-mediated checkpoint activation (Zou and Elledge, 2003). RPA also recruits RAD18 (E3 ubiquitin protein ligase) that monoubiquitinates PCNA at K164 aided by RAD6 (Bi, 2015). Upon ubiquitination, PCNA interacts with Spartan, which stabilizes RAD18 and the ubiquitinated (ub)-PCNA at the damage site. Then, the TLS polymerase POLη (POLH) interacts with ub-PCNA and adds a nucleotide directly opposite the lesion. The addition is extended by another TLS polymerase, POLζ (POLZ). Once the extension by POLZ is complete, it is replaced by the high-fidelity replicative DNA polymerase. USP1 (ubiquitin-specific peptidase 1) deubiquitinates PCNA, and DNA synthesis resumes with the replicative polymerase (Bi, 2015; Ghosal and Chen, 2013; Zafar and Eoff, 2017). The molecular mechanisms regulating the various steps of the TLS pathway remain unclear, and remain a major focus for future studies.

TLS polymerases are also an active component in ICL repair (Knipscheer et al., 2009). Over activation of any TLS polymerase can be detrimental to cell survival, as it increases mutagenic events in the DNA. Several studies have implicated increased TLS polymerase activity in tumorigenesis as well as chemoresistance (Zafar and Eoff, 2017).

1.4.6. DSB repair: – Non-Homologous End Joining (NHEJ) and Homologous Recombination (HR)

DSB arises from a variety of sources, including IR, RF collapse, meiotic recombination, or inefficient SSB repair. Mammalian cells employ two major repair pathways to repair DSBs: NHEJ and HR. Both pathways are complex and involve a plethora of proteins that do not overlap between the pathways. The choice between HR and NHEJ is dependent on the stage of the cell cycle. NHEJ is considered a faster repair pathway than HR and available throughout the cell cycle (Lieber, 2010; Sancar et al., 2004).

1.4.6.1. Non-homologous end-joining

NHEJ is considered a error-prone repair pathway, as it ligates the broken ends of DNA together, potentially compromising the genomic region affected by the break (Mao et al., 2008). NHEJ-mediated DSB repair does not rely on the homologous strand and is the predominant repair pathway in the G1 phase of the cell cycle (Hartlerode and Scully, 2009). In response to DSBs, Ku heterodimers (Ku70 and Ku80) rapidly bind the broken ends of the DNA and recruit DNA-dependent protein kinase (DNA-PK) (DNA-PK catalytic subunits, DNA-PKcs) to the damage site (Lees-Miller and Meek, 2003). DNA-PK is an important kinase in the same PIKK family as ATM and ATR. DNA-PK was the first PIKK kinase to be identified as a dsDNA-phosphorylating protein (Walker et al., 1985). Subsequent work established that DNA-PK plays a crucial role in regulating DSB repair by stabilizing the DSB ends and inhibiting end-processing (Jette and Lees-Miller, 2015; Lees-Miller and Meek, 2003). Once DNA-PK

is recruited to the DSB, it autophosphorylates at two distinct sites: T2609 and S2056. Studies have suggested that DNA-PK autophosphorylation at T2609 destabilizes its interaction with the DSB end, enabling end-processing by ARTEMIS (DNA cross-link repair 1C) (Lees-Miller and Meek, 2003). However, phosphorylation at S2056 protects the DNA from excessive end-processing and excludes the HR proteins (Jette and Lees-Miller, 2015). Once ARTEMIS processes the broken ends minimally, DNA-PK recruits XRCC4/LIG4 to ligate the broken ends together in coordination with XLF (Fig. 3) (Ciccia and Elledge, 2010).

As NHEJ is responsible for repairing DSBs, the loss of any factor has a severe effect on cells. The NHEJ pathway is not only important for resolving damage-induced DSB, but also plays an important role in V(D)J recombination (Khanna and Jackson, 2001). During V(D)J recombination, T and B cells randomly assemble different gene segments to generate unique receptors for recognizing different molecules. NHEJ proteins aid the formation of these VDJ receptors by aiding the ligation of the broken DNA ends (Sishc and Davis, 2017). Hence, the loss of any NHEJ proteins results in early arrest in T and B cell development causing immunodeficiency (Chang et al., 2017; Sishc and Davis, 2017). Defective NHEJ signaling can also result in radiosensitivity, genomic instability, growth retardation, developmental and immune defects, and predisposition to cancer (Hakem, 2008).

1.4.6.2. Homologous recombination (HR)

HR is the other DSB repair pathway that functions in an error-free manner. Unlike NHEJ, HR is dependent on a homologous sister chromatid that serves as a template to

repair the DSB. Given the requirement for homology, HR is restricted to be functional only during the S or G2 phases of the cell cycle (Ciccia and Elledge, 2010; Jasin and Rothstein, 2013). Accurate DNA end resection is the most critical step for initiating HR. In response to DSBs, along with ATM activation, the MRN complex can also interact with the broken DNA ends using the RAD50 (RAD50 DSB repair protein) ATPase domain (Bhaskara et al., 2007; Williams et al., 2007). Once the MRN complex stabilizes the DNA ends, it recruits CtIP nuclease to the damage site, aided by ATM kinase activity (Wang et al., 2013b). It is important to note that BRCA1 also interacts with both the MRN and CtIP complex and ubiquitinates CtIP, stabilizing its association at the damage site (Jasin and Rothstein, 2013; Sartori et al., 2007). CtIP performs the initial DNA resection; however, two other nucleases are recruited for extensive resection: EXO1 and BLM (Nimonkar et al., 2011). The loss of any of the nucleases' activity results in significantly reduced ssDNA formation and RPA foci (Huertas, 2010). Once the ssDNA filaments are exposed, RPA coats them, providing a template for RAD51 loading. RAD51 binds ssDNA and forms nucleoprotein filaments (Shinohara et al., 1992). RAD51 displaces RPA from the single strand, and several proteins regulate RAD51 loading, including ATM, ATR, BRCA1, BRCA2, and PALB2 (partner and localizer of BRCA2) (Ahlskog et al., 2016; Davies et al., 2001; Sy et al., 2009; Zhao et al., 2017). RAD51 lies at the core of the HR pathway, as it mediates homology search and performs strand invasion in the sister chromatid, forming D-loops (Ciccia and Elledge, 2010). The D-loop structure is resolved by two methods: synthesis-dependent strand annealing (SDSA) or the Holliday junction (HJ) (Haber, 2000). In SDSA, RTEL1 (regulator of telomere elongation 1 helicase 1) aids

RAD51 removal and D-loop resolution (Barber et al., 2008). However, several methods are used to resolve a HJ structure. HJ can be dissolved by BLM and TopIII (DNA topoisomerase III), or in most cases, a plethora of nucleases (MUS81/EME1 [MUS81 structure-specific endonuclease subunit/essential meiotic structure-specific endonuclease 1], SLX1/4 (structure-specific endonuclease subunit SLX4), GEN1 [GEN1, HJ 5′ flap endonuclease]) are recruited to cleave the HJ and resolve the structure (Fig. 3) (Popuri et al., 2008; Rass et al., 2010; Wyatt et al., 2013).

HR is considered a significant pathway in organismal viability. The loss of most HR genes manifests as embryonic lethality in mice (Hakem, 2008). *Brca1/2* gene mutations are associated with a variety of cancers (Ford et al., 1998; Miki et al., 1994). In summary, several human disorders, developmental defects, increased genomic instability, and tumorigenesis are associated with defective HR repair (Hustedt and Durocher, 2016). The detrimental effects due to loss of HR machinery loss outweighs that of all other repair pathways.

1.4.6.3. Relationship between BRCA1 and 53BP1 in repair choice

Along with the proteins in both NHEJ and HR, two major proteins are critical for pathway choice: BRCA1 and 53BP1. BRCA1 is an E3 ubiquitin ligase that plays a central role in various cellular processes, including DNA repair, checkpoint signaling, transcription, fork stability, and chromatin architecture (Feng et al., 2015; Ray Chaudhuri et al., 2016; Rondinelli et al., 2017; Taglialatela et al., 2017). Most importantly, BRCA1 promotes DNA end resection aided by CtIP to initiate HR (Yun and Hiom, 2009). In contrast, 53BP1 promotes the NHEJ pathway by preventing

excessive resection (Bunting et al., 2010). BRCA1 and 53BP1 have an antagonistic relationship. Interestingly, removing 53BP1 can rescue embryonic lethality, HR defects, and tumor predisposition in *Brca1*-deficient mice, demonstrating the importance of the 53BP1–BRCA1 pathway in cellular viability (Bunting et al., 2010).

In the past decade, extensive studies have dissected the molecular details underlying the 53BP1–BRCA1 pathway functions. Given the dependence of HR on the cell cycle, 53BP1 and BRCA1 also function in accordance with different phases of the cell cycle, where BRCA1 actively promotes HR-mediated DSB repair during S/G2 (Daley and Sung, 2014). Studies have suggested that the loss of BRCA1 leads to 53BP1 recruitment at the DSB during G2 (Zhu and Dutta, 2006). Conversely, 53BP1 depletion promotes BRCA1 loading during G1, suggesting that BRCA1 loading is inhibited during G1 in a 53BP1-dependent manner, and vice versa (Escribano-Díaz et al., 2013). Recent studies have shown that BRCA1 promotes 53BP1 dephosphorylation in a PP4C (protein phosphatase 4- catalytic subunit)-dependent manner, and subsequent removal of the 53BP1 binding partner RIF to promote EXO1 mediates DSB resection and HR (Isono et al., 2017). In contrast, another deubiquitinating enzyme, USP48 (ubiquitin-specific peptidase 48), antagonizes BRCA1-mediated ubiquitination of H2A, restricting resection and promoting 53BP1 activity (Uckelmann et al., 2018). Further studies will reveal more details regarding the relationship between 53BP1 and BRCA1. Understanding the molecular mechanism of these proteins will provide novel insights into the balancing of DSB repair, and this knowledge could be exploited for therapeutic benefits.

1.4.6.4. Other DSB repair pathways

Within the realm of DSB repair, a few other offshoot repair pathways can be activated to perform error-prone DSB repair in the absence of NHEJ or HR. One such pathway is microhomology-mediated end-joining (MMEJ or alt-EJ), where DSB ends are resected and anneal once homology between a few base pairs is found. Somewhat analogous to MMEJ, cells also perform single-strand annealing (SSA), where resection and annealing occurs upon the identification of a larger homology area. In both pathways, end annealing at the homology regions is followed by DNA flap processing aided by endonucleases, followed by DNA ligation (Dietlein et al., 2014; Jasin and Rothstein, 2013).

Given the toxic nature of unrepaired DSBs, cells have evolved several mechanisms to resolve and repair them. Both the HR and NHEJ pathways are still not fully characterized, and growing interest has seen more details regarding new interactions and molecular functioning emerge.

1.4.7. Fanconi anemia pathway–mediated DNA ICL repair

During ICL formation, the two DNA strands are linked covalently, which physically impedes the DNA replication and transcription machinery (Heyer et al., 2010; Lopez-Martinez et al., 2016). Several repair pathways, including HR and NER, and several other protein complexes, coordinate the recognition and repair of ICLs.

DNA ICLs are recognized by the DNA-binding protein with an accessory helicase motif, FANCM (FA complementation group M). Along with FANCM,

FAAP24 (FA core complex–associated protein 24), MHF1 (histone fold protein 1), and MHF2 also localize to the chromatin, providing a platform for assembling the FA core complex (Huang et al., 2010). The FA core complex consists of 13 FA proteins (FANCA, FANCB, FANCC, FANCE, FANCG, FANCL, FANCM, FANCT, FAAP100, MHF1, MHF2, FAAP20, and FAAP24) (Collis et al., 2008). Once the core complex is assembled at the ICL, FANCI–FANCD2 (ID2) are recruited to the damage site, and their recruitment is dependent on ATR-mediated ID2 phosphorylation (Andreassen et al., 2004; Ho et al., 2006). It has been suggested that the role of ATR and BRCA1 is also important in FA core complex formation; however, it remains a controversial topic in this field (Lopez-Martinez et al., 2016; Zhu and Dutta, 2006). On another note, FANCL monoubiquitinates FANCD2; however, the timing of the monoubiquitination remains unclear. Some studies argue that FANCL monoubiquitinates FANCD2 before the ID2 heterodimer is loaded onto the chromatin, whereas others have suggested that it occurs post-chromatin loading (Liang et al., 2016; Longerich et al., 2014). Several proteins (UBE2T [ubiquitin-conjugating enzyme E2 T], USP1–UAF1 [USP1-associated factor 1]) regulate the FANCD2 ubiquitination levels in response to ICLs (Knipscheer et al., 2009). Nevertheless, ID2 localization to the chromatin facilitates recruitment of the downstream endonucleases (SLX4/FANCP, ERCC4/FANCQ, and MUS81) that can cleave one strand on each side of the lesion (Lopez-Martinez et al., 2016). Once the lesion is cut and unhooked, TLS polymerase REV1 (REV1, DNA-directed polymerase) or REV3–7 can bypass the lesion and complete DNA synthesis, followed by ligation (Ceccaldi et al., 2016). This leaves the complementary strand with the DSB to be repaired by the HR machinery.

Several HR genes are also known as FA genes, such as *RAD51*/*FANCR*, *BRCA1*/*FANCS*, *BRCA2*/*FANCD1*, *PALB2*/*FANCN*, *BRIP1* (BRCA1-interacting protein C-terminal helicase 1)/*FANCJ*, and *RAD51C*/*FANCO (Nalepa and Clapp, 2018)*. In conclusion, ICL repair relies on the FA pathway to coordinate different components of NER, TLS, and HR machinery (Fig 1.3).

Growing research has identified new FA proteins; so far, the FA pathway encompasses 23 proteins, and mutation in any of these 23 genes can result in FA. FA is a rare genetic disorder, patients are characterized by bone marrow failure, congenital defects, physical abnormalities, and increased risk for certain cancers (Nalepa and Clapp, 2018). The cells of patients with FA are prone to genomic instability and radial chromosome formation resulting from faulty ICL repair (Knipscheer et al., 2009).

1.5. The RAD9A–HUS1–RAD1 (9-1-1) complex

The 9-1-1 complex is a heterotrimeric clamp that interacts with DNA and shares structural similarity with another DNA-binding clamp, PCNA (Weiss et al., 2000c). Like PCNA, it does not have any enzymatic activity; however, it has residues that facilitate interaction with DNA and other proteins (Parrilla-Castellar et al., 2004). The 9-1-1 complex functions by activating ATR-mediated checkpoint signaling and DNA repair following DNA damage (Weiss et al., 2003). In the following sections, I will elaborate on the dual role of the 9-1-1 complex and its physiological relevance to organismal survival.

1.5.1. Identification of the 9-1-1 complex

During the early 1990s, a series of molecular and genetic studies in both fission (*Schizosaccharomyces pombe*) and budding yeast (*S. cerevisiae*) identified genes essential for DNA replication and DNA damage checkpoints. In fission yeast, six genes (*hus*1+, *rad*1+, *rad*3+, *rad*9+, *rad*17+, *rad*26+) were identified as important for the DDR (al-Khodairy and Carr, 1992; al-Khodairy et al., 1994; Kostrub et al., 1997; Weiss et al., 2000c). Cells deficient in these genes were hypersensitive to several replication stress–inducing agents, such as HU, UV, and bleomycin, and exhibited cell division defects under stressed conditions (Enoch et al., 1992; Kostrub et al., 1997). The names of the proteins were derived from genetic screens, i.e., hydroxyurea sensitive (*Hus1*) and radiation sensitive (*Rad9*, *Rad1*). Soon after their discovery, homologs of these genes were identified in several other species, marking them as highly evolutionary conserved genes (Thelen et al., 1999; Volkmer and Karnitz, 1999; Weiss et al., 1999). Additionally, paralogs of both HUS1 and RAD9A (HUS1B and RAD9B, respectively) were identified and shown to be conserved in several species (Dufault et al., 2003; Hang et al., 2002). HUS1B and RAD9B are significantly enriched in meiotic germ cells and have defined roles in meiosis (unpublished data, Weiss Lab).

1.5.2. Structure and loading of the 9-1-1 complex

The 9-1-1 complex is a toroidal DNA-binding clamp that has DNA- and protein-binding residues. Computational modelling and extensive electron microscopy (EM) analysis have been applied to elucidate the structural details of the proteins. Several

studies have used biochemical assays to identify the functionally important residues of the 9-1-1 complex (Delacroix et al., 2007; Dore et al., 2009).

Comparison of their subunits shows that RAD1 and HUS1 are more closely related and RAD9A is the most distantly related. Unlike PCNA, the 9-1-1 complex has an additional 120 nucleotides that comprise the floppy unstructured tail of RAD9A (Xu et al., 2009). Due to the unstructured nature of the RAD9A tail, the 9-1-1 complex crystal structure is devoid of that region. Hence, there is very limited information on the RAD9A tail structure. Like PCNA, the 9-1-1 complex contains an elliptical hole as the complex is formed. This hole is sufficient for the DNA duplex to pass through in a titled orientation (Dore et al., 2009). Several key positive-charge residues are present in the inner side of the clamp, mediating the clamp interaction with DNA; details on the important residues in HUS1 facilitating DNA interaction are discussed in the following chapter.

Comparison of the outer surface of the 9-1-1 complex with PCNA shows a high amount of topological similarity between the two complexes. Like PCNA, all 9-1-1 complex subunits contain an interdomain connecting (IDC) loop. The IDC loops in the 9-1-1 subunits run from the N- to C-terminal, forming the grooves on the outer surface of the subunits comprised of hydrophobic residues. These hydrophobic grooves are conserved elements within the β DNA clamp, as they are considered to facilitate protein interactions with the clamp (Sohn and Cho, 2009). However, the IDC loops within the subunits are not conserved, providing specificity in the interaction of proteins with the subunits (Dore et al., 2009). In PCNA, the IDL and the second globular domain forms a hydrophobic pocket that acts as a docking site for PCNA-

interacting proteins (PIP). Several PIPs contain a PIP box motif that promotes their interaction with PCNA. Like PCNA, RAD9A and HUS1 contain a topologically similar hydrophobic pocket, potentially promoting interaction with several proteins with the PIP motif (Dore et al., 2009; Sohn and Cho, 2009). The hydrophobic pockets between RAD9A and HUS1 also have some structural differences, further promoting distinct protein–protein interactions. Along with the PCNA-like hydrophobic pocket, HUS1 also contains a novel hydrophobic pocket with a strong positive electrostatic potential at its base (Lim et al., 2015). The importance of these hydrophobic pockets will be discussed in the next chapter.

As with most DNA binding clamps, the 9-1-1 complex also depends on a clamp loader complex for its recruitment onto the DNA. Primarily, RAD1 interacts with the clamp loader RAD17–RFC2-5 complex and facilitates the complex's interaction with DNA (Zou et al., 2002). Studies have determined that the RAD9A–RAD1 interaction is the weakest bond among the subunits, and during recruitment to the DNA, this interaction provides opening of the complex for loading onto the DNA (Kaur et al., 2001b). Interestingly, the 9-1-1 complex also loads onto 5′ recessed DNA ends; however, PCNA loads at 3′ recessed ends. In either case, both clamps require an ssDNA–dsDNA junction for effective loading (Xu et al., 2009).

1.5.3. Role of the 9-1-1 complex in checkpoint signaling and DNA repair

Upon loading on the DNA, the 9-1-1 complex interacts with TopBP1 using the phosphorylated C-terminal tail of RAD9A (Lee et al., 2007). In humans, RAD9A phosphorylation at S341 and S387 by Casein Kinase 2 (CK2) is critical for the 9-1-1

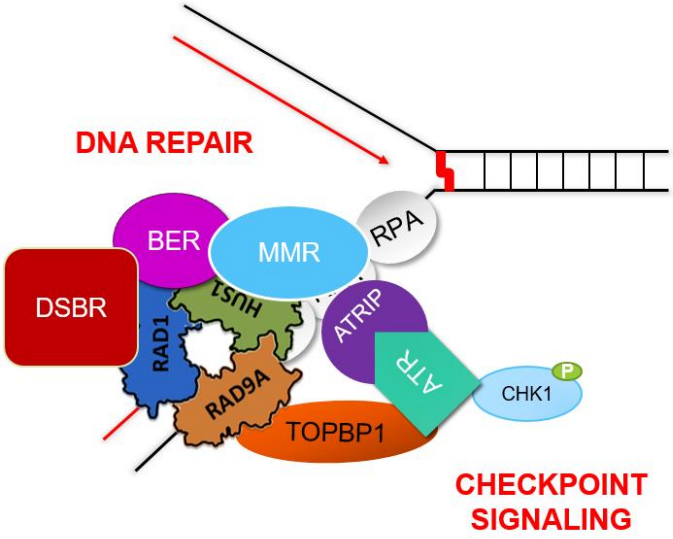

Fig 1.4. Simplified model depicting the distinct role for the 9-1-1 complex in response to replication stress. The 9-1-1 complex two distinct roles upon DNA damage, activation of ATR-mediated checkpoint signaling and DNA repair. Several independent studies have identified repair proteins in same and other repair pathways to mediate interactions with the 9-1-1 complex. The table in this figure, lists the name of repair protein that have been identified to interact with the 9-1-1 complex.

Table 1.1. A list of DNA repair proteins that interact with the 9-1-1 complex

Model system	DNA repair component	Repair pathway	Interacting partner(s)
S. pombe	SpMYH	BER	SpRad9, SpHus1, SpRad1
H. sapiens	FEN1		RAD9, HUS1, RAD1
	Pol β		RAD9, HUS1, RAD1
	DNA Ligase I		RAD9, HUS1, RAD1
	APE1		RAD9, HUS1, RAD1
	NEIL1 glycosylase		RAD9, HUS1, RAD1
	TDG glycosylase		RAD9, HUS1, RAD1
	hOGG1 glycosylase		RAD9, HUS1, RAD1
	WRN helicase		RAD9, RAD1
	MYH		HUS1
S. cerevisiae	EXO1	Multiple	Mec3 (HUS1)
H. sapiens	MSH2	MMR	RAD9, HUS1, RAD1
	MSH3		RAD9, HUS1, RAD1
	MSH6		RAD9, HUS1, RAD1
	MLH1		RAD9
S. cerevisiae	Rev7 (Pol ζ)	TLS	Mec3 (Hus1)
			Ddc1 (Rad9)
S. pombe	DinB (Pol κ)		SpHus1, SpRad1
S. cerevisiae	Rad14 (XPA?)	NER	Ddc1 (Rad9)
H. sapiens	Metnase	NHEJ	Rad9
M. musculus	Rad51	HR	Rad9
H. sapiens	Pol λ	MMEJ	RAD9, HUS1, RAD1

complex interaction with TopBP1 and the subsequent activation of checkpoint signaling (Takeishi et al., 2010; Ueda et al., 2012). Upon interacting with RAD9A, TopBP1 interacts with and activates ATR (Fig. 4). As mentioned earlier, activated ATR phosphorylates various downstream substrates, including CHK1 and p53, initiating checkpoint activation.

Besides stimulating checkpoint activity, the 9-1-1 complex also regulates DNA repair (Eichinger and Jentsch, 2011). Like PCNA, the 9-1-1 complex interacts physically with several repair proteins using outer surface hydrophobic pockets. Several of these proteins utilize their PIP box motif (Q-x-x-[ILM]-x-x-[FY]-[FY]) to facilitate their interaction with the 9-1-1 complex (Xu et al., 2009). Independent studies have shown 9-1-1 complex interaction with several repair proteins regulating NER, BER, HR, and the TLS pathway; however, a global approach for identifying all interactors of the complex has not been conducted (Fig.4). In addition, the physiological relevance of interactions involving the 9-1-1 complex remains unclear. In Chapter 4, I will discuss a proteomic approach utilized by our lab in collaboration with the Smolka Lab to identify novel interactors of the 9-1-1 complex and provide insight into the functional significance of these interactions.

1.5.4. Physiological relevance of the 9-1-1 complex

DDR proteins, including the 9-1-1 complex, play an essential role in maintaining genomic integrity, and the loss of any 9-1-1 complex subunit can be detrimental to cell viability. The 9-1-1 complex is highly conserved in eukaryotes, implying its essential

functionality. In yeast, loss of the 9-1-1 complex does not affect cell viability under non-stressed conditions; however, the cells are extremely sensitive to genotoxic stress and later were found to increased genomic instability (al-Khodairy et al., 1994; Kostrub et al., 1997). Similarly, in Drosophila, *Hus1* and *Rad9* loss exhibits oocyte nuclear defects, and impaired repair of DSBs during meiotic recombination (Kadir et al., 2012; Peretz et al., 2009). Fertility defects were also observed upon Rad9 deletion in *Echinococcus* granulosus (Cabrera et al., 2008). Work in C. elegans showed requirement of the 9-1-1 complex in telomere replication and genome maintenance (Boerckel et al., 2007; Randal Hofmann et al., 2002).

In mice, the loss of RAD9A or HUS1 causes mid-gestational embryonic lethality (Hopkins et al., 2004; Weiss et al., 2000a). *Hus1*$^{-/-}$ embryos exhibit developmental defects, reduced size, morphological abnormalities, and failed axial rotational at 9.5 days post-coitum (dpc) (Weiss et al., 2003). Furthermore, *Hus1*$^{-/-}$ embryos also displayed increased apoptosis and chromosomal abnormalities. To promote survival and avoid cell cycle arrest in *Hus1*$^{-/-}$ cells, a candidate gene that enforces cell cycle arrest, *p21*, was inactivated. *Hus1*$^{-/-}$ *p21*$^{-/-}$ cells exhibited hypersensitivity towards replication stress–inducing agents, e.g., UV, HU, and bleomycin (Levitt et al., 2005; Weiss et al., 2000a; Weiss et al., 2003).

As *Hus1* knockout is lethal, a hypomorphic *Hus1* allele was established to elucidate the functional importance of the 9-1-1 complex *in vivo*. Here, a neomycin resistance cassette (neo) was introduced between exon 1 and exon 2, enabling reduced expression of *Hus1*. Additionally, exon 1 was deleted in another *Hus1* allele (Δ1), abolishing *Hus1* expression. These alleles were used to generate a hypomorphic allelic

series of *Hus1* expression in mice (*Hus1*$^{+/+}$, *Hus1*$^{+/neo}$, *Hus1*$^{+/\Delta 1}$, *Hus1*$^{neo/neo}$, *Hus1*$^{neo/\Delta 1}$), where *Hus1* expression by the *Hus1*$^{neo/\Delta 1}$ allele was reduced to 20% as compared to that of *Hus1*$^{+/+}$ (Levitt et al., 2005). *Hus1*$^{neo/\Delta 1}$ mice were born at the expected Mendelian ratio and were grossly normal; however, they exhibited increased genomic instability, premature senescence, and hypersensitivity to replication stress–inducing agents (Levitt et al., 2007). Recently, in collaboration with Andrew White's laboratory, we identified that, in response to UV radiation, *Hus1*$^{neo/\Delta 1}$ mice grossly displayed increased inflammation and insufficient wound healing compared to wild-type mice (unpublished data). Furthermore, the mice exhibited hyperplasia and increased melanocyte epithelial migration, suggesting a role for *Hus1* in regulating UV sensitivity in mice.

Analogous to the *Hus1* hypomorph allelic series, a Cre-Lox system was also utilized to generate *Hus1* conditional knockout (CKO) cells and mice. Upon the addition of Cre adenovirus, Cre recombinase will excise the loxP sites flanking exons 2 and 3 of *Hus1*, generating *Hus1*-null cells (Zhu and Weiss, 2007). Conditional inactivation of *Hus1* in primary mouse embryonic fibroblasts (MEFs) resulted in increased common fragile site expression, cell proliferation defects, and increased apoptosis (Zhu and Weiss, 2007). Using the same system, dual *Hus1* and *p53* inactivation in mouse mammary glands resulted in the accumulation of DNA damage, followed by increased apoptosis and morphological defects in mammary gland structure and function (Yazinski et al., 2009). Finally, *Hus1* CKO in the testis resulted in meiotic defects, germ cell depletion, and severely compromised fertility (Lyndaker et al., 2013a). Similar meiotic phenotypes were observed in response to *Rad9A* loss in

meiotic germ cells (Hopkins et al., 2004).

Dissection of the molecular function of the 9-1-1 complex makes it evident that the loss of any 9-1-1 complex subunit will have a severe effect on checkpoint signaling and repair. Chromosomal aberration and hypersensitivity to replication-induced genotoxins are direct outcomes of the loss of 9-1-1 complex functions. The loss of several other DDR genes result in similar phenotypes (Wang et al., 2006b). Reports have shown *Hus1* knockdown compromised effective HR repair efficiency. Lyndaker et al. showed that, besides the gross meiotic defects, RAD9A localized with RAD51, and HUS1 loss resulted in persistent RAD51 foci formation and increased γH2Ax flares, implying a regulatory role of the 9-1-1 complex in HR and DSB repair during meiosis (Lyndaker et al., 2013a).

In the context of DDR in normal cells, the 9-1-1 complex orchestrates two major roles mentioned above: regulating DNA repair and activating ATR-mediated checkpoint signaling. Similarly, reports suggest that the 9-1-1 complex plays a role in combating replication stress in cancer cells (Broustas and Lieberman, 2014b). During the early stages of tumor initiation, the 9-1-1 complex plays a protective role in maintaining genome integrity by aiding accurate DNA repair and DNA damage checkpoint signaling. However, post-cell transformation, increased cell proliferation causes increased replication stress, leading to 9-1-1 complex upregulation to initiate DNA repair and resolve replication stress to aid proliferation. Unpublished data from our lab suggest that, in cancer mouse models, *Hus1* impairment causes decreased cell transformation and reduced tumor burden. Details regarding the role of the 9-1-1 complex in regulating tumorigenesis will be discussed in the following chapters.

In conclusion, the evidence suggests that *Hus1* acts in both tumor progression and suppression; however, the molecular details remain unclear. Similarly, evidence suggests *Rad9* loss also reduced tumor burden in mice and reduced prostate cancer cell proliferation and survival in vitro (Broustas et al., 2012). On the contrary, Rad1 deletion in mice enhanced susceptibility for skin tumor development (Han et al., 2010). Further studies elucidating the role of the 9-1-1 complex in tumorigenesis and genome maintenance will enable better understanding of the pathway and identify novel interactions that could be exploited for therapeutic benefits.

1.6. Crosstalk between replication fork stability and DNA repair for genome maintenance

Faithful transmission of genetic material is prominently dependent on accurate duplication of the genome by the DNA replication machinery. However, DNA lesions arising from endogenous or exogenous sources pose a challenge to replication fork (RF) progression (Lopes et al., 2001). The RF is a multi-protein complex comprising of DNA helicases, DNA polymerases, and other accessory proteins that aid DNA synthesis. Replication stress perturbs DNA replication, often resulting in stalling or slowing of the RF (Johnson and O'Donnell, 2005). In response to small DNA lesions, polymerase and helicase uncoupling is initiated to promote extended helicase activity (Atkinson and McGlynn, 2009). Subsequently, either the processive polymerase is replaced with a TLS polymerase to bypass the lesion, or repriming downstream of the lesion is initiated (Branzei and Foiani, 2010). In either case, the RF can rescue replicating the DNA. However, in chemical-induced DNA damage (ICL) or bulky

adduct formation, RFs are arrested at the damage site and require accessory proteins for stabilization (Lopes et al., 2001). Resolving stalled RFs requires a complex signaling pathway not only to coordinate lesion repair, but also to promote fork processing to avoid fork collapse and DSB formation from destabilization of the stalled RFs.

ssDNA accumulation due to RF stalling intrinsically triggers activation of ATR-mediated checkpoint signaling in coordination with the 9-1-1 complex and TopBP1 (Delacroix et al., 2007). Upon activation, ATR phosphorylates a plethora of substrates including CHK1, which mediates cell cycle arrest (Zhao and Piwnica-Worms, 2001). Apart for halting new origin firing, ATR promotes RF stability by regulating several key downstream proteins in fork reversal and restart (Blackford and Jackson, 2017). In response to stalled RFs, ATR phosphorylates the BLM and WRN (Werner syndrome RecQ-like helicase) helicases; these phosphorylation events are required for accurate fork restart (Friedel et al., 2009). Checkpoint kinases also regulate the activity of several nucleases that participate in fork restart (Trenz et al., 2006). Apart from the checkpoint machinery, several other proteins, including HR proteins, nucleases, translocases, and many more, play a significant role in overseeing the resolution of stalled RFs.

In mammalian cells, HR is considered a critical repair pathway for error-free DSB repair. Remarkably, growing evidence highlights key roles for several HR pathway members, such as RAD51 and BRCA1/2, in protecting stalled RFs (Lemacon et al., 2017; Mijic et al., 2017; Pasero and Vindigni, 2017; Ray Chaudhuri et al., 2016; Zellweger et al., 2015). RAD51 promotes strand invasion and HJ resolution during

HR-mediated DSB repair (Krejci et al., 2012). At stalled RFs, BRCA2 and accessory proteins promote the stabilization and formation of the RAD51 nucleoprotein filament on the ssDNA, protecting the nascent strands from nuclease-dependent fork degradation (Schlacher et al., 2011; Schlacher et al., 2012).

Another important aspect of fork protection and restart involves accurate nucleolytic resection at the DNA damage region. Similar to HR proteins, nucleases such as MRE11, EXO1, DNA2 (DNA replication helicase/nuclease 2), and CtIP are largely studied in the context of DSB repair; however, a novel role for these nucleases in stalled RF remodeling has recently been identified (Pasero and Vindigni, 2017). For example, MRE11 in coordination with CtIP can initiate DNA resection and generate ssDNA gaps at stalled fork regions, priming it for RAD51 nucleofilament formation, facilitating HR-mediated repair (Lemacon et al., 2017). In the absence of fork protection proteins, such as HR/FA proteins, uncontrolled nuclease activity can result in the degradation of stalled RFs and fork collapse (Feng and Jasin, 2017; Lemacon et al., 2017; Rondinelli et al., 2017; Taglialatela et al., 2017). Hence, maintaining tight control over the nuclease activity is essential for stabilizing stalled RFs.

With the use of single molecule technique to measure DNA replication, i.e., DNA fiber analysis, the Jasin Lab was the first to propose a novel role for HR proteins, including BRCA2 and RAD51, in maintaining RF stability against MRE11-dependent fork degradation (Schlacher et al., 2011; Schlacher et al., 2012). Their data suggested that, *BRCA2* deficiency led to destabilization and degradation of the stalled forks by MRE11, leading to genomic instability. Subsequently, crosstalk between the HR and FA proteins was implicated in modulating stalled RFs, where FA/BRCA

proteins stabilized RAD51 loading at stalled RFs to protect nascent strands from MRE11-dependent fork degradation. The expansion of these studies to *Brca1/2*-deficient cells uncovered a novel role for the histone methyltransferases MLL3/4 as well as PTIP in regulating MRE11 recruitment at stalled RFs. As loss MLL3/4 and PTIP led to the restoration of RF stability and chemoresistance without restoring HR in *Brca1/2* deficienct cells. (Ray Chaudhuri et al., 2016). These data reveal a novel mechanism in which protecting stalled RFs can promote synthetic viability and drug resistance in *Brca1/2*-deficient cells irrespective of their HR capability. In parallel, D'Andrea's group revealed another pathway led by EZH2 (enhancer of zeste 2 polycomb repressive complex 2 subunit)–MUS81 in stabilizing stalled RFs and conferring PARP inhibitor (PARPi) resistance in *BRCA2*-deficient cancers (Rondinelli et al., 2017). Interestingly, EZH2, a methyltransferase, methylates H3K27 at stalled forks, promoting MUS81 endonuclease recruitment and subsequent MUS81-mediated fork degradation. The loss of either EZH2 or MUS81 can promote fork stabilization, causing PARPi resistance in *Brca*2-deficient tumors. Interestingly, the MUS81–EZH2 pathway does not regulate fork protection in *Brca1*-deficient tumors, suggesting the possibility of separate facilitating mechanisms of BRCA1 and BRCA2 functions in fork protection (Rondinelli et al., 2017). These studies also raise an important point regarding how BRCA1/2 and RAD51 orchestrate the separable functions of HR and fork protection. Recently, studies describing the separation of function mutants in both RAD51 and BRCA2 have been published, shedding new light on the molecular mechanisms of genome maintenance (Feng and Jasin, 2017; Wang et al., 2015).

To resolve stalled RFs, cells remodel and reverse the stalled RF, forming a

"chicken foot" structure, known as a reversed fork (RVF) (Sogo et al., 2002). RVFs are typically defined as the remodeling of a typical three-way junction stalled RF into a four-way junction by annealing the two newly synthesized DNA strands to generate a regressed arm at the stalled point (Neelsen and Lopes, 2015). RVFs were first identified by the Foiani group in 2001; later, RVFs were visualized using EM by several labs, including the Lopes and Vindigni groups (Lopes et al., 2001; Sogo et al., 2002; Vindigni and Lopes, 2017). Restructuring a stalled RF into RVF not only stabilizes the fork, but also promotes accurate fork restart. Optimally, RF reversal promotes the transient stalling of replication to restrict extensive ssDNA accumulation, extends DNA repair time, and promotes replication completion by a second incoming fork during ICL repair (Neelsen and Lopes, 2015). However, recent studies have suggested that abnormal RF reversal can lead to adverse pathological consequences. For example, fork remodeling can promote DNA strand misalignment, contributing to genomic instability. Unregulated fork reversal can also stimulate extensive nuclease activity, leading to fork degradation and the formation of aberrant DNA structures (Lemacon et al., 2017; Pasero and Vindigni, 2017; Schlacher et al., 2011). RVFs are also frequently observed in response to oncogene-induced replication stress, underscoring the importance of RVFs in cancer (Neelsen and Lopes, 2015).

RAD51 initiates the reversal of stalled replication forks. RAD51 initiates fork reversal independently of its association with BRCA2 (Zellweger et al., 2015). Interestingly, other HR mediators, such as RAD54, RAD51 paralogs, MMS22L–TONSL (MMS22-like, DNA repair protein–tonsoku-like, DNA repair protein), support BRCA2-independent RAD51 loading during fork reversal (Krejci et al., 2012;

Piwko et al., 2016; Somyajit et al., 2015). Unlike BRCA2 deficiency, loss of RAD51 reduced fork reversal, inhibited MRE11-dependent fork degradation, and restored fork stability in *Brca2*-deficient cells (Mijic et al., 2017). Together, these data indicate the importance of the BRCA2-independent function of RAD51 in fork reversal and fork protection. However, the consequent nucleoprotein filament formation and stabilization of RAD51 requires BRCA2 activity and is vital for protecting the RVF against nuclease-dependent fork degradation (Feng and Jasin, 2017). These separable roles for RAD51 were first observed in a patient-derived $RAD51^{T131P}$ mutant cell line. The mutant RAD51 T131P could interact with DNA; however, it failed to form stable nucleofilament even in presence of BRCA2; consequently, the $RAD51^{T131P}$ mutant cells exhibited increased ssDNA accumulation, RPA exhaustion, and increased DNA2 and WRN activity, resulting in faulty ICL repair (Wang et al., 2015). Furthermore, the Costanzo lab showed that $RAD51^{T131P}$ mutant cells were competent for fork reversal, but lacked RVF protection against MRE11-dependent degradation (Kolinjivadi et al., 2017b). On the contrary, RAD51 overexpression promotes increased fork reversal, leading to fork degradation and replication-associated DSBs (Couch et al., 2013; Dungrawala et al., 2017). Recent proteomic analysis has revealed that RADX prevents aberrant fork remodeling by sequestering RAD51 away from the stalled RFs (Dungrawala et al., 2017). Elevated RAD51 levels also disrupt DNA replication, elongation, and unscheduled origin firing, resulting in increased genomic instability (Parplys et al., 2015). In conclusion, along with its function in HR-mediated repair, RAD51 plays multiple roles in the context of RF stability: fork protection and fork reversal, and the consequences of RAD51 perturbation vary with which role is

affected. It is also important to note that independent of HR/FA fork protection proteins, ABRO1 (abraxas 2, BRISC complex subunit) and BOD1L (biorientation of chromosomes in cell division 1–like 1) protect stalled RF against DNA2- and EXO1-dependent fork degradation (Higgs et al., 2015; Xu et al., 2017). Recent work from our lab also identified that loss of the checkpoint protein complex, 9-1-1 causes MRE11-dependent fork degradation upon replication stress (unpublished data).

Along with RAD51, several translocases, such as SMARCAL1 (SWI/SNF-related, matrix-associated, actin-dependent regulator of chromatin, subfamily a-like 1), HLTF (helicase-like transcription factor), and ZRANB3 (zinc finger RANBP2-type containing 3), are implicated in initiating fork reversal. Initially, *SMARCAL1* was identified as a gene of interest in patients with Schimke immuno-osseous dysplasia (Elizondo et al., 2009). Subsequent work from the labs of Elledge and Cortez demonstrated the importance of the RPA-interacting protein SMARCAL1 in regulating fork reversal to maintain genomic stability (Bansbach et al., 2009; Ciccia et al., 2009). However, SMARCAL1 activity must be tightly regulated by RPA and ATR, as SMARCAL1 activity loss or overexpression can be deleterious for the genome (Poole and Cortez, 2017). The concentration and DNA-binding orientation of RPA dictates its interaction with SMARCAL1, thereby regulating SMARCAL1-dependent fork reversal. If SMARCAL1 bypasses RPA regulation, post-DNA localization, SMARCAL1 can undergo ATR-mediated phosphorylation, which suppresses SMARCAL1-dependent fork reversal activity (Poole and Cortez, 2017). Similarly, ZRANB3 was also uncovered by the Elledge group as a PCNA interacting protein that promotes fork reversal upon its interaction with polyubiquitinated PCNA

(K164) (Ciccia et al., 2012). Polyubiquitinated PCNA can also be regulated by the yeast RAD5 homolog HLTF, and the HIRAN domain of HLTF can stimulate fork reversal activity (Poole and Cortez, 2017). Other DNA translocases, such as RAD54, and FANCM have also been implicated in playing a role in fork reversal (Quinet et al., 2017). More recently, studies have revealed that the loss of SMARCAL1 and other translocases such as ZRANB3 and HLTF can rescue fork degradation in *BRCA1/2*-deficient cells in response to replication stress (Ciccia et al., 2012; Kolinjivadi et al., 2017b; Lemacon et al., 2017; Mijic et al., 2017; Taglialatela et al., 2017). Unlike PTIP or MLL3/4 depletion, SMARCAL1 depletion did not confer chemoresistance in *BRCA1*-deficient cells, even though genomic stability was restored (Taglialatela et al., 2017). Although the extensive mechanistic details of these fork-remodeling proteins have not been uncovered, recent studies underscore the importance of these fork-remodeling enzymes in genome maintenance.

Interestingly, the mechanisms of chemoresistance in *BRCA1*- and *BRCA2*-deficient cells vary dramatically. One possible explanation for this disparity might be cell line specificity, which enforces one or another mechanism, or the fact that both BRCA proteins participate in mechanisms that effect chemoresistance and genomic stability in a distinct manner. Nevertheless, several labs have recently extensively characterized the effect of *Brca2* deficiency on RF stability. The role of BRCA2 in regulating fork dynamics appears straightforward, as it promotes the formation of RAD51 nucleofilament that prevents MRE11-mediated fork degradation (Schlacher et al., 2011). Later, it was clarified that the MRE11-mediated fork degradation is facilitated by several proteins, including PTIP, MLL3/4, and EZH2 (Ray Chaudhuri et

al., 2016; Rondinelli et al., 2017). Recently, it was shown that RAD52 promotes stalled fork degradation in *Brca2*-deficient cells by priming MRE11-dependent stalled fork resection (Mijic et al., 2017). Initial work from the Jasin lab demonstrated that *Brca2* deficiency led to increased nascent strand degradation but maintained relatively normal fork restart activity (Schlacher et al., 2011). Until recently, the mechanisms that facilitated the fork restart activity in *Brca2*-deficient cells remained unclear. Lemacon et al. showed that in *Brca2*-deficient cells, MUS81 cleaved the partially resected RVF with a ssDNA flap to ensure POLD3-dependent fork restart and cell survival, suggesting a possible synthetic lethal effect in cells upon BRCA2 and MUS81/POLD3 depletion. Interestingly, D'Andrea demonstrated that MUS81 disruption in BRCA2-deficient cells restored fork stability and conferred resistance to PARPi, which Lemacon et al. did not observe (Lemacon et al., 2017; Rondinelli et al., 2017). This discrepancy in the role of MUS81 in regulating fork stability could be related to its ability to process diverse types of substrates.

In normal fork restart, there are two distinct mechanisms through which a cell can promote fork regression and restart RVFs. The RECQ family helicases RECQ1, BLM, and WRN are primarily responsible for replication fork restoration (Neelsen and Lopes, 2015). RECQ1 is an ATP-dependent DNA helicase that interacts with RVFs, unwinding the leading strand at the stalled RF and promoting branch migration (Berti et al., 2013). However, PARP1-mediated ADP ribosylation keeps RECQ1 activity at the stalled forks in check. PARP1 activity is stimulated at regions of strand discontinuity and at replication blocks (Margalef et al., 2018). RECQ1 activity remains inhibited by the activated PARP1 until replication stress is relived. This

mechanism prevents premature RVF restoration (Neelsen and Lopes, 2015). Independent of RECQ1, WRN, and BLM, other members of the RECQ family helicases can also promote fork restart activity in a HR-dependent manner (Pasero and Vindigni, 2017). Interestingly, unlike other RECQ helicases, WRN has 3′ to 5′ exonuclease activity, making it the prime candidate for restoring forks containing gaps in the leading strand (Atkinson and McGlynn, 2009). Another helicase/nuclease, DNA2, facilitates the production of 3′ overhang at RVF regions aided by WRN/BLM ATPase activity. Aided by RAD51, this overhang can initiate strand invasion and form Holliday Junction (HJ), which HR machinery subsequently resolves (Popuri et al., 2008). However, both WRN and BLM have pro- and anti-recombinogenic activity, where instead of promoting HR and crossover action, they promote fork restart by dissolving HJs (Patel et al., 2017). It is also important to mention that RECQ1 actively inhibits DNA2 activity during RECQ1-mediated restart via brank migration (Nimonkar et al., 2011). The Pasero group identified SAMHD1 (SAM and HD domain–containing dNTP triphosphohydrolase 1), a dNTP hydrolase, as a potential cofactor of MRE11 in promoting gapped fork resection. SAMHD1 loss results in defective processing of the stalled forks by RECQ1 (RecQ-like helicase), which promotes ssDNA release in the cytoplasm, inducing interferon signaling (Coquel et al., 2018). Hence, the regulation of error-free restoration of the stalled fork by RECQ-family helicases is tightly regulated to ensure genomic integrity.

A common conclusion that has emerged from all of the above studies is that RF stability and remodeling involve tightly regulated balancing acts among several proteins from different pathways. Moreover, fork remodeling has come to the fore as a

major contributor to chemoresistance and cancer. Hence, the identification and characterization of new factors involved in stalled RF and its restoration will provide novel insight into the mechanistic regulation and physiological relevance.

1.7. Role of DDR proteins in tumorigenesis and anti-cancer therapeutics

With constant DNA insults, complete and faithful genome repair and duplication is of paramount importance for organismal survival (Zhou and Elledge, 2000). The DDR is a tightly controlled signaling network that ensures DNA fidelity in response to DNA damage. However, a compromised DDR can trigger genomic instability in cells, resulting in the accumulation of mutations and heralding the onset of several disorders, including cancer (Ciccia and Elledge, 2010; Ghosal and Chen, 2013; Hakem, 2008; Harper and Elledge, 2007; Kerzendorfer and O'Driscoll, 2009; Stocker and Hafen, 2000). With the advancements in cancer genomics, it has become evident that various cancer entities display impaired DDR and reduced DNA repair activity (Broustas and Lieberman, 2014b; Knijnenburg et al., 2018).

Genomic instability is considered a hallmark of cancer. For example, in humans, early neoplastic lesions often display signs of DNA damage and signs of senescence (Dietlein et al., 2014). These phenotypes in early precancerous cells are the result of oncogene-induced replication stress, where the senescence and active DDR act as obstacles against malignant transformation (Halazonetis et al., 2008). DDR activation results in activation of the checkpoint kinases ATR and ATM, forming a barrier against precancerous cell transformation (Bracey et al., 1997; Braig et al.,

2005; Gorgoulis et al., 2005; O'Connor, 2015). Notably, signs of increased DNA damage checkpoint activation, including characteristic phosphorylation of ATM, CHK2, and H2AX, are observed in precancerous lesions (Damia and Broggini, 2004; Gorgoulis et al., 2005; Yoo et al., 2004). However, with inactivating mutation in the DDR proteins, precancerous cells can bypass the barrier and complete malignant transformation. Due to increased proliferative demands, cancer cells rely heavily on the DDR to combat replication stress to sustain their error-prone cellular proliferation (Bartkova et al., 2005; Halazonetis et al., 2008; Luo et al., 2009). Increased expression of several components of the ATR pathway genes, such as *RAD9A*, *CHK1*, and *HUS1*, has been observed in different cancer types (Bartkova et al., 2005; Cheng et al., 2005; de la Torre et al., 2008; Doerr et al., 2017; Tho et al., 2012). Our lab has shown that *Hus1* impairment causes decreased cell transformation and reduced tumor burden in cancer mouse models (unpublished data). The Cancer Genome Atlas (TCGA) and Oncomine analyses revealed elevated expression of 9-1-1 complex and other ATR pathway genes in different cancer types. Interestingly, some tumor cells that rely on the alternative lengthening of telomeres (ALT) pathway exhibit hypersensitivity towards ATR inhibition, as the role of ATR lies in regulating telomere maintenance (Karnitz and Zou, 2015). Together, these studies suggest that DDR pathway components are prime candidates for targeted cancer therapy (Fig. 1.5).

Traditionally, to target the DDR defects of cancer cell, the US Food and Drug Administration (FDA) approved small molecules that induce replication stress and activate the replication stress response, such as DNA-crosslinking agents, topoisomerase toxins, and alkylating agents. However, these drug treatment courses

also adversely affect healthy tissues, resulting in significant and potentially life-threatening adverse effects (Forment and O'Connor, 2018). To address this issue, studies have been designed to perform targeted therapy. With the idea of targeted therapy, the concept of synthetic lethality is applied, where cell death is induced upon loss-of-function events in two genes, but mutation in individual genes allows for cell viability. PARPi were one of the most celebrated therapies used for targeting the DDR pathway (O'Connor, 2015). During PARPi development, it was well-known that *BRCA1* and/or *BRCA2* mutations result in faulty HR-mediated DSBs and are the leading cause of breast and ovarian cancers (Ford et al., 1998; Heikkinen et al., 2005; Miki et al., 1994). Given the mechanism of PARP, where it facilitates SSB repair, PARPi were designed to trap the PARP–DNA complex leading to DSB formation. In normal cells, competent HR machinery, including functional BRCA1 and BRCA2, would mediate error-free DSB repair. However, in BRCA1/2-deficient tumors, the loss of HR function leads to activation of the error-prone repair NHEJ pathway, leading to unsustainable genomic stability and cell death in response to PARP inhibition (Fong et al., 2009). With the massive success of PARPi, over eight PARPi are being explored in more than 25 phase III clinical trials (O'Connor, 2015). Along with PARP, inhibitors of several components of the checkpoint pathways, such as ATR, CHK1, and WEE1 (WEE1 G2 checkpoint kinase), are under investigation in clinical trials (Forment and O'Connor, 2018).

The idea of “mutator phenotype” was coined to demonstrate that inactivating mutations in genome maintenance pathways contribute to greater accumulation of mutations within the genome, paving the way for genomic instability and cancer

promoting genomic aberrations (Bartkova et al., 2005; Halazonetis et al., 2008; Jackson and Bartek, 2009b; Loeb, 1998; Lord and Ashworth, 2012). Given the central role for the DDR and the results from current preclinical trials with PARP inhibitor being encouraging; continued work in developing new DDR targets would provide breakthrough in identifying novel cancer therapies.

1.8. Summary

A eukaryotic cell harnesses an intricate network of molecular signaling pathways to maintain its genomic integrity. The DDR is an integral part of genome maintenance as it regulates checkpoint signaling, DNA repair, DDT, and apoptosis pathways. Recent advances in the field have identified hundreds of DDR proteins, however the molecular mechanism regulating their activity still remain unclear. Resolution of the intricate network making up the DDR pathway will be essential for understanding the functional consequences that may determine cancer progression and guide in precision therapy.

The 9-1-1 complex is an important DDR protein complex that maintains genomic integrity, through its role of activating ATR- mediated checkpoint signaling and DNA repair. The role of 9-1-1 in activating ATR-mediated checkpoint signaling has been well established in the field, however its role in DNA repair remains unexplored. Hence, I focused on exploring the cross-talk between the checkpoint signaling and DNA repair proteins, as it holds promise in the field of molecular therapeutics. To conduct this study, I will focus on HUS1, a 9-1-1 complex subunit, which is essential for 9-1-1 functions, as a model.

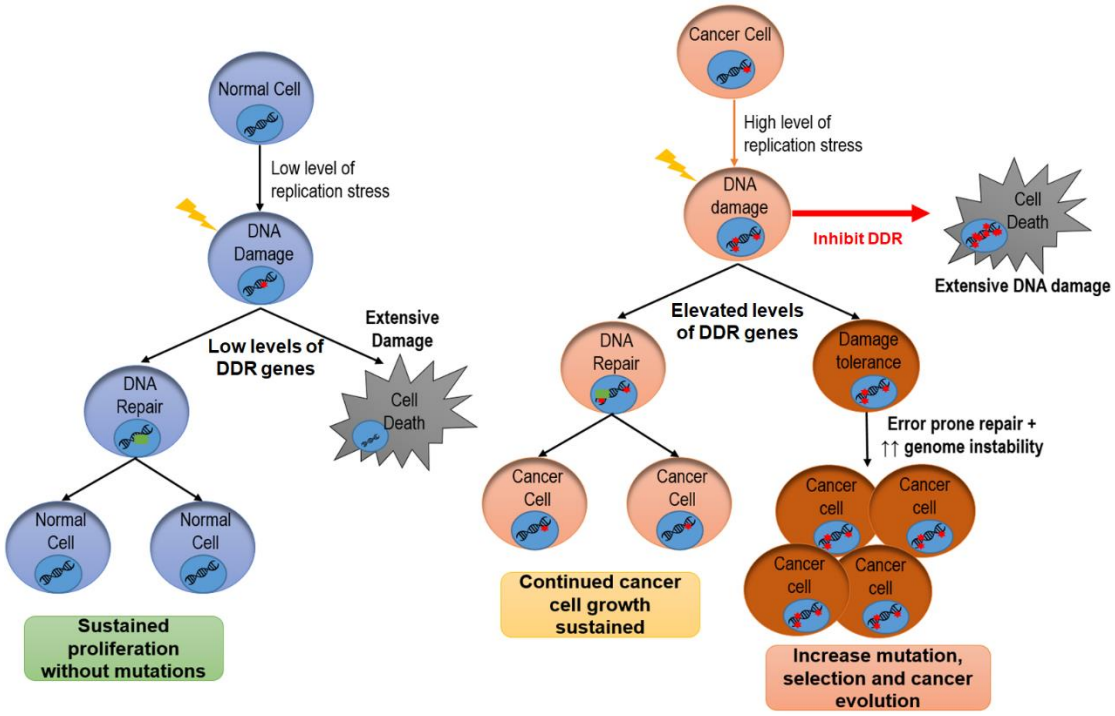

Fig. 1.5 – Therapeutic targeting of DDR genes for treatment against oncogenic-induced replication stress in cancer cells. At any given time, normal cells exhibit low levels of replication stress that is combating with the help of the DDR genes for sustained proliferation with genome alteration. Conversely, cancer cells experience extensive amount of replication stress resulting in increased DDR protein expression. With effective DNA repair in cancer cells, high cellular proliferation is sustained without additional mutation, however if the elevated levels of DDR promote damage tolerance, cancer cell can accumulate additional mutations and significantly impact cancer evolution. Hence, targeted therapy against DDR proteins would be an effective way for combat cancer cell growth.

Loss of *Hus1* leads to various cellular defects such as embryonic lethality, genomic instability, reduced repair efficiency, and tumor resistance. Using the crystal structure of HUS1, we generated several point mutations that allowed us to characterize the residues that facilitated the clamp assembly, DNA interaction and downstream effector functions. During this study we were also able to generate separation of function 9-1-1 mutants (Chapter 2).

Next, using mass spectrometry and the separation of function HUS1 mutants, I performed a comprehensive screen to isolate novel interactors of the 9-1-1 complex, as well as to identify HUS1 specific interactions. Our preliminary study has also identified components of the neddylation pathway, implicated in repair complex resolution, in concert with HUS1. With these promising results, this study will uncover the role of HUS1 in regulating the neddylation pathway (Chapter 3). We also uncovered a novel role for the 9-1-1 complex in regulating FA-mediated ICL repair and replication fork stability (Chapter 4).

Given the role of DDR proteins in aiding targeted cancer therapy, exploring the function of the 9-1-1 complex in the context of cancer would provide valuable insights for novel therapeutics. Using mutant *Kras* induction in *Hus1* hypomorph and WT mice, we demonstrated that HUS1 supports tumorigenesis. Finally, by studying the alternative polyadenylation (APA) mechanism of *Hus1*, the study revealed a regulatory mechanism employed by cells to regulate the *Hus1* expression levels. In conclusion, these studies outlined the significance of HUS1 in DNA repair by uncovering novel protein interactions with HUS1 and helped identify mechanisms that facilitate tumorigenesis.

CHAPTER 2

GENOME PROTECTION BY THE 9-1-1 COMPLEX SUBUNIT HUS1 REQUIRES CLAMP FORMATION, DNA CONTACTS, AND ATR SIGNALING-INDEPENDENT EFFECTOR FUNCTIONS*

2.1 ABSTRACT

The RAD9A-HUS1-RAD1 (9-1-1) complex is a heterotrimeric clamp that promotes checkpoint signaling and repair at DNA damage sites. In this study, we elucidated HUS1 functional residues that drive clamp assembly, DNA interactions, and downstream effector functions. First, we mapped a HUS1-RAD9A interface residue that was critical for 9-1-1 assembly and DNA loading. Next, we identified multiple positively charged residues in the inner ring of HUS1 that were crucial for genotoxin-induced 9-1-1 chromatin localization and ATR signaling. Finally, we found two hydrophobic pockets on the HUS1 outer surface that were important for cell survival after DNA damage. Interestingly, these pockets were not required for 9-1-1 chromatin localization or ATR-mediated CHK1 activation, but were necessary for interactions between HUS1 and its binding partner MYH, suggesting that they serve as interaction domains for the recruitment and coordination of downstream effectors at damage sites.

*The data presented in this chapter has been published: Pei Xin Lim, Darshil R. Patel, Kelsey Poisson, Manpreet Basuita, Charlton Tsai, Amy M. Lyndaker, Bor-Jang Hwang, A-Lien Lu, and Robert S. Weiss. Genome protection by the 9-1-1 complex subunit HUS1 required clamp formation, DNA contacts, and ATR signaling-independent effector functions – *JBC*. 2015 June 12; 290(24): 14826-14840. Figures 2.6B-D and 2.7 were generated by Darshil Patel.

Together, these results indicate that, once loaded onto damaged DNA, the 9-1-1 complex executes multiple, separable functions that promote genome maintenance.

2.2 INTRODUCTION

When left unchecked, DNA insults from exogenous and endogenous sources can lead to premature aging, developmental defects, and tumorigenesis (Jackson and Bartek, 2009a). To prevent these deleterious outcomes, cells have evolved DNA damage response (DDR) pathways that are responsible for triggering an appropriate protective reaction to genome damage. Central to DDR pathways are checkpoint proteins that regulate cell cycle transitions, DNA repair, replication fork stability, and apoptosis (Cimprich and Cortez, 2008).

The RAD9A-HUS1-RAD1 (9-1-1) clamp is a toroidal heterotrimeric DNA clamp that regulates checkpoint signaling after DNA damage (Eichinger and Jentsch, 2011). It is essential for cell survival after genotoxin exposure and during various physiological processes, such as embryogenesis, adult tissue homeostasis, and spermatogenesis (Han et al., 2010; Hopkins et al., 2004; Lyndaker et al., 2013b; Vasileva et al., 2013; Weiss et al., 2000b; Yazinski et al., 2009). The 9-1-1 clamp is structurally related to proliferating cell nuclear antigen (PCNA), a homotrimeric processivity factor for DNA replication and repair (Moldovan et al., 2007). Like PCNA, each 9-1-1 subunit folds into two globular domains linked by an interdomain connecting (IDC) loop (Dore et al., 2009; Sohn and Cho, 2009; Xu et al., 2009). The subunits associate in a head-to-tail manner to form a stable heterotrimeric complex. A clamp loader composed of RFC1-5 loads PCNA at 3’ recessed DNA ends, whereas 9-

1-1 is loaded by RAD17/RFC2-5 at 5' recessed ends (Bermudez et al., 2003; Ellison and Stillman, 2003; Majka et al., 2006a). Once loaded at damage sites, 9-1-1 stimulates ATR kinase activation through interactions with TOPBP1 (Delacroix et al., 2007). Activated ATR phosphorylates several substrates, including the effector kinase CHK1, which induce cell cycle arrest, stabilize stalled forks and inhibit origin firing (Cimprich and Cortez, 2008).

In addition to its checkpoint signaling functions, 9-1-1 also acts directly in DNA repair through its role as a molecular scaffold (Eichinger and Jentsch, 2011; Helt et al., 2005; Madabushi and Lu, 2011). The 9-1-1 clamp physically interacts with and stimulates the activity of factors in many DNA repair pathways, including base excision, mismatch, and nucleotide excision repair, as well as homologous recombination, non-homologous end joining and translesion synthesis. Evaluating the physiological significance of these interactions is challenging because genetic approaches to ablate 9-1-1 function typically compromise both checkpoint signaling and all other functions executed by the clamp.

In order to resolve the relative importance of the checkpoint signaling-dependent and -independent functions of the 9-1-1 complex, we endeavored to identify residues that are essential for these functions and describe here residues in murine HUS1 (mHUS1) that mediate three critical 9-1-1 activities: clamp formation, DNA association, and interaction with downstream effectors. Consistent with the idea that 9-1-1 has critical signaling-independent roles, we identified HUS1 domains that are dispensable for ATR-mediated signaling to CHK1 but nevertheless required for the cellular response to DNA damage.

2.3 MATERIALS AND METHODS

Plasmids and mutagenesis – All mutations were introduced into *mHus1* using a QuikChange Lightning Multi Site-Directed Mutagenesis kit (Agilent technologies) and the primers listed in Table 2.1. Most mutagenesis was performed on the pBP2-mHus1 retroviral plasmid (Weiss et al., 2002) as the template with 2 exceptions. In the first case where compound mutations had to be made sequentially, pBP2-mHus1 plasmids with intermediate mutations were used as the template. In the second case, residues K2, F3, R4 and K6 of mHUS1 were mutagenized with the pGEX2T-mHus1 plasmid as the template because 5' retroviral long terminal repeats in the pBP2-mHus1 plasmid interfered with mutagenesis. Subsequently, the pGEX2T-mHus1 mutants were subcloned into pBP2 plasmid. Functionally defective mutant constructs were further subcloned into pCMV-neo-Bam_3 plasmid (Hinds et al., 1990) for mutant mHUS1 immunoblot detection, as well as into p3XFLAG-CMV^{TM}-14 (Sigma) for IF and chromatin fractionation assays. All mutations were verified by DNA sequencing.

Cell culture, retroviral infection and transfection – All cultured cells were grown on gelatinized dishes in Dulbecco's Modified Eagle's Medium (Corning) supplemented with 10% Bovine Calf Serum (Thermo Scientific Hyclone, SH30072), 1% nonessential amino acids (Corning Cellgro, 25-025-CI), 1% L-glutamate (25-005-CI) and 1% penicillin and streptomycin (30-002-CI). Expression of the various *mHus1* constructs in *Hus1*$^{-/-}$*p21*$^{-/-}$ MEFs and HEK293T cells (ATCC) was done in two ways. The first method was pBabe-based retroviral transduction for low-level ectopic *Hus1* expression as previously described (Weiss et al., 2002). The second method was

plasmid transfection of pCMV-mHus1 and pCMV-mHus1-3XFLAG high-level expression constructs done as follows: a mix of 575µl DMEM, 40µg polyethyleneimine, 4µg pCMV plasmid and 1µg pGK-puro plasmid was dripped onto 10^6 *Hus1*$^{-/-}$ *p21*$^{-/-}$ MEFs seeded the day before in a 10cm dish. Transfected cells were selected in culture medium containing 1.83µg/ml puromycin, replaced every other day for a week. Stable drug-resistant cells made from both methods were cultured according to the 3T3 passaging protocol for maintenance and experimental use. For co-IP assays, pCMV-mHUS1 constructs were co-transfected with pCMV-hRad9a-Myc and pCMV-hRad1-HA plasmids.

Survival assays – For short term viability assays, cells were seeded in 6-well plates and either left untreated or treated with 50ng/ml 4NQO or 0.5µM aphidicolin for 24 hours. Mitomycin C (MMC) treatment was for 1 hour. After 3 days, the cells were collected by trypsinization and counted using a Moxi^{TM} Z mini automated cell counter (ORFLO technologies). Percent survival was calculated by dividing the number of cells after treatment by the number of untreated cells. Error bars ± SD. Statistical analysis was by Student's T-test, and p-values of <0.05 were considered significant. For clonogenic survival assays, cells were seeded in 6-well plates and treated with 4NQO or aphidicolin for 24 hours or with MMC for 1 hour. After 6 days, the cells were fixed with methanol and stained with crystal violet overnight. The plates were then washed, dried and scanned.

Table 2.1. Primers used for site-directed mutagenesis of *mHus1*.

Mutations	Primer [a]
RAD9-interacting residue	
R128E	5'-gtctccatcgagcagcagcgaaatcgtggtgcatgatatc-3'
Inner ring hydrophobic cleft	
V19A, M22A, I23A	5'-cttgtctgaatcatttcacacgagccagtaacgcggcagccaagcttgccaaaacctgcac-3'
V247A	5'-gccggacagcaagcgactcccaccaag-3'
V271A, L273A	5'-atttgctcctggaagacgcctccgctcagtatttcatcccagc-3'
R18A	5'-ctatcatgttactgactgctgtgaaatgattcagacaagccagg-3' [b]
R18Q	5'-cttgtctgaatcatttcacacaagtcagtaacatgatagccaa-3'
R18Q M22T	5'-cttgtctgaatcatttcacacaagtcagtaacacgatagccaagcttgcca-3'
Inner ring positively charged residues	
R18A	5'-ctatcatgttactgactgctgtgaaatgattcagacaagccagg-3' [b]
K25A	5'-ggtgcaggttttggcaagcgcggctatcatgttactgact-3' [b]
K25A K28A	5'-atgcggagggtgcaggttgcggcaagcgcggctatcatgttactgac-3' [b]
K93A	5'-tctggagttctgggcagttgccaaggctcgagataagttt-3' [b]
R90A, K93A	5'-tggagttctgggcagttgccaaggctgcagataagttttccgacgttaattctaa-3' [b]
K165A	5'-ccacaacactcttcatcatcgccaaggctggtaagcaaatac-3' [b]
K165A, K168A	5'-gtttctcatttttccacaacactcgccatcatcgccaaggctggtaagcaaatactgacg-3'

	[b]
K173A, R175A	5'-ttcaatcacaagctgattgctgatgtttgccattgcttccacaacactcttcatcatcttcaag-3' [b]
K236A, K237A	5'-aagaaactggaggagtgccgctatgtcaatgtgcaccttggccatgtcttct-3' [b]
Outer ring hydrophobic pocket	
P150A	5'-gtggaaggacttacaagaagcctccatcccagac-3'
P150A, I152A, P153A, C155A	5'-gactgtggaaggacttacaagaagcctccgccgcagacgctgacgtcagtatttgctt-3'
V257A, T261A	5'-caaggcagtgtgcaatattgcgaataacagagctgttcattttgatttgctc-3'
F276A, P278A	5'-aagacgtctcccttcagtatgccatcgcagccttgtcctagg-3'
S53R	5'-gctcacaccacatcctcacgcctccac-3' [b]
I152R	5'-gacttacaagaaccctccagaccagactgtgacgtcag-3'
I152Y	5'-aaggacttacaagaaccctcctacccagactgtgacgtcagtatt-3'
I152F	5'-cttacaagaaccctcctttcccagactgtgacgt-3'
Outer ring novel pocket	
F3A	5'-[ccgcgtggatcc]atgaaggctcgcgccaagatcg-3' [c]
F3R	5'-cgcgtggatccatgaagcgtcgcgccaagatcgtggacc-3'
F3R, R4A	5'-cgcgtggatccatgaaggctgccgccaagatcgtggacct-3'
G71W	5'-gaacttttttagtgaatttcaaatggaatgggtctctgaagaaaacaacgagattt-3'
I79A	5'-aggagtctctgaagaaaacaacgaggcttatttagaattaacgtcggaaaac-3'
L105A	5'-ccagagccttgaaaatcaaggcgactaacaaacactttccct-3'

K104A, L105A, T106A	5'-ccagaactccagagccttgaaaatcgcggcggctaacaaacactttccctgtcttac-3'
V138A, L139D	5'-gcatgatatccccataaaggctgatccgagaagactgtggaagg-3'
L105R	5'tccagagccttgaaaatcaagaggactaacaaacactttccctg-3'
L139R	5'-tcgtggtgcatgatatccccataaaggttagaccgagaagactgtgg-3'
R4D	5'-[cgcgtggatcc]atgaagtttgacgccaagatcgtggacc-3' [c]
F3R, R4D	5'-[cgcgtggatcc]atgaagcgtgacgccaagatcgtggacc-3' [c]
Outer ring positively charged residues	
K2A, R4A, K6A	5'-gacaagccaggtccacgatcgcggcggcaaacgccat[gaatccacgcgg]-3' [b,c]
R99A, K102A, K104A	5'-gggaaagtgtttgttagtcagcgcgattgccaaggctgcggagttctgggcagttttcaagg-3' [b]
K108A, H109A	5'-cagacacggtaagacagggaaaggctgcgttagtcagcttgattttcaagg-3' [b]
K137A, R141A, R142A, K145A	5'-ggttcttgtaagtccgcccacagtgctgccggaagaaccgctatggggatatcatgcaccacga ttc -3' [b]
BII4-6 loop	
Δ215-227	5'-gtgcaccttggccat()taatagagggttttcaagatccttaaaa-3' [b,d]
Δ215-227::hHus1 loop	5'-attttaaggatcttgaaaaccctctattagcctctgaaagtacccatgaaaacagacacccagaagacatggc ca-3'

	5'-gcctctgaaagtacccatgaagacagaaacgtagaacacatggccaaggtgcaca-3'
Δ215-227::PCNA loop	5'-cattttaaggatcttgaaaaccctctattacaaactagcaatgtcgatcaaaacagacaccca gaagacatggc caag-3' 5'-cttgaaaaccctctattacaaactagcaatgtcgataaagaagaagaggcagtagacatgg ccaaggtgcac at-3'

[a] The positions of nucleotides altered to create desired mutations are underlined.

[b] antisense primers. Primer orientation was chosen based on lower energy cost of mismatches.

[c] [pGEX-2T sequences]

[d] (39 nucleotides deleted)

ConSurf evolutionary conservation and surface electrostatic potential analyses – Amino acid sequences of PCNA, RAD9A, HUS1 and RAD1 from 44 organisms that represent a broad range of taxa were curated from UniProtKB database (http://www.uniprot.org) (Table 2.2). Multiple sequence alignments were created with ClustalX ver2.1 (Julie D. et al., 1997) and uploaded to the ConSurf server (http://consurf.tau.ac.il) (Ashkenazy et al., 2010) for calculation of evolutionary conservation scores (Bayesian method) with reference to the human counterparts of each protein. The scores were projected on available protein structures of PCNA (PDB 1VYM) and RAD9A-HUS1-RAD1 (PDB 3GGR) to identify functional surface residues. All images were created using PyMOL. The surface electrostatic potential of HUS1 was calculated and displayed using the Adaptive Poisson-Boltzmann Solver (APBS) plugin in PyMOL. In the calculations, dielectric constants of 1.0 and solvent ionic strength equivalent to 75mM KCl were used. Side chains of lysine and arginine residues were given a net positive charge, aspartate and glutamate negative, and other residues neutral. Positive and negative color contours were set at +/- 10kT/e.

Immunofluorescence (IF) – *Hus1*$^{-/-}$*p21*$^{-/-}$ MEFs stably expressing WT or mutant mHUS1-3XFLAG proteins were grown on gelatinized cover slips overnight and treated with MMC for 23 hrs. Cells were immunostained with mouse α-FLAG and rabbit α-RAD9A primary antibodies and Alexa Fluor 488 goat α-mouse and 555 goat α-rabbit secondary antibodies for IF detection according to antibody manufacturer's protocol. Overlapping FLAG and RAD9A foci in 50 randomly picked cells from each sample were quantified and analyzed by one-way ANOVA.

Table 2.2. List of UniProtKB accession numbers of the PCNA, RAD9A, HUS1 and RAD1 sequences used for evolutionary conservation analysis.

		Accession numbers			
ORGANISM	SYMBOL	PCNA	RAD9A	HUS1	RAD1
Ailuropoda melanoleuca (Giant panda)	AILME	D2HQS7	G1L1M9	G1LDT0	G1L9B8
Arabidopsis thaliana (Mouse-ear cress)	ARATH	Q9M7Q7	F4J7B7	Q709F6	Q8L7G8
Bos taurus (Bovine)	BOVIN	Q3ZBW4	Q5EAC3	E1BG06	E1BB72
Caenorhabditis elegans (Nematode worm)	CAEEL	O02115	Q9NBJ6	G5EFI9	G5EC44
Callithrix jacchus (White-tufted-ear marmoset)	CALJA	F7GZC8	U3DMA2	F7G3C8	F7I3N9
Canis familiaris (Dog)	CANFA	E2R0D6	F6XPS6	F1Q245	E2QYH8
Cavia porcellus (Guinea pig)	CAVPO	H0VE65	H0VIK1	H0WC14	H0VEA3
Ceratitis capitata (Mediterranean fruit fly)	CERCA	W8B157	W8C9F2	W8C4C2	W8B5C0
Gallus gallus (Chicken)	CHICK	Q9DEA3	R4GG06	E1C8I4	E1C4I3

Chlamydomonas reinhardtii (Chlamydomonas smithii)	CHLRE	A8JHX0	A8IS48	A8J5N4	A8IFX0
Dictyostelium discoideum (Slime mold)	DICDI	Q54K47	Q869Q1	Q54NC0	Q55E62
Drosophila melanogaster (Fruit fly)	DROME	P17917	O96533	Q9VN60	Q9VQD4
Felis catus (Cat)	FELCA	M3WAR4	M3W096	M3XC14	M3WY16
Equus caballus (Horse)	HORSE	F6R950	F6QXP4	F7BM24	F6YZW4
Homo sapiens (Human)	HUMAN	P12004	Q99638	O60921	O60671
Hydra vulgaris (Hydra)	HYDVU	T2MHJ2	T2M799	T2MIV2	T2MID6
Lepisosteus oculatus (Spotted gar)	LEPOC	W5NF42	W5MKE2	W5N6Y6	W5N1G5
Loxodonta africana (African elephant)	LOXAF	G3SY50	G3T2S3	G3TJN6	G3SZN1
Macaca mulatta (Rhesus macaque)	MACMU	F6ZD63	H9FXY2	F7F1Y2	F7A5K9
Mus musculus	MOUSE	P17918	Q9Z0F6	Q8BQY8	Q9QWZ

(Mouse)					1
Mustela putorius furo (European domestic ferret)	MUSPF	M3Y491	M3XXF9	M3Z395	M3YUM0
Myotis lucifugus (Little brown bat)	MYOLU	G1NW67	G1P3Z2	G1NTI5	G1PS54
Neovison vison (American mink)	NEOVI	U6DX35	U6D1D1	U6CPZ2	U6CY10
Nomascus leucogenys (Northern white-cheeked gibbon)	NOMLE	G1R863	G1R3F3	G1QWZ3	G1RWE2
Oreochromis niloticus (Nile tilapia)	ORENI	I3KAK2	I3JC68	I3K6T5	I3JLK1
Ornithorhynchus anatinus (Duckbill platypus)	ORNAN	F7BRC7	F6REC2	F7BS27	F6UI60
Otolemur garnettii (Small-eared galago)	OTOGA	H0XLL4	H0XWZ7	H0X7H9	H0XC10
Pan troglodytes (Chimpanzee)	PANTR	H2QJX3	K7DL38	H2QUJ9	K7BUE0
Sus scrofa (Pig)	PIG	I3L813	F1RUX7	B6UV60	F1SND5
Polysphondylium pallidum (Cellular slime mold)	POLPA	D3BSY5	D3BA05	D3BR17	D3BPJ7
Pongo abelii	PONAB	H2P1A0	H2NCN7	H2PXG5	Q5R7X9

(Sumatran orangutan)					
Oryctolagus cuniculus (Rabbit)	RABIT	G1SKZ3	G1TKX6	G1TRN1	G1T7G8
Rattus norvegicus (Rat)	RAT	P04961	D3ZXM2	D3ZNA8	D3ZC52
Sarcophilus harrisii (Tasmanian devil)	SARHA	G3WDY3	G3VT27	G3W0W1	G3WBB6
Schizosaccharomyces pombe (Fission yeast)	SCHPO	Q03392	P26306	P78955	P22193
Ovis aries (Sheep)	SHEEP	W5Q6P4	W5PNJ1	W5PS82	W5PPP9
Spermophilus tridecemlineatus (Thirteen-lined ground squirrel)	SPETR	I3NDE1	I3NF38	I3MYM9	I3MDU2
Strongylocentrotus purpuratus (Purple sea urchin)	STRPU	W4Z5C9	W4YCU0	W4ZAK8	W4ZIN8
Tetraodon nigroviridis (Spotted green pufferfish)	TETNG	H3DD39	H3D6H6	H3D7M2	H3BWC7
Wickerhamomyces ciferrii (Yeast)	WICCF	K0KS34	K0KG77	K0KFL9	K0KTE1
Xenopus laevis (African clawed frog)	XENLA	P18248	Q7ZZU5	Q8JHD8	Q8AY27
Xenopus tropicalis	XENTR	Q66KJ8	Q6DJ26	Q6DF51	A9ULD8

(Western clawed frog)					
Xiphophorus maculatus (Southern platyfish)	XIPMA	M4AKD0	M4A625	M4AET7	M3ZPZ4
Saccharomyces cerevisiae (Baker's yeast)	YEAST	P15873	Q08949	Q02574	P48581

Survival assays – For short term viability assays, cells were seeded in 6-well plates and either left untreated or treated with 50ng/ml 4NQO or 0.5µM aphidicolin for 24 hours. Mitomycin C (MMC) treatment was for 1 hour. After 3 days, the cells were collected by trypsinization and counted using a Moxi^{TM} Z mini automated cell counter (ORFLO technologies). Percent survival was calculated by dividing the number of cells after treatment by the number of untreated cells. Error bars ± SD. Statistical analysis was by Student's T-test, and p-values of <0.05 were considered significant. For clonogenic survival assays, cells were seeded in 6-well plates and treated with 4NQO or aphidicolin for 24 hours or with MMC for 1 hour. After 6 days, the cells were fixed with methanol and stained with crystal violet overnight. The plates were then washed, dried and scanned.

Immunoprecipitation and immunoblotting – For analysis of 9-1-1 subunit interactions, HEK293T transiently transfected with pCMV-mHus1, pCMV-hRad9a-Myc and pCMV-hRad1-HA constructs were irradiated with 100J/m^2 UV and 2 hours later cell lysates for co-immunoprecipitation (co-IP) were prepared. Lysates were incubated with anti-MYC (Santa Cruz) or anti-HA (Covance) antibodies, followed by incubation with protein A/G resin (Thermo Scientific). For analysis of HUS1-MYH interactions, HEK293T transiently transfected with pCMV-mHus1-3XFLAG or pCMV-R4D+I152Y-3XFLAG constructs were treated with 1mM H_2O_2 and 3 hours later cell lysates for co-IP were prepared. Lysates were incubated with anti-FLAG resin (Sigma). Immunoprecipitates or total cell lysates (input) were resolved by SDS-PAGE. Standard immunoblotting procedures were performed using antibodies specific

for HUS1 (Lyndaker et al., 2013b), RAD9A (Lyndaker et al., 2013b), MYC (Santa Cruz), HA (Covance), FLAG (Sigma), pCHK1 Ser345 (Cell Signaling), Histone 3 (Abcam), GAPDH (Advanced ImmunoChemical), MYH (Gu and Lu, 2001), TOPBP1 (Rendtlew Danielsen et al., 2009) or β-actin (Sigma).

Chromatin fractionation – *Hus1*$^{-/-}$*p21*$^{-/-}$ MEFs stably expressing WT or mutant mHUS1-3XFLAG proteins were irradiated with 100J/m^2 UVC and fractionated 2 hours post-treatment using a previously described extraction protocol (Abmayr et al., 2001) with modifications. Cells were swollen in hypotonic buffer (10mM HEPES pH7.9, 1.5mM $MgCl_2$, 75mM KCl, 0.2mM PMSF and 0.5M DTT) for 6 min in 37°C and lysed with Dounce homogenizer. After centrifugation at 14,000 rpm for 15 min, the supernatant was separated for cytoplasmic extract preparation. The nuclei pellet was resuspended in equal volumes of low-salt and high-salt buffers (20mM HEPES pH7.9, 25% glycerol, 1.5mM $MgCl_2$, 0.2M or 1.2M KCl, 0.2mM EDTA, 0.2mM PMSF and 0.5M DTT) in sequential order to extract the soluble nuclear fraction. After centrifugation at 14,000 rpm for 30 min, the supernatant was separated for nuclear extract preparation. The pellet was resuspended in RIPA buffer supplemented with aprotinin, leupeptin, sodium orthovanadate and phenylmethylsulfonyl fluoride (PMSF), sonicated at 24-30W for 1 min (Misonix Sonicator 3000), and centrifuged to produce the chromatin fraction in the supernatant. The cytoplasmic and nuclear fractions were dialyzed in dialysis buffer (20mM HEPES pH7.9, 20% glycerol, 100mM KCl, 0.2mM EDTA, 0.2mM PMSF and 0.5M DTT) overnight before use. 20μg of each fraction was used for immunoblotting.

2.4 RESULTS

A systematic structure/function analysis of HUS1

We used published crystal structure analyses of human 9-1-1 (Dore et al., 2009; Sohn and Cho, 2009; Xu et al., 2009), computational modeling of 9-1-1 subunit and DNA interactions (Querol-Audi et al., 2012; Xu et al., 2013), and evolutionary conservation analysis to predict functionally important mHUS1 residues. Initially we screened mHUS1 mutants with targeted mutations in 7 specific regions (Table 2.3) for the ability to complement the genotoxin sensitivity of *Hus1*$^{-/-}$*p21*$^{-/-}$ mouse embryonic fibroblasts (MEFs), which are hypersensitive to DNA damage (Weiss et al., 2000b). As detailed below, 3 HUS1 regions (the HUS1/RAD9A interface, the positively-charged inner surface of HUS1, and two hydrophobic pockets on the HUS1 outer surface) emerged as having the greatest functional significance in complemented cells challenged with 4NQO, a UV mimetic, or aphidicolin, a replication stress-inducing DNA polymerase inhibitor.

HUS1-RAD9A interaction is critical for 9-1-1 clamp formation and function

Stable inter subunit interactions are required to allow 9-1-1 clamp formation and maintain clamp integrity during the loading process (Dore et al., 2009; Sohn and Cho, 2009; Xu et al., 2009). We tested the impact of disrupting inter subunit interactions by targeting mHUS1 R128 (127 in hHUS1) located at the HUS1-RAD9A interface (Figure 2.1A), as its polar interactions were predicted to contribute substantially to the interaction between these subunits (Xu et al., 2013). Indeed, mutation of the orthologous residue in *S. pombe hus1* (N121) impairs association with spRAD9A

Table 2.3. Summary of clonogenic survival and short-term viability assay results for all mHUS1 mutants analyzed.

Mutations	Expression	Clonogenic survival[a]		Short term viability[a]	
		4NQO	Aphidicolin	4NQO	Aphidicolin
RAD9-interacting residue					
R128E	Yes	Null	Null	Null	Null
Inner ring hydrophobic cleft					
V19A, M22A, I23A	partial	WT	WT	WT	WT
V247A, V271A, L273A	partial	WT	WT	WT	WT
V19A, M22A, I23A, V247A, V271A, L273A	partial	WT	Partial	Partial	Null
R18A	Yes	N/A[a]	N/A	WT	WT
R18Q	Yes	N/A	N/A	WT	WT
R18Q M22T	Yes	N/A	N/A	WT	WT
Inner ring positively charged residues					
K93	N/A	WT	WT	WT	WT
K25	N/A	WT	WT	WT	WT
K25, K93	Yes	WT	WT	WT	WT
K25, K236, K237 (3A)	Yes	Partial	Partial	Partial	WT
K173, R175, K236, K237 (4A-1)	Yes	WT	Partial	Partial	Partial
K25, K93, K236, K237 (4A-2)	Yes	Null	Null	Null	Null
K25, K93, K173, R175, K236, K237 (6A)	Yes	Null	Null	Null	Null
R90, K93 (C1)	Yes	WT	WT	WT	Partial
R18, K25, K28 (C2)	N/A	WT	WT	WT	WT

K236, K237 (C3)	N/A	WT	WT	WT+	WT
K165, K168, K173, R175 (C4)	Yes	WT	Partial	WT	Partial
R18, K93, K165 (C5)	Yes	WT	Partial	Partial	WT
K173, R175	N/A	WT	WT	WT+	WT
K165, K168	N/A	WT	WT	N/A	N/A
K25A K28A K165A	Not stable	N/A	N/A	N/A	N/A
Outer ring hydrophobic pocket					
P150A, I152A, P153A, C155A	Partial	WT	WT	Partial	Partial
V257A, T261A, F276A, P278A	Yes	WT	WT	WT	WT
P150A, I152A, P153A, C155A, V257A, T261A, F276A, P278A	Partial	WT	Partial	N/A	N/A
P150A, V257A, T261A, F276A, P278A	Partial	WT	Partial	WT	Partial
P150A, I152A, P153A, C155A, F276A, P278A	Not stable	Partial	Partial	Partial	Partial
S53R	Yes	N/A	N/A	WT	WT
I152R	Partial	N/A	N/A	Partial	Partial
I152Y	Yes	Partial	WT	Partial	Partial
I152F	Yes	N/A	N/A	WT	WT
Outer ring novel pocket					
F3A, G71W, I79A, L105A	Not stable	Null	Null	N/A	N/A
F3A, G71W	N/A	WT	WT	N/A	N/A
F3A, I79A	N/A	WT	WT	N/A	N/A
F3A, L105A	N/A	WT	WT	N/A	N/A

F3A, I79A, L105A	Not stable	WT	Null	N/A	N/A
F3R	Not stable	Partial	Partial	Partial	WT
F3R, R4A	N/A	Partial	Partial	Partial	WT
K104A, L105A, T106A	N/A	WT	WT	WT	Partial
K104A, L105A, T106A, V138A, L139D	Not stable	Null	Null	Null	Null
L105R	Not stable	N/A	N/A	N/A	N/A
L139R	Not stable	N/A	N/A	N/A	N/A
R4D	Yes	Partial	WT	Partial	Partial
R4D, I152Y	Yes	Partial	WT	Partial	Partial
Outer ring positively charged residues					
K2A, R4A, K6A	N/A	WT	WT	N/A	N/A
R99A, K102A, K104A	N/A	WT	WT	N/A	N/A
K108A, H109A	N/A	WT	WT	N/A	N/A
K137A, R141A, R142A, K145A	N/A	WT	WT	N/A	N/A
BII4-6 loop					
Δ215-227	Not stable	Null	Null	N/A	N/A
Δ215-227::hHus1 loop	N/A	WT	WT	N/A	N/A
Δ215-227::PCNA loop	N/A	WT	WT	N/A	N/A

[a] Survival outcomes were categorized into: WT+ (better than WT mHUS1 complemented cells), WT (similar to WT mHUS1 complemented cells), Partial (worse than WT mHUS1 complemented cells but better than *Hus1* null cells), and Null (similar to *Hus1* null cells).

[b] not tested

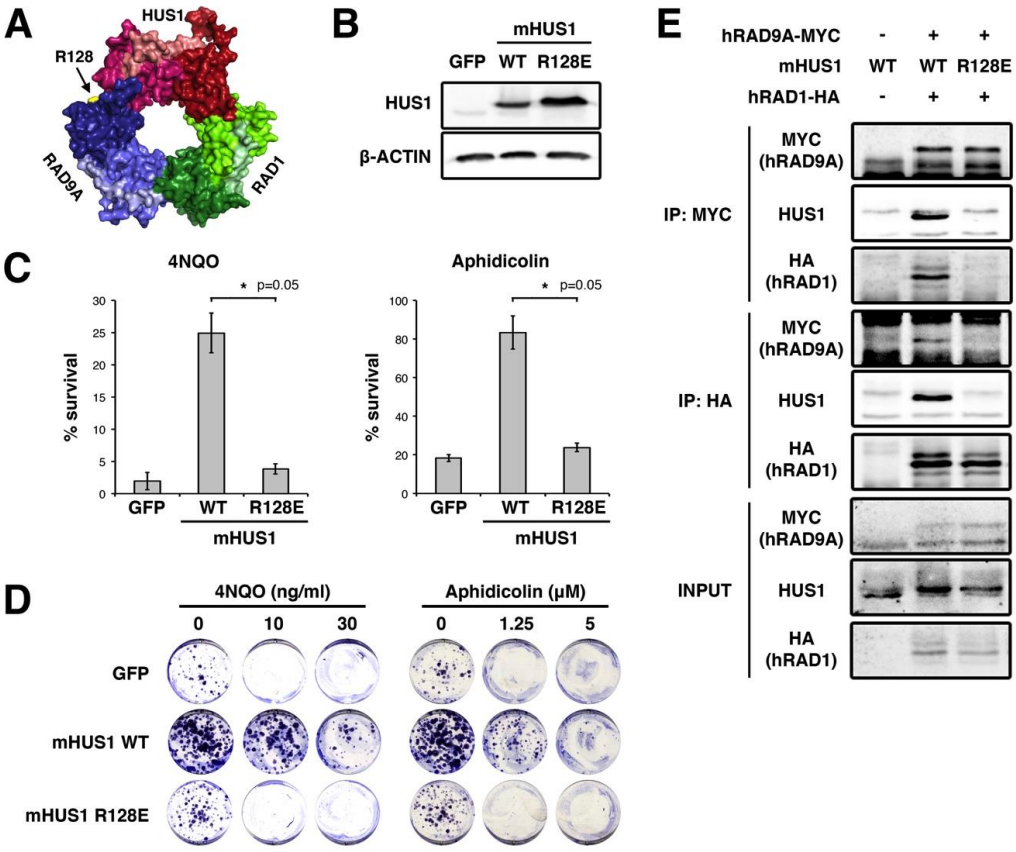

FIGURE 2.1. mHUS1 residue R128 is crucial for 9-1-1 clamp formation. (A) R128 (arrow) is located at the HUS1-RAD9A interface (PDB 3GGR). (B) Immunoblotting using antibodies specific for HUS1 or β-ACTIN was performed to compare the stability of WT and R128E mHUS1 proteins in HEK293T cells. (C-D) Short term viability and clonogenic survival were measured for *Hus1*-null MEFs stably expressing mHUS1 R128E after 4NQO or aphidicolin treatments. MEFs expressing GFP or WT mHUS1 served as negative and positive controls, respectively. Each experiment in (C) was repeated 5 times with 2 independently generated cell lines. (E) Interaction of mHUS1 R128E with hRAD9 and hRAD1 was assessed by co-IP.

(Kaur et al., 2001a). Hence, we mutated R128 to E (R128E) to reverse the charge of the residue and analyzed 9-1-1 clamp formation and cell survival after genotoxin treatment.

After confirming the stability of R128E mutant protein (Fig. 2.1B), we subjected R128E-expressing *Hus1*-null MEFs to short term viability and clonogenic survival assays (Fig. 2.1C and D). In both assays, mHUS1 R128E failed to rescue the genotoxin hypersensitivity of *Hus1*-null MEFs. Next, co-immunoprecipitation (co-IP) assays were performed to test interactions between mHUS1 R128E and RAD9A (Fig. 2.1E). Whereas wild-type (WT) mHUS1 co-IP'd with hRAD9A-MYC, mHUS1 R128E did not. Interestingly, in R128E-expressing cells hRAD1-HA also was not detected in the MYC IP, and neither mHUS1 R128E nor hRAD9A-MYC was detected in the reciprocal HA IP (Fig. 2.1E). These results indicate that reversing the charge of a single residue at the HUS1-RAD9A interface fully disrupted the stability and function of the entire trimeric 9-1-1 complex.

Multiple positively charged residues on the HUS1 inner surface facilitate HUS1-DNA interactions in a synergistic manner.

Like PCNA, 9-1-1 is thought to interact with the DNA phosphate backbone, affording proper loading and scaffolding activity on chromatin (McNally et al., 2010). The inner HUS1 surface consists of 4 parallel α-helices containing 11 positively-charged residues (Fig. 2.2A). In order to determine the importance of mHUS1-DNA contact, alanine mutants of several of these residues (K25, K93, K173, R175, K236 and K237) were generated and functionally tested. These mutations did not disrupt mHUS1

protein stability (Fig. 2.2B), but all caused loss of function as evidenced by partial (mutants 3A and 4A-1) or complete (4A-2 and 6A) genotoxin hypersensitivity phenotypes (Fig. 2.2C and 2.2D). These defects were not due to disruption of 9-1-1 clamp formation, as both mHUS1 4A-2 and 6A co-IP'd with hRAD9A-MYC and hRAD1-HA to the same extent as WT mHUS1 (Fig. 2.2E). Notably, the hHUS1 residues equivalent to those mutated in 4A-2 and 6A were computationally predicted to directly contact DNA (Querol-Audi et al., 2012). We generated additional mutants in different alignments (Fig. 2.3A and Table 2.3) to investigate the possible involvement of alternative DNA contacts. However, these mutants were not associated with pronounced hypersensitivity phenotypes (Fig. 2.3B). Taken together, these results indicate that 6 specific positively-charged HUS1 residues synergistically facilitate HUS1-DNA contacts and are necessary for cell survival following DNA damage.

HUS1 has two functional hydrophobic pockets that are important for genome maintenance.

Like PCNA, the 9-1-1 clamp stimulates the activity of many DNA repair factors via direct physical interactions. To identify HUS1 functional domains that might bind effectors, we conducted an evolutionary conservation analysis with the assumption that functional residues would be evolutionarily conserved. As a proof of principle, we first performed this analysis on PCNA (Fig. 2.4A). Two clusters of conserved residues were apparent on the PCNA outer ring surface, one for the well-characterized primary PCNA interacting protein (PIP)-box binding pocket, and the

FIGURE 2.2. Multiple positively-charged residues on the HUS1 inner ring are synergistically important for genotoxic stress responses. (A) mHUS1 has 11 arginines and lysines (black circles) distributed on 4 α-helices in the inner ring surface (PDB 3GGR). Alanine substitutions of these residues (3A-6A) were made. (B) Protein expression was measured as in Figure 1B. (C-D) Genotoxin sensitivity was measured as in Figures 1C and 1D. Each experiment in (C) was repeated 3 times with 3 independently generated cell lines. (E) Interaction of mHUS1 mutant proteins with hRAD9 and hRAD1 was assessed by co-IP.

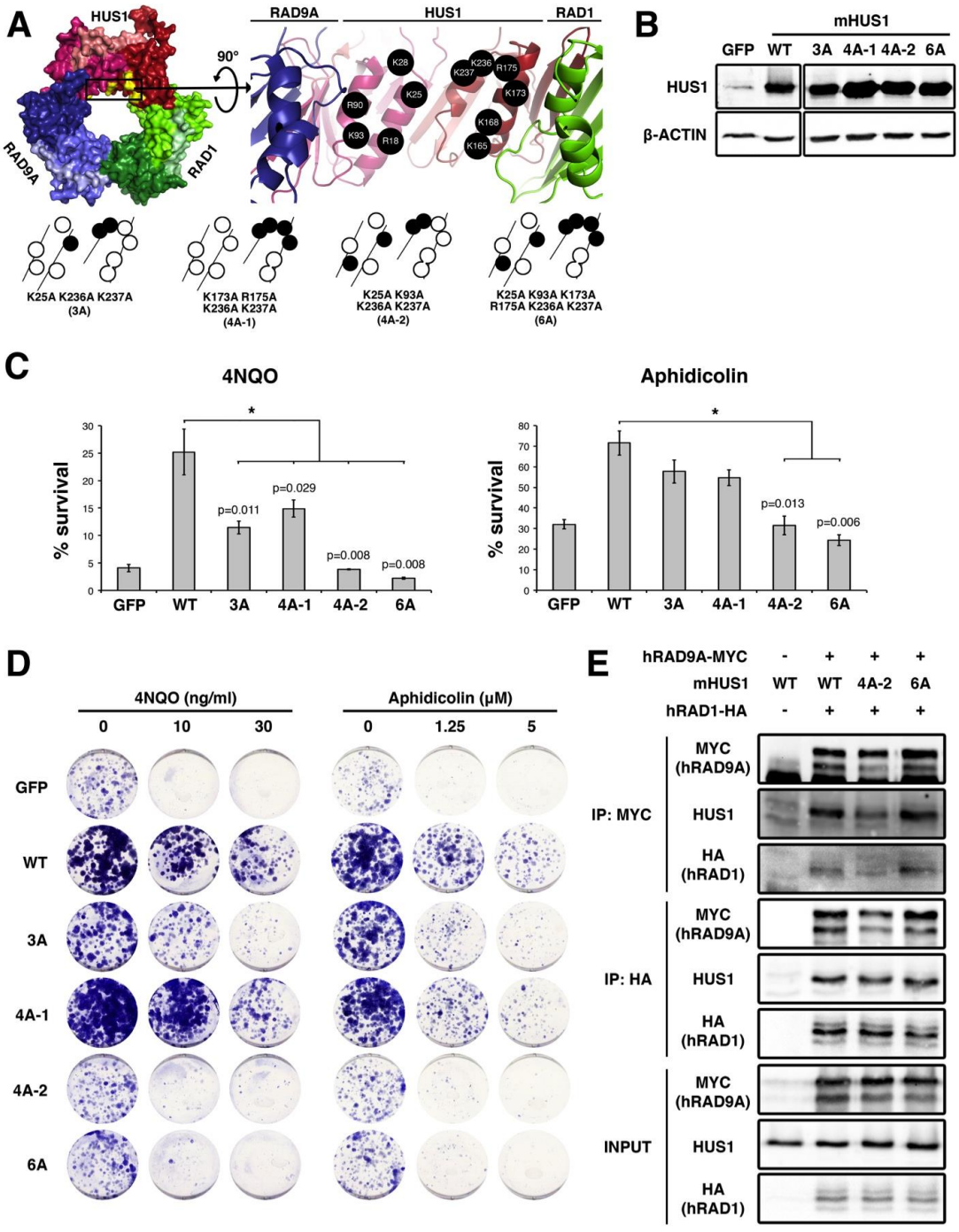
A
HUS1
RAD9A
RAD1
90°
RAD9A
HUS1
RAD1
K28
K25
R90
K93
R18
K236
K237
R175
K173
K168
K165
K25A K236A K237A
(3A)
K173A R175A
K236A K237A
(4A-1)
K25A K93A
K236A K237A
(4A-2)
K25A K93A K173A
R175A K236A K237A
(6A)
B
mHUS1
GFP WT 3A 4A-1 4A-2 6A
HUS1
β-ACTIN
C
4NQO
Aphidicolin
% survival
p=0.011
p=0.029
p=0.008
p=0.008
p=0.013
p=0.006
GFP WT 3A 4A-1 4A-2 6A
D
4NQO (ng/ml)
0 10 30
Aphidicolin (μM)
0 1.25 5
GFP
WT
3A
4A-1
4A-2
6A
E
hRAD9A-MYC - + + +
mHUS1 WT WT 4A-2 6A
hRAD1-HA - + + +
IP: MYC
IP: HA
INPUT
MYC (hRAD9A)
HUS1
HA (hRAD1)

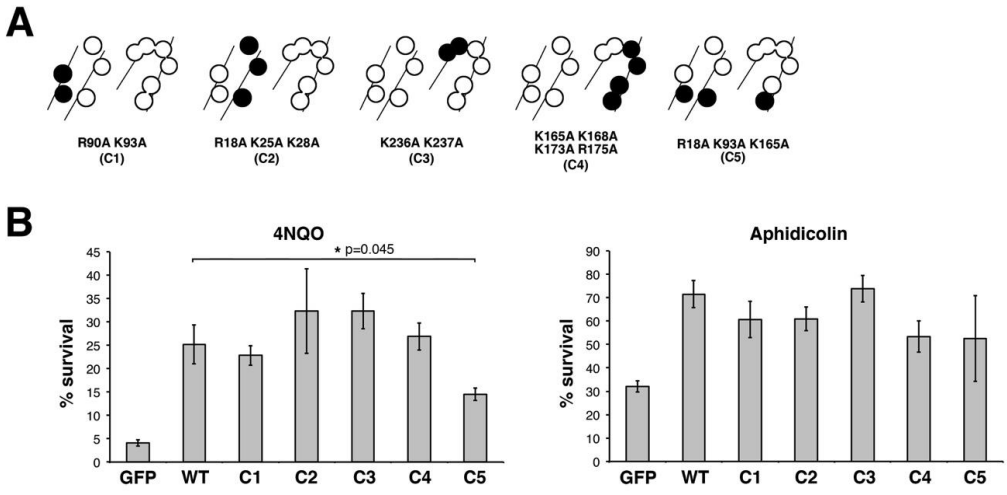

FIGURE 2.3. Certain configurations of positively charged residues in the inner ring of HUS1 are dispensable for genotoxic stress responses. (A) Alanine substitutions of positively charged residues were made in various combinations (C1-C5), as indicated by the filled circles. (B) Short term viability of *Hus1*$^{-/-}$ *p21*$^{-/-}$ MEFs stably expressing mHUS1 inner ring mutants C1-C5 after 4NQO or aphidicolin treatments was measured. Each experiment was repeated 4 times using 3 independently generated cell lines. No significant differences in survival between wild-type mHUS1 and mutants C1-C5 were identified, except for C5 with 4NQO treatment.

FIGURE 2.4. The identification of a novel conserved hydrophobic pocket in the outer ring of HUS1. (A, B) The evolutionary conservation values of each amino acid position in the protein structures of PCNA, RAD9A, HUS1 and RAD1 were calculated using the Consurf bioinformatics server (see Experimental Procedures). Multiple sequence alignments of 44 organisms that encompass a wide range of taxa were used (see Table 2.2). Residues pseudo-colored in cyan have diverged and are variable, whereas those in magenta are conserved. Dotted lines outline conserved regions that potentially mediate protein-protein associations. The circled regions correspond to the PIP box-binding hydrophobic pocket of PCNA and the analogous conserved region of RAD9A. A second conserved region for PCNA and HUS1 is outlined with a rectangle and in the case of HUS1 corresponds to a novel pocket on the side of globular domain 1 comprised of 3 conserved hydrophobic residues. (C) HUS1 atomic surface and surface electrostatic potential models reveal a positively charged groove at the base of the novel pocket. The charge is contributed by an arginine at position 4.

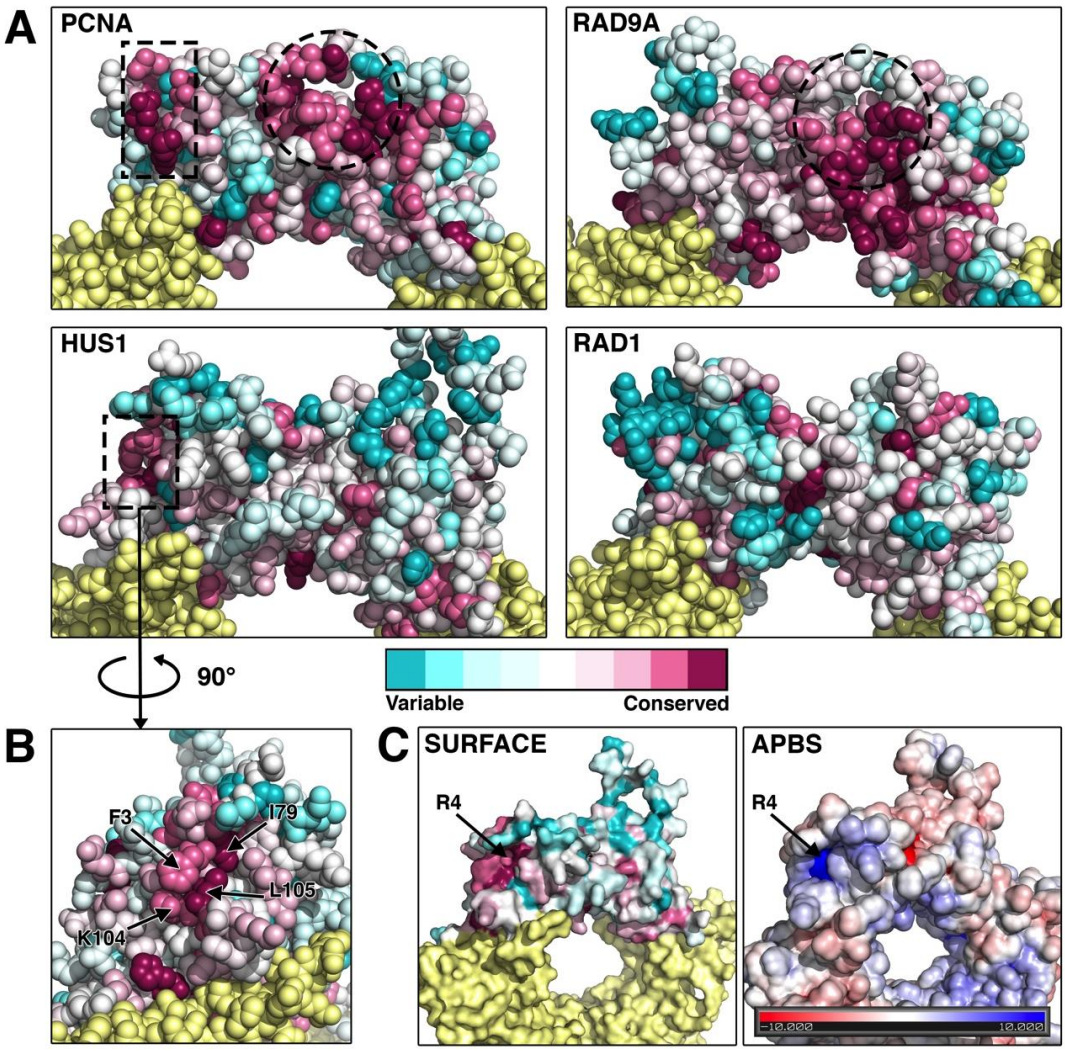
A
PCNA
RAD9A
HUS1
RAD1
90°
Variable
Conserved
B
F3
I79
L105
K104
C
SURFACE
R4
APBS
R4
−10.000
10.000

other for a secondary domain that also associates with sequences C-terminal to the PIP box motif in some PCNA effectors (Gulbis et al., 1996; Sakurai et al., 2005).

The same analysis was then applied to RAD9A, HUS1 and RAD1 (Fig. 2.4A). Structural studies had previously identified PCNA-like hydrophobic pockets in RAD9A and HUS1 (Dore et al., 2009). However, the distribution of conserved residues for each subunit varied from PCNA and from each other. RAD9A showed conservation of the primary PCNA-like hydrophobic pocket but HUS1 and RAD1 did not. However, when analyzing only mammalian sequences, conservation of HUS1 and RAD1 residues at the equivalent position for the primary PCNA-like hydrophobic pocket became evident (data not shown). We also identified a cluster of conserved HUS1 residues in the topologically equivalent region of the PCNA secondary binding site. This pocket is formed by 3 hydrophobic HUS1 residues (F3, I79 and L105) along with R4 at the pocket base, creating a strong positive electrostatic potential surrounded by a neutral field (Fig. 2.4B and 2.4C).

To assess the functional significance of the HUS1 outer surface domains, we first targeted hydrophobic residues that form the PCNA-like primary and secondary pockets, but various alanine mutants either disrupted HUS1 protein stability or did not cause loss of function in survival assays (Table 2.3). We then generated mutations predicted to physically or electrostatically block the pockets (Fig. 2.5A). For the primary pocket, we changed I152 (V151 in hHUS1) to Y (I152Y) to block the pocket with a bulky side chain. For the secondary pocket, R4 was mutated to D (R4D) to reverse the charge at the base. We also generated the double pocket mutant (R4D+I152Y) to test whether the pockets functioned independently or in conjunction

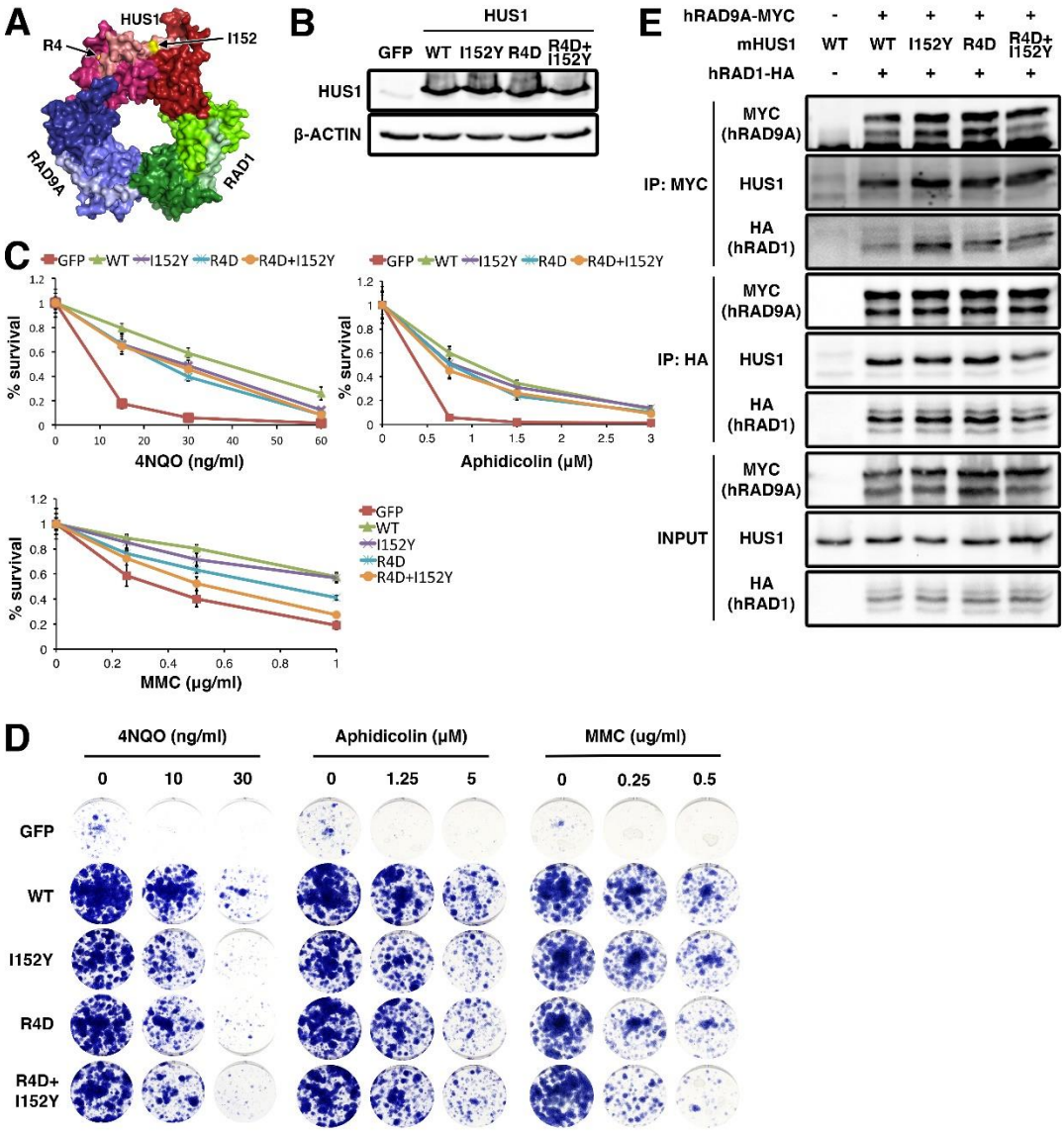

FIGURE 2.5. Two hydrophobic pockets on the outer surface of HUS1 are required for genotoxic stress responses. (A) R4 and I152 (arrows) are located on the outer ring surface (PDB 3GGR). (B) Protein expression was measured as in Figure 1B. (C-D) Genotoxin sensitivity was measured as in Figures 1C and 1D, as well as with MMC treatment. Each experiment in (C) was repeated 2 times with 2 independently generated cell lines. (E) Interaction of the pocket mutants with hRAD9 and hRAD1 was assessed by co-IP.

with each other. Although all three mutants were stably expressed and competent for clamp formation (Fig. 2.5B and 2.5E), *Hus1* deficient cells expressing the double pocket mutant were no more sensitive to 4NQO or aphidicolin than those expressing either single pocket mutant (Fig. 2.5C and 2.5D). Interestingly, when challenged with MMC, cells expressing the double pocket mutant showed a synergistic increase in hypersensitivity as compared to the single mutants. These results suggest that the two HUS1 outer surface pockets function have separable roles in response to certain forms of DNA damage, such as DNA crosslinks, but act in conjunction for other DNA lesions, such as those induced by 4NQO or aphidicolin.

DNA damage-induced HUS1 chromatin localization is disrupted in clamp destabilizing and DNA interaction mutants, but occurs normally in pocket mutants.

In order to determine how the different classes of HUS1 mutations affected the ability of HUS1 to localize on chromatin after DNA damage, we performed immunofluorescence (IF) assays in *Hus1*-null MEFs complemented with 3XFLAG-tagged mHUS1 mutants, including R128E (RAD9A interface), 4A-2 or 6A (DNA binding), or I152Y or R4D (outer surface pockets) (Fig. 2.6A). We quantified RAD9A and FLAG IF co-staining in cells treated with MMC (Fig. 2.6C). MMC-induced RAD9A foci were absent in *Hus1*-null MEFs but were present after restoration of mHUS1 expression. While RAD9A and FLAG foci colocalized in MEFs expressing WT mHUS1-3XFLAG, likely representing 9-1-1 accumulation on damaged DNA, the clamp destabilizing HUS1 mutant R128E-3XFLAG failed to form FLAG or RAD9A

foci. Similar results were observed for 4A2-3XFLAG and 6A-3XFLAG DNA interaction mutants. By comparison, inner ring mutants with less severe genotoxin sensitivity phenotypes showed an intermediate average number of MMC-induced foci formation (Fig. 2.6B and 2.6D), suggesting that 9-1-1 loading requires clamp-DNA interactions, as is the case for PCNA (McNally et al., 2010). By contrast, mHUS1 pocket mutants I152Y-3XFLAG, R4D-3XFLAG and R4D+I152Y-3XFLAG retained the ability to form MMC-induced foci and colocalize with RAD9A to the same extent as WT mHUS1-3XFLAG (Fig. 2.6A and 2.6C).

To verify the IF results, we performed immunoblotting of fractionated cells after UV irradiation (Fig. 2.6E). WT mHUS1-3XFLAG was detected in the nuclear and chromatin compartments after UV damage. Consistent with the IF results, this response was ablated in MEFs expressing R128E-, 4A2- or 6A-3XFLAG, but not in MEFs expressing the pocket mutants. Thus, genotoxin-induced 9-1-1 clamp accumulation on damaged DNA requires proper 9-1-1 clamp formation and DNA interactions, but not HUS1 pocket-mediated functions.

HUS1 pocket mutants are competent for checkpoint signaling but defective for effector interactions

To determine if the various mHUS1 mutants affected ATR activation and checkpoint signaling, we assessed UV-induced CHK1 phosphorylation (pCHK1) (Fig. 2.7A). As previously reported (Weiss et al., 2002), *Hus1*-null MEFs were impaired for CHK1 phosphorylation upon UV treatment. This defect was rectified by complementation with WT mHUS1. However, in cells complemented with the mHUS1 R128E, 4A-2 or

FIGURE 2.6. DNA damage-induced HUS1 localization is defective in HUS1 clamp forming and DNA interacting mutants, but not in HUS1 pocket mutants. (A-B) MMC-treated *Hus1*-null MEFs stably expressing the indicated constructs were stained with DAPI (blue), and α-FLAG (green) and α-RAD9A (red) antibodies. Scale bar=10μm. (C-D) Quantifications of colocalized FLAG and RAD9A foci are presented in quartile box and dot plots. NS = not significant. (D) Immunoblotting using antibodies specific for FLAG or β-ACTIN was performed to compare the stability of 3XFLAG-tagged WT and mutant mHUS1 proteins (C1, C4 and C5) in HEK293T cells. (E) Cells were UV-treated, fractionated into cytoplasmic (cyt), nuclear (nuc) and chromatin (chr) fractions, and immunoblotted. GAPDH and Histone 3 served as fractionation controls. Arrows indicate HUS1 band; asterisks denote a non-specific band.

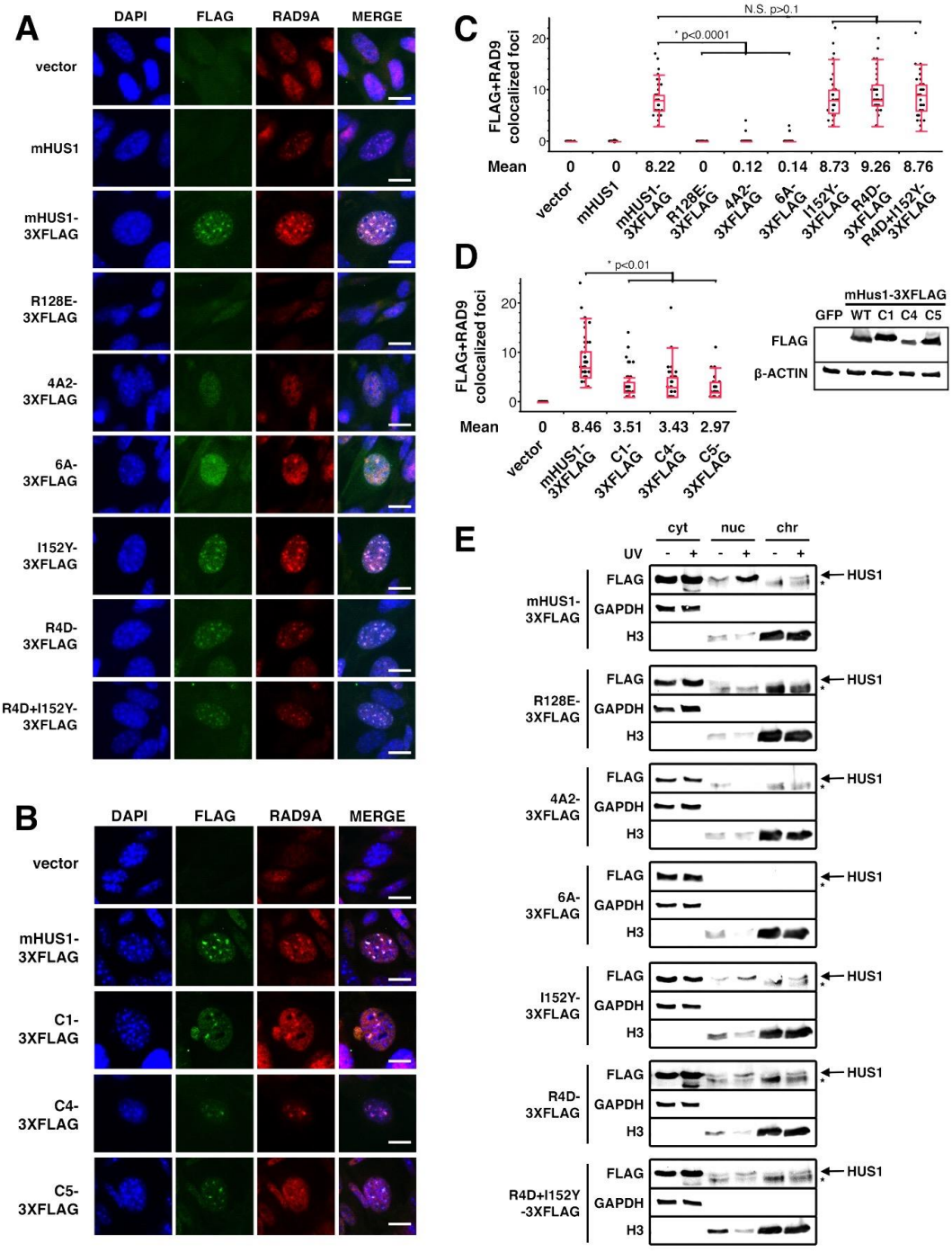
A
DAPI
FLAG
RAD9A
MERGE
vector
mHUS1
mHUS1-3XFLAG
R128E-3XFLAG
4A2-3XFLAG
6A-3XFLAG
I152Y-3XFLAG
R4D-3XFLAG
R4D+I152Y-3XFLAG
B
DAPI
FLAG
RAD9A
MERGE
vector
mHUS1-3XFLAG
C1-3XFLAG
C4-3XFLAG
C5-3XFLAG
C
FLAG+RAD9 colocalized foci
N.S. p>0.1
* p<0.0001
Mean
0
0
8.22
0
0.12
0.14
8.73
9.26
8.76
vector
mHUS1
mHUS1-3XFLAG
R128E-3XFLAG
4A2-3XFLAG
6A-3XFLAG
I152Y-3XFLAG
R4D-3XFLAG
R4D+I152Y-3XFLAG
D
FLAG+RAD9 colocalized foci
* p<0.01
Mean
0
8.46
3.51
3.43
2.97
vector
mHUS1-3XFLAG
C1-3XFLAG
C4-3XFLAG
C5-3XFLAG
mHus1-3XFLAG
GFP
WT
C1
C4
C5
FLAG
β-ACTIN
E
cyt
nuc
chr
UV
- + - + - +
mHUS1-3XFLAG
R128E-3XFLAG
4A2-3XFLAG
6A-3XFLAG
I152Y-3XFLAG
R4D-3XFLAG
R4D+I152Y-3XFLAG
FLAG
GAPDH
H3
HUS1

6A mutants, the pCHK1 response was abrogated to the same extent as with complete *mHus1* deficiency. These data indicate that unstable subunit-subunit and mHUS1-DNA interactions significantly impair ATR activation, consistent with the observations that these mutant proteins failed to properly localize to DNA damage sites. By contrast, cells expressing mHUS1 pocket mutants I152Y, R4D or R4D+I152Y retained normal levels of UV-induced CHK1 phosphorylation (Fig. 2.7A), as might be expected since interactions between 9-1-1 and the ATR activator TOPBP1 occur through RAD9A (Delacroix et al., 2007). This result suggests that the genotoxin sensitivity phenotype shown by cells expressing the pocket mutants might be due to disruption of checkpoint signaling-independent HUS1 functions.

The 9-1-1 clamp is known to interact with several DNA repair proteins, including many from the base excision repair pathway (Helt et al., 2005; Madabushi and Lu, 2011). Among the well-established 9-1-1 binding partners is the DNA glycosylase MutY Homolog (MYH) (Chang and Lu, 2005; Shi et al., 2006). In order to determine if HUS1 outer surface pockets were important for protein-protein interactions, R4D+I152Y-3XFLAG protein was expressed and immunoprecipitated for the detection of association with endogenous MYH (Fig. 2.7B). Whereas wild-type HUS1-3XFLAG effectively pulled down MYH, less MYH was detected in the R4D+I152Y-3XFLAG immunoprecipitation. Notably, TOPBP1 co-immunoprecipitated with the HUS1 outer surface mutant to a similar extent as with wild-type HUS1, consistent with our observation that this mutant was capable of promoting UV-induced CHK1 phosphorylation.

FIGURE 2.7. 9-1-1-dependent checkpoint signaling requires clamp formation and DNA associations but not HUS1 outer surface pocket function, which is necessary for effector interactions. (A) DNA damage-induced CHK1 phosphorylation is hampered in HUS1 clamp formation and DNA interaction mutants, but is intact for HUS1 outer surface pocket mutants. Lysates from cells treated with 0 or 100 J/m^2 UV were immunoblotted using antibodies specific for phospho-CHK1 or β-ACTIN. (B) HUS1 pocket mutant R4D+I152Y is impaired for interaction with base excision repair protein MYH. Lysates prepared from HEK293T cells overexpressing 3XFLAG-tagged WT or R4D+I152Y mHUS1 proteins were immunoprecipitated with antibody specific for FLAG and immunoblotted using antibodies specific for MYH and TOPBP1. (C) Model for HUS1-mediated function in DNA damage response. WT HUS1 forms 9-1-1 clamps, localizes to DNA damage sites, and mediates ATR checkpoint signaling and DNA repair functions. When the RAD9A interacting residue is dysfunctional, HUS1 cannot form 9-1-1 clamp, causing loss of all downstream functions. HUS1 mutants defective for DNA interactions are still able to form 9-1-1 clamps but cannot localize to DNA damage sites, similarly causing loss of all downstream functions. Only HUS1 pocket mutants are able to form 9-1-1 clamps, localize to DNA lesions, and activate ATR for checkpoint signaling. However, checkpoint-independent functions of HUS1 are perturbed in the pocket mutants, likely causing increased genotoxin hypersensitivity due to impaired DNA repair.

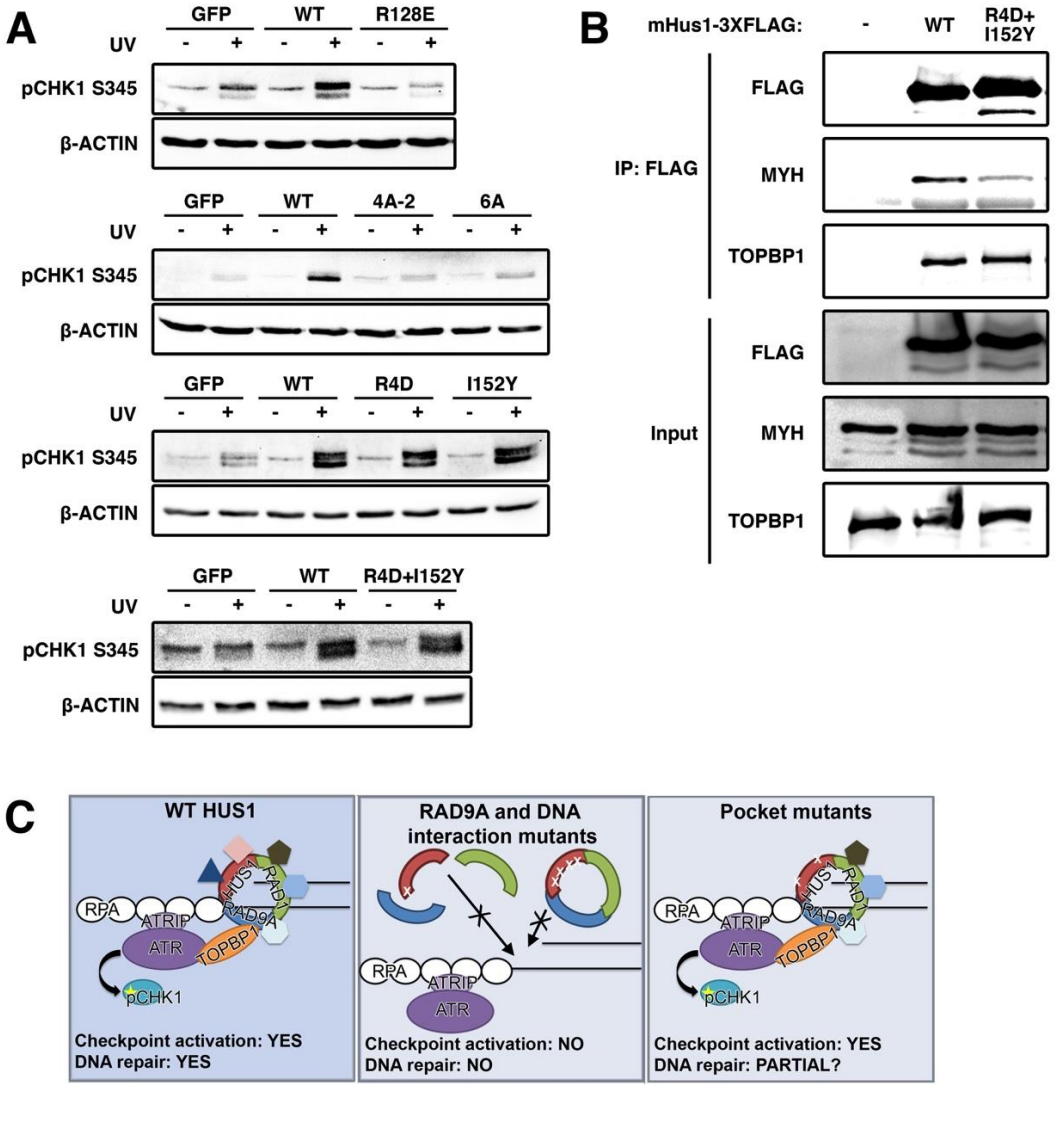
A
GFP
WT
R128E
UV
pCHK1 S345
β-ACTIN
GFP
WT
4A-2
6A
UV
pCHK1 S345
β-ACTIN
GFP
WT
R4D
I152Y
UV
pCHK1 S345
β-ACTIN
GFP
WT
R4D+I152Y
UV
pCHK1 S345
β-ACTIN
B
mHus1-3XFLAG:
-
WT
R4D+ I152Y
IP: FLAG
FLAG
MYH
TOPBP1
Input
FLAG
MYH
TOPBP1
C
WT HUS1
RAD9A and DNA interaction mutants
Pocket mutants
RPA
ATRIP
ATR
TOPBP1
HUS1
RAD1
RAD9A
pCHK1
Checkpoint activation: YES
DNA repair: YES
Checkpoint activation: NO
DNA repair: NO
Checkpoint activation: YES
DNA repair: PARTIAL?

Together, these results indicate that the mHUS1 outer surface mutant is defective for the recruitment of DNA repair proteins despite properly localizing to damaged DNA and supporting ATR checkpoint signaling, highlighting ATR-independent effector functions downstream of HUS1 (Fig. 2.7C).

2.5 DISCUSSION

Checkpoint signaling in coordination with appropriate DNA repair is crucial for a successful DDR in cells experiencing various genotoxic stresses. Understanding this concerted action is important for appreciating how normal cells are protected from the deleterious effects of genomic instability and how malignant cells manage genomic and cellular integrity in the face of numerous physiological stresses (Ciccia and Elledge, 2010; Hanahan and Weinberg, 2011; Helleday et al., 2008; Hoeijmakers, 2001). In this study, we sought to understand the molecular interactions that underlie a robust DDR involving the 9-1-1 clamp and in doing so defined the molecular requirements for both stimulation of ATR-induced CHK1 phosphorylation and CHK1-independent functions for the 9-1-1 complex mediated by outer surface residues of the HUS1 subunit.

Maintaining sufficient inter-subunit contacts is the most crucial initial step for 9-1-1 clamp formation, failure of which will abrogate all downstream clamp functions. Remarkably, reversing the polarity of a single residue (R128 of mHUS1) at the RAD9A/HUS1 interface fully disrupted 9-1-1 clamp integrity and function, even though there are at least 8 other HUS1 residues predicted to contribute to RAD9A-HUS1 interactions (Xu et al., 2013). Interestingly, the RAD9A/HUS1 interface

mutation also disrupted HUS1-RAD1 and RAD1-RAD9A associations. One possible explanation is that active repulsion of HUS1-RAD9A indirectly weakens HUS1-RAD1 and RAD9A-RAD1 interactions. Alternatively, the findings may suggest that clamp assembly occurs in an ordered, stepwise process as reported for the heterotrimeric PCNA of *Sulfoflobus solfataricus* (*Sso*PCNA) (Dionne et al., 2003), or that all three 9-1-1 interfaces function cooperatively during trimerization.

The inner surface of PCNA consists of four parallel alpha-helices that contain positively charged residues, some of which contact the negatively charged DNA sugar-phosphate backbone and are necessary for efficient clamp loading and mobility on DNA (Georgescu et al., 2008). Similarly, the HUS1 inner surface also is comprised of four parallel alpha-helices containing numerous positively charged residues, and here we report that HUS1 function requires a specific set of synergistically important residues that are aligned in a transhelical manner analogous to those of PCNA. Notably, our findings are consistent with predicted HUS1-DNA contacts from computational modeling (Querol-Audi et al., 2012). It is remarkable that loss of DNA contacts for the HUS1 subunit alone leads to severe checkpoint signaling defects and hypersensitivity to genotoxins, since modeling of 9-1-1 on DNA indicates that the three subunits contribute almost equally for DNA backbone associations (Querol-Audi et al., 2012), although it remains possible that certain DNA structures might lead to other 9-1-1 conformations on DNA. The HUS1 inner surface mutants stably associate with the other 9-1-1 subunits but do not show substantial DNA damage-induced accumulation on chromatin, suggesting that interactions between 9-1-1 and DNA are necessary for stable loading of the clamp.

Much knowledge about PCNA function was gained by structure/function studies that identified a PCNA hydrophobic pocket as the docking site for most PIP box motif-carrying proteins (Naryzhny, 2008). Based on the structural similarity between the 9-1-1 complex and PCNA, we hypothesized that the outer surface of HUS1 would mediate physical interactions with downstream effectors. Our evolutionary conservation analysis revealed that among all 9-1-1 subunits, RAD9A showed the greatest conservation of the hydrophobic pocket that is analogous to the site where PCNA interacts with PCNA interacting protein box motifs, consistent with the idea that RAD9A is the subunit most closely related to PCNA (Dore et al., 2009). The same region was conserved among mammalian HUS1 proteins but not in a broader representation of species. This suggests that while the RAD9A pocket is evolutionarily conserved, HUS1 and RAD1 have undergone greater divergence, potentially reflecting specialization of clamp subunits. Consurf analysis of HUS1 additionally revealed a second hydrophobic pocket on the outer surface that showed substantial evolutionary conservation. Disruption of these two HUS1 outer surface pockets caused partial loss of function without disturbing clamp formation or its recruitment to chromatin following DNA damage. That cells expressing these pocket mutants were not as hypersensitive to genotoxic stress as cells that completely lack HUS1 likely relates to the fact that they remain functional for genotoxin-induced CHK1 activation, as would be expected since interactions between 9-1-1 and the ATR activator TOPBP1 occur through the C-terminal tail of RAD9A (Delacroix et al., 2007). It also remains possible that RAD9A and RAD1 provide some level of redundancy when HUS1 is dysfunctional, as in some cases, RAD9A, HUS1 and

RAD1 can all interact with the same repair protein albeit with different binding affinities (Bai et al., 2010; Friedrich-Heineken et al., 2005; Gembka et al., 2007; Guan et al., 2007; Park et al., 2009; Smirnova et al., 2005). We favor the possibility that each 9-1-1 subunit binds at least some unique downstream effectors, with the idea that each subunit is specialized to some extent to mediate specific functions. Indeed, the subunits of the archael heterotrimeric PCNA each interact with distinct binding partners, a characteristic that provides a means to diversify and coordinate clamp functions (Beattie and Bell, 2012).

PCNA-effector interactions invariably involve PIP box sequences, but there is mixed evidence regarding a role for PIP box motifs in 9-1-1-effector interactions (Eichinger and Jentsch, 2011), and the role of the secondary HUS1 pocket is unknown. It may stabilize interactions with PIP box-containing effectors that bind the primary pocket, resembling PCNA interactions with FEN1 and p21 (Gulbis et al., 1996; Sakurai et al., 2005). Combining the outer surface mutations (R4D+I152Y) did not further increase hypersensitivity to 4NQO or aphidicolin beyond that for either single mutant (Table 2.3), suggesting a related function for the two pockets. However, cells expressing the double mutant R4D+I152Y showed increased sensitivity to MMC, consistent with our previous findings (Balmus et al., 2015). Here we further show that the double mutant R4D+I152Y confers great MMC hypersensitivity than either of the corresponding single mutants, implying that at certain DNA lesions the two HUS1 pockets can have separate roles that cooperatively improve cell survival. In such circumstances, the secondary HUS1 pocket might interact with distinct effectors independently of the primary pocket, through a different motif, like the recently

reported Mec3-Mcm10 interaction, which involves both a PIP box and other sequences in MCM10 (Alver et al., 2014). With its close proximity to the RAD9A primary PCNA-like pocket, the secondary HUS1 pocket also may be involved in RAD9A-HUS1 inter subunit-effector binding, as has been reported for the interaction between the equivalent budding yeast proteins (DDC1-MEC3) and their partner RED1 (Eichinger and Jentsch, 2010). Bacterial β-clamp and *Sso*PCNA display intersubunit interactions with TLS polymerases (Bunting et al., 2003; Xing et al., 2009).

An open question has been to what extent the requirement for the 9-1-1 complex in genome maintenance reflects its role in TOPBP1-induced ATR activation, versus direct functions for 9-1-1 subunits in other processes. By mutating the HUS1 outer surface pockets, we have successfully separated these 9-1-1 functions and demonstrate that HUS1 has roles apart from checkpoint signaling that also are crucial for cell survival following DNA damage. Continued analysis of this collection of HUS1 mutants, especially further dissection of the genotoxin-specific functions of both HUS1 outer surface pockets, as well as the outer surface domains of RAD9A and RAD1, holds promise for shedding light on 9-1-1 functions in genome maintenance and highlighting potential targets that can be exploited for anti-cancer therapies.

2.6 ACKNOWLEDGEMENT

This work was supported by NIH grant R01 CA108773 (R.S.W). Additionally, we thank Ivaylo Ivanov from Georgia State University, and Alba Guarne from McMaster University for suggestions on strategies for mutagenesis. We also thank Joseph Peters, and Marcus Smolka for helpful discussions and comments on the manuscript.

CHAPTER 3

THE 9-1-1 DNA DAMAGE RESPONSE COMPLEX ACTS UPSTREAM OF BRCA1, FANCD2 AND RAD51 DURING DNA INTERSTRAND CROSSLINK REPAIR TO MAINTAIN GENOMIC STABILITY*

3.1 ABSTRACT

In mammalian cells, the Fanconi anemia (FA) pathway plays a central role in the multifaceted cellular response to DNA interstrand crosslinks (ICLs) that stabilizes stalled replication forks and coordinates ICL repair. Here, we tested the requirement for the RAD9A-RAD1-HUS1 (9-1-1) complex for ICL responses. Our studies showed that *Hus1* deficiency resulted in Mitomycin C (MMC) hypersensitivity, radial chromosome formation, and disrupted MMC-induced chromatin loading of FANCD2. The 9-1-1 complex physically associated with several FA proteins and additionally was necessary for recruitment of RAD51 and BRCA1 onto DNA in response to MMC-induced ICLs. Furthermore, *Hus1* protected stalled replication forks against MRE11-induced fork degradation during replication stress. Analysis of separation of function mutants indicated that chromatin loading of FANCD2 and RAD51 was mediated through the outer surface of the 9-1-1 complex, whereas BRCA loading, fork protection, and prevention of radial chromosome formation occurred through 9-1-1-dependent checkpoint signaling. Together, these results indicate that the 9-1-1

Robert S. Weiss, Joanna Mleczko, Catalina Pereira, Pei Xin Lim, Georgios Karras, and Maria Jasin contributed to the work presented in this chapter. Full acknowledge can be found in section 3.6.

complex coordinates multiple signaling and repair proteins required for efficient and accurate ICL repair.

3.2 INTRODUCTION

Accurate genome replication and continuous surveillance for damaged DNA are essential to organismal survival. Failure to resolve DNA lesions can result in blockage of DNA replication and transcription, leading to genomic instability, tumorigenesis and other disorders (Zhou and Elledge, 2000). DNA-ICLs are one form of DNA damage initiated by endogenous aldehydes or exogenous crosslinking agents that result in fork stalling and replication stress (Knipscheer et al., 2009).

When replication forks stall at an ICL, cells initiate DNA damage induced checkpoint signaling to ensure cell cycle arrest (Ciccia and Elledge 2010). A key trigger for this response is the accumulation of ssDNA, which becomes coated with RPA and prompting the independent recruitment of the checkpoint kinase ATR in complex with ATRIP, as well as the 9-1-1 complex at the damage site (Delacroix et al., 2007; Weiss et al., 2003). The 9-1-1 complex is a DNA-binding sliding clamp that is structurally similar to PCNA (Proliferation Cell Nuclear Antigen) and both serve as molecular scaffolds lacking enzymatic activity (Eichinger and Jentsch, 2011). Upon loading at damage sites, the 9-1-1 complex stimulates ATR kinase signaling through interactions between RAD9A and the ATR activator TOPBP1. Activated ATR phosphorylates downstream effectors including the kinase CHK1 resulting in cell cycle arrest and initiation of DNA repair, or apoptosis in cases of severe damage (Delacroix et al., 2007). In addition to activating ATR-mediated checkpoint signaling,

the 9-1-1 complex also promotes DNA repair via physical interactions with numerous proteins involved in different repair pathways (Lim et al., 2015; Stergiou et al., 2011).

The importance of the 9-1-1 complex in maintaining genomic instability is striking, as loss of any of the clamp subunits results in severe genomic instability, increased apoptosis, cellular proliferation defects, sensitivity to genotoxins, and embryonic lethality (Han et al., 2010; Hopkins et al., 2004; Levitt et al., 2005; Weiss et al., 2000a; Weiss et al., 2000c). The 9-1-1 complex is particularly important for responding to replication stress, including that caused by ICL inducing agents such as MMC (Balmus et al., 2016). A recent proteomic screen revealed that the 9-1-1 complex is recruited at the damage site upon ICL formation, prior to loading of the key ICL repair proteins (Raschle et al., 2015). Taken together, these studies implicate the 9-1-1 complex as a key player in the cellular response to ICLs, although the underlying molecular mechanisms have not been resolved.

Fanconi Anemia (FA) is a genomic instability syndrome caused by mutations in any of the twenty-two known genes that participate in the FA pathway (Cheung and Taniguchi, 2017; Michl et al., 2016). A subset of FA proteins assemble at the ICL to form the FA core complex (Ceccaldi et al., 2016; Zhang and Walter, 2014). The FA core complex is responsible for the recruitment and ubiquitination of the FANCI-FANCD2 (ID2) heterodimer at the damage site, events often used experimentally as a marker of FA pathway activation (Knipscheer et al., 2009; Smogorzewska et al., 2007). The ID2 dimer then recruits downstream endonucleases (SLX4, XPF1-ERCC1) that unhook the ICL, releasing the covalent linkage between the complementary strands and generating a double strand break (DSB) (Kim et al., 2013). After

unhooking, translesion polymerases bypass the lesion, and synthesis of the lesion containing strand is completed. The unhooked ICL is later removed by nucleotide excision repair, while the double-stranded break (DSB) is repaired by homologous recombination (HR) (Long et al., 2011; Michl et al., 2016).

One consequence of dysfunctional ICL repair, as seen in FA patients, is the formation of aberrant chromosomal structures known as radial chromosomes, believed to reflective defective repair events involving non-homologous chromosomes. Mutations in several HR/FA genes, such as BRCA1/2, RAD51, and FANCD2, result in radial formation and other FA phenotypes (Long et al., 2011). Recent studies showed that BRCA1/2 deficient cells, nascent DNA strands at stalled replication forks undergo MRE11-dependent fork degradation in response to replication stress, implicating BRCA1/2 in maintaining fork stability (Ray Chaudhuri et al., 2016; Schlacher et al., 2011; Schlacher et al., 2012). Along with BRCA1 and BRCA2, RAD51 and FANCD2 additionally function as central players in stabilizing stalled replication forks (Ray Chaudhuri et al., 2016; Rondinelli et al., 2017; Schlacher et al., 2012; Sotiriou et al., 2016; Xu et al., 2017). Interestingly, HUS1 loss also resulted in radial chromosome formation and decreased HR repair efficiency in cells, further hinting at an interplay between the 9-1-1 complex, HR and fork stability pathways (Balmus et al., 2016; Levitt et al., 2007; Wang et al., 2006b).

Given that *Hus1* deficiency results in hallmark features of FA, we tested its roles in responding to ICLs. In addition to interacting with several FA proteins, the 9-1-1 complex was found to be required for recruitment of FANCD2 as well as the HR proteins RAD51 and BRCA1 onto chromatin upon MMC-induced DNA-ICLs.

Furthermore, *Hus1* deficiency resulted in MRE11-dependent fork degradation following replication stress. The outer surface of the 911 complex was found to be necessary for FANCD2 and RAD51 localization, functions that were independent of checkpoint signaling. Meanwhile ATR activation by 9-1-1 was essential for BRCA1 recruitment, protection against fork degradation, and suppression of radial chromosome formation. These findings highlight dual roles for the 9-1-1 complex in regulating FA-mediated ICL repair and stabilizing stalled replication forks to maintain genome integrity.

3.3 MATERIALS AND METHODS

Cell culture and treatments - *Hus1*$^{-/-}$*p21*$^{-/-}$ and *Hus1*$^{+/+}$*p21*$^{-/-}$, *Hus1*$^{-/-}$*p53*$^{-/-}$ and *Hus1*$^{+/-}$ *p53*$^{-/-}$, MEFs were described previously in (Lim et al., 2015). *Rad9a*$^{+/+}$ or *Rad9a*$^{SA/SA}$ cells and *Fancd2*- or *Fanca*-null MEFs were generated from 13.5 days old embryos and immortalized with Large T antigen. MEFs and 293T cells were grown in DMEM with 10% BCS cells and 1% Penicillin-Streptomycin, 1% NEA and 1% L-Glutamine. Stable cell lines were created by selection in 1.83μg/mL puromycin. Generation of *Hus1*$^{-/-}$ cells complemented empty vector, WT-HUS1 or PM4-HUS1 is previously described in (Lim et al., 2015) (Refer to Table 3.1 for details).

Survival assays - Short term viability assays were carried out by seeding 10,000 cells in triplicate in 6-well plates 24 hour prior to treatment with and without genotoxin. For treatment with MMC (Abcam), 0.20μg, 0.30μg, or 0.40μg for 1 hour. For trioxsalen,

cells were treated for 20 minutes with either 100μM, 1μM, or 0.1μM of psoralen and then activated with 5.0J/cm^2 of UVA. 72 hours post treatment cells were stained with Trypan blue dye and counted using a hemocytometer. Percent survival was calculated by dividing the average of cells treated with genotoxin by cells untreated. Error bars ± SD. Statistical analysis was carried out by Student's T-test, and p-values of <0.05 were considered significant.

Chromatin fractionation - *Hus1*$^{-/-}$*p21*$^{-/-}$ MEFs stably expressing WT, PM4 and A6 HUS1 proteins were treated with 20 μg of MMC overnight before fractionating the cells as described in (Méndez and Stillman, 2000) with a few modifications. Cells were hypotenized using Buffer 1 (10 mM HEPES, pH7.9; 10mM KCl; 1.5 mM $MgCl_2$; 0.34 M sucrose; 10% glycerol; 1mM DTT; 0.3 mM PMSF) for 5 minutes, before centrifuging them at 5000g for 5 minutes to separate the cytoplasmic (supernatant) and nuclear fraction (pellet). The pellet (nuclear fraction) was lysed using Buffer 2 (3 mM EDTA, 0.2 mM EGTA, 1mM DTT, 0.3 mM PMSF) and incubated for 30 minutes on ice. After centrifugation at 5000g for 5 minutes, the supernatant (soluble nuclear fraction) was collected and the pellet (chromatin fraction) was resuspended with Buffer 3 (10 mM Tris-HCl pH 8.0, 5 mM KCl, and 1mM $CaCl_2$) along with 1 unit of Micrococcus nuclease. The solution was incubated at 37^{o}C for 10 minutes before centrifuging at 14000 rpm for 10 minutes to produce the chromatin fraction in the supernatant. 20 μg of the chromatin fraction were used for immunoblotting.

Table 3.1 - Key Resources Table

Reagent or Resource	Source
Mouse monoclonal anti-Flag	Sigma-Aldrich
Rabbit polyclonal anti-FANCD2	Novus Biological
Mouse monoclonal anti-γH2Ax	Millipore
Rabbit monoclonal anti-GAPDH	Cell Signaling Technology
Mouse monoclonal anti-αtubulin	Sigma-Aldrich
Rabbit polyclonal anti-Histone3	Cell Signaling Technology
Mouse polyclonal anti-Histone3	Sigma-Aldrich
Mouse monoclonal anti-HA	Covance
Rabbit polyclonal anti-pCHK1 (S317)	Cell Signaling Technology
Rabbit polyclonal anti-RAD51	Millipore
Rabbit polyclonal anti-pRPA32 (S4/S8)	Bethyl Laboratories
Rat monoclonal anti-RPA32	Cell Signaling Technology
Rat monoclonal anti-BrdU	Abcam
Mouse monoclonal anti-BrdU	BD Biosciences
Mouse monoclonal anti-BrdU	Cell Signaling Technology
Rabbit monoclonal anti-mBRCA1	R. Greenberg Lab (UPenn)
Rabbit polyclonal anti-53BP1	Novus Biologicals
Mouse monoclonal anti-PCNA	Santa Cruz
Rabbit polyclonal anti-MRE11	Novus Biologicals
Rabbit anti-MRE11	J. Petrini Lab (MSKCC)
Goat anti-rat Alexa Fluor 594	Thermo Fisher
Goat anti-mouse Alexa Fluor 488	Thermo Fisher
Goat anti-rabbit Alexa Fluor 594	Thermo Fisher
Goat anti-rabbit Alexa Fluor 488	Thermo Fisher
Goat anti-rat Alexa Fluor 488	Cell Signaling Technology
Goat anti-mouse Alexa Fluor 555	Thermo Fisher
Goat polyclonal anti-rabbit HRP	Southern Biotech
Horse anti-mouse HRP	Cell Signaling Technology
CldU	Sigma-Aldrich
IdU	Sigma-Aldrich
BrdU	Sigma-Aldrich
Hydroxyurea	Sigma-Aldrich
Puromycin	Corning
Mirin	Sigma-Aldrich
Mitomycin C	Abcam
Lipofectamine 3000	Thermo Fisher Scientific
Trioxsalen	Tokyo Chemical Industry Co.
ATR inhibitor (AZD6738)	Selleckchem
DNA-PK inhibitor (NU7441)	Selleckchem
ATM inhibitor (KU55933)	Selleckchem
CHK1 inhibitor (**AZD7762**)	Selleckchem

KaryoMAX Colcemid	Thermo Fisher Scientific
Micrococcal Nuclease	Thermo Fisher Scientific
Anti-FLAG M2 affinity gel	Sigma-Aldrich
HEK293T	(Lim et al., 2015)
MEFs (*Hus1*)	(Lim et al., 2015)
MEFs (*Rad9a*)	This Study
MEFs (*Fancd2*, *Fanca*)	(Balmus et al., 2015)
Plasmid: HUS1-3xFLAG	(Lim et al., 2015)
Plasmid: HUS1-HA	This Study
Plasmid: FANCI-HA	This Study
Plasmid: FANCG-FLAG	This Study
Plasmid: pCMV14-3xFlag	Sigma-Aldrich
Plasmid: pBABE-puro-EV	(Lim et al., 2015)
Plasmid: pBABE-puro-HUS1	(Lim et al., 2015)
Plasmid: pBABE-puro-PM4	(Lim et al., 2015)
Prism	GraphPad
FlowJo	FlowJo
Photoshop	Adobe

Metaphase spread preparation - MEFs were seeded in 10cm dishes and grown until 70% confluence was reached. Then, cells were treated with 20ng, 30ng or 40ng/ml for 24 hours. Cells were then incubated in 0.10 μg/ml Colcemid for 1 h. Cells were then harvested by trypsinization, incubated for 7 min at 37°C in hypotonic buffer (0.034M KCl, 0.017M $Na_3C_6H_5O_7$), and fixed for at least 20 min at 4°C in 75% methanol-25% acetic acid three times. Cells in fixative were then spotted onto microscope slides and stained with 2.0% Giemsa in Gurr buffer (pH 6.8).

Immunofluorescence Staining -For IF staining cells were seeded on 0.01 % gelatin coated glass coverslips in 6 well dishes and allowed to attach for 24 hours. Then cells were treated with 5μM Hydroxyurea, 2000ng of MMC or 10 Gy of IR at indicated time points. When staining for FANCD2, cells were pre-extracted with 0.5 % Triton-X 100 for 1 minute before fixation with 4% PFA for 20 min at RT. Following fixation cells were washed in 1X PBS, then permeabilized with 0.5 % NP40 for 20 min. Cells were then blocked in PBG (0.2% cold water fish gelatin and 0.5% BSA for 20 minutes and incubated in primary antibody solution at a concentration of 1:500 overnight. The next day, cells were triple rinsed in 1X PBS and incubated in a 1:1000 dilution of secondary antibody (Alexafluor 488 A11034 anti-rabbit) for two hours in the dark. Cells were mounted in DAPI containing 0.05% DAPI mounting medium and imaged the same day using a Leica DMRE fluorescence microscope. For γH2AX immunofluorescence staining cells were grown and treated as above but fixed with methanol, triple rinsed in 1X PBS and permeablized in 3% BSA. Next, cells were incubated with anti-γH2AX primary antibody and goat anti-mouse Alexa Fluor 488

secondary antibody. Immunofluorescence co-staining was performed on *Hus1*$^{-/-}$*p21*$^{-/-}$ MEFs stably expressing WT or mutant mHUS1-3XFLAG proteins. Cell were grown and treated as described above, then immunostained with mouse α-FLAG and rabbit α-FANCD2 primary antibodies overnight one antibody at a time. Alexa Fluor 488 goat α -mouse and 555 goat α-rabbit secondary antibodies were used for IF detection according to antibody manufacturer's instruction.

For RPA32, BRCA1, 53BP1, FANCD2 and RAD51 staining, cells were pre-extracted with CSK buffer for 5 minutes on ice followed by 4% PFA fixing for 15 minutes. Cells were further fixed by incubating them in 75% ethanol for 5 minutes on ice, followed by 15% BCS + 2% BSA block. Cells were incubated with the respective antibodies (RPA32 and RAD51) overnight at 1:1000 concentration (4^{o}C), followed by 1:500 secondary incubation at room temperature for 1 hour. Finally, cells were mounted in DAPI containing 0.05% DAPI mounting medium and imaged the same day using a Leica DMRE fluorescence microscope.

For MRE11 staining, cells were pre-extracted with CSK buffer for 5 minutes on ice followed by methanol fixing for 15 minutes at -20^{o}C. Rest of the protocol similar as above (Refer to Table 3.1 for details).

LUMIER with BACON - Was performed as described before (Barrios-Rodiles et al., 2005) 3xFLAG-tagged constructs were transfected in 96-well format in duplicates into HEK293T-derived reporter cell lines using polyethylenimine. To avoid spatial gradients in transfection efficiency plates were incubated at room temperature for 30 minutes before transfer to 37°C (5% CO_2). Two days after transfection, cells were

washed in 1xPBS using an automated plate washer (Biotek ELx406) and lysed in 50mM HEPES [pH 7.9]/150mM NaCl/10mM $MgCl_2$/20mM Na_2MoO_4/0.7% TritonX-100/5% glycerol, protease and phosphatase inhibitors, benzonase and RNAseA. The lysates were transferred with an automated liquid handler (Tecan) into 384-well plates that had been coated with monoclonal anti-FLAG M2 antibody (Sigma-Aldrich, F1804) and blocked with 3% BSA/5% sucrose/0.5% Tween 20. Plates were incubated at 4°C for 3 hr, after which plates were washed with HENG buffer (Taipale et al., 2012) using an automated plate washer. Luminescence was measured with a plate reader using Gaussia Flex luciferase kit. To determine FLAG bait protein expression levels, after luminescence measurement, HRP-conjugated anti-FLAG antibody in ELISA buffer (1xPBS, 2% goat serum, 5% Tween 20) was added to wells. Plates were incubated for 90 minutes at room temperature and were subsequently washed in 1xPBS/0.05% Tween 20 with an automated plate washer. ELISA signal was detected using a chemiluminescent substrate. LUMIER Interaction Scoring. To correct for variability in cell number across wells LUMIER signal was normalized against the luminescence of the total cell extract (5%). Background ratios fit a log-normal distribution, and thus we calculated z-scores for each protein-protein interaction. Three independent experiments were performed and average z-scores and standard deviations were plotted.

Co-Immunoprecipitation and Immunoblotting - To analyze the interaction of HUS1 with FANCD2, FANCG and FANCI protein, HEK293T cells transiently transfected with pCMV-HUS1-3xFLAG, or pCMV-HUS1-HA and FANCI-HA or

FANCG-3xFLAG constructs were treated with 20 µg of MMC or DMSO as control. After 24 hours of treatment, the cells were fractionated to isolate nuclear fraction and subsequently protein lysates are prepared for co-IP analysis. Lysates were incubated with Anti-Flag M2 resin or Anti-HA antibody overnight before immunoblotting. For analysis of HUS1 mutants' interaction with FANCI and FANCD2, HEK293T cells were transiently transfected with pCMV-3XFLAG construct containing either wildtype HUS1, HUS1-R4D (PM1), HUS1-V151Y (PM3) or HUS1-R4D+V151Y (PM4). Cells were treated with 20 µg of MMC, before fractionation and cell lysate preparation described above. Lysates were incubated with Anti-FLAG resin. Immunoprecipitates and total cell lysates were resolved by SDS-PAGE. Standard immunoblotting procedures were performed (Refer to Table 3.1 for details).

ssDNA BrdU assay - *Hus1*$^{-/-}$*p21*$^{-/-}$ and control cells were incubated in 10 µg/ml of BrdU for at least 24 hours before plating as described above. The cells were maintained in BrdU for the duration of the MMC or mock treatment. The staining was performed according to the manufacturer's instructions.

Flow cytometry based chromatin protein detection - *Hus1*$^{-/-}$*p21*$^{-/-}$ and control cells were treated with 2000ng of MMC at indicated time points. The cells were subject to protocol described in (Forment and Jackson, 2015).

DNA Fiber Analysis - DNA fiber assays (Fig 5A-C and S7A) were performed as previously described (Schlacher et al., 2011). Cells were pulse labeled with 100 µM

CldU and 100 μM IdU for 20 minutes followed by untreated or treated with 4 mM HU as indicated. 2000–4000 cells were lysed in lysis buffer (0.5% SDS, 200 mM Tris-HCl pH 7.4, 50 mM EDTA). DNA fibers were spread on microscope slides and fixed in methanol/acetic acid (3:1 by volume). DNA was denatured in 2.5 M HCl for 30 min, followed by 1 h blocking buffer (10% goat serum and 0.1% Triton-X in PBS). Slides were incubated with primary antibodies, anti-CldU (1:100) and anti-IdU (1:75) followed by secondary antibodies, anti-rat Alexa Fluor 488 and anti-mouse Alexa Fluor 594 (1:100), for 1 h each in blocking buffer at room temperature. Slides were mounted in Prolong with DAPI before image acquisition under Axio2 microscope (Zeiss). Images were analyzed with FIJI (ImageJ) software (Refer to Table 3.1 for details).

DNA Combing Analysis - DNA combing assays were performed as previously described (Rondinelli et al., 2017). Cells were pulse labeled with 50 μM CldU and 250 μM IdU for 30 minutes followed by untreated or treated with 4 mM HU with or without 25uM of Mirin as indicated. Preparation of plugs and molecular combing was performed according to the manufacture's protocol (Genomic Vision). Post DNA combing, the glass slides were denatured using 0.5M NaOH and 1M NaCl for 8 minutes before blocking with Block-Aid for 30 minutes. Slides were incubated with primary antibodies, anti-CldU (1:100) and anti-IdU (1:75) followed by secondary antibodies, anti-rat Alexa Fluor 488 and anti-mouse Alexa Fluor 594 (1:100), for 1 h each in blocking buffer at room temperature. Slides were mounted in Prolong with DAPI before image acquisition.

3.4 RESULTS

9-1-1 complex dysfunction causes cellular hypersensitivity to DNA crosslinking agents and leads to ICL-induced radial chromosome formation.

Previous studies indicated that *Hus1*-deficient cells are hypersensitive to ICL-inducing agents (Lim et al. 2015; Balmus et al. 2016). To compare the degree of MMC sensitivity in *Hus1*-null cells to that of *Fanca*- or *Fancd2*-null cells, we performed short term survival assays on MMC-treated and untreated mouse embryonic fibroblasts (MEFs). Direct comparison among the cell lines revealed *Hus1*-null cells to be comparably sensitive to MMC as *Fanca*- or *Fancd2*-null MEFs (Fig. 3.1A and B). Hypersensitivity was also observed in *Hus1*-null MEFs upon treatment with UVA-activated Trioxsalen, another crosslinking agent (Fig. 3.1C).

The sensitivity of *Hus1*-null cells to crosslinking agents raised the possibilities of faulty ICL repair. To test this hypothesis, we monitored chromosomal integrity following low dose MMC treatment of cells. Multiple independent *Hus1*-null MEF lines showed increased chromosomal damage relative to control lines (Fig. 3.1D, 3.1E, 3.2A, and 3.2B), including chromosome breaks, fusion events and radial chromosome formation (Table 3.2). Because the 9-1-1 complex forms punctate nuclear foci in MMC treated cells (Lim et al., 2015), we next tested if the 9-1-1 clamp co-localizes with FA proteins at damage sites by immunofluorescence. FANCD2 and HUS1-FLAG co-localized in a subset of MMC-treated cells (Fig 3.1F). Overall, these data indicate a connection between the 9-1-1 complex and FA pathway during ICL responses.

Figure 3.1. 9-1-1 complex dysfunction causes cellular hypersensitivity to DNA crosslinking agents and leads to ICL-induced radial chromosome formation. A-B. *Hus1*$^{-/-}$*p21*$^{-/-}$, control (*Hus1*$^{+/+}$*p21*$^{-/-}$), *Fancd2*$^{-/-}$, *Fanca*$^{-/-}$, and their respective controls (*Hus1*$^{+/+}$;*p21*$^{-/-}$, *Fancd2*$^{+/+}$, *Fanca*$^{+/+}$) were treated with the indicated doses of MMC and after 72 hours the number of viable cells was quantified. **C**. *Hus1*$^{-/-}$*p21*$^{-/-}$, and control (*Hus1*$^{+/+}$*p21*$^{-/-}$) cells were treated with the indicated doses of trioxsalen for 20 minutes and then exposed to 2.5 J/cm^2 UVA after 72 hours the number of viable cells was quantified. **D and E.** Metaphase chromosome analysis of *Hus1*$^{-/-}$*p21*$^{-/-}$ and control (*Hus1*$^{+/+}$*p21*$^{-/-}$) cells was performed following mock treatment or treatment with 60ng/ml MMC for 24h. **F.** Immunofluorescence co-staining for FANCD2 and HUS1 (FLAG) in *Hus1*$^{-/-}$*p21*$^{-/-}$ cells complemented with *Hus1-3xFLAG* following treatment with 2µg/ml MMC for 24h. Cells were counterstained with 0.05% DAPI.

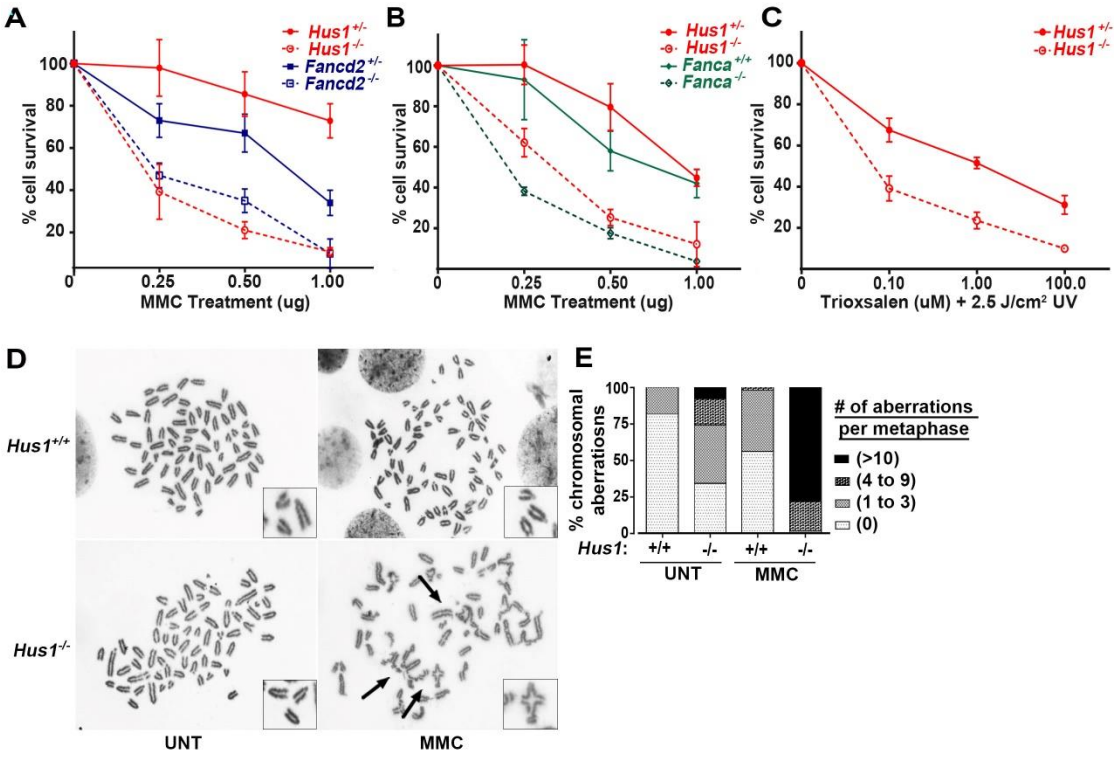
A
B
C
Hus1+/-
Hus1-/-
Fancd2+/-
Fancd2-/-
Fanca+/+
Fanca-/-
% cell survival
MMC Treatment (ug)
Trioxsalen (uM) + 2.5 J/cm² UV
D
Hus1+/+
Hus1-/-
UNT
MMC
E
% chromosomal aberrations
# of aberrations per metaphase
(>10)
(4 to 9)
(1 to 3)
(0)
Hus1:
+/+
-/-
UNT
MMC
F
FLAG
FANCD2
DAPI
MERGE
Hus1-/- +HUS1 3xFLAG
UNT
MMC

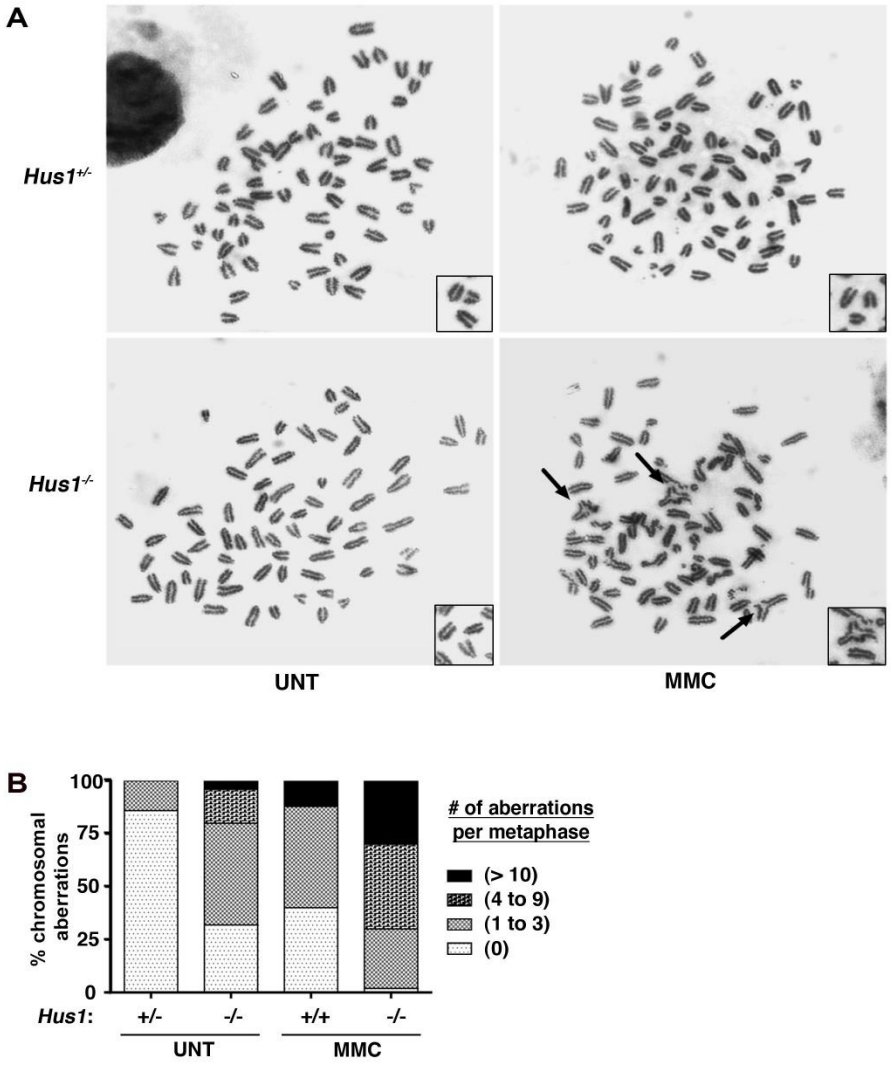

Figure 3.2. The 9-1-1 complex is required for suppresing radial chromosome formation upon MMC treatment. A and B. Metaphase chromosome analysis and quantification of *Hus1*-deficient (*Hus1*$^{-/-}$*p53*$^{-/-}$) and control (*Hus*$^{+/-}$ *p53*$^{-/-}$) cells following mock treatment or treatment with 60ng/ml MMC for 24h shown in independent cell line. Spreads categorized based on number of aberrations per spread.

Table 3.2. Chromosomal aberrations in *Hus1*$^{-/-}$ *p21*$^{-/-}$ and *Hus1*$^{+/+}$ *p21*$^{-/-}$ control cells following MMC treatment [a].

Genotype	Breaks/Gaps	Fusions	Acentric	Radials
Hus1$^{+/+}$ *p21*$^{-/-}$ (UNT)	3	5	4	0
Hus1$^{-/-}$ *p21*$^{-/-}$ (UNT)	8	27	72	0
Hus1$^{+/+}$ *p21*$^{-/-}$ (MMC)	6	6	15	0
Hus1$^{-/-}$ *p21*$^{-/-}$ (MMC)	139	143	303	24

[a] *Hus1*-deficient and control cells were treated with Mitomycin C (MMC) at 60ng/ml for 24 hours or mock treated (UNT). Then chromosome spreads were prepared and 50 spread per condition were counted.

HUS1 is required for FANCD2 focus formation and chromatin loading in response to ICLs.

FANCD2-FANCI heterodimer localization to damage sites is essential for FA pathway activation (Knipscheer et al., 2009). To elucidate the requirement for the 9-1-1 complex in FA pathway activation, we evaluated FANCD2 focus formation, a classic marker of FA pathway activation, in *Hus1*-null and control cells. MMC-induced FANCD2 foci were readily observed in presence of *Hus1*, but were not detected in multiple independent cell lines lacking *Hus1* (Fig. 3.3A, 3.4A, 3.4B and 3.4C). Importantly, complementation with WT-HUS1 restored MMC-induced FANCD2 focus formation in *Hus1*-null cells (Fig. 3.3B and C), affirming the role for HUS1 in FANCD2 loading during ICLs.

To rule out the possibility that the FANCD2 defect was due to a lower level of MMC-induced DNA damage in the absence of *Hus1*, we performed staining for γH2AX (3.3D, 3.4D and 3.4E). γH2AX focus formation occurred to a similar extent in *Hus1*-null and control cells, indicating that cells lacking *Hus1* failed to form FANCD2 foci despite experiencing MMC-induced damage. To confirm these findings, we performed chromatin fractionation on MMC-treated *Hus1*-null and control cells. MMC-treated *Hus1*-proficient cells showed the expected increase in the FANCD2 chromatin loading, however, chromatin loading of FANCD2 failed to occur in *Hus1*-null cells following treatment (Fig. 3.3E). Collectively, these results confirm a critical role for the 9-1-1 complex in FANCD2 recruitment to MMC-induced ICLs.

Figure 3.3. HUS1 is required for FANCD2 focus formation and chromatin loading in response to ICL. **A.** Parental *Hus1*$^{-/-}$*p21*$^{-/-}$, and *Hus1*$^{+/+}$*p21*$^{-/-}$ cells were treated with 1μg/ml MMC for 24h and stained for FANCD2. Nuclei were counterstained with 0.05% DAPI. **B.** *Hus1*$^{-/-}$*p21*$^{-/-}$ and *Hus1*$^{+/+}$*p21*$^{-/-}$ cells complemented with *Hus1*, or empty vector as a control, were treated and stained as in A. **C.** Quantification of the FANCD2 staining data shown in B. The number of FANCD2 foci per cell was counted in 50 cells per condition. **D.** Immunofluorescence staining for FANCD2 or γH2AX in MMC- or mock-treated cells of the indicated genotypes. **E.** Cells of the indicated genotypes were treated with 0.5 μg/mL of MMC, harvested, and subjected to chromatin fractionation. The chromatin fraction (CHR) or whole cell lysate (WCL) was immunoblotted with antibodies specific to FANCD2, GAPDH (cytosolic control), or Histone H3 (chromatin control).

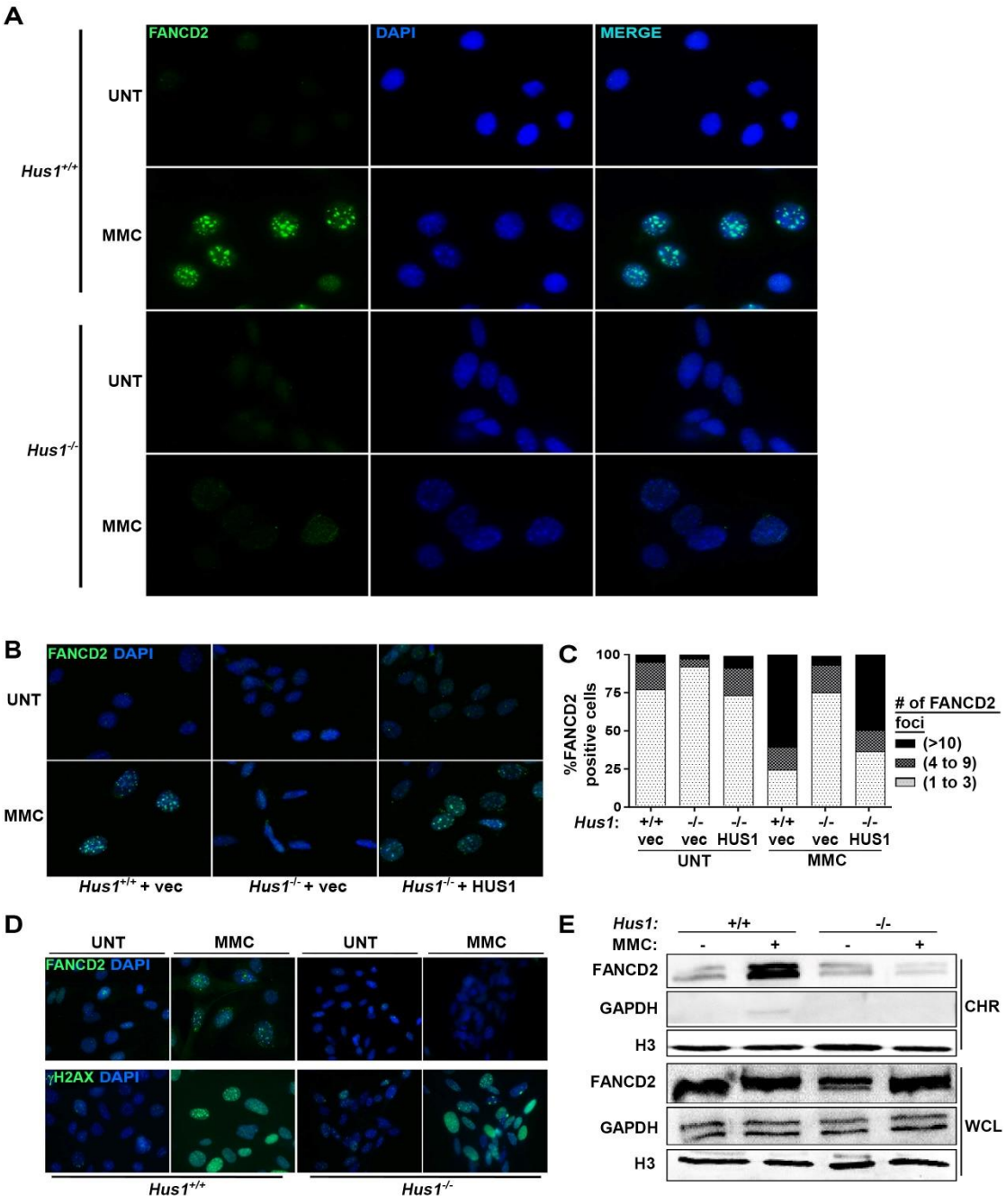
A
FANCD2
DAPI
MERGE
UNT
MMC
Hus1+/+
Hus1-/-
B
FANCD2 DAPI
UNT
MMC
Hus1+/+ + vec
Hus1-/- + vec
Hus1-/- + HUS1
C
%FANCD2 positive cells
100
75
50
25
0
# of FANCD2 foci
(>10)
(4 to 9)
(1 to 3)
Hus1:
+/+ vec
-/- vec
-/- HUS1
+/+ vec
-/- vec
-/- HUS1
UNT
MMC
D
UNT
MMC
UNT
MMC
FANCD2 DAPI
γH2AX DAPI
Hus1+/+
Hus1-/-
E
Hus1:
+/+
-/-
MMC:
-
+
-
+
FANCD2
GAPDH
H3
CHR
FANCD2
GAPDH
H3
WCL

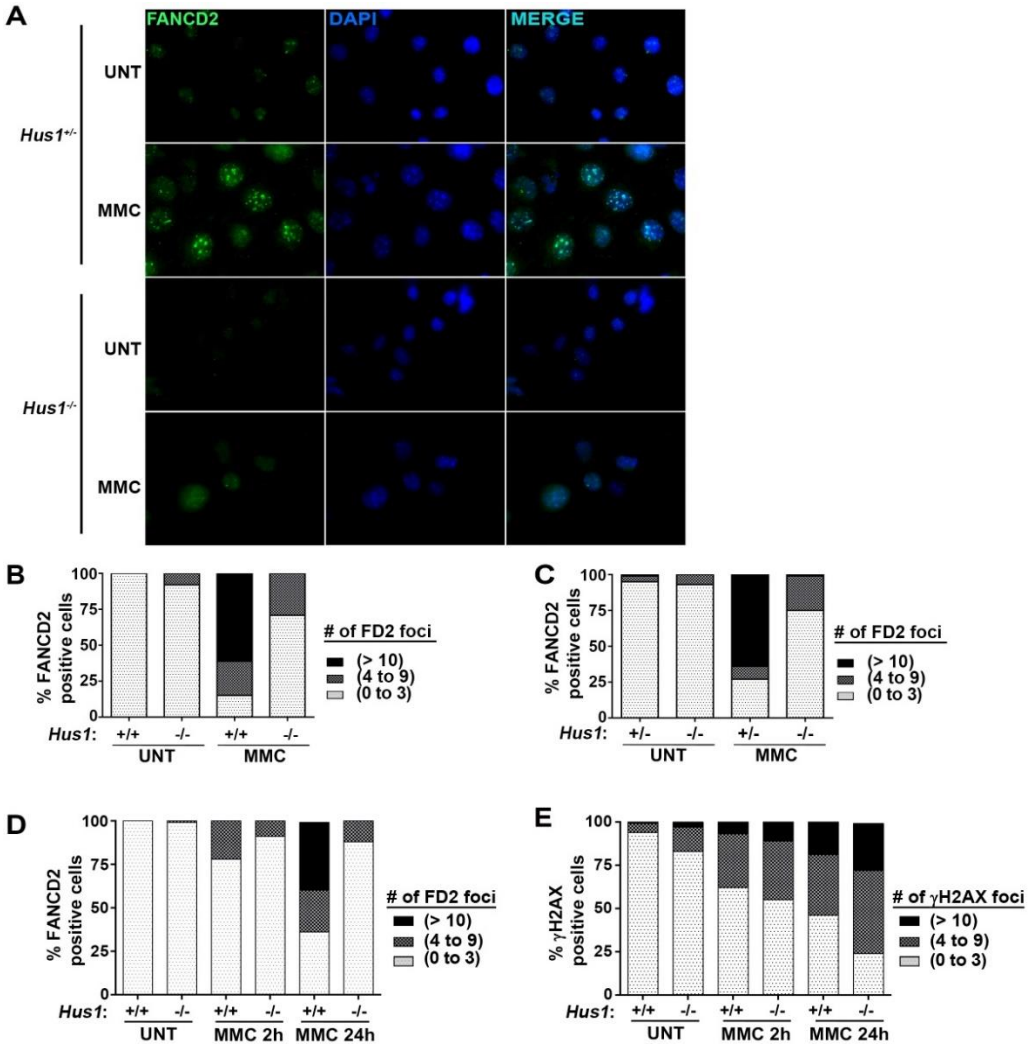

Figure 3.4. *Hus1* deficiency leads to loss of MMC-induced FANCD2 but not γH2AX focus formation. A. Immunofluorescence staining for FANCD2 in independent *Hus1* cell lines. *Hus1*-deficient (*Hus1*$^{-/-}$*p53*$^{-/-}$) and control (*Hus1*$^{+/-}$*p53*$^{-/-}$) cells were treated with 1μg/ml MMC for 24h. Nuclei were counterstained with 0.05% DAPI. **B.** Quantification of the FANCD2 staining data shown in Figure 2A. **C.** Quantification of the FANCD2 staining data shown in Supp. Figure 2A. **D.** Quantification of FANCD2 and **E.** γH2AX staining data after 2 and 24h of MMC treatment. The number of FANCD2 and γH2AX foci per cell was counted in 50 cells per condition.

The 9-1-1 complex physically associates with multiple Fanconi Anemia pathway proteins.

The 9-1-1 complex in known to interact with a plethora of DNA repair proteins, often binding multiple factors in the same pathway (Li et al., 2013; Lim et al., 2015; Ngo et al., 2014; Pandita et al., 2006; Takeishi et al., 2010). The defective cellular and molecular responses to crosslinking agents in *Hus1*-deficient cells raised the possibility of physical association between 9-1-1 and FA proteins. To screen for potential physical interactions, we performed luminescence-based mammalian interactome mapping (LUMIER) assays (Taipale et al., 2012). In LUMIER, FLAG-tagged bait and Renilla luciferase-tagged prey proteins are co-expressed in mammalian cells, and their ability to interact is quantified by a luciferase assay following FLAG IP. Luciferase-tagged 9-1-1 subunits were individually expressed in 293T cells and tested for interaction with FLAG tagged FA proteins, with luciferase-tagged PCNA serving as the negative control. Notably, LUMIER assays revealed that HUS1 and RAD9A-ΔC (lacking the C-terminal tail of RAD9A) interacted with several FA proteins (Fig. 3.5A). RAD9A showed the most robust interactions with FA proteins, including FANCG, FANCL, FANCM, PALB2, SLX4 and FANCF (listed in decreasing score for strength of interaction). HUS1 on the other hand showed significant interaction with PALB2, FANCG, FANCL, FANCA, FANCF, and FANCD2. Other pathway components fell just below our rigorous threshold for significance (z-score of 2), but nevertheless could be legitimate interactors, particularly since the LUMIER assay was done without genotoxin treatment. FANCC and FANCI were found to interact with luciferase alone and therefore were excluded

from further analysis. Interestingly, RAD1 displayed weak interactions with FA proteins but strongly associated with HUS1 as expected, suggesting that the assay reads out direct interactions rather than indirect contacts via associated 9-1-1 subunits. Overall, the results from LUMIER assays suggest that the 9-1-1 complex may promote FA signaling by acting as a scaffold that interacts with several pathway components.

To validate the potential physical interactions identified in the LUMIER screen, we performed co-immunoprecipitation (co-IP) experiments using FLAG-tagged HUS1 to detect either endogenous FANCD2 or overexpressed HA-FANCI. Both subunits of the ID dimer weakly interacted with FLAG-tagged HUS1 in the absence of MMC. However, a significant increase in nuclear HUS1 levels and robust interactions with FANCD2 and HA-FANCI accompanied MMC treatment (Fig. 3.5B and C). To test interactions between 9-1-1 and an FA core complex component, we co-expressed HA-HUS1 and FLAG-FANCG and found that HUS1 and FANCG interacted with each other in a treatment dependent manner (Fig. 3.5D).

9-1-1 complex subunits associate with binding partners via the outer surface of the clamp, paralleling the mechanism utilized by PCNA. Indeed, FANCD2 is known to interact with PCNA in this manner (Howlett et al., 2009). We recently established that the HUS1 outer surface features two functionally important and conserved hydrophobic pockets where effector proteins are likely to bind. To disrupt protein interaction mediated through these pockets, we mutated one residue in each pocket, creating HUS1 mutants R4D (pocket mutant 1; PM1) and V151Y (PM3). Expression of the double mutant (R4D+V151Y (PM4)) in *Hus1*-null cells caused MMC hypersensitivity greater than either single mutant and was also found to be impair

Figure 3.5. 9-1-1 subunits directly interact with multiple Fanconi Anemia pathway components. A. LUMIER BACON analysis to reveal interactions between RAD9-HUS1-RAD1 subunits with FA proteins. Luciferase tagged 9-1-1 complex subunits and FLAG tagged FA proteins were used to perform this assay. **B-D.** Co-immunoprecipitation (co-IP) analysis to assess interactions between human FANCD2, FANCI-HA, or FANCG-3XFLAG and HUS1. 293T were transiently transfected with vector alone or plasmids encoding HUS1-3xFLAG (B, C), FANCI-HA (C), FANCG-FLAG (D), or HUS1-HA (D). Protein lysates were prepared from isolated nuclei after treatment of the cells with 0.5 μg/mL MMC or DMSO. Immunoprecipitations were performed with anti-FLAG M2 resin followed by immunoblotting with antibodies specific to FLAG M2, HA, or FANCD2. **E, F**. Co-IP analysis of interaction between FANCD2 or FANCI-HA and wildtype or mutant HUS1-3xFLAG. Nuclear proteins were isolated after treating the cells with 0.5 μg/mL MMC and immunoprecipitations and immunoblotting were performed as in B-D.

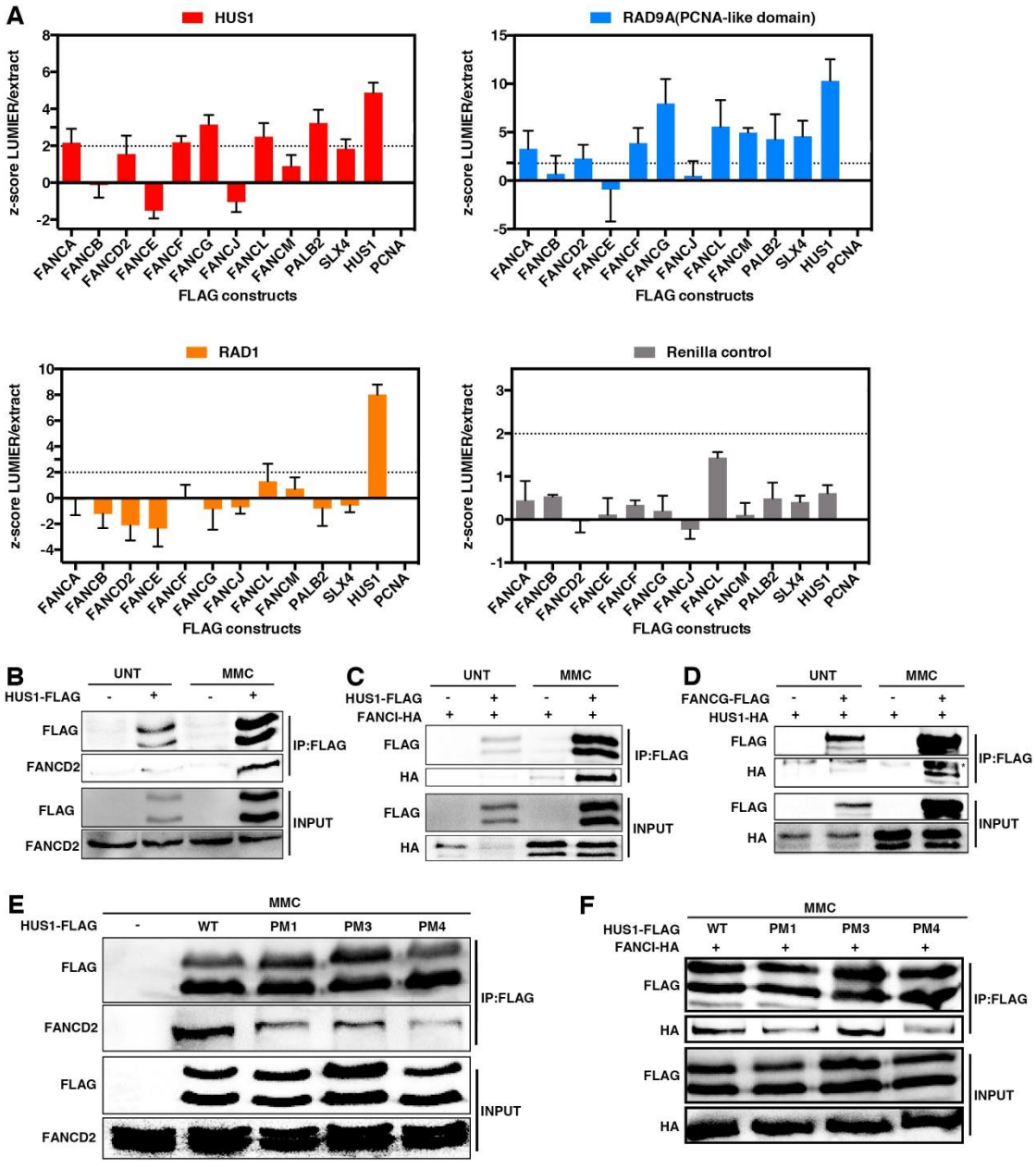
A
HUS1
RAD9A(PCNA-like domain)
RAD1
Renilla control
z-score LUMIER/extract
FANCA FANCB FANCD2 FANCE FANCF FANCG FANCJ FANCL FANCM PALB2 SLX4 HUS1 PCNA
FLAG constructs
B
UNT
MMC
HUS1-FLAG
FLAG
FANCD2
IP:FLAG
INPUT
C
HUS1-FLAG
FANCI-HA
HA
D
FANCG-FLAG
HUS1-HA
E
WT
PM1
PM3
PM4
F

interaction between HUS1 and a known binding partner, MYH1 (Lim et al., 2015). Importantly, all the HUS1 outer surface mutants were fully functional for clamp formation, chromatin loading, and activation of ATR checkpoint signaling (Lim et al., 2015). Hence, these separation of function mutants are useful for distinguishing between the checkpoint signaling-dependent and -independent roles of the 9-1-1 complex in DNA repair. Co-IP revealed modest reduction in FANCD2 binding with PM3 mutant, a more substantial defect in both FANCD2 and FANCI binding with PM1 mutant. However, the greatest disruption of FANCD2 and FANCI binding with HUS1 was observed with the PM4 double mutant (Fig. 3E and F). These results suggest that both HUS1 outer surface hydrophobic pockets contribute to interactions between HUS1 and the ID2 dimer.

The 9-1-1 complex promotes RAD51 localization to chromatin in response to MMC-induced replication stress.

The FA pathway activation defect in *Hus1*-deficient cells prompted us to additionally assess downstream events in the response to ICLs. During ICL repair, the generation of DSB following ICL unhooking initiates endonuclease-mediated DNA end resection. The resected DNA ends provide a template for RAD51 loading and nucleoprotein filament formation, which is necessary for strand invasion and error free repair (Long et al., 2011). To examine downstream HR activity during ICL repair, we measured RAD51 focus formation in *Hus1*-null and control cells. RAD51 focus formation was completely abolished in MMC- treated *Hus1*-deficient cells at all investigated time points (2-24h) (Fig. 3.6A, 3.7A, C, 3.8A). In MMC-treated *Hus1*-

proficient cells, RAD51 foci were readily formed as early as 2h and the foci persisted up to 24h (Fig. 3.6A, 3.7A, C, 3.8A). Similar results were observed with another replication stress-inducing agent, hydroxyurea (HU), but IR treatment induced RAD51 foci irrespective of *Hus1* status (Fig. 3.6A). Detailed time course analysis revealed that RAD51 foci were slightly decreased in *Hus1*-null cells after prolonged exposure to IR treatment (24h); however, they remained similar between the genotypes at other times post IR (2, 6 and 12h) (Fig. 3.7B,D, S4). Similarly, chromatin fractionation analysis confirmed the RAD51 chromatin loading defects after MMC treatment in *Hus1*-null cells compared to those complemented with wild-type HUS1 (Fig. 3.6B). By contrast, RAD51 chromatin loading was observed after IR treatment even in the absence of *Hus1* (Fig 3.6C). Both *Hus1*-null and control cells displayed similarly increased γH2AX focus formation following MMC, HU, or IR, indicating that RAD51 loading fails despite extensive DNA damage (Fig. 3.8C). These results indicate that the 9-1-1 complex is important for RAD51 loading in a lesion-specific manner.

RAD51 loading fails to occur in *Hus1*-deficient cells despite the presence of RPA-coated ssDNA after MMC.

RAD51 loading has been found to precede DSB formation following ICL-induced replication stress (Zhang and Walter, 2014), suggesting that the RAD51 loading defect in *Hus1*-deficient cells was not merely a consequence of FANCD2 dysfunction. Consistent with this, RAD51 foci were readily visualized in both *Fancd2*$^{-/-}$ and *Fancd2*$^{+/+}$ cell lines upon MMC treatment (Fig. 3.7E-F). Thus, the 9-1-1 complex independently recruits both FANCD2 and RAD51 to chromatin in response to MMC.

Figure 3.6. The 9-1-1 complex promotes RAD51 localization to the DNA in response to MMC-induced replication stress. A. Immunofluorescence staining for RAD51 in *Hus1*$^{-/-}$*p21*$^{-/-}$, and *Hus1*$^{+/+}$*p21*$^{-/-}$ following treatment with 0.5 µg/ml MMC, 1mM HU or 10Gy of IR treatment for 16 hours. Cells were counterstained with 0.05% DAPI. **B-C**. Immunoblot analysis of chromatin fractions (CHR) or whole cell lysate (WCL) prepared from cells of the indicated genotypes were treated with 0.5 µg/mL MMC **(B)** or 10Gy of IR **(C)** treatment. Antibodies specific to RAD51, phospho-RPA32 (S4/S8), RPA32, FANCD2, GAPDH and Histone H3 were used. **D.** Immunofluorescence staining for RPA in *Hus1*$^{-/-}$*p21*$^{-/-}$, and *Hus1*$^{+/+}$*p21*$^{-/-}$ following treatment with 0.5 µg/ml MMC, 1mM HU or 10Gy of IR treatment for 16 hours. Cells were counterstained with 0.05% DAPI. **E.** Quantification of the RPA staining data shown in C.

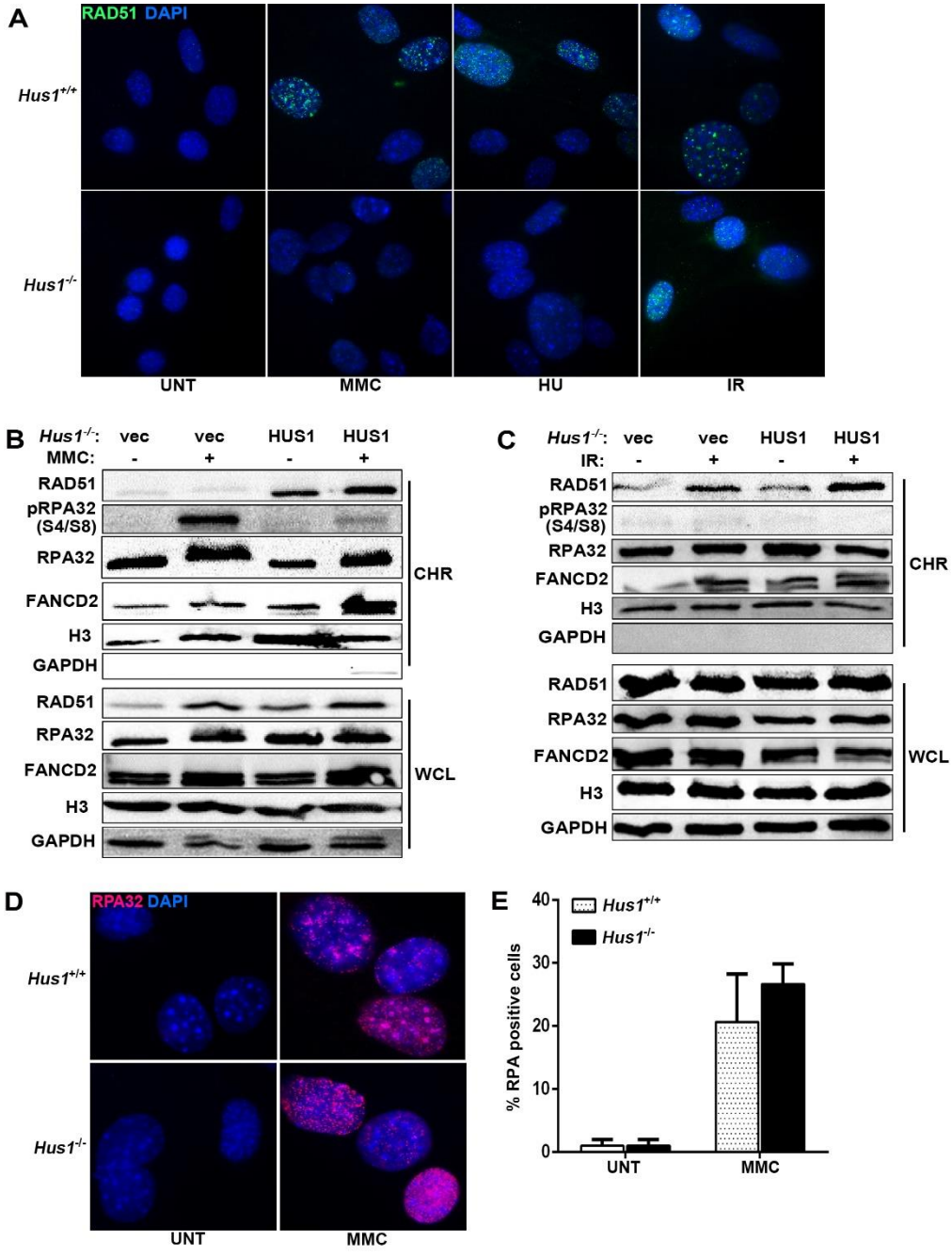
A
RAD51 DAPI
Hus1+/+
Hus1-/-
UNT
MMC
HU
IR
B
Hus1-/-: vec vec HUS1 HUS1
MMC: - + - +
RAD51
pRPA32 (S4/S8)
RPA32
FANCD2
H3
GAPDH
CHR
RAD51
RPA32
FANCD2
H3
GAPDH
WCL
C
Hus1-/-: vec vec HUS1 HUS1
IR: - + - +
RAD51
pRPA32 (S4/S8)
RPA32
FANCD2
H3
GAPDH
CHR
RAD51
RPA32
FANCD2
H3
GAPDH
WCL
D
RPA32 DAPI
Hus1+/+
Hus1-/-
UNT
MMC
E
Hus1+/+
Hus1-/-
% RPA positive cells
40
30
20
10
0
UNT
MMC

Figure 3.7. HUS1 is required for RAD51 function in response to replication stress. A-B. Immunofluorescence staining for RAD51 in *Hus1*-deficient (*Hus1*$^{-/-}$*p21*$^{-/-}$) and control (*Hus1*$^{+/+}$ *p21*$^{-/-}$) cells were treated with 0.5 μg/ml MMC or 10Gy of IR for a time course from 2 to 24h. Nuclei were counterstained with 0.05% DAPI. **C-D.** Quantification of results from A-B. **E.** Immunofluorescence staining for RAD51 in *Fancd2*-deficient (*Fancd2*$^{-/-}$) and control (*Fancd2*$^{+/-}$) cells. Cells were treated with 0.5 μg/ml MMC, for 4 hours. Nuclei were counterstained with 0.05% DAPI. **F.** Quantification of RAD51 staining shown in E.

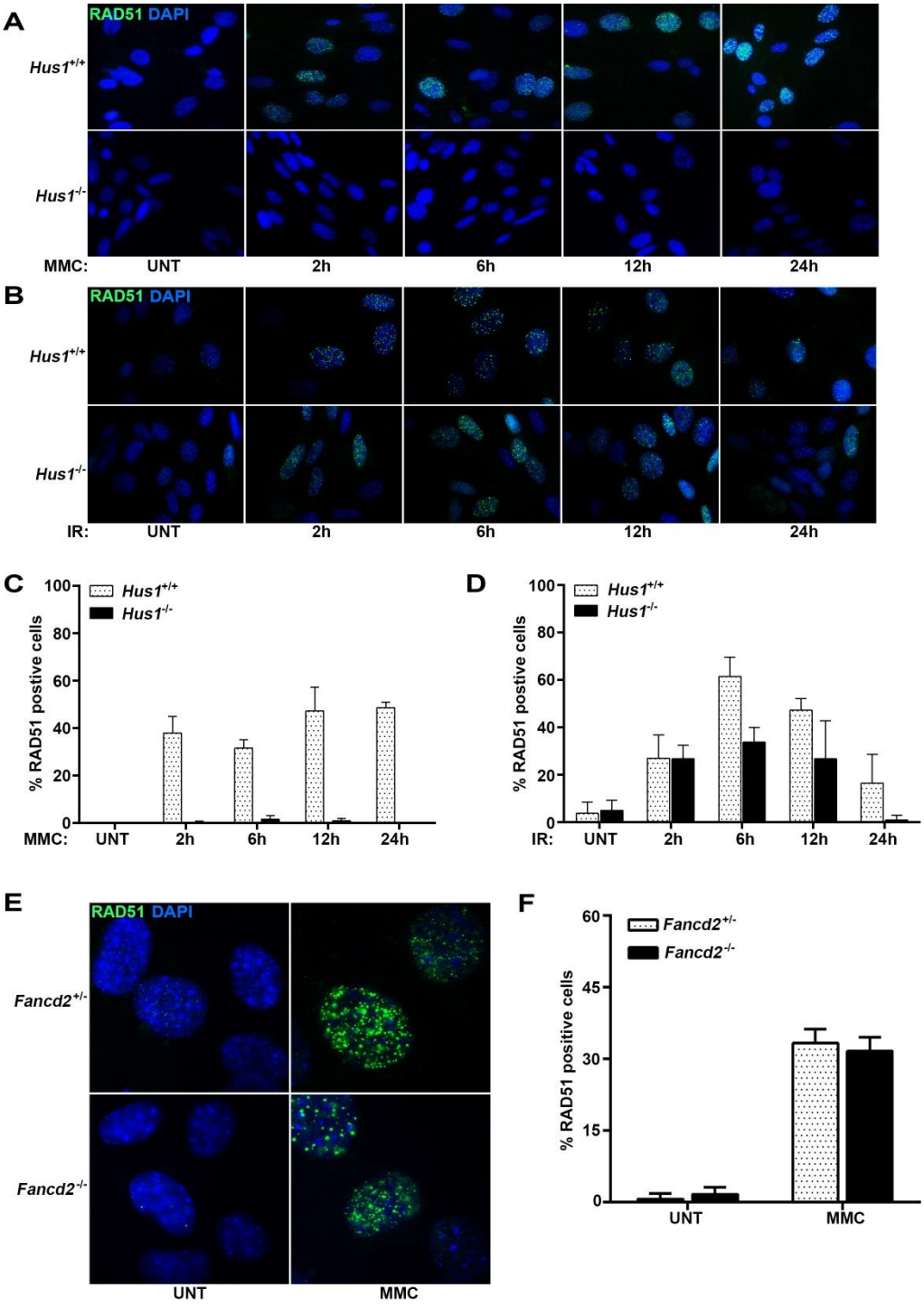
A
RAD51 DAPI
Hus1+/+
Hus1-/-
MMC:
UNT
2h
6h
12h
24h
B
RAD51 DAPI
Hus1+/+
Hus1-/-
IR:
UNT
2h
6h
12h
24h
C
Hus1+/+
Hus1-/-
% RAD51 postive cells
100
80
60
40
20
0
MMC:
UNT
2h
6h
12h
24h
D
Hus1+/+
Hus1-/-
% RAD51 postive cells
IR:
UNT
2h
6h
12h
24h
E
RAD51 DAPI
Fancd2+/-
Fancd2-/-
UNT
MMC
F
Fancd2+/-
Fancd2-/-
% RAD51 positive cells
60
45
30
15
0
UNT
MMC

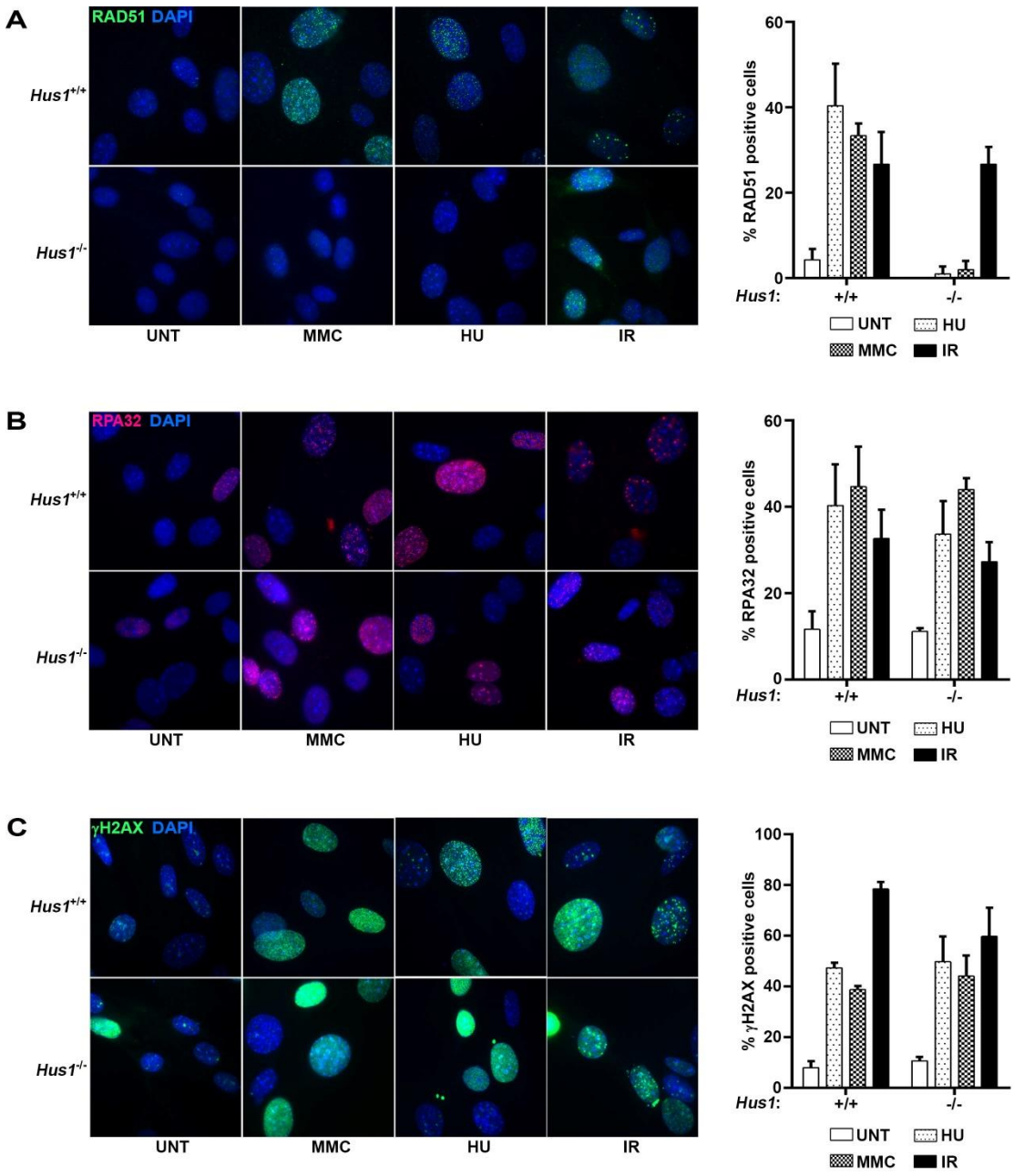

Figure 3.8. RAD51 defects observed upon *Hus1* loss are replication stress specific. **A-C.** Immunofluorescence staining for **A.** RAD51, **B.** RPA32 and **C.** γH2Ax carried out side by side, in *Hus1*-deficient (*Hus1*$^{-/-}$*p21*$^{-/-}$) and control (*Hus1*$^{+/+}$ *p21*$^{-/-}$) cells. Cells were treated with 0.5 μg/ml MMC, 10Gy of IR or 1mM of HU for 4 and 16 hours. Nuclei were counterstained with 0.05% DAPI.

During HR, RAD51 loading occurs on RPA-coated ssDNA, and failure of upstream events such as end resection and RPA loading could potentially contribute to RAD51 loading defects in MMC-treated *Hus1*-null cells (Huang et al., 2010; Kolinjivadi et al., 2017a). To confirm the presence of MMC-induced ssDNA in *Hus1*-null cells, we used native BrdU staining to observe ssDNA accumulation. It has been previously reported that MMC-induced ICLs do not produce long ssDNA stretches needed for detection of BrdU in this assays (Huang et al., 2010), and indeed we did not observe native BrdU staining in MMC-treated cells regardless of Hus1 status. We therefore induced replication stress using HU which does generate long stretches of ssDNA in wild-type cells and like MMC fails to trigger RAD51 loading in the absence of HUS1. Both *Hus1*-null and control cells showed similar native BrdU staining after HU (Fig. 3.9A), suggesting that the failure of replication stress-induced RAD51 loading in *Hus1*-deficient cells is not due to a lack of ssDNA formation.

Next, we investigated RPA localization, as RPA coating of ssDNA is a precursor to RAD51 loading. RPA foci were readily apparent in both *Hus1*-null and control cells following MMC treatment (Fig. 3.6D-E, 3.8B). Similarly, chromatin fractionation analysis confirmed genotoxin-induced RPA loading onto DNA, irrespective of *Hus1* status (Fig. 3.6B-C). The initial kinetics of RPA loading at early timepoints (2-12h) after MMC were similar in *Hus1*-null and control cells. However by 24h after MMC treatment, *Hus1*-null cells showed increased RPA foci as compared to controls (3.9B, C). An independent flow cytometry-based assay for chromatin binding also revealed increased RPA loading in *Hus1*-null cells compared to control cells at 16hr after MMC treatment (3.9D). Collectively, these findings suggest that the

failure of replication stress-induced RAD51 loading in *Hus1*-null cells does not stem from defects in ssDNA formation or RPA loading.

Interestingly, the RPA immunoblot revealed an increased molecular weight band in MMC-treated *Hus1*-null cells, suggesting the possibility of RPA hyperphosphorylation. RPA hyperphosphorylation at S4/S8 by ATM and/or DNAPKs has been found to suppress RAD51 loading onto DNA, although some studies suggest otherwise (Liu et al., 2012; Patel et al., 2017). MMC-treated *Hus1*-null cells displayed significantly elevated pRPA (S4/S8) levels and restoration of *Hus1* expression suppressed RPA S4/S8 hyperphosphorylation (Fig. 3.6B). To test whether RPA phosphorylation contributed to the RAD51 loading defect, we attempted to block RPA hyperphosphorylation by treating cells with the DNA-PK inhibitor (NU7441) and the ATM inhibitor (KU55933). Combined inhibitor treatment significantly reduced pRPA (S4/S8) levels, but failed to restore RAD51 loading in MMC-treated *Hus1*-null cells. (Fig. 3.10A).

The 9-1-1 complex protects stalled replication forks against MRE11-dependent fork degradation.

Recent studies have identified additional role for FANCD2 and RAD51 in stabilizing stalled replication forks and preventing MRE11-dependent fork degradation following replication stress (Schlacher et al., 2012). To assess the impact of *Hus1* loss on replication fork stability, we monitored nascent replication tracts by pulsing cells with CldU and IdU, followed by treatment with HU or MMC. As shown in Figure 3.11A, reduced *Hus1* levels in *Hus1* hypomorph cells were associated with a reduction in

Figure 3.9. RAD51 loading fails to occur in *Hus1*-deficient cells despite the presence of RPA-coated ssDNA after MMC. A. Immunofluorescence staining for BrdU carried out in *Hus1*-deficient (*Hus1*$^{-/-}$*p21*$^{-/-}$*)* and control (*Hus1*$^{+/+}$ *p21*$^{-/-}$*)* cells. Cells were untreated or treated with either 1mM HU or 1μg/ml MMC for 16 hours before analysis. One set of untreated cells were incubated with 1M HCl for 20 mins and used as positive control for BrdU staining. **B.** Immunofluorescence staining for RPA32 in *Hus1*-deficient (*Hus1*$^{-/-}$*p21*$^{-/-}$*)* and control (*Hus1*$^{+/+}$ *p21*$^{-/-}$*)* cells were treated with 0.5 μg/ml MMC for a time course from 2 to 24h. Nuclei were counterstained with 0.05% DAPI. **C.** Quantification of results from B. **D.** Flow cytometry-based chromatin binding protein assay was performed on *Hus1*-deficient (*Hus1*$^{-/-}$*p21*$^{-/-}$*)* and control (*Hus1*$^{+/+}$ *p21*$^{-/-}$*)* cells were either untreated or treated with 0.5 μg/ml MMC for 16 hours. Antibody against RPA32 was used to observe the RPA chromatin binding in the cells.

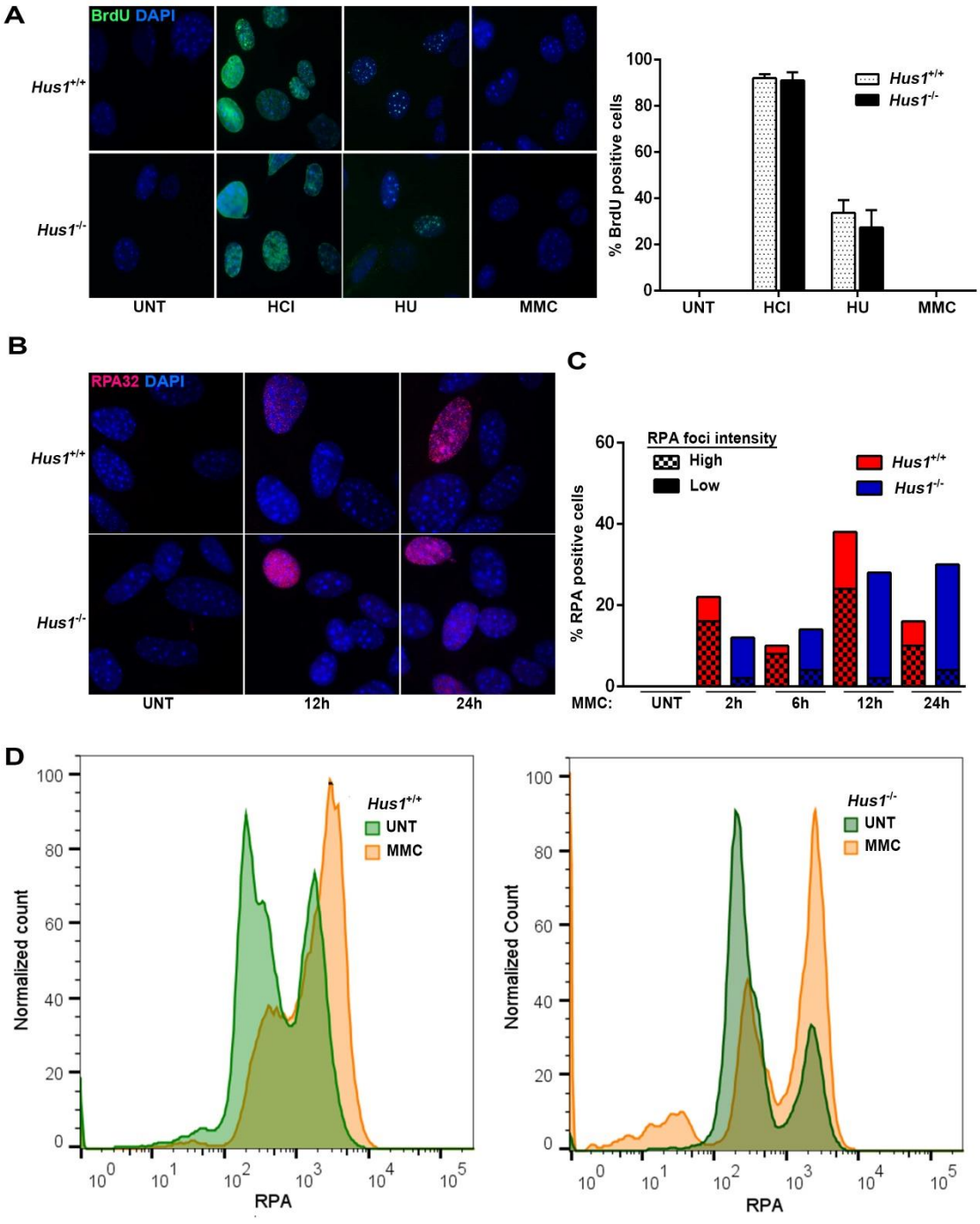
A
BrdU DAPI
Hus1+/+
Hus1-/-
UNT
HCl
HU
MMC
% BrdU positive cells
100
80
60
40
20
0
Hus1+/+
Hus1-/-
UNT
HCl
HU
MMC
B
RPA32 DAPI
Hus1+/+
Hus1-/-
UNT
12h
24h
C
RPA foci intensity
High
Low
Hus1+/+
Hus1-/-
% RPA positive cells
60
40
20
0
MMC:
UNT
2h
6h
12h
24h
D
Normalized count
Hus1+/+
UNT
MMC
RPA
Normalized Count
Hus1-/-
UNT
MMC
RPA

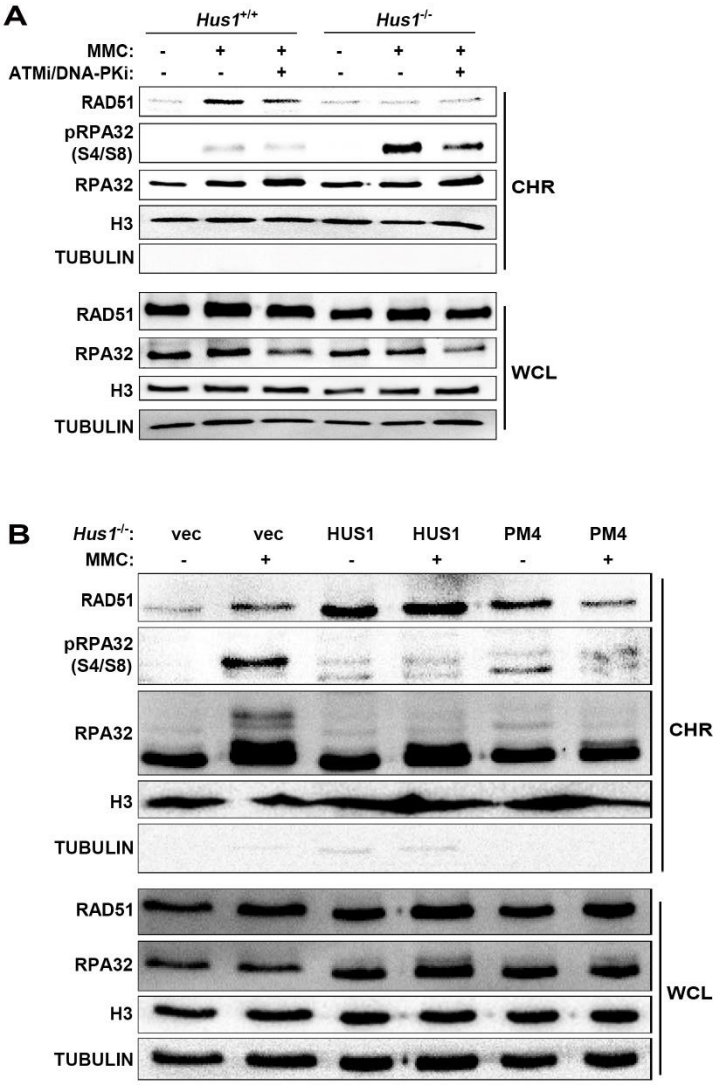

Figure 3.10. HUS1 regulates the pRPA32 and RAD51 loading during ICL repair. **A.** Immunoblotting analysis of chromatin fractionation and whole cell lysate. Cells were treated with 0.5ug/mL MMC for 4h and with or without the addition of ATM and DNA-PK inhibitors. **B.** Immunoblotting analysis of chromatin fractionation and whole cell lysates using *Hus1*-deficient (*Hus1*$^{-/-}$*p21*$^{-/-}$) cells, complemented with empty vector, WT-HUS1, and HUS1-PM4 mutants. Cells were treated with 0.5ug/mL MMC for 24h. GAPDH and H3 were used as cytoplasmic and nuclear controls respectively.

Figure 3.11. The 9-1-1 complex protects stalled replication forks against MRE11-dependent fork degradation. A. Dot plot of CldU to IdU tract length ratios for individual replication forks in the HU-treated WT and *Hus1*$^{neo/\Delta 1}$ MEFs. **B.** DNA Fiber analysis measuring the tract length of restarted fork or new replication origins in the MEF cells described in A. **C.** Quantification of the MRE11 staining data shown in D. **D.** Immunofluorescence staining for MRE11 in *Hus1*$^{-/-}$*p21*$^{-/-}$ and *Hus1*$^{+/+}$*p21*$^{-/-}$ cells were treated with 0.5 µg/ml MMC for 4h. Nuclei were counterstained with 0.05% DAPI. **E.** Dot plot of CldU to IdU tract length ratios for individual replication forks in the MMC-treated *Hus1*$^{-/-}$*p21*$^{-/-}$ and *Hus1*$^{+/+}$*p21*$^{-/-}$ cells with or without Mirin. **F.** Quantification of the BRCA1 staining data shown in G. **G.** Immunofluorescence staining for BRCA1 in *Hus1*$^{-/-}$*p21*$^{-/-}$, and *Hus1*$^{+/+}$*p21*$^{-/-}$ following treatment with 0.5 µg/ml MMC for a time course from 2 to 24h. Cells were counterstained with 0.05% DAPI.

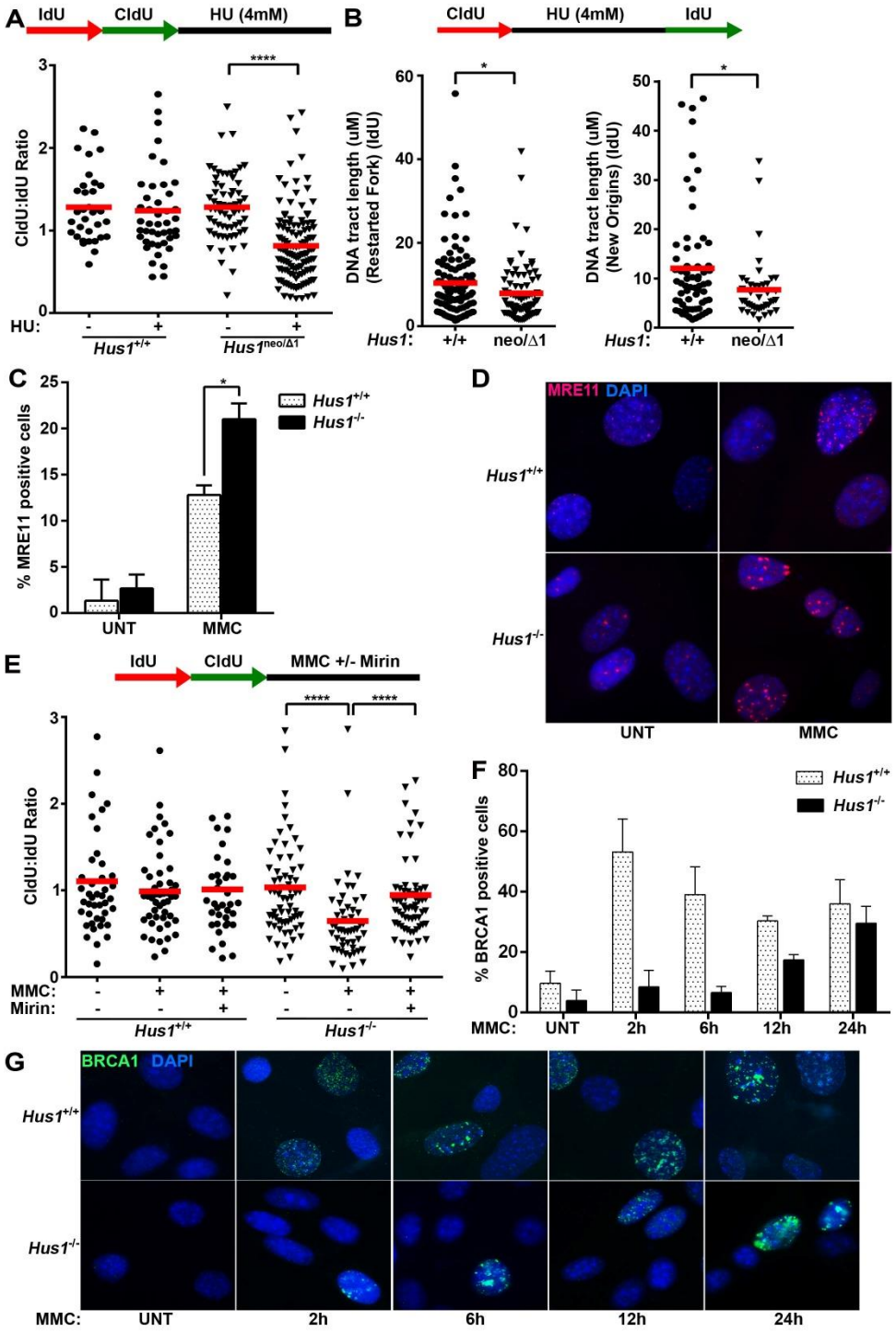
A
IdU
CldU
HU (4mM)
CldU:IdU Ratio
HU:
Hus1+/+
Hus1neo/Δ1
B
CldU
HU (4mM)
IdU
DNA tract length (uM) (Restarted Fork) (IdU)
DNA tract length (uM) (New Origins) (IdU)
Hus1:
+/+
neo/Δ1
C
% MRE11 positive cells
Hus1+/+
Hus1-/-
UNT
MMC
D
MRE11 DAPI
Hus1+/+
Hus1-/-
UNT
MMC
E
IdU
CldU
MMC +/- Mirin
CldU:IdU Ratio
MMC:
Mirin:
Hus1+/+
Hus1-/-
F
% BRCA1 positive cells
Hus1+/+
Hus1-/-
MMC:
UNT
2h
6h
12h
24h
G
BRCA1 DAPI
Hus1+/+
Hus1-/-
MMC:
UNT
2h
6h
12h
24h

Figure 3.12. The 9-1-1 complex promotes BRCA1 loading following ICL induction. A. Dot plot of CldU to IdU tract length ratios for individual replication forks in the HU-treated *Hus1*$^{+/+}$ and *Hus1*$^{neo/\Delta 1}$ MEFs with or without Mirin. **B.** Quantification of results from D. **C.** Quantification of results from E. **D.** Immunofluorescence staining for 53BP1 carried out in *Hus1*-deficient (*Hus1*$^{-/-}$*p21*$^{-/-}$*)* and control (*Hus1*$^{+/+}$ *p21*$^{-/-}$*)* cells. Cells were untreated or treated with either 0.5µg/ml MMC for 2-24 hours before analysis. Nuclei were counterstained with 0.05% DAPI. **E.** Immunofluorescence staining for BRCA1 carried out in *Hus1*-deficient (*Hus1*$^{-/-}$*p21*$^{-/-}$*)* and control (*Hus1*$^{+/+}$ *p21*$^{-/-}$*)* cells. Cells were untreated or treated with either 0.5µg/ml MMC or 10Gy of IR for 4h and 16h before analysis. Nuclei were counterstained with 0.05% DAPI.

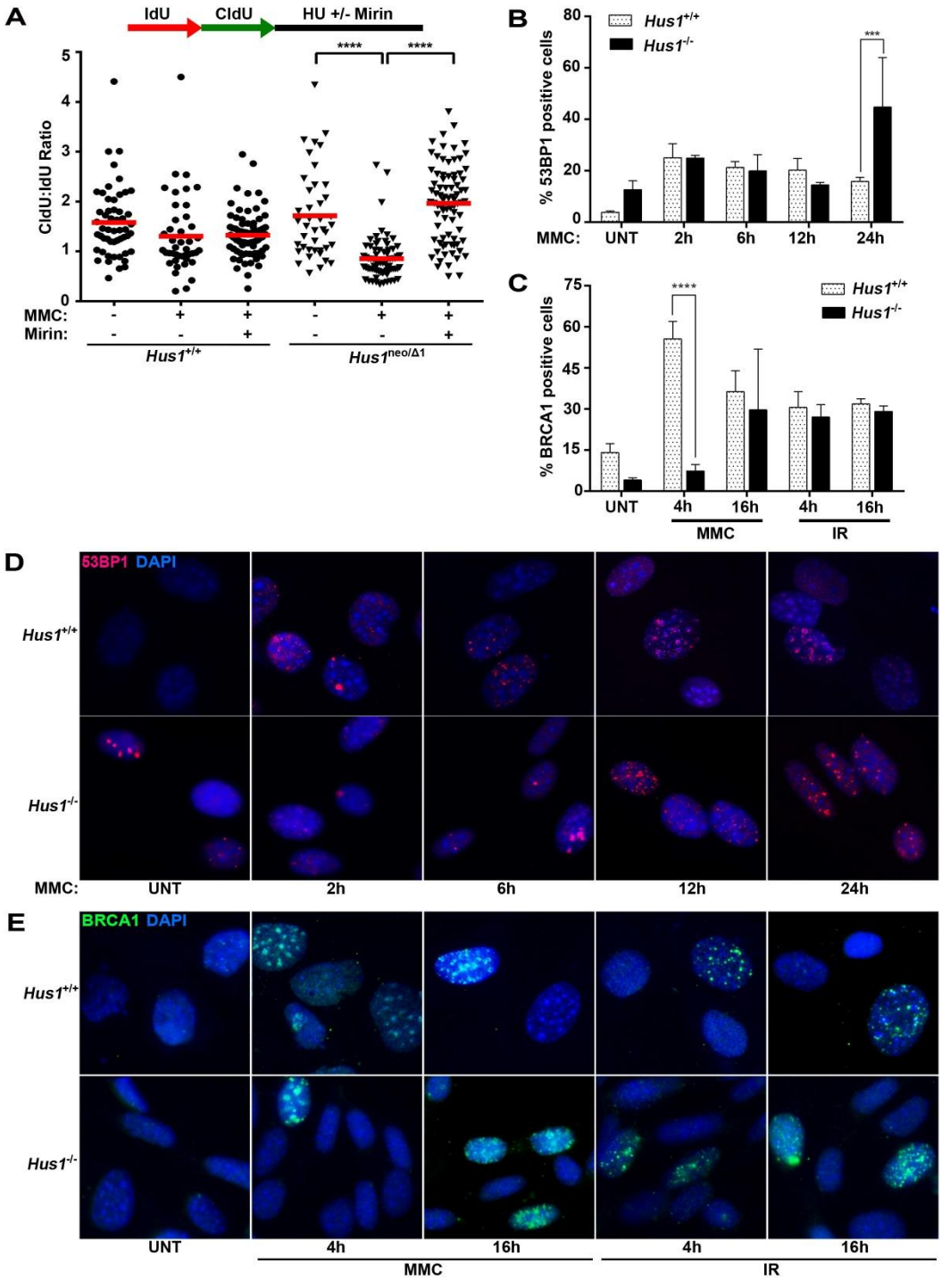
A
IdU
CldU
HU +/- Mirin
****
****
CldU:IdU Ratio
MMC:
Mirin:
Hus1+/+
Hus1neo/Δ1
B
Hus1+/+
Hus1-/-
% 53BP1 positive cells
***
MMC:
UNT
2h
6h
12h
24h
C
Hus1+/+
Hus1-/-
% BRCA1 positive cells
****
UNT
4h
16h
4h
16h
MMC
IR
D
53BP1 DAPI
Hus1+/+
Hus1-/-
MMC:
UNT
2h
6h
12h
24h
E
BRCA1 DAPI
Hus1+/+
Hus1-/-
UNT
4h
16h
4h
16h
MMC
IR

CldU:IdU median tract length, suggesting that HUS1 protects against nascent strand degradation following replication stress. Similar results were observed in *Hus1*-null cells (Fig 3.11E). Compared to control cells, *Hus1* hypomorph MEFs also exhibited short tract lengths at restarted forks and newly fired origins, suggesting impaired replication restart following fork stalling (Fig. 3.11B). Given that the MRE11 nuclease is known to degrade nascent DNA at deprotected replication forks, we examined MRE11 focus formation in *Hus1*-null cells. MRE11 foci were significantly increased in MMC-treated *Hus1*-null cells compared to control cells (Fig 3.11C-D). Importantly, the MRE11 inhibitor (Mirin) suppressed nascent degradation after MMC treatment in both *Hus1*-hypomorph and *Hus1*-null cells (Fig. 3.11E, 3.12A). Together, these findings suggest a role for HUS1 in protecting stalled replication forks against MRE11-dependent fork degradation.

The 9-1-1 complex promotes BRCA1 loading following ICL induction.

53BP1 and BRCA1 are two additional key regulators of repair pathway choice and fork stability (Bunting et al., 2010; Daley and Sung, 2014; Isono et al., 2017). To understand their relationship to the 9-1-1 complex following replication stress, we measured BRCA1 and 53BP1 focus formation in MMC-treated *Hus1*-null and control cells. MMC treatment induced 53BP1 focus formation to a similar extent regardless of *Hus1* status. However, cells lacking HUS1 had a higher basal level of 53BP1 foci prior to treatment and at late time points (24 hr) also showed significantly increased 53BP1 focus formation relative to control cells, possibly reflecting increased genome

damage in *Hus1*-null cells prior to and following extended replication stress (Fig. 3.12B, D). Interestingly, BRCA1 focus formation was significantly impaired in *Hus1*-null cells relative to controls, although BRCA1 foci did increase after prolonged MMC exposure (12-24h) even in the absence of HUS1 (Fig 3.11F-G). Following IR treatment, BRCA1 focus formation was equivalent in *Hus1*-null or control cells at all investigated time points (Fig. 3.12C, E). These results identify a crucial role for the 9-1-1 complex in regulating BRCA1 recruitment to chromatin specifically in the context of replication stress.

The HUS1 outer surface is important for repair protein recruitment in response to MMC-induced ICLs.

Our LUMIER and co-IP data revealed complex formation between HUS1 and several FA proteins, and analysis of the PM4 mutant implicated the HUS1 outer surface in these associations. To test the functional importance of the HUS1 outer surface in ICL responses, we generated mutant cell lines by complementing *Hus1*-null cells with empty vector, WT-HUS1 or PM4-HUS1. Immunoblot analysis revealed increased pCHK1 upon MMC treatment of cells expressing WT- or PM4-HUS1 (Fig. 3.13A), confirming complementation of the *Hus1*-null cells and the capacity of both WT and PM4 HUS1 to support genotoxin-induced CHK1 activation (Lim et al., 2015). As shown in Fig. 3.13B and Fig. 3.14A, FANCD2 focus formation after MMC treatment was significantly reduced in *Hus1*-null cells containing the empty vector, and PM4-HUS1 failed to rescue this defect, whereas WT-HUS1 restored FANCD2 focus formation. PM4-HUS1 expression in *Hus1*-null cells also failed to fully rescue

Figure 3.13. The HUS1 outer surface is important for repair protein recruitment in response to MMC-induced ICLs. A. Immunoblot analysis on *Hus1*$^{-/-}$*p21*$^{-/-}$ cells complemented with empty vector, WT, or PM4. Antibodies specific to pCHK1 (S317) and Actin were used. **B.** Quantification for FANCD2, **C.** RAD51, **D.** BRCA1, and **E.** MRE11 staining in *Hus1*$^{-/-}$*p21*$^{-/-}$ cells complemented with empty WT, vector, or PM4. Cells were treated with 0.5µg/ml MMC for 8 hours and counterstained with 0.05% DAPI. **F.** Dot plot of IdU to CldU tract length ratios for individual replication forks in the MMC-treated *Hus1*$^{-/-}$*p21*$^{-/-}$ cells complemented with either WT, empty vector or PM4. **G.** Quantification of *Hus1*$^{-/-}$*p21*$^{-/-}$ cells complemented with WT, PM4, or empty vector following mock treatment or treatment with 60ng/ml MMC for 24h.

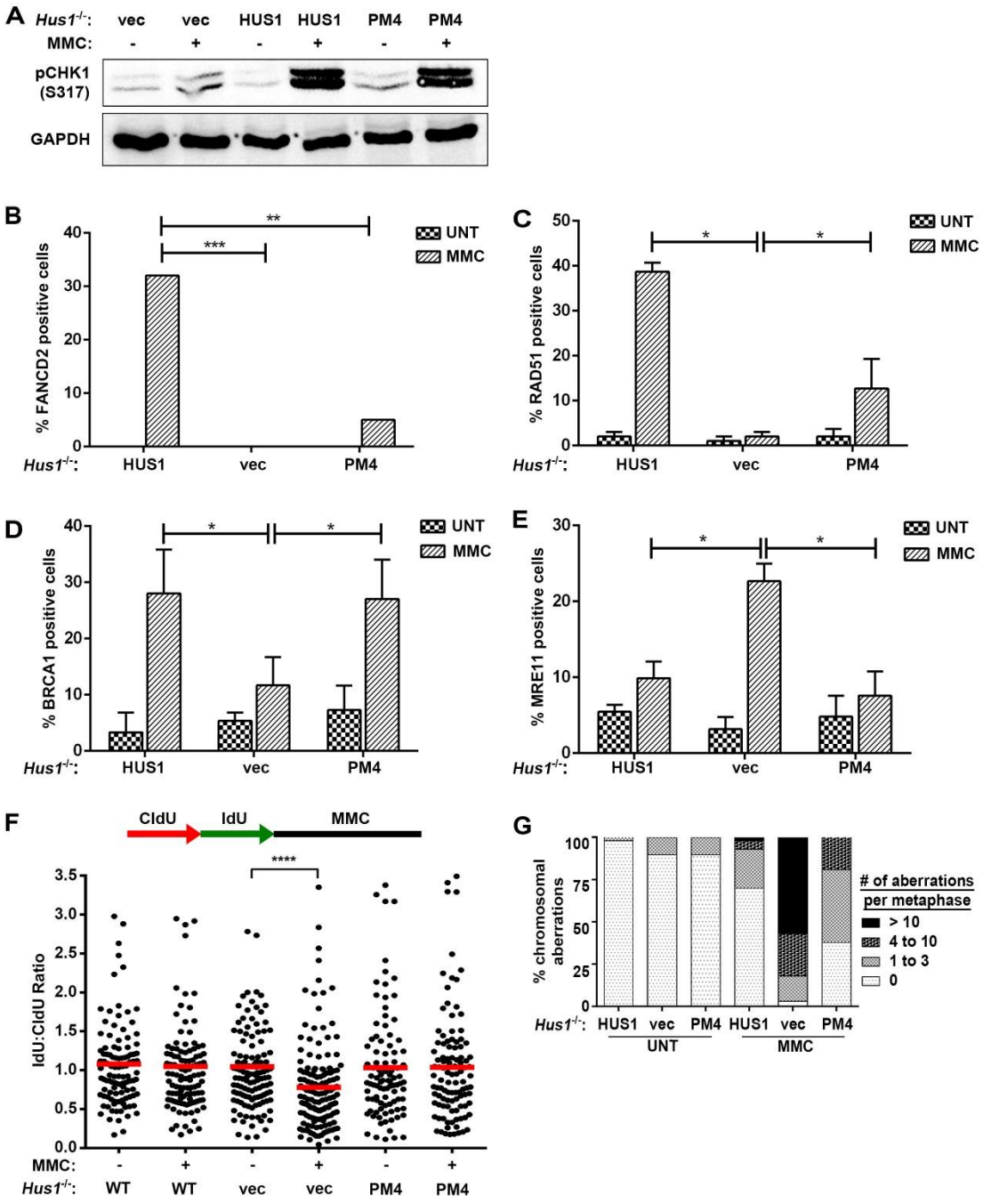
A
Hus1-/-: vec vec HUS1 HUS1 PM4 PM4
MMC: - + - + - +
pCHK1 (S317)
GAPDH
B
% FANCD2 positive cells
UNT
MMC
Hus1-/-: HUS1 vec PM4
C
% RAD51 positive cells
D
% BRCA1 positive cells
E
% MRE11 positive cells
F
CldU
IdU
MMC
IdU:CldU Ratio
MMC: - + - + - +
Hus1-/-: WT WT vec vec PM4 PM4
G
% chromosomal aberrations
# of aberrations per metaphase
> 10
4 to 10
1 to 3
0
UNT
MMC

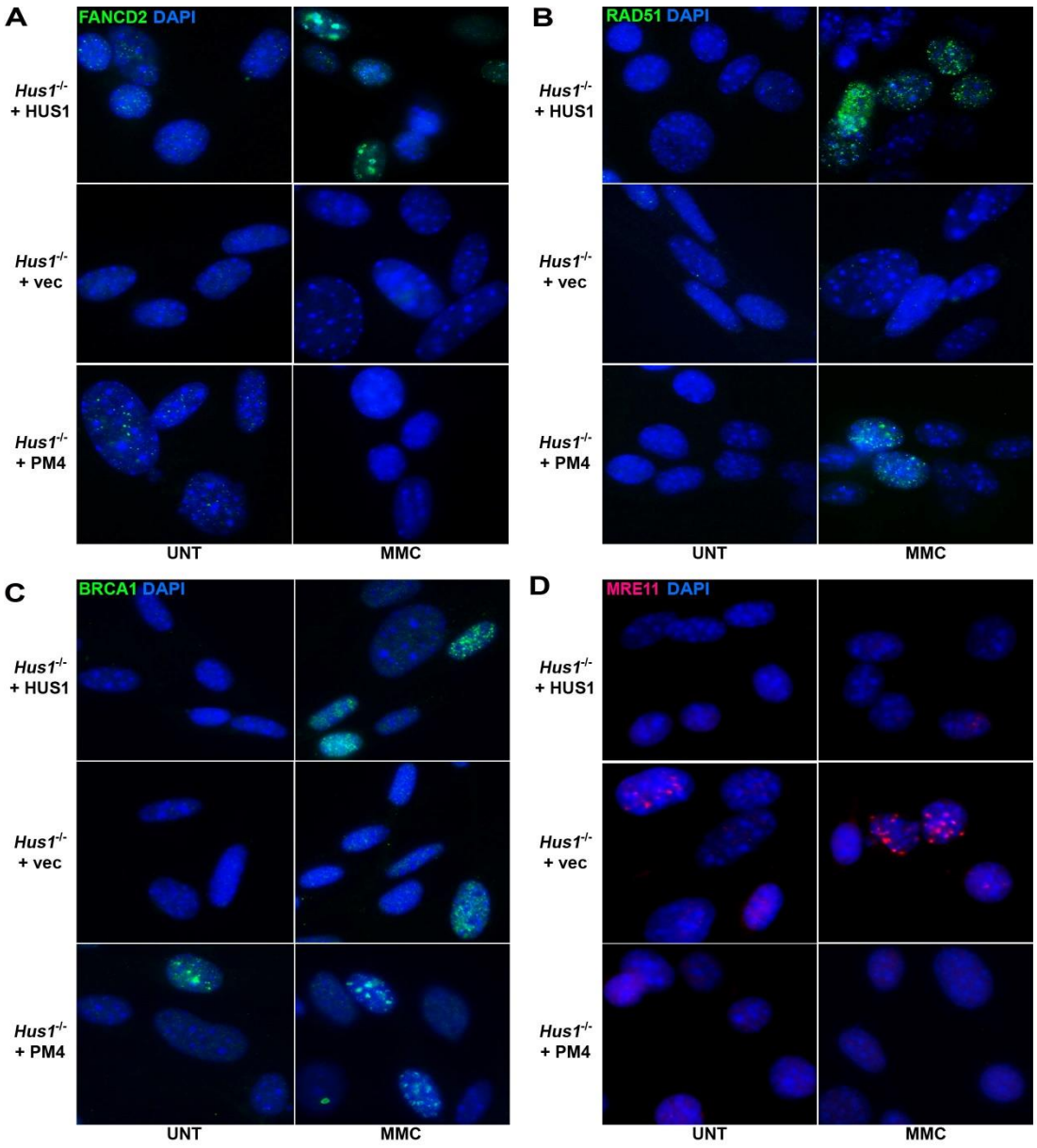

Figure 3.14. Outer surface of HUS1 is important for recruitment of FANCD2 and RAD51. A-D Immunofluorescence staining for **A.** FANCD2, **B.** RAD51, **C.** BRCA1, and **D.** MRE11 in *Hus1*-deficient (*Hus1*$^{-/-}$*p21*$^{-/-}$) cells complemented with empty vector, WT, or PM4. Cells were treated with 0.5µg/ml MMC for 4h. Nuclei were counterstained with 0.05% DAPI.

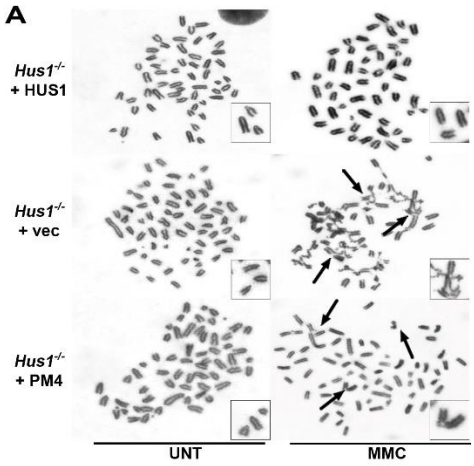

Figure 3.15. Outer surface of HUS1 is not essential for suppressing radial chromosome formation. A. Metaphase chromosome analysis of *Hus1*$^{-/-}$*p21*$^{-/-}$ cells complemented with WT, PM4, or empty vector following mock treatment or treatment with 60ng/ml MMC for 24h.

Table 3.3. Chromosomal aberrations in *Hus1*$^{-/-}$ +HUS1, *Hus1*$^{-/-}$ +vec and *Hus1*$^{-/-}$ +PM4 cells following MMC treatment [a].

Genotype	Breaks/Gaps	Fusions	Acentric	Radials
Hus1$^{-/-}$ +HUS1 (UNT)	1	0	1	0
Hus1$^{-/-}$ +vec (UNT)	5	1	6	0
Hus1$^{-/-}$ +PM4 (UNT)	6	2	1	0
Hus1$^{-/-}$ +HUS1 (MMC)	17	17	2	6
Hus1$^{-/-}$ +vec (MMC)	178	189	83	23
Hus1$^{-/-}$ +PM4 (MMC)	16	36	25	6

[a] *Hus1*$^{-/-}$ +HUS1, *Hus1*$^{-/-}$ +vec and *Hus1*$^{-/-}$ +PM4 cells were treated with Mitomycin C (MMC) at 60ng/ml for 24 hours or mock treated (UNT). Then chromosome spreads were prepared and 50 spread per condition were counted.

RAD51 focus formation after MMC treatment. The outer surface HUS1 mutant supported greater RAD51 focus formation than that observed in *Hus1*-null cells containing the empty vector, but failed to reach the level of RAD51 recruitment achieved with WT-HUS1 (Fig. 3.13C, 3.14B). Chromatin fractionation assays yielded similar results. *Hus1*-null cells containing the empty vector were defective for loading RAD51 onto chromatin and had elevated pRPA, phenotypes that were corrected by WT-HUS1 expression (Fig. 3.13B). PM4-HUS1 expressing cells showed a partial RAD51 loading defect but normal levels of RPA phosphorylation relative to WT-HUS1 complemented cells. No differences were observed in MMC-induced BRCA1 or MRE11 focus formation between *Hus1*-null cells complemented with WT-HUS1 or PM4-HUS1 (Fig. 3.13D-E, 3.14C-D). Lastly, PM4-HUS1 complemented cells were competent for replication fork protection after MMC treatment (Fig. 3.13F) and showed a low level of MMC-induced chromosomal aberrations that was similar to that observed in cells expressing WT-HUS1 and much lower than that observed in *Hus1*-null cells containing the empty vector (Fig. 3.13G, Table 3.3, 3.15). Collectively, the above findings indicate that the HUS1 outer surface participates in FANCD2 and RAD51 recruitment to chromatin in response to replication stress but appears to be dispensable for BRCA1 and MRE11recruitment as well as for suppressing radials and other chromosomal aberrations.

9-1-1 mediated checkpoint signaling is essential for MMC-induced BRCA1 recruitment, replication fork protection, and the prevention of chromosomal instability.

In light of the signaling-independent functions of the 9-1-1 complex in facilitating recruitment of FANCD2 and RAD51, we next assessed the role of 9-1-1 mediated ATR checkpoint signaling in the response to replication stress, as ATR has previously been implicated in FA pathway signaling (Ahlskog et al., 2016; Andreassen et al., 2004; Ho et al., 2006; Tomida et al., 2013). We therefore generated another separation of function mutant that was selectively disabled for checkpoint signaling. Using CRISPR, we mutated a phosphorylation site in the RAD9A C-terminal tail (S385A) that is essential for interaction with TOPBP1 and 9-1-1 mediated ATR activation. To verify the defect in 9-1-1 mediated ATR activation, we examined MMC-induced CHK1 phosphorylation in *Rad9a*$^{SA/SA}$ and control *Rad9a*$^{+/+}$ MEFs. Immunoblot analysis revealed that MMC elicited CHK1 phosphorylation (S317) in wild type cells but not in *Rad9a*$^{SA/SA}$ mutant cells (Fig. 3.16A). Both *Rad9a*$^{SA/SA}$ and wild-type cells were competent for MMC-induced FANCD2 and RAD51 focus formation (Fig 3.16B-C, 3.17A-B), consistent with our observations that these functions require the HUS1 outer surface. On the other hand, *Rad9a*$^{SA/SA}$ cells showed significantly reduced BRCA1 and increased MRE11 focus formation following MMC, relative to wild-type cells (Fig. 3.16D-E, 3.17C-D). Reduced BRCA1 focus formation persisted in *Rad9a*$^{SA/SA}$ cells even after 16h of MMC treatment, unlike in *Hus1*-null cells where it reached wild-type levels at late timepoints, hinting that secondary damage capable of attracting BRCA1 independently of the 9-1-1 complex may not arise in *Rad9a*$^{SA/SA}$ cells (Fig. 3.17E-F). Furthermore, *Rad9a*$^{SA/SA}$ cells were defective for replication fork protection, displaying reduced CldU:IdU median tract length upon replication stress (HU and MMC) that could be rescued by MRE11 inhibition (Fig. 3.16F, 3.18B, C).

Thus 9-1-1-mediated ATR signaling is crucial for BRCA1 recruitment and protection of stalled replication forks against nascent strand degradation by MRE11. These functions were paramount for chromosome maintenance, as a significant increase in chromosomal aberrations, including breaks and radials were observed after MMC treatment of *Rad9a*$^{SA/SA}$ cells, as compared to *Rad9a*$^{+/+}$ controls (Fig. 3.16G, 3.18A). Taken together with earlier results, these data indicate that the 9-1-1 complex suppresses radial formation via checkpoint signaling-dependent BRCA1 recruitment and fork protection, and not through outer surface functions necessary for FANCD2 and RAD51 chromatin recruitment.

To independently validate the importance of 9-1-1 mediated ATR checkpoint signaling in ICL responses, we tested how treatment of wild-type cells with ATR or CHK1 inhibitors impacted FANCD2, RAD51 and BRCA1 focus formation. Consistent with our analysis of the 9-1-1 separation of function mutants, MMC elicited FANCD2 and RAD51 focus formation even after CHK1 inhibition (Fig 3.19 A-B, D-E). Also consistent with our analysis of *Rad9a*$^{SA/SA}$ cells, MMC-induced BRCA1 focus formation was significantly diminished in WT cells upon CHK1 inhibition (Fig. 3.19C, F). In contrast to the more selective effect of CHK1 inhibition, ATR inhibition completely abolished MMC-induced focus formation by FANCD2, RAD51 and BRCA1, in line with previous reports (Fig 3.19). These results suggest that 9-1-1 mediated checkpoint signaling through CHK1 is mainly crucial for BRCA1 recruitment and fork protection upon replication stress, and that MMC-induced FANCD2 and RAD51 recruitment is promoted by both signaling-independent roles of the 9-1-1 complex as well as 9-1-1 and CHK1 independent signaling by ATR.

Figure 3.16. 9-1-1 mediated checkpoint signaling is essential for MMC-induced BRCA1 recruitment, replication fork protection, and the prevention of chromosomal instability. A. Immunoblot analysis of whole cell lysates prepared from cells of the indicated genotypes were treated with 0.5 ug/mL MMC for 8hr. Antibodies against pCHK1 (S317) and GAPDH were used. **B.** Quantification of FAND2, **C.** RAD51, **D.** BRCA1, and **E.** MRE11staining carried out in *Rad9a*$^{SA/SA}$ and *Rad9a*$^{+/+}$ cells. Cells were treated with 0.5 µg/ml MMC for 8 hours and counterstained with 0.05% DAPI. **F.** Dot plot of IdU to CldU tract length ratios for individual replication forks in the MMC-treated *Rad9a*$^{+/+}$ and *Rad9a*$^{SA/SA}$ MEFs with or without Mirin. **G.** Metaphase chromosome spread quantification of *Rad9a*$^{SA/SA}$ and *Rad9a*$^{+/+}$ cells following mock treatment or treatment with 60ng/ml MMC for 24 hours.

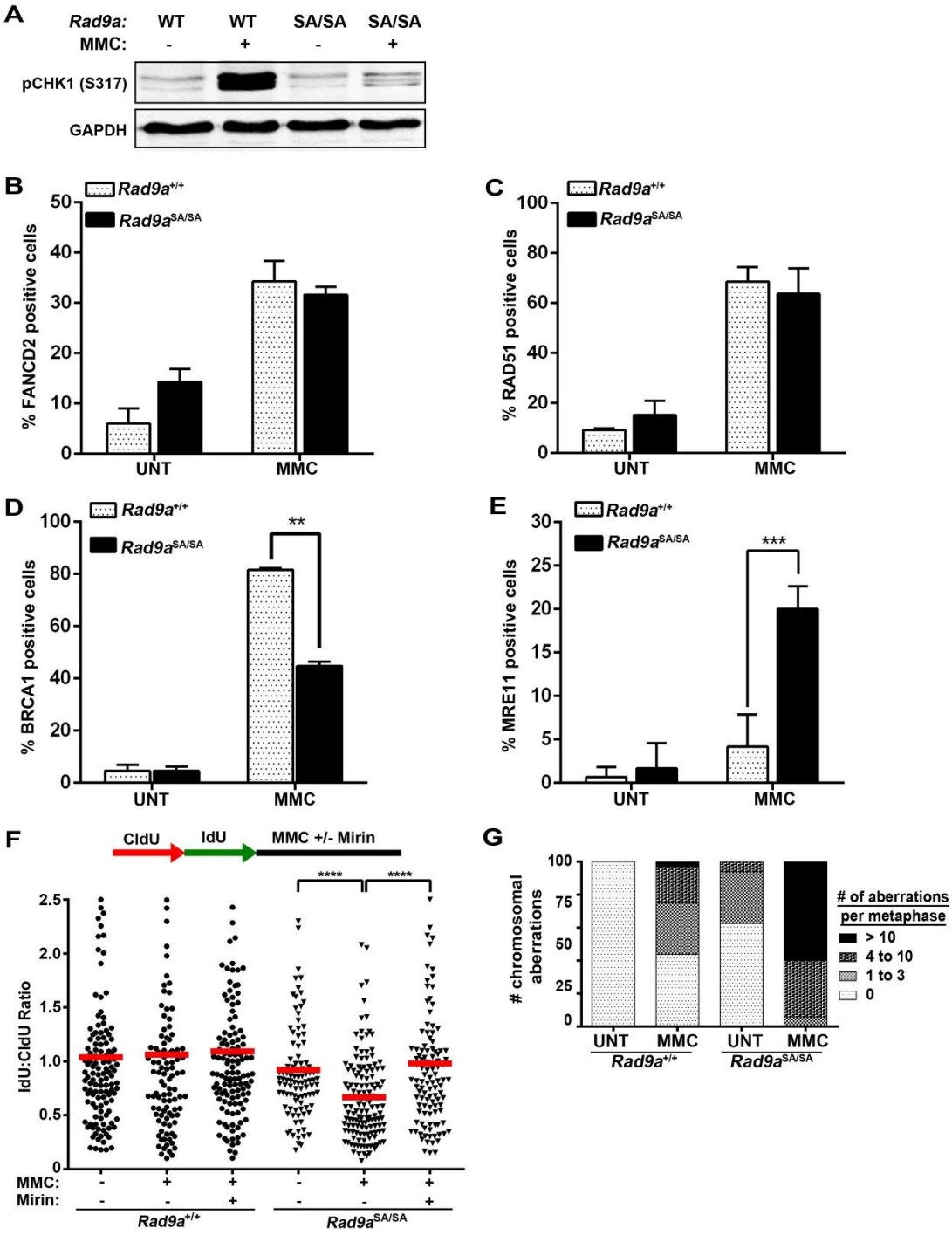
A
Rad9a: WT WT SA/SA SA/SA
MMC: - + - +
pCHK1 (S317)
GAPDH
B
Rad9a+/+
Rad9aSA/SA
% FANCD2 positive cells
UNT
MMC
C
% RAD51 positive cells
D
% BRCA1 positive cells
**
E
% MRE11 positive cells
***
F
CldU
IdU
MMC +/- Mirin
****
IdU:CldU Ratio
MMC:
Mirin:
G
chromosomal aberrations
of aberrations per metaphase
> 10
4 to 10
1 to 3
0

Figure 3.17. 9-1-1 mediated checkpoint signaling is critical for recruitment of BRCA1. A-D Immunofluorescence staining for **A.** FANCD2, **B.** RAD51, **C.** BRCA1, and **D.** MRE11 in *Rad9a*^{WT} or *Rad9a*$^{SA/SA}$ cells. Cells were treated with 0.5μg/ml MMC for 4h. Nuclei were counterstained with 0.05% DAPI. **E.** Immunofluorescence staining for BRCA1 foci carried out in *Rad9a*^{WT} or *Rad9a*$^{SA/SA}$ cells after 4h and 16h of MMC treatment. **F.** Quantification of results from E.

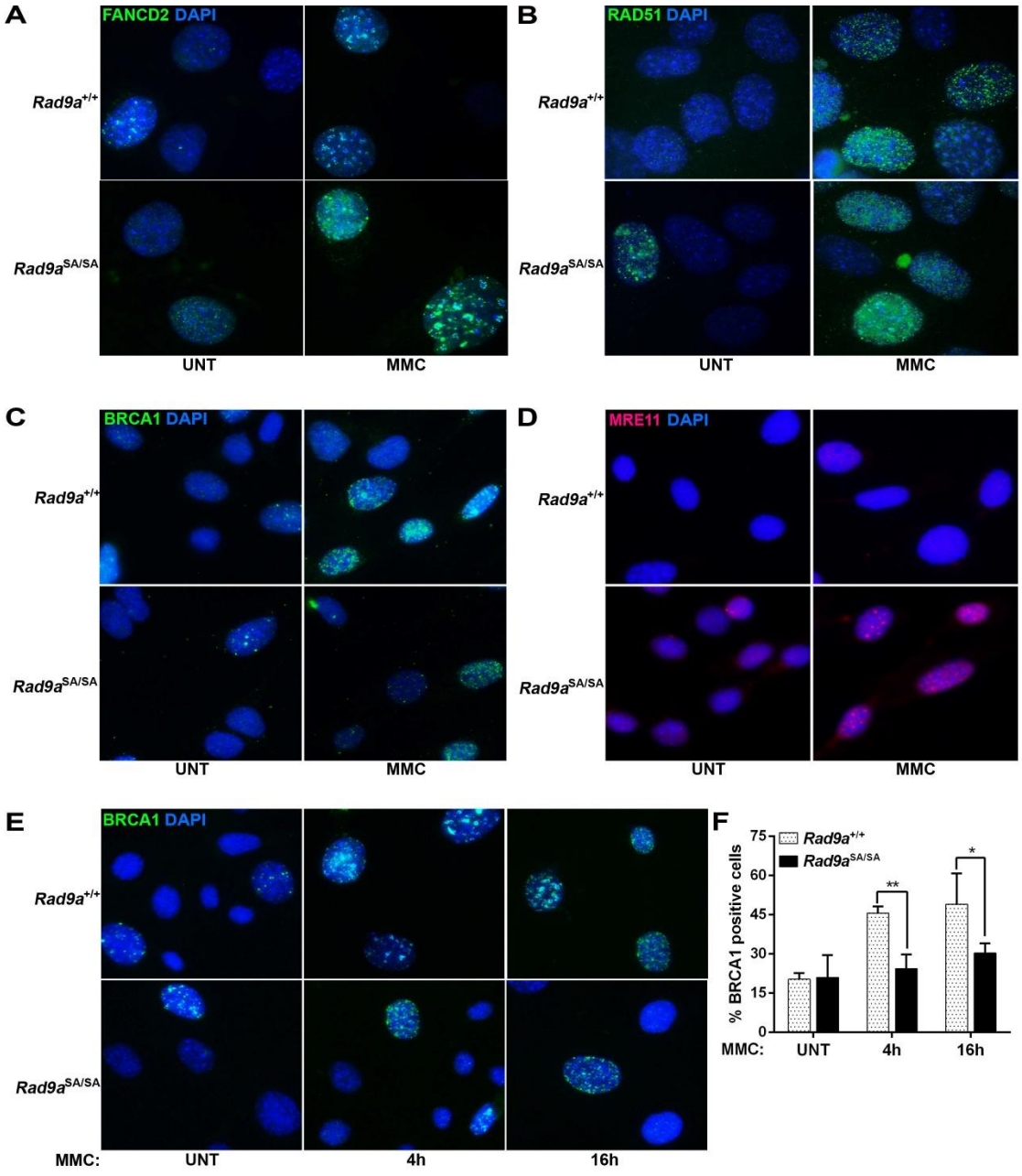
A
FANCD2 DAPI
Rad9a+/+
Rad9aSA/SA
UNT
MMC
B
RAD51 DAPI
Rad9a+/+
Rad9aSA/SA
UNT
MMC
C
BRCA1 DAPI
Rad9a+/+
Rad9aSA/SA
UNT
MMC
D
MRE11 DAPI
Rad9a+/+
Rad9aSA/SA
UNT
MMC
E
BRCA1 DAPI
Rad9a+/+
Rad9aSA/SA
MMC:
UNT
4h
16h
F
Rad9a+/+
Rad9aSA/SA
% BRCA1 positive cells
75
60
45
30
15
0
**
*
MMC:
UNT
4h
16h

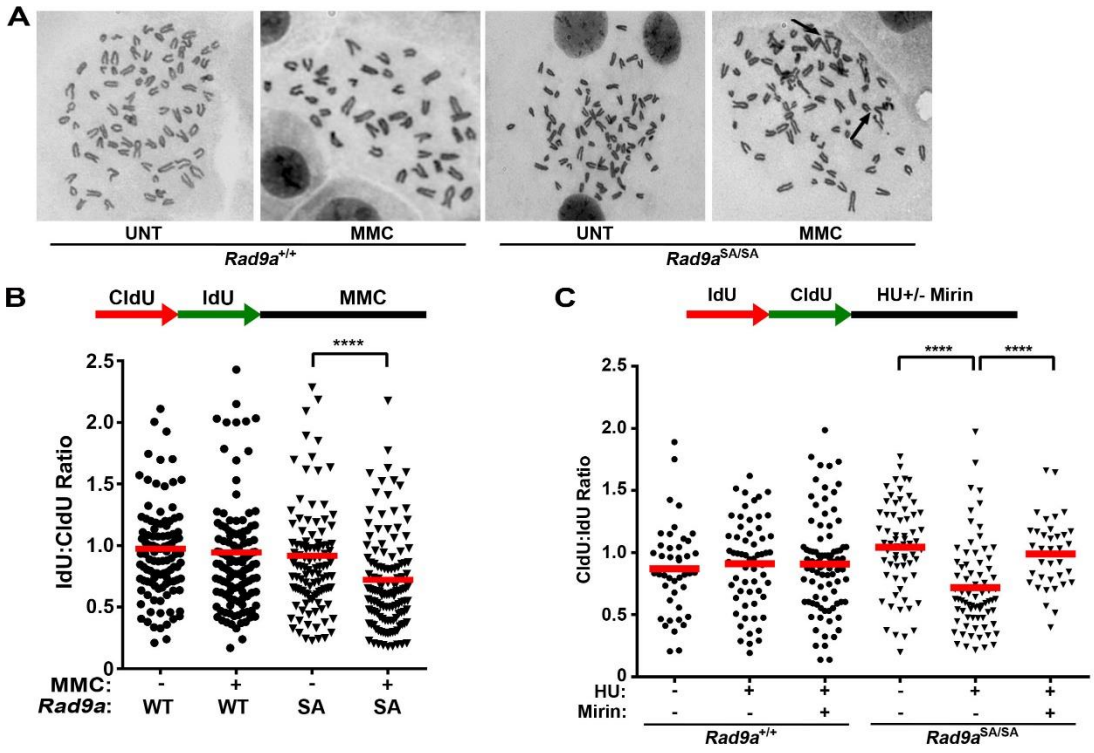

Figure 3.18. 9-1-1 mediated checkpoint signaling is essential for replication frok protection and the prevention of chromosomal instability. A. Metaphase chromosome analysis and quantification of *Rad9a*^{WT} or *Rad9a*$^{SA/SA}$ cells following mock treatment or treatment with 60ng/ml MMC for 24h. **B.** Dot plot of IdU to CldU tract length ratios for individual replication forks in the MMC-treated *Rad9a*^{WT} and *Rad9a*$^{SA/SA}$ MEFs. C**.** Dot plot of CldU to IdU tract length ratios for individual replication forks in the HU-treated *Rad9a*^{WT} and *Rad9a*$^{SA/SA}$ MEFs with or without Mirin.

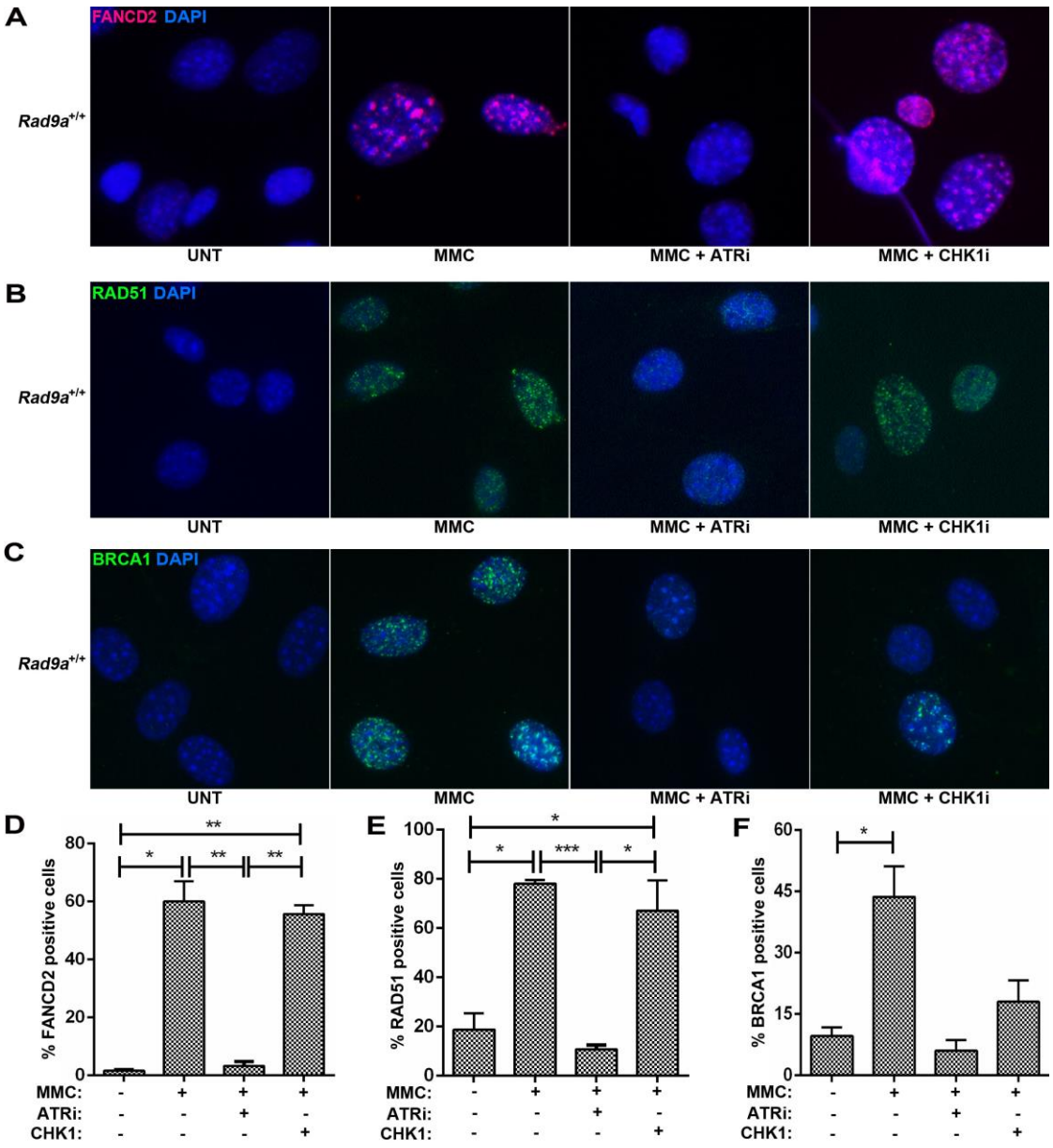

Figure 3.19. CHK1 inhibition phenocopies *Rad9a*$^{SA/SA}$ mutant cells. **A-C** Immunofluorescence staining for **A.** FANCD2, **B.** RAD51, and **C.** BRCA1 in *Rad9a*$^{+/+}$. Cells were treated with 0.5µg/ml MMC for 4h with/without ATR inhibitor and CHK1 inhibitor. Nuclei were counterstained with 0.05% DAPI. **D-F.** Quantification of results from A-C.

3.5 DISCUSSION

Based on recent findings that the 9-1-1 complex is recruited to ICLs (Raschle et al., 2015), together with our observations that *Hus1* deficiency confers hypersensitivity to ICL inducing agents and is associated with predisposition to radial chromosome formation, we endeavored to resolve the molecular functions of the 9-1-1 complex in responding to ICLs. The 9-1-1 complex shares structural similarity with the toroidal DNA clamp PCNA, although the RAD9A subunit also includes a C-terminal extension that is not present in PCNA. Thus the 9-1-1 has PCNA like activity involving protein-protein interactions with the outer surface of the clamp, and additionally functions in a manner distinct from PCNA by stimulating checkpoint signaling via the C-terminal RAD9A tail. Here we report multiple new functions for the 9-1-1 complex in aiding the chromatin recruitment of RAD51 and FANCD2 in response to ICLs, and protecting stalled replication forks via BRCA1 recruitment and MRE11 exclusion.

Both the ICL hypersensitivity and chromosomal fragility in *Hus1*-null cells are properties shared with cells defective in the Fanconi anemia signaling pathway, providing a rationale for investigating the crosstalk between HUS1 and DNA crosslink repair. FANCD2 focus formation is a classic marker of FA pathway activation, and we found it to be defective in cells lacking HUS1. We had previously reported that MMC-induced FANCD2 ubiquitination is also impaired in *Hus1*-null cells, although the level of FANCD2 ubiquitination is elevated in the absence of damage when HUS1 is absent (Balmus et al., 2015). It is known that phosphorylation of the ID2 heterodimer by ATR also is required for their activity, including FANCD2 focus

formation (Ho et al., 2006). However, using separation of function mutants we show that FANCD2 focus formation is independent of the signaling role of 9-1-1 mediated by the C-terminal tail of RAD9A. Given the PCNA-like properties of 9-1-1 complex as a molecular scaffold and a previous report that FANCD2 interacts with PCNA (Howlett et al., 2009), we predicted physical interactions between 9-1-1 and FANC proteins. Both our LUMIER screen and co-IP experiments identified interactions between the 9-1-1 complex and FANCD2-FANCI, as well as multiple additional components of the FA pathway. Interactions between the 9-1-1 complex and multiple components of individual repair pathways has emerged as a common theme, first established with base excision repair and now extended to the FA pathway (Gembka et al., 2007; Guan et al., 2007). We speculate that contacts with multiple proteins that act in sequence in responding to particular lesions might help ensure repair completion once the process is initiated.

However, the methods used to evaluate interactions between the 9-1-1 complex and FANCD2 did not differentiate the roles of the clamp in checkpoint signaling versus PCNA-like protein-protein interactions. Our findings using two separation of function mutants, HUS1-PM4 (repair defective) and RAD9A-SA (checkpoint defective), confirmed a direct role for HUS1 in FANCD2 recruitment via its interaction with outer surface hydrophobic pockets of the clamp, rather than a checkpoint signaling defect. Given that the 9-1-1 complex both facilitates recruitment of FANCD2/I at damage sites and stimulates ATR activity, it may be that one role of 9-1-1 is to bring substrates into proximity of ATR for subsequent phosphorylation and activation.

Consistent with our analysis of 9-1-1 mutants, we determined that ATR but not CHK1 inhibition completely abolished FANCD2 focus formation. FANCD2 formation in cells expressing the RAD9A-SA mutant, argues for a 9-1-1 independent ATR activating mechanism that can facilitate ATR-mediated FANCD2 phosphorylation and subsequent foci formation. Recent work has identified a new ATR activator, ETAA1 that can activate ATR in response to replication stress in the absence of the 9-1-1 complex or TOPBP1 (Bass et al., 2016; Haahr et al., 2016; Zou et al., 2017). The CHK1 inhibitor data further suggests CHK1-independent signaling by ATR for FA pathway activation.

In addition to a role in promoting FA signaling, our data also indicate a requirement for HUS1 in RAD51 focus formation and chromatin loading following MMC or HU treatment. Interestingly, HUS1 was dispensable for IR-induced RAD51 foci, suggesting that the requirement for 9-1-1 for RAD51 chromatin loading is specific to replication stress. To understand the mechanism responsible for the failure of RAD51 focus formation in MMC-treated *Hus1*-null cells, we closely examined the role of HUS1 in multiple steps of the HR pathway. Our results suggest that ssDNA accumulation and RPA loading, prerequisites for RAD51 loading, occur in the absence of *Hus1*. Growing evidence also suggested that RPA32 hyperphosphorylation at sites S4/S8 by ATM and DNA-PK impair RAD51 loading onto ssDNA, resulting in failed DSB repair (Lee et al., 2010; Zuazua-Villar et al., 2015). We also observed increased levels of RPA32 S4/S8 phosphorylation in the absence of *Hus1*; however, reducing pRPA (S4/S8) levels using ATM and DNK-PK inhibitors did not rescue RAD51 loading (Fig S6A). Interestingly, hyperphosphorylation of RPA (S4/S8) is also

considered as a marker for ssDNA accumulation (Kottemann et al., 2018). The increased RPA loading observed in response to long term replication stress in Hus1-null cells, together with RPA hyperphosphorylation, raises the possibility that uncontrolled resection may lead to failed RAD51 recruitment and subsequent genome instability. Several nucleases, such as MRE11 and EXO1, have been implicated in hyper-resection at damage sites in the absence of functional HR (Huertas, 2010). Hyper-resection can result in ssDNA accumulation and RPA exhaustion leading to replication catastrophe (Toledo et al., 2017). Given previous studies reporting a role for the 9-1-1 complex in stimulating DNA resection by DNA2 and EXO1 (Ngo et al. 2014; Blaikley et al., 2014) further investigation into the role of the 9-1-1 complex role in regulating resection at stalled forks as well as at DNA ends.

Although RPA binding to ssDNA is a precursor to RAD51 loading, formation and stabilization of RAD51 nucleofilaments requires a host of additional proteins, lincluding RAD51 paralogs, BRCA2 and PALB2 (Krejci et al., 2012; Long et al., 2011). An interaction between RAD9A and RAD51 has been demonstrated in a damage specific manner, suggesting a possible role for the 9-1-1 complex in regulating the RAD51 loading (Pandita et al., 2006). The data from our separation of function mutants implicate the HUS1 outer surface in facilitating RAD51 recruitment to MMC-induced DNA damage. As RAD51 loading was only partially disrupted in cells expressing the HUS1 PM4 mutant, it may be that RAD51 also interacts with other 9-1-1 complex subunits such as RAD9A (Pandita et al., 2006). In contrast, no changes in MMC-induced RAD51 focus formation was observed in cells expressing the RAD9A-S385A mutant, suggesting that 9-1-1 stimulated checkpoint signaling is

not needed for RAD51 focus formation. Similar to the results noted above for FANCD2, MMC-induced RAD51 focus formation was ablated by ATR but not CHK1 inhibitor treatment, again suggesting that ATR can signal in a 9-1-1 independent manner and through substrates other than CHK1. Although our data indicate that both FANCD2 and RAD51 chromatin loading after MMC require the HUS1 outer surface, our findings also indicate that the RAD51 defect is not a downstream consequence of the FANCD2 defect, as Fancd2-null MEFs were proficient for MMC-induced RAD51 loading.

Nucleolytic resection at stalled replication forks is highly controlled and necessary for efficient fork restart and continued DNA replication (Pasero and Vindigni, 2017). Recent studies have identified several HR/FA proteins, such as FANCD2, RAD51, and BRCA1/2, as crucial guardians against the degradation of stalled replication forks (Kolinjivadi et al., 2017; Lemacon et al., 2017; Ray Chaudhuri et al., 2016; Schlacher et al., 2011; Taglialatela et al., 2017). In the absence of RAD51 and FANCD2, replication forks undergo MRE11-mediated fork degradation (Schlacher et al., 2012). Several other nucleases, such as EXO1, DNA2 and MUS81, have been linked to processing stalled replication forks to facilitate fork restart or fork degradation (Mijic et al., 2017; Rondinelli et al., 2017). Likewise, our data implicated *Hus1* in stabilizing stalled replication fork during replication stress, as *Hus1* deficiency led to MRE11-dependent replication fork degradation. Interestingly, *Hus1* deficiency also led to shortening of the track length at restarted forks, as well as at newly fired origins following replicatin stress. These data are in accord with previous studies that showed ATR inhibition destabilized stalled replication forks and

caused nascent strand degradation (Branzei and Foiani, 2010; Cimprich and Cortez, 2008). ATR phosphorylation of SMARCAL1 is one mechanism for replication fork stablization, as well as accurate fork restart (Couch et al., 2013). Further investigation of SMARCAL1, and other factors like ZRANB3 and HLTF3, needed for fork reversal and restart may provide additional insights into mechanisms of fork protection by the 9-1-1 complex.

Studies in Xenopus egg extracts argue that replication fork convergence is required to initiate ICL repair (Zhang et al., 2015). Replication is halted 20-40 bases away from the ICL with the help of the CMG replicative helicase complex. CMG is subsequently removed, allowing for recruitment of FANCD2 (Ceccaldi et al., 2016; Long et al., 2014). BRCA1 is a key protein not only in regulating ICL repair, but also in protecting replication forks, promoting HR, and regulating transcription (Kolinjivadi et al., 2017; Taglialatela et al., 2017; Venkitaraman, 2001). Interestingly, our data show that *Hus1* deficiency resulted in significantly delayed BRCA1 focus formation upon MMC treatment. However IR-induced BRCA1 focus formation was normal in Hus1-deficient cells at all investigated time points. We hypothesize that the 9-1-1 complex promotes early BRCA1 loading upon replication stress in order to stabilize the stalled replication forks. Prolonged exposure to MMC in the absence of *Hus1*, resulted in an elevated level of DNA damage and increased DSBs at later time points, allowing for BRCA1 loading through other mechanisms that do not require HUS1. Consistent with this possibility, staining for 53BP1, which localizes to DSB, was elevated at late timepoints post MMC in Hus1-null cells. Notably, reduced BRCA1 foci were observed in MMC-treated *Rad9a*$^{SA/SA}$ cells but not in HUS1-PM4

mutant cells. These data suggest that BRCA1 is regulated through 9-1-1 mediated ATR/CHK1 signaling, as BRCA1 is known to be phosphorylated by ATR during genotoxic stress (Tibbetts et al., 2000) and both ATR and CHK1 inhibition impaired BRCA1 focus formation.

Interestingly, a significant decrease in BRCA1 foci was observed at both early (4h) and late (16h) time points after MMC treatment in *Rad9a*$^{SA/SA}$ cells, unlike the eventual late BRCA1 focus formation seen in *Hus1*-null cells at 12 to 24h (Fig. 7D, S9E-F). This may suggest that *Rad9a*$^{SA/SA}$ cells do not experience the extensive DNA damage seen in *Hus1*-null cells, such that the structures needed for 9-1-1 independent RAD51 loading are not created. *Rad9a*$^{SA/SA}$ cells also underwent MRE11-dependent fork degradation in response to replication stress, and displayed increased chromosomal aberrations and radial chromosome formation. These observations suggest that the 9-1-1 complex works upstream of BRCA1 via its ATR/CHK1 signaling activation function to prevent fork degradation and genomic instability. Although it may seem surprising that failed FANCD2 and RAD51 focus formation in the HUS1-PM4 mutant did not lead to appreciable radial chromosome formation, other studies indicate that radial formation can be achieved through other repair mechanisms besides HR (Hanlon Newell et al., 2008; Adamo et al., 2014).

RAD51 initiates fork reversal independently of its association with BRCA2 (Zellweger et al., 2015). Several other HR mediators, such as RAD54, RAD51 paralogs, MMS22L–TONSL (MMS22-like, DNA repair protein–tonsoku-like, DNA repair protein), support BRCA1/2-independent RAD51 loading during fork reversal (Krejci et al., 2012; Piwko et al., 2016; Somyajit et al., 2015). However, without

BRCA2, RAD51 fails to form a stable nucleofilament on ssDNA, resulting in failed fork protection and HR. Similarly, in our system, BRCA1-independent mechanisms are responsible for loading RAD51 as the delayed BRCA1 focus formation in *Hus1*-null cells was not associated with detectable RAD51 focus formation. Moreover *Rad9a*$^{SA/SA}$ cells were competent for RAD51 but not BRCA1 focus formation, further strengthening the idea of BRCA1-independent RAD51 loading at ICLs. However, caution should be used when drawing conclusions from focus formation data as some functional protein loading could still occur at lower levels even when focus formation is not apparent.

Taken together, our findings underscore the importance of the 9-1-1 complex in regulating DNA ICL repair. The 9-1-1 complex stabilizes stalled replication forks via its checkpoint function in concert with BRCA1, and promotes recruitment of other crucial repair and fork stabilizing proteins, such as RAD51 and FANCD2. Future studies characterizing the interaction of 9-1-1 complex with these proteins can provide a novel insight into the mechanisms that drive genome instability as well as open up avenue for drug therapeutics.

3.6 ACKNOWLEDGMENTS

The authors thank Drs. John Schimenti, Marcus Smolka, Paula Cohen and Adrian McNairn for reagents and helpful discussions, and members of the Weiss lab for feedback and technical assistance. The Weiss lab extends special appreciation to Dr. Warren Zipfel's laboratory for assistance with UVA/Trioxsalen experiments. We would also like to thank Dr. Roger Greenberg and Dr. John Petrini for providing

BRCA1 and MRE11 antibodies, respectively. The authors are also grateful to Markus Grompe for *Fancd2* mice. We would like to thank Alexander Bishop's lab for providing guidance with the DNA combing. We are also grateful to Paula Cohen and Andrew White for granting access to their microscope. This work was supported by NIH grant R01 CA108773 to RSW; funding for DP from NIH training grant T32 GM07273; an NSF predoctoral fellowship to CP; and a National Center for Research Resources grant (S10RR023781) for instrumentation.

CHAPTER 4

A NOVEL ROLE FOR 9-1-1 DNA DAMAGE CLAMP IN REGULATING NEDDYLATION FOR GENOME MAINTAINENCE*

4.1. ABSTRACT

DNA damage checkpoints are activated in response to DNA damage, and initiate cell cycle arrest and DNA repair, or apoptosis in cases of severe DNA damage. Among several important checkpoint proteins, the RAD9A–HUS1–RAD1 (9-1-1) complex, a heterotrimeric DNA clamp, promotes genome maintenance. Assembly and loading of the 9-1-1 complex on DNA at damaged sites is required for cell survival in various contexts. The 9-1-1 complex promotes ATR-mediated checkpoint signaling and has also been implicated in DNA repair via physical interactions with numerous repair factors. However, the physiological significance of these interactions are not fully known in most cases. Using a proteomics approach, we have uncovered novel repair factors that interact with the 9-1-1 complex, including key members of the protein neddylation (a key post-translational modification) pathway. HUS1 interacted and promoted the recruitment of Cullin family proteins, which are known substrates for neddylation. Furthermore, we also used auxin inducible degron technology to establish a system for rapid degradation of endogenous HUS1 in human cells. Taken together,

* Yi Liu, Dongsong Kim, Marcus Smolka, Hyeongsun Moon, Andrew White and Robert S Weiss helped with the experiments in this chapter. Full acknowledgement can be found in section 4.6.

these studies provide insights into how the 9-1-1 complex promotes the recruitment of the neddylation pathway at the DNA damage sites and highlight its importance for cell survival following DNA damage.

4.2. INTRODUCTION

Alterations in cellular genome content, whether inflicted by genotoxic insults from endogenous or exogenous sources, may result in pathological conditions, such as aging, developmental defects, neurological disorders, and carcinogenesis (Bartkova et al., 2005; Friedberg et al., 2004; Gorgoulis et al., 2005; Hoeijmakers, 2009; Jackson and Loeb, 2001). To recognize and address these insults, cells mount a coordinated DNA damage response (DDR) that promotes activation of the DNA damage checkpoint (Zhou and Elledge, 2000). Activated DNA damage checkpoint signaling results in cell cycle arrest, transcriptional changes, the initiation of DNA repair, and in the case of severe damage, apoptosis (Chen et al., 2006; Harper and Elledge, 2007; Zhou and Elledge, 2000). The role of transmitting the early DNA damage signal is filled by two major pathways led by members of the phosphatidylinositol 3-kinase–related kinase (PIKK) family, ATM and ATR, which are at the core of the DDR (Abraham, 2001; Sancar et al., 2004). ATM is primarily activated by double-strand breaks (DSBs) and promotes checkpoint signaling through CHK2 (Khanna and Jackson, 2001). Analogously, ATR responds to ssDNA generated during the processing of DNA lesion as a results of replication stress induced by chemical agents such as aphidicolin or hydroxyurea (Cimprich and Cortez, 2008). The physiological relevance of these kinases in maintaining genome integrity is demonstrated by patients

with *ATM* and *ATR* mutations, which result in a range of severe organismal defects (Blackford and Jackson, 2017; Brown and Baltimore, 2000).

It is well established that ATR activation is dependent on TOPBP1 and the DNA checkpoint clamp known as the RAD9A-HUS1-RAD1 (9-1-1) complex (Lee et al., 2007). The 9-1-1 complex shares structural homology with proliferating cell nuclear antigen (PCNA) and is loaded on chromatin at DNA damage sites (Parrilla-Castellar et al., 2004). Upon loading, the 9-1-1 complex stimulates ATR signaling through interactions between RAD9A and the ATR activator TOPBP1 (Lee et al., 2007; Mordes et al., 2008). *Hus1* deficiency in cultured MEFs promotes increased apoptosis, genomic instability, hypersensitivity to replication stress, and cellular proliferation defects (Balmus et al., 2016; Levitt et al., 2007; Weiss et al., 2003; Zhu and Weiss, 2007).

Both the 9-1-1 complex and PCNA serve as DNA-binding molecular scaffolds that lack enzymatic activity. PCNA is a central coordinator of DNA replication, chromatin assembly, cohesion establishment, and DNA damage repair (Mailand et al., 2013; Moldovan et al., 2007). PCNA interacts with a plethora of proteins via a PCNA-interacting protein (PIP) box-binding pocket (Gilljam et al., 2009). The PIP box sequence consists of Q-x-x-[ILM]-x-x-[FY]-[FY], allowing for interaction of the proteins containing this sequence to bind a hydrophobic pocket on PCNA (Gilljam et al., 2009; McNally et al., 2010; Tsanov et al., 2014). Apart from its signaling function, the 9-1-1 complex also directly contributes to DNA repair by interacting with and recruiting several DNA repair proteins to damage sites. Independent studies have shown 9-1-1 interacts with several repair proteins in different repair pathways.

However, no comprehensive screen for 9-1-1 binding partners has been reported, and additional 9-1-1 effectors likely remain to be relevant.

Interestingly, a recently uncovered neddylation, has sparked interest in the field of cancer therapeutics. Neddylation is a post-translational modification, an ubiquitin-like protein, NEDD8 (neural precursor cell expressed developmentally downregulated protein 8), is conjugated onto a target protein (Rabut and Peter, 2008; Soucy et al., 2010). Neddylation is initiated by the NEDD8 E1 activating enzyme, NAE1-UBA3, which adenylates the C-terminal glycine residue of NEDD8 to form a NEDD8–thioester bond. Following the linkage, UBE2M (ubiquitin-conjugating enzyme E2 M) (E2) and RBX1 (ring-box 1) (E3) conjugate the activated NEDD8 to the substrates (Brown and Jackson, 2015). Along with the neddylating enzymes, there are the deneddylases, e.g., CSN (COP9 signalosome, COPS) complex and CAND1 (cullin-associated and neddylation-dissociated 1), which deneddylate target proteins (Pick et al., 2012). Unlike ubiquitin, it remains unclear whether NEDD8 can form a poly-protein chain. However, there is some evidence implicating NEDD8 mixed chain formation with ubiquitin in budding yeast and human cells (Singh et al., 2012). Given the recent discovery of the neddylation pathway, knowledge on its molecular determinants and substrates remains limited. The ubiquitin E3 ligase family of cullin (CUL)-RING ligases (CRLs) is a well-characterized target of RBX1 (E3). CULs (1, 2, 3, 4A, 4B, 5, 7) serve as molecular scaffolds for the CRL complex (Lee and Zhou, 2010). CUL protein neddylation increases their ubiquitylation activity, resulting in the poly-ubiquitination of substrate proteins and subsequent degradation of the substrates (Fig 2A) (Enchev et al., 2015). Hence, the neddylation machinery regulates protein

degradation by controlling the CUL-dependent poly-ubiquitination machinery. Interestingly, a small-molecule inhibitor of NAE1-UBA3, MLN4924, is currently being explored for cancer therapy, and initial clinical trials have reported promising results (Soucy et al., 2010; Vanderdys et al., 2018). Recent studies have implicated a role for the neddylation pathway in DSB repair, yet the mechanistic details and physiological relevance of protein neddylation remain unclear (Brown et al., 2015; Jimeno et al., 2015; Li et al., 2014; Ma et al., 2013; Meir et al., 2015).

Here, we performed a comprehensive proteomic screen to uncover novel protein interactors of the 9-1-1 complex, as well as to isolate HUS1-specific interactions. This proteomic study identified neddylation pathway components as potential HUS1 interactors. Functional analysis of the interaction suggested a novel role for the 9-1-1 complex in promoting the neddylation pathway in response to DNA damage.

4.3. MATERIALS AND METHODS

Mice - *Hus1*$^{+/+}$, *Hus1*$^{+/\Delta 1}$, and *Hus1*$^{+/neo}$ mice (Levitt et al., 2005; Levitt et al., 2007) were maintained on a FVB inbred genetic background. To generate experimental *Hus1*$^{Neo/\Delta 1}$ mice, as well as littermate controls, *Hus1*$^{+/\Delta 1}$ and *Hus1*$^{+/Neo}$ mice were bred, and first generation offspring were used for the experiments. All animals were genotyped by PCR analysis of DNA extracted from tail tip biopsies. All animals used in this study were handled in accordance with federal and institutional guidelines, under a protocol approved by the Cornell University Institutional Animal Care and Use Committee (IACUC).

Cell culture - *Hus1*$^{+/+}$*; p21*$^{-/-}$ *and Hus1*$^{-/-}$*; p21*$^{-/-}$ were grown on gelatinized dishes in Dulbecco's Modified Eagle's Medium (Corning) supplemented with 10% Bovine Calf Serum (Thermo Scientific Hyclone, SH30072), 1% nonessential amino acids (Corning Cellgro, 25-025-CI), 1% L-glutamate (25-005-CI) and 1% penicillin and streptomycin (30-002-CI). For the proteomic screen, HEK293T cells were grown in SILAC (Stable Isotope Labeling of Amino acids in Culture) DMEM media lacking arginine and lysine (88425; Thermo Fisher Scientific) supplemented with 10% dialyzed FBS and 1% penicillin and streptomycin (30-002-CI. "Light" DMEM was supplemented with normal arginine and lysine; ''heavy'' DMEM was supplemented with lysine ($^{13}C_6$) and arginine ($^{13}C_6$). McCoy's 5A medium (Thermo Fisher Scientific) supplemented with 10% FBS (Gibco), 100 U/ml penicillin, and 100 µg/ml streptomycin. Cells were grown in a 37°C humid incubator with 5% CO_2. HCT116 cells used to generate the mAID tagged HUS1 were grown in McCoy's 5A medium (Thermo Fisher Scientific) supplemented with 10% BCS (Gibco), 2 mM l-glutamine, 100 U/ml penicillin, and 100 µg/ml streptomycin.

Proteomic Screen - Cells grown (15cm plates) in the "heavy" DMEM were co-transfected with 18ug of DNA consisting of pCMV-*HUS1-3xFLAG*, pCMV-*hRAD9A* and pCMV-*hRAD1* plasmids were previously described in (Lim et al., 2015), whereas the "light" DMEM were co-transfected with 18ug of DNA consisting of untagged version of pCMV-*HUS1*, pCMV-*hRAD9A* and pCMV-*hRAD1* plasmids, using lipofectamine 2000 (Life Technologies) for 12h, followed by 0.5 µg/mL Mitomycin C

(MMC) treatment for 24 h before preparing cell lysates. Next, lysates were incubated with anti-FLAG resin (Sigma). Immunoprecipitated proteins were reduced, alkylated and subjected to trypsin digestion overnight. Trypsin digested peptides were subjected to C18 column (Waters) clean up and processed as described in (Liu et al., 2017), before being analyzed by liquid chromatography-tandem mass spectrometry (LC-MS/MS) (Q-Exactive Orbitrap, Thermo Fisher Scientific). Detailed report regarding the instrument and analysis are described in (Liu et al., 2017).

Immunoprecipitation (IP) and immunoblotting - To analyze HUS1 subunit interactions with neddylation proteins, HEK293T transiently transfected with pCMV-hHUS1-3xFLAG construct were irradiated with 100J/m^2 UV or treated with 0.5 µg/mL MMC and 16 hours later, cell lysates for co-immunoprecipitation (co-IP) were prepared using IP Buffer (50mM Tris-HCl pH 7.5, 100mM NaCl, 0.4% NP-40 along with Protein A/L, protease inhibitors). Lysates were incubated with anti-FLAG (Sigma) and immunoprecipitates were subjected to standard immunoblotting. For auxin-treated HUS1-mAID cells, cells were treated with 0.5 µg/mL MMC and 500 µM auxin (abcam) for 8 hours before lysing the cells. Immunoblotting procedures were performed using antibodies specific for pCHK1 Ser317 (Cell Signaling), CUL4A (Bethyl Lab), RPA (Cell Signaling), PLK1 (Cell Signaling), UBE2M (Abcam), γH2AX (Millipore), DDB2 (Santa Cruz), XPC (ProteinBiotech), NEDD8 (Santa Cruz), Histone 3 (Abcam), GAPDH (Advanced ImmunoChemical), COPS6 (Enzo), TOPBP1 (Rendtlew Danielsen et al., 2009), mAID (MLB Intl.), or β-actin (Sigma).

Chromatin fractionation – *Hus1*$^{-/-}$*p21*$^{-/-}$ and *Hus1*$^{+/+}$*p21*$^{-/-}$MEFs were treated as mentioned above. To fractionate, cells were swollen in hypotonic buffer (10mM HEPES pH7.9 (Sigma), 1.5mM $MgCl_2$, 75mM KCl, 0.2mM PMSF and 0.5M DTT) for 6 min in 37°C and lysed with Dounce homogenizer. After centrifugation at 14,000 rpm for 15 min, the supernatant was separated for cytoplasmic extract preparation. The nuclei pellet was resuspended in equal volumes of low-salt and high-salt buffers (20mM HEPES pH7.9, 25% glycerol, 1.5mM $MgCl_2$, 0.2M or 1.2M KCl, 0.2mM EDTA, 0.2mM PMSF and 0.5M DTT) in sequential order to extract the soluble nuclear fraction. After centrifugation at 14,000 rpm for 30 minutes, the supernatant was separated for nuclear extract preparation. The pellet was resuspended in RIPA buffer supplemented with aprotinin (Sigma), leupeptin (Sigma), sodium orthovanadate (Sigma) and phenylmethylsulfonyl fluoride (PMSF) (Sigma), sonicated at 24-30W for 1 min (Misonix Sonicator 3000), and centrifuged to produce the chromatin fraction. The cytoplasmic and nuclear fractions were dialyzed in dialysis buffer (20mM HEPES pH7.9, 20% glycerol, 100mM KCl, 0.2mM EDTA, 0.2mM PMSF and 0.5M DTT) overnight. 20μg of each fraction was used for immunoblotting. Standard immunoblotting procedure were used as described in (Lim et al., 2015).

UVB-mediated melanocyte migration assay - To perform UVB irradiation on the skin region of interest, mice were anesthetized using isoflurane, and then 180 mJ cm^{-2} UVB was irradiated onto the shaved dorsal skin. A control section of skin was also shaved at the time of irradiation, but was protected by a covering with a UV resistant material. To reduce UVB-induced acute inflammation, 10 μg g^{-1}dexamethasone was

subcutaneously injected 1 day prior to and post UVB-irradiation. The mice were euthanized on day 11 post UVB treatment, followed by tissue harvesting and preservation.

Tissue immunostaining - Formalin-fixed paraffin-embedded (FFPE) tissue sections were cut at 5 μm and frozen tissues were cut at 6-8 μm for hematoxylin and eosin staining, and immunostaining. Immunofluorescence staining on fresh frozen sections and immunohistochemistry on FFPE tissue sections were performed as previously described in (White et al., 2011). Immunohistochemistry was performed with antigen retrieval using antigen unmasking solution (citric acid based, Vector) for 30 min at 90°C. Antibodies were used as anti-Trp2 (1:200), anti-K5 (1:600) together with suitable Alexa Fluor or biotinylated secondary antibodies for immunofluorescence and immunohistochemistry. The immunohistochemistry signal was amplified and detected using VECTASTAIN Elite ABC HRP Kit and AEC Peroxidase Substrate Kit followed by mounting using ImmunoHistoMount (Sigma). Prolong Gold antifade mountant with DAPI were used for IF staining.

Generation of HUS1-mAID cells – Using MIT CRISPR generation tool, we generated a guide RNA target close to the stop codon of *HUS1*. Oligos encompassing the guide sequences were ordered and cloned into LentiCRISPRv2 plasmid using the standard Zhang Lab CRISPR cloning protocol described in (Shalem et al. 2011). Next, to design the *HUS1* G-block, DNA sequences180 bp upsteam and 180 bp downstream of the CRISPR cut site were isolated. In the DNA sequence, the STOP codon from the

last exon of HUS1 was removed and a silent mutation in the PAM was introduced to generate a ECORV cut site right after the last codon of HUS1. At the end of the sequences, a 20 bp homology overlapping the destination vector (pCDNA5/FRT/TO) were added to the g-block. The g-block was synthesized by Genewiz, which was interested into the pcDNA5 vector using Gibson cloning. The g-block containing pcDNA5 vector was digested with ECORV and gel purified. Next, mAID-hygro and mAID-Neo were amplified from vectors provided by (Natsume et al., 2016) using primers that contain additional 20 bp corresponding to the internal region of the g-block adjacent to the cut site. Gibson cloning was performed using digest pcDNA5-g-block and PCR amplified neo-mAID and hygro-mAID sequences to generate the donor plasmids. Detailed cloning strategy is described in (Natsume et al., 2016). The HCT116 cells stably expressing CMV-OsTIR were obtained from (Natsume et al., 2016). To the stable HUS1-mAID cell lines, cells were grown in a six-well plate before CRISPR/Cas and donor plasmids were transfected using Lipofectamine 3000 (Life technologies). Two days after transfection, cells were selected using 1 μg/ml puromycin, 700 μg/ml G418, and/or 100 μg/ml HygroGold. After 10–12 days, colonies were picked for further selection in a 96-well plate. To induce the degradation of AID-fused proteins, 500 μM indole-3-acetic acid (IAA), a natural auxin, was added to the medium for 2-24 hr. See Table 4.1 for primer list.

Survival assays – For short term viability assays, HUS1-mAID cells were seeded in 6-well plates and either left untreated or treated with 80ng/mL of Mitomycin C (MMC) treatment was for 1hr. After 3 days, the cells were collected by trypsinization

Table 4.1. Oligonucleotide sequences for mAID cloning

HUS1 – CRISPR Guide sequence	5’ TGCATGCCAACTCCAGCGAC 3’
mAID-F	5’-TCATCCCTGCGCTGTCCGATGGTGCAGGCGCCAAGGAGAA-3’
mAID-R-Neomycin	5’ TGCATGCCAACTCCAGCGACGATAACGACCCAACACCGTG 3’
mAID-R-Hygromycin	5’ TGCATGCCAACTCCAGCGACGATTAGTGAACCTCTTCGAG 3’
HUS1-gblock	TGTGGTGGAATTCTGCAGATAGGAGGTGCAGGCTGGGAAGGCTGTTCTGAAAAAGTAGAGATCAAAATGTGTGTGCTGCACTAGGTCTCTAAAATCATGGCTTTTCTCTTCCCAGATATTGTGAATAACAAGATGGTGCATTTTGATCTGCTTCATGAAGACGTGTCCCTTCAGTATTTCATCCCTGCGCTGTCCGATATCGTCGCTGGAGTTGGCATGCAGAGACTTTGTCAGGATGGGAGAGGCCGCAGGTGTTGTGTTCTGATCACTGGTCTGTGCCCTCACAGCACCGCACATCGACACACTGTACTTATTTGTCCCTCTCTAACATTTTAACTAAAAGTTGATTCAACAACACACAGTTGGATAAACATATCACTATCCAGCACAGTGGCGGCCG

and counted. Percent survival was calculated by dividing the number of cells after treatment by the number of untreated cells. Error bars ± SD. Statistical analysis was by Student's T-test, and p-values of <0.05 were considered significant.

For clonogenic survival assays, cells were seeded in 6-well plates and treated with 100uM HU for 24 hours. Cells were fed new growth media every 5 days. After 14 days, the cells were fixed with methanol and stained with Giemsa stain for 2 hours. The plates were then washed, dried and scanned.

Immunofluorescence staining - Cells were seeded on coverslips in 6 well dishes allowed to attach for 24 hours and treated with 0.5µg/mL of MMC for 4 hours, before pre-extracting with CSK buffer for 5 minutes on ice followed by 4% PFA fixing for 15 minutes. Cells were further fixed by incubation in 75% ethanol for 5 minutes on ice, followed by 15% Bovine Calf Serum (BCS) + 2% Bovine Serum Albumin (BSA) block. Cells were incubated with RAD51 antibody (Millipore) overnight at 1:1000 concentration (4^{o}C), followed by 1:500 secondary incubation at room temperature for 1 hour. Finally, cells were mounted in DAPI containing 0.05% DAPI mounting medium and imaged the same day using a Leica DMRE fluorescence microscope.

4.4. RESULTS

Proteomic analysis revealed novel 9-1-1 interactions

As a molecular scaffold, the 9-1-1 complex orchestrates the assembly of the repair and signaling complexes through physical interactions with various binding partners.

Independent studies have reported several candidate proteins that mediate interaction with the 9-1-1 complex; however, without a high-throughput proteome-wide screen for the 9-1-1 interactors, a significant number of interactions remains unknown. To identify novel factors that might be associated with the 9-1-1 complex in a DNA damage-dependent manner, we conducted a proteomic study by overexpressing the 9-1-1 complex subunits, including 3xFLAG tagged HUS1 in HEK293T cells cultured in SILAC (stable isotope labeling with amino acids in cell culture) medium. The cells transfected with untagged version of the 9-1-1 complex were cultured in the "Light: DMEM media, whereas the cells transfected with 9-1-1 complex with 3xFLAG-HUS1 were grown in "Heavy" DMEM media. Growing the cells in different SILAC (Heavy and Light) media allows for mass separation between the peptides isolated in MS. Samples were treated with mitomycin C (MMC) for 24 h before the lysates were co-immunoprecipitated using FLAG antibody, and the quality of the immunoprecipitates was tested by immunoblotting (Fig. 4.1A). Nuclear lysates containing HUS1–3xFLAG successfully pulled down TOPBP1, whereas the whole-cell lysate and cytoplasmic fraction showed no detectable interaction between TOPBP1 and HUS1–3xFLAG (Fig. 4.1B). The nuclear lysates underwent LC-MS/MS, and upon applying a stringent cutoff of >2-fold enrichment for 9-1-1–specific binding, the proteomic data revealed >200 protein interactions for the 9-1-1 complex (Fig. 4.1C). To ensure the precision and eliminate labeling bias, we repeated the experiment by switching the heavy and light incorporation in the transfected cells. Figure 4.1C represents proteins identified in two separated experiments. Several known 9-1-1 complex interactors were identified in the screen, validating the screen.

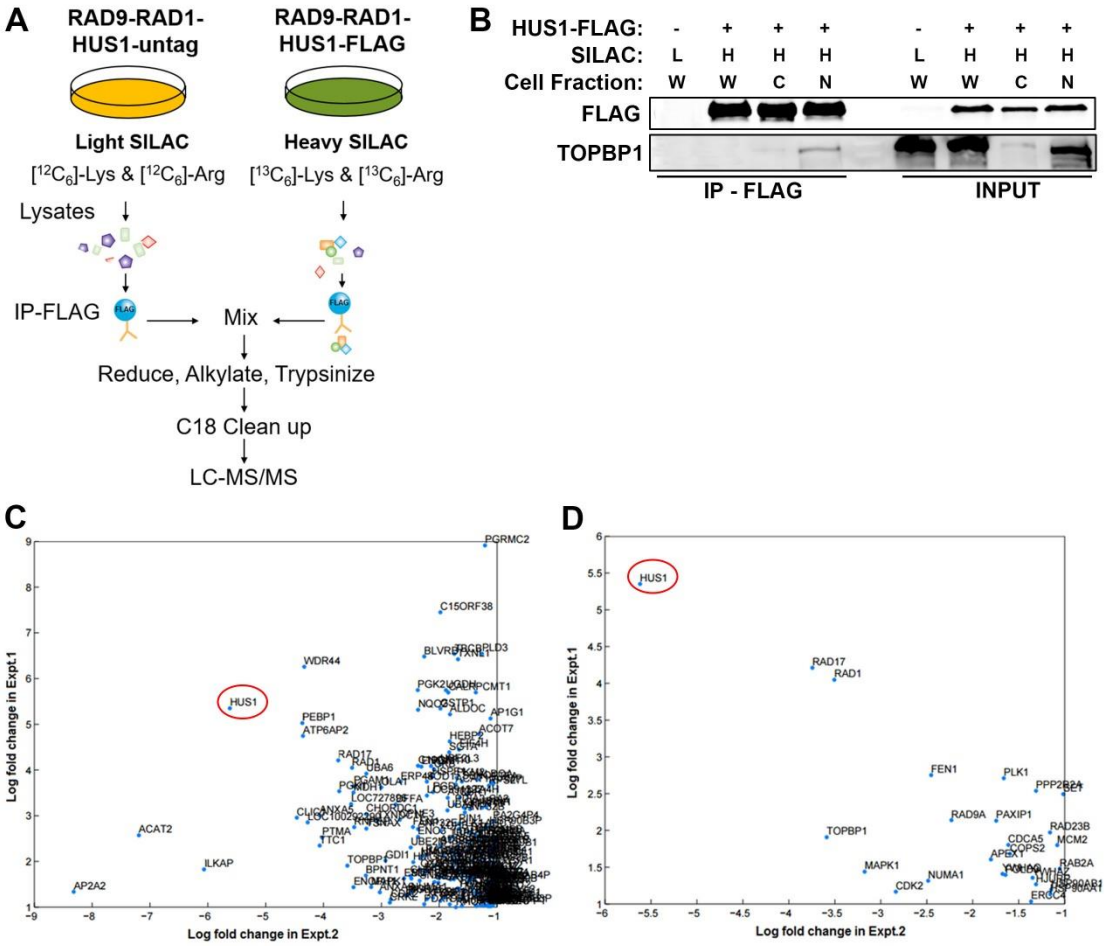

Figure 4.1. Proteomics screens identified novel 9-1-1 complex interacting proteins. (A) Strategy for SILAC-based IP-MS using HUS1-3xFLAG and untagged HUS1 (B) Western blot analysis of lysates from 293T cells transfected with the 9-1-1 subunits, HUS1-3xFLAG or untagged HUS1, followed by nuclear fractionation. (C) Distribution of SILAC-based all identified proteins, which were enriched as HUS1 interacting proteins in two independent experiments. (D) Distribution of SILAC-based all DDR proteins, which were enriched as HUS1 interacting proteins in two independent experiments. Red circle indicates the bait protein (HUS1).

Table 4.2. List of 9-1-1-interacting DDR proteins identified in the proteomics screen. Green depict the bait (9-1-1 complex subunits); blue depicts the known 9-1-1 complex interactors and red colored proteins are novel 9-1-1 interacting proteins

	Peptides Recovered		
Proteins	**Untagged HUS1**	**HUS1-3xFlag**	**Pathway**
HUS1	13	170	9-1-1 Clamp Subunits
RAD9A	32	114	
RAD1	17	99	
TOPBP1	0	15	Checkpoint Protein
FEN1	2	7	Base Excision Repair
APEX1	0	5	
MSH6	0	6	Mismatch Repair
MSH6	1	26	
RAD51	1	4	Homologous Recombination
FANCI	7	40	Fanconi Anemia Pathway
FANCD2	0	15	
FANCA	0	3	
ERCC2	2	9	Nucleotide Excision Repair
ERCC6	3	11	
NEK9	2	12	Mitosis
PLK1	1	19	
CUL2	4	14	Neddylation Pathway
CUL4	0	3	
SKP1	5	12	
COPS6	0	7	
UBE2M	0	3	
NAE1	0	3	

Interestingly, several novel candidate proteins belonging to the DNA replication machinery, DNA repair pathways, and DDR proteins were also identified (Fig. 4.1D, Table 4.2). Overall, the proteomic screen revealed a robust network of 9-1-1 interactions.

HUS1 interacts with multiple neddylation factors

Excitingly, many factors of the neddylation pathway appeared to be abundant in our screen. In Figure 4.2A, all underlined and bolded proteins related to neddylation were identified in the MS screen as potential HUS1 interactors, suggesting a possible role for the 9-1-1 complex in the neddylation pathway. Neddylation is required for activating the CRLs that subsequently polyubiquitinate target proteins and tag them for proteasomal degradation (Brown et al., 2015). Along with the neddylation machinery, the screen also identified CRL protein and CRL modifier (Fig. 4.2A). Using HEK293T, we validated the interactions by immunoprecipitating the neddylation factor, UBE2M with HUS1–HA, upon DNA damage (Fig. 4.2B). Additionally, endogenous CRL member, CUL4A also co-immunoprecipitated with HA–HUS1 (Fig. 4.2B). Together, our results illustrate a novel role for the 9-1-1 complex in binding neddylation pathway proteins.

HUS1 regulates UBE2M and CUL4A protein expression

With the data supporting physical interaction between the 9-1-1 complex and neddylation pathway proteins along with CRLs, we focused on elucidating the physiological relevance of the interaction. To test this, we used immunoblotting to

observe the total expression of neddylation proteins and CRLs in *Hus1*-proficeint (*Hus1*$^{+/+}$) and *Hus1*-deficient (*Hus1*$^{-/-}$) cells. We observed that UBE2M and CUL4A protein expression varied in response to HUS1 levels. Relative to the *Hus1*$^{+/+}$ cells, *Hus1*$^{-/-}$ cells had decreased CUL4A levels and significantly increased UBE2M levels (Fig. 4.3A). As there is evidence that both the 9-1-1 complex and neddylation proteins regulate DNA repair during replication stress (Brown et al., 2015; Parrilla-Castellar et al., 2004), we tested if the 9-1-1 complex regulates neddylation factors during replication stress. In *Hus1*$^{-/-}$ cells, UBE2M levels were significantly upregulated in response to prolonged replication stress induced by MMC (Fig 4.3B). On the contrary, UBE2M levels in *Hus1*$^{+/+}$ cells declined steadily post-MMC treatment (Fig 4.3B). We observed no difference in CUL4A levels irrespective of genotype or treatment. Next, we conducted chromatin fractionation analysis using *Hus1*$^{-/-}$ and *Hus1*$^{+/+}$ cells to test if the chromatin recruitment of these proteins is dependent on the 9-1-1 complex. In the *Hus1*$^{+/+}$ cells, UBE2M and COPS6 protein levels were significantly reduced on the DNA in response to MMC- and HU-induced replication stress; in contrast, levels of both protein were enriched in the chromatin fraction of the *Hus1*$^{-/-}$ cells post-treatment. Together, these data suggest that *Hus1* regulates the expression and localization of the neddylation proteins in response to DNA damage.

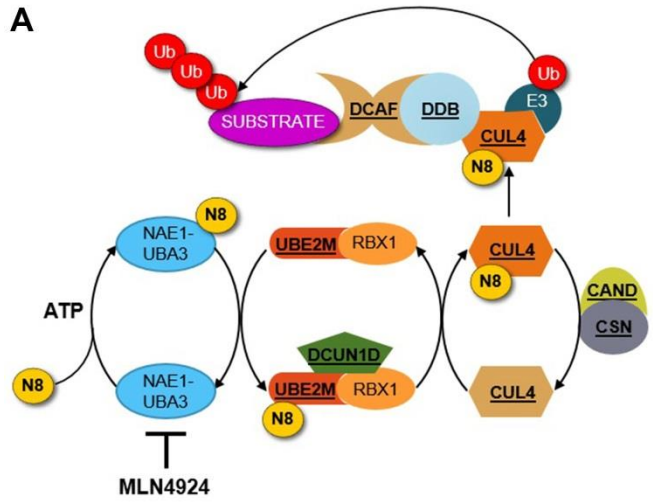

Proteins	Hit on MS Screen	
	Repeat 1	Repeat 2
NAE1	Y	N
UBA3	Y	N
UBE2M	Y	Y
DCUN1D4	Y	Y
CUL1,2,4	Y	Y
CAND1	Y	Y
CSN	Y	Y

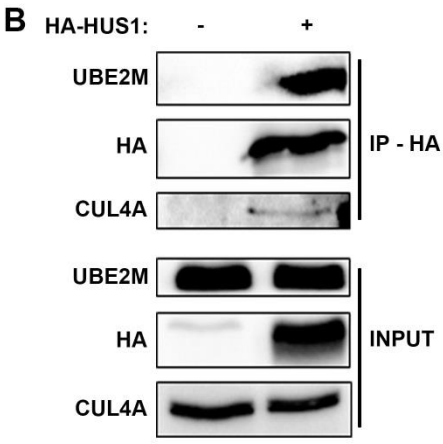

Figure 4.2. HUS1 physically interacts with neddylation proteins. (A) Representation of major neddylation pathway components. NEDD8 (N8) is conjugated to E1 (NAE1-UBA3) in an ATP-dependent manner, it gets shuttles to E2/3 (UBE2M/RBX) and finally onto CUL4 substrates. CAND1 and CSN complex can remove the N8 from CUL4. CUL4 upon N8 conjugation can poly-ubiquitinate substrate protein with help of other accessory factors (DDB and DCAF). MLN4924 inhibits UBA3. The figure was adapted from (Brown and Jackson, 2015). (B) Interaction with endogenous UBE2M and CUL4A by immunoprecipitated HA-HUS1, and was analyzed by immunoblotting.

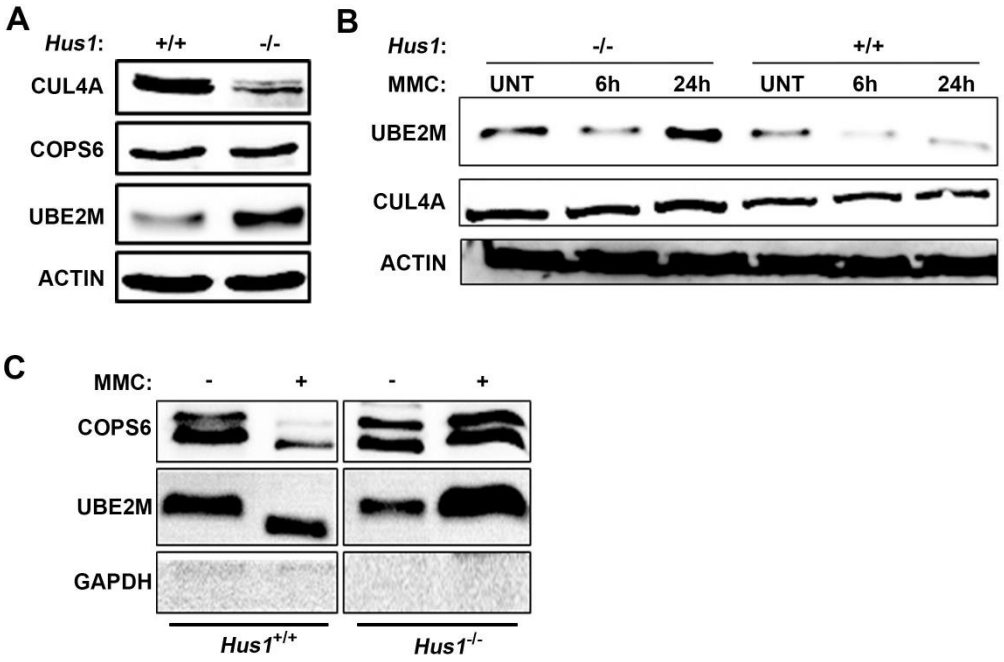

Figure 4.3. HUS1 regulates the expression and recruitment of neddylation proteins. (A) Immunoblot performed using antibody against CUL4A, COPS6, UB2EM, and ACTIN (Control) in *Hus1*$^{+/+}$ and *Hus1*$^{-/-}$ MEFs. (B) Immunoblot performed using antibody against CUL4A, UB2EM, and ACTIN (Control) in *Hus1*$^{+/+}$ and *Hus1*$^{-/-}$ MEFs with MMC treatment at indicated times. (C) Chromatin fractionation analysis in *Hus1*$^{+/+}$ and *Hus1*$^{-/-}$, analyzed by immunoblotting using antibody against COPS6, UB2EM, and GAPDH (Control) MEFs with or without 24h of MMC treatment.

HUS1 is important for UV-induced DNA damage response

The nucleotide excision repair (NER) pathway is the primary protective mechanism against UV DNA damage, facilitating the removal of helix-distorting DNA adducts (Garfinkel and Bailis, 2002). Recent publication revealed the importance for the neddylation pathway in regulating UV-induced NER repair (Hu et al., 2015). Interestingly, the 9-1-1 complex has also been implicated in regulating UV responses, as 9-1-1 complex loss confers UV hypersensitivity in cells. Upon UV-induced DNA damage, melanocytes production and migration towards the wounded area is stimulated, which promotes efficiency of NER (Jarrett et al., 2017; Wu et al., 2004). To fully understand the role of the 9-1-1 complex in UV-induced NER, we examined UVB-mediated melanocyte migration in *Hus1*$^{+/+}$ and *Hus1*$^{neo/\Delta1}$ mice (Fig. 4.4A). Given that *Hus1* loss manifests as embryonic lethality, we used *Hus1*$^{neo/\Delta1}$ mice as generated previously (Levitt et al., 2007). *Hus1*$^{neo/\Delta1}$ mice contain a neomycin resistance cassette between exon 1 and 2 in one allele; exon 1 is deleted from the other allele, resulting in 20% *Hus1* expression compared to the wild type (WT). *Hus1*$^{neo/\Delta1}$ mice are born at the expected mendelian ratio, and also exhibit grossly normal morphology; however, *Hus1*$^{neo/\Delta1}$ mice are extremely sensitive to replication stress (Levitt et al., 2007). Gross analysis of the *Hus1*$^{+}$ and *Hus1*$^{neo/\Delta1}$ mice after UVB treatment revealed increased inflammation in *Hus1*$^{neo/\Delta1}$ mice compared to *Hus1*$^{+}$ mice (Fig. 4.4B). Interestingly, melanocytes stem cells (MCSC) upon stimulation by UVB induce MCSC activation and translocation via an inflammation-dependent process (Moon et al., 2017). However, both *Hus1*$^{+}$ and *Hus1*$^{neo/\Delta1}$ mice exhibited similar levels of TRP2 (a melanocyte marker) positive cells migrated to the interfollicular epidermis

(IFE) upon UVB irradiation at day 0 and day 2 (Fig. 4.4C). Next, we tested if UVB irradiation directly affected migrated melanocytes at the IFE by adding an extra UVB treatment on day 8. The *Hus1*$^{neo/\Delta 1}$ mice a displayed moderate increase in IFE hyperplasia and hyperkeratosis after 3rd UVB irradiation (Fig. 4.4D). Interestingly, the *Hus1*$^{neo/\Delta 1}$ mice also had increased melanocytes at the IFE (Fig. 4.4E), suggesting a role for *Hus1* in regulating inflammation and melanocyte proliferations following UV damage.

From a mechanistic point of view, the DNA adducts induced by UV are recognized by a NER sensor protein, XPC (XPC complex subunit, DNA damage recognition and repair factor), along with DDB1 (damage-specific DNA-binding protein 1)–DDB2 (XPE), subunits of the CRL4 complex (CUL4A–DDB–ROC1). A recent study identified a role for NEDD8–CUL4A in fine-tuning XPC ubiquitination levels and subsequent NER (Yang et al., 2016). One of the subunit of the 9-1-1 complex, RAD9A has been shown to colocalize with XPC at damage sites (Li et al., 2013). Given the role for 9-1-1 complex and neddylation protein in NER, we planned to investigate the chromatin localization of the neddylation and NER proteins in response to UV-induced DNA damage in *Hus1*$^{+/+}$ and *Hus1*$^{-/-}$ cells. However, we were unable to test XPC, and other NER and neddylation proteins due unavailability of effective antibodies that are compatible with mouse proteins.

Figure 4.4. HUS1 is important for UV-induced DNA damage response. (A) Experimental schematic for UVB treatment to observe melanocyte migration in *Hus1*$^{+}$ and *Hus1*$^{neo/\Delta1}$ mice. (B) Gross analysis of *Hus1*$^{+}$ and *Hus1*$^{neo/\Delta1}$ mice after two rounds of UVB exposure. The images were taken five days after the first UVB exposure. (C) Lineage tracing of melanocytes using antibody against TRF2, following two rounds of UVB treatment in *Hus1*$^{+}$ and *Hus1*$^{neo/\Delta1}$ mice. Tissues were counterstained with anti-TRF2 antibody, serving as a marker for melanocytes, anti-KRT5 (marker for interfollicular epidermis) and DAPI for DNA staining. (D) Haematoxylin and eosin (H&E) staining of *Hus1*$^{+}$ and *Hus1*$^{neo/\Delta1}$ mice tissues after three rounds of UVB treatment. IF counterstained with DAPI. (E) Lineage tracing of melanocytes using antibody against TRF2, following three rounds of UVB treatment in *Hus1*$^{+}$ and *Hus1*$^{neo/\Delta1}$ mice. Tissues were counterstained with anti-TRF2 antibody, serving as a marker for melanocytes, anti-KRT5 (marker for interfollicular epidermis) and DAPI for DNA staining.

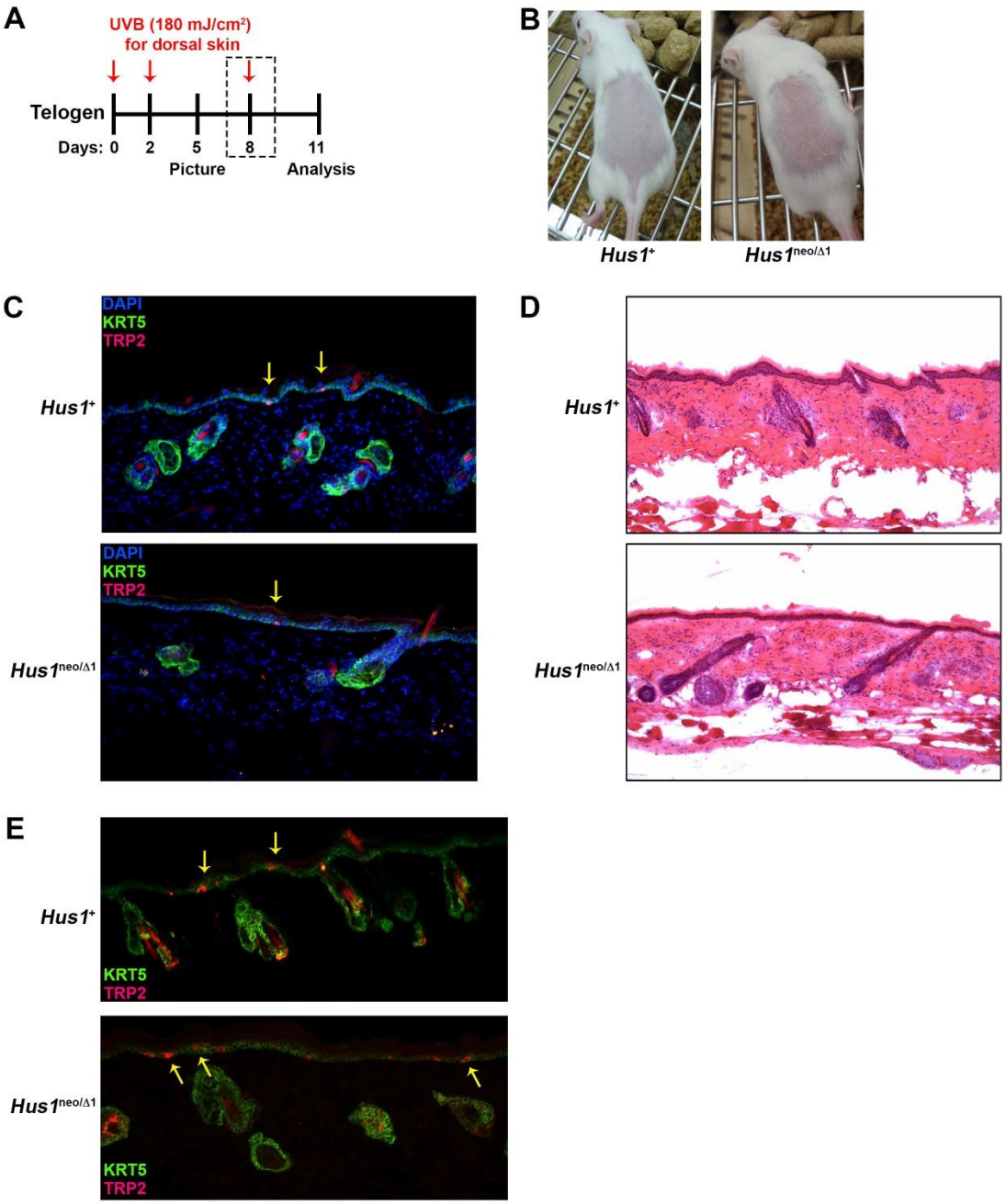
A
UVB (180 mJ/cm²)
for dorsal skin
Telogen
Days: 0 2 5 8 11
Picture
Analysis
B
Hus1+
Hus1neo/Δ1
C
DAPI
KRT5
TRP2
Hus1+
Hus1neo/Δ1
D
Hus1+
Hus1neo/Δ1
E
Hus1+
KRT5
TRP2
Hus1neo/Δ1
KRT5
TRP2

Auxin-inducible degron (AID) tagging of *HUS1* allowed rapid depletion of endogenous HUS1 in human cells

With our proteomics data identifying the 9-1-1 interactors using human HEK293T cells, and the lack of specific mouse protein antibodies, we established a human cell line-based system to test the impact of *Hus1* loss. This system would also allow us to access the role for the 9-1-1 complex using human cells. We utilized the AID (auxin-indubile degron) tagging system established in (Natsume et al., 2016), which allowed us to deplete endogenous HUS1 protein upon auxin treatment. Using CRISPR/Cas, we generated a DSB after the last codon of the *Hus1* to insert an in-frame mAID cassette into the parental cell lines (Fig 4.5A). The parental HCT116 cells already expressed *Oryza sativa* TIR1 (OsTIR1), an auxin responsive F-box protein that forms a functional SCF^{TIR1} ubiquitin ligase within the eukaryotic cells. Upon addition of auxin, mAID tagged HUS1 will bind auxin allowing the OsTIR complex to poly-ubiquitinate and subsequently degrade the mAID fused protein.

To test our HUS1-mAID system, we subjected the mAID-tagged HUS1 cells with genotoxic stress and measured their ability to form colonies and proliferate. As expected, auxin treated HUS1-mAID cells conferred hypersensitivity to MMC treatment (Fig 4.5B). Similarly, auxin treatment in the HUS1-mAID cells also displayed colony formation defect without any genotoxic stress, and the defect was enhanced upon addition of hydroxyurea (Fig. 4.5C). Immunoblot analysis using antibody against pCHK1 (S317) confirmed disruption of MMC induced 9-1-1 mediated ATR-mediated checkpoint in auxin treated HUS1-mAID cells compared to non-auxin treated HUS1-mAID and control cells (Fig 4.5D). Auxin treated HUS1-

mAID cells also resulted in reduced MMC-induced RAD51 focus formation compared to untreated cells (Fig 4.5E). Lastly, we utilized DR-GFP system to see if homology-directed recombination (HDR) is impacted with loss of *HUS1*. As expected, auxin treated HUS1-mAID cells had reduced HDR compared to untreated control cells (Fig. 4.5F). Overall, these findings indicated that HUS1-mAID cells promote auxin induced acute HUS1 depletion in human cells and phenocopies the defects observed in *Hus1*$^{-/-}$ MEFs.

4.5. DISCUSSION

The role of the 9-1-1 complex in activating ATR-mediated checkpoint signaling is very well established; however, its function in DNA repair remains largely unexplored. Herein, we elucidate the role of the 9-1-1 complex in DNA repair and identify novel 9-1-1 complex–interacting proteins using proteomic analysis. Among the candidates, an interesting subset of the neddylation machinery proteins was identified as potential 9-1-1 interactors. The 9-1-1 complex not only interacted with the neddylation factors, but also regulated their expression and recruitment upon DNA damage. In absence of HUS1, UBE2M levels were significantly increased, but only the non-neddylated form of UBE2M was observed onto the chromatin. On the contrary, UBE2M-mediated neddylation target CUL4A levels were significantly reduced upon *HUS1* depletion. Hence, our data suggest a novel role for the 9-1-1 complex in promoting the neddylation pathway by regulating the UBE2M-NEDD8-CUL4A interaction during DNA damage.

Figure 4.5. Auxin-inducible degron (AID) tagging of *HUS1* allowed rapid depletion of endogenous HUS1 in human cells. (A) Experimental scheme used to generate HUS1-mAID cells. A PCR-amplified DNA containing mAID sequence along with neomycin or hygromycin selection marker cassette was cloned in pcDNA5 vector between 200 base pair (bp) *HUS1* homology arms. Donor vectors carrying neomycin and hygromycin, along with a CRISPR/Cas vector targeting *HUS1* locus were transfected in CMV-OsTIR expressing HCT116 cells. Post transfection, cells were subjected with G418 and hygromycin selection, and single cell colonies were isolated and tested to generate HUS1-mAID expressing cells. (B) Short term viability measured in HUS1-mAID expressing HCT116 cells with and without MMC and auxin treatment. (C) Clonogenic survival measured in HUS1-mAID expressing HCT116 cells and control cells with and without HU and auxin treatment. (D) Immunoblot performed using antibody against pCHK1 (S317), mAID, and ACTIN (Control) in HUS1-mAID expressing HCT116 cells and control cells with and without 4h of 0.5 μg/ml MMC and 500 μM auxin treatment. (E) Immunofluorescence staining for RAD51 (Green) in HUS1-mAID expressing HCT116 cells with and without 4h of 0.5 μg/ml MMC and 500 μM auxin treatment. Nuclei were counterstained with 0.05% DAPI (Blue). (F) Analysis of the DR-GFP activity in HUS1-mAID cells with and without auxin treatment.

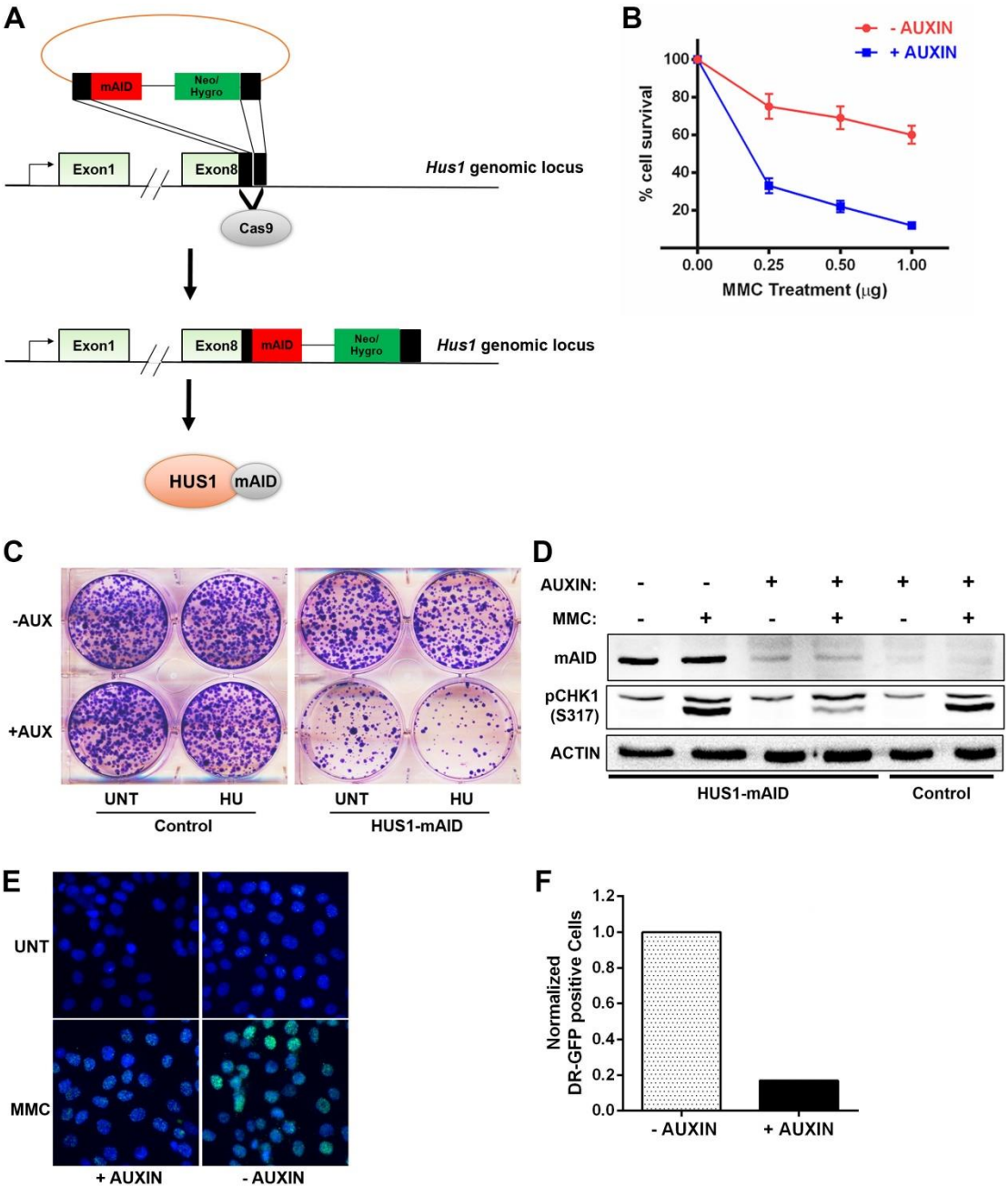
A
mAID
Neo/
Hygro
Exon1
Exon8
Hus1 genomic locus
Cas9
Exon1
Exon8
mAID
Neo/
Hygro
Hus1 genomic locus
HUS1
mAID
B
- AUXIN
+ AUXIN
% cell survival
100
80
60
40
20
0.00
0.25
0.50
1.00
MMC Treatment (μg)
C
-AUX
+AUX
UNT
HU
UNT
HU
Control
HUS1-mAID
D
AUXIN:
MMC:
mAID
pCHK1
(S317)
ACTIN
HUS1-mAID
Control
E
UNT
MMC
+ AUXIN
- AUXIN
F
Normalized
DR-GFP positive Cells
1.2
1.0
0.8
0.6
0.4
0.2
0.0
- AUXIN
+ AUXIN

Advancements in technology have resulted in the identification of several new DDR factors, clarifying the DDR network and their mechanistic regulations. Our proteomics screen is one such tool that promotes the expansion of the DDR network by uncovering novel interactions mediated by the 9-1-1 complex in response to DNA damage. Our proteomics screen pulled down several known 9-1-1–interacting proteins effectively, i.e., TOPBP1, mutS homolog 2 (MSH2)/6, and flap structure–specific endonuclease 1 (FEN1), providing confidence in our data (Xu et al., 2009; Warren et al., 2007; Delacroix et al., 2007). Among the novel interactors, our data identified several Fanconi anemia (FA) pathway members, i.e., FANCI, FANCD2, and FANCA, as potential 9-1-1 interactors (Raschle et al., 2015). Interestingly, independent of the proteomics screen, our lab had also identified FANCD2, FANCA, and several other FA proteins as RAD9A- and HUS1-binding proteins using another high-throughput approach: LUMIER (**lu**minescence-based **m**ammalian **i**nt**er**actome). With another assay identified the same proteins as 9-1-1 interactors, this served as another validation point of our proteomic screen. Another interesting protein identified as a potential 9-1-1 binding partner was PLK1 (polo-like kinase 1). Sufficient evidence suggests that PLK1 interacts physically with TOPBP1 (Moudry et al., 2016); thus, these results lead to the question of whether our MS screen identified direct protein–protein interaction with bait protein or if it showed indirect "neighboring" interactions. To identify 9-1-1–specific interactors, conducting a proteomic screen utilizing a separation-of-function *HUS1* mutant would be important. A recent study in our lab identified residues (R4 and I152) on HUS1 exterior surface hydrophobic pockets that mediated HUS1 interaction with repair proteins (Lim et al., 2015).

Mutating those residues (R4D and I152Y) disrupted the ability of HUS1 to bind DNA repair proteins without perturbing the role of the 9-1-1 complex in ATR activation. Immunoprecipitation (IP)-MS analysis of mutant vs. WT HUS1 proteins would reveal HUS1-specific interactions, eliminating the possibility of direct vs. indirect protein–protein interactions. Further analysis of the RAD9A and RAD1 subunits would also be required to elucidate an accurate 9-1-1 complex interactome.

One of the most interesting novel HUS1 binding partners in our proteomics experiments are cellular neddylation pathway components that modify target proteins with the ubiquitin-like protein NEDD8. A recent publication also implicated the neddylation pathway in regulating UV damage repair protein dynamics by facilitating systematic degradation of repair factor to enable DNA site accessibility to the downstream repair factors (Yang et al., 2016). The pathway has strong translational significance, as neddylation factors are often altered in cancer, and a NAE1 inhibitor, MLN4924, has shown promising results in clinical trials as a cancer therapeutic (Soucy et al., 2010). Notably, RNA interference (RNAi) screen identified synthetic lethality when MLN4924 was applied to *Hus1* knockdown cells, implying a role for HUS1 in regulating neddylation process, however the molecular details still remain unclear (Garcia et al., 2014). This study elaborates the mechanistic role of the interaction dynamics between HUS1 and neddylation proteins. Not only do neddylation proteins interact with the 9-1-1 complex, their expression levels also appear to be altered in response to *Hus1* levels. Being a molecular scaffold, the 9-1-1 complex also alters neddylation factor recruitment at the damage site. UBE2M levels remained elevated in response to *Hus1* loss; however, the chromatin recruitment of

NEDD8–UBE2M and COPS6 was significantly diminished following MMC-induced DNA damage in *Hus1*$^{-/-}$ cells compared to *Hus1*$^{+/+}$ cells. Along with the neddylation factor, CUL4A levels, which are targets of NEDD8 conjugation, were also decreased in *Hus1*$^{-/-}$ cells. This is an interesting observation, as NEDD8 conjugation to CUL4A E3 ubiquitin ligase activates the enzyme promoting CUL4A-mediated polyubiquitination of target proteins that undergo proteasomal degradation. Recently, it was revealed that chromatin-bound PCNA interacts with proteins containing a PIP degron (PIP box encompassing two additional residues), and allows for targeted degradation via CUL4A E3 ubiquitin ligase (Huh and Piwnica-Worms, 2013; Tsanov et al., 2014; Zhang et al., 2013). As the 9-1-1 complex shares structural similarity (PIP box motif-binding pocket) with PCNA, and our HUS1 MS data suggest interaction with neddylation proteins, it implies a role for HUS1 in promoting neddylation to regulate repair factor degradation.

The screen also identified interaction between two important NER proteins, i.e., ERCC2 (ERCC excision repair 2, TFIIH core complex helicase subunit) and ERCC6 (ERCC excision repair 6, chromatin remodeling factor), with the 9-1-1 complex. Some evidence in the literature implicates the 9-1-1 complex in regulating NER; however, as studies are limited, most of the mechanistic details remain unknown (Li et al., 2013). *Hus1* loss can cause hypersensitivity to UV treatment in cells, and RAD9A mediates interaction with the NER protein XPC (Li et al., 2013; Weiss et al., 2003). Here, we determined that, following UV radiation, partial *Hus1* loss resulted in increased inflammation and increased melanocyte epithelial migration, suggesting a role for *Hus1* in regulating UV sensitivity in mice. Unfortunately, due to

limited antibody reagents, we could not measure XPC recruitment and its ubiquitination directly, which would be a better marker for NER activity. Similar to the 9-1-1 complex, CRL neddylation also promotes the ubiquitin-mediated proteolysis of $CRL4^{DDB2}$ to regulate XPC levels and subsequent NER (Yang et al., 2016). Using our HUS1-mAID cells, we could use human anti-XPC antibody to test its ubiquitination levels as well as its activity in absence of *HUS1*. Since the neddylation pathway and the 9-1-1 complex are implicated in regulating tumorigenesis, continued use of the HUS1-mAID system in a human cancer cell line will better help in elucidating the clinical relevance for their interactions. With the possibility of HUS1-mAID system establishment in different cell lines, we could also measure the global neddylation levels with and without HUS1 in tumor and non-tumorigenic cell lines. Further investigation will also decode the mechanism through which the 9-1-1 complex mediates the interactions between UV-induced DNA damage repair proteins and neddylation factors to maintain genomic integrity.

Taken together, we know that: 1) *Hus1*-deficient cells are hypersensitive to UV damage, 2) HUS1 interacts with the neddylation pathway upon genotoxic stress, and 3) neddylation is required during UV-induced DNA repair. The data suggest that the 9-1-1 complex may play a central role in repairing UV-induced DNA damage by orchestrating neddylation and CUL proteins assembly at the damage site to initiate repair. Upon UV-induced DNA damage, physical interaction with the 9-1-1 complex is responsible for the localization and coordination of neddylation proteins at the damage site. We propose a model where, following CUL activation by the neddylation machinery, the 9-1-1 complex facilitates repair protein degradation to promote access

of the downstream NER repair factors to the DNA lesion for repair.

4.6. ACKNOWLEDGEMENT

We would like to thank Marcus Smolka, and members of the Smolka lab for performing and conducting the analysis of the proteomics data, as well as their assistance for providing the reagents for the mAID system. We would also like to thank Dr. Andrew White and Dr. Hyeongsun Moon for conducting the UVB treatment and melanocyte migration assays. Finally, we appreciate the feedback and helpful comments received from the members of the Weiss lab.

CHAPTER 5

TUMOR PROMOTING FUNCTIONS FOR THE DNA DAMAGE RESPONSE PROTEIN HUS1*

5.1. ABSTRACT

DNA damage checkpoint pathways have distinct, stage-specific roles in tumorigenesis. Checkpoints protect against cancer-initiating mutations in normal cells, but in some cases support tumor growth at later stages, allowing cancers to tolerate elevated stress levels associated with malignant transformation. Here, we tested the role of the DNA damage response protein HUS1 in malignant transformation. As a 9-1-1 complex component, HUS1 participates in DNA repair and promotes ATR activation. *Hus1* impairment increased oncogene-induced chromosomal aberrations and checkpoint activation, impeding both cell proliferation and cell transformation. Moreover, *Hus1* inactivation decreased tumorigenesis in mouse models of lung and skin cancer. HUS1 levels were elevated in multiple cancer cell lines through a mechanism involving alternative polyadenylation. Unlike their normal counterparts, which express *Hus1* as a long isoform with an extensive 3'UTR, cancer cells utilized a proximal polyadenylation site, yielding a short isoform with a truncated 3'UTR lacking sequences for negative regulation of *Hus1* expression. These data suggest that

* Stephanie Yazinski, Gabriel Balmus, Pei Xin Lim, Kelly Hume, Tim Dinh, John Stupinski, Lee M. Gerwitz, Tiffany Shand, Nedra Holmes, Sharon Guzman, Teresa Southard, Praveen Sethupathy and Robert S Weiss helped with the experiments in this chapter. Full acknowledgement can be found in section 5.6.

cancer cells have an elevated dependency on HUS1 that is satisfied in part by upregulating HUS1 expression through alternative polyadenylation.

5.2. INTRODUCTION

A hallmark of cancer is the presence of elevated cellular stresses that accompany malignant transformation, including replication, proteotoxic, mitotic, metabolic, and oxidative stresses (Halazonetis et al., 2008; Luo et al., 2009). Consequently, neoplastic cells have a greater dependence on stress response proteins, such as heat shock proteins, antioxidant enzymes, and DNA damage response factors. The term "non-oncogene addiction" refers to the concept that cancer cells are "addicted" to these and other non-oncogenic cellular functions that are necessary for them to survive transformation and sustain tumor development (Luo et al., 2009).

The checkpoint pathway headed by the kinase ATR plays a critical role in responding to DNA damage and stalled replication forks (Blackford and Jackson, 2017; Cimprich and Cortez, 2008; Friedel et al., 2009). It follows that the requirement for the ATR pathway may be higher in cells undergoing increased proliferation or hyper-replication, such as that associated with transformation and oncogene-induced proliferation. HUS1 is a critical component of the ATR pathway that, along with RAD9 and RAD1, forms a heterotrimer termed the 9-1-1 complex (Parrilla-Castellar et al., 2004). This PCNA-like clamp functions as a scaffold at DNA damage sites, with interactions between RAD9 and TOPBP1 promoting ATR activation and stress-induced CHK1 phosphorylation (Delacroix et al., 2007; Lee et al., 2007; Weiss et al., 2003; Zhao and Piwnica-Worms, 2001). The 9-1-1 complex additionally physically

interacts with numerous DNA repair proteins, inducing and coordinating their activities at damage sites (Lim et al., 2015) . HUS1 is particularly important during S-phase, with *Hus1* loss resulting in chromosomal instability and embryonic lethality (Weiss et al., 2000a; Weiss et al., 2003; Zhu and Weiss, 2007). We hypothesize that sustained *Hus1* expression may be necessary for cancer cells to survive the stresses associated with malignant transformation.

Several human cancers show increased expression of ATR pathway components, including *RAD9* up-regulation in breast and prostate cancers (Broustas and Lieberman, 2014a; Cheng et al., 2005; Yun et al., 2014), increased *HUS1* expression in ovarian tumors (de la Torre et al., 2008), and *CHK1* overexpression in colorectal and breast cancers (Karnitz and Zou, 2015; Tho et al., 2012; Verlinden et al., 2007). Tumor initiating cells in a mouse mammary tumor model also show up-regulation of several DNA damage response and repair proteins, including *Hus1* (Zhang et al., 2008), suggesting an increased dependence on these proteins during tumorigenesis. Accordingly, mouse models with impaired ATR function in several cases display reduced tumorigenesis following oncogene activation or carcinogen exposure (Bartkova et al., 2005; Chen et al., 2017; Karnitz and Zou, 2015). DNA damage checkpoint inactivation as a therapeutic strategy is currently being tested through kinase inhibitors targeted against ATR and its downstream effector CHK1 (Dietlein et al., 2014; Forment and O'Connor, 2018; Karnitz and Zou, 2015; O'Connor, 2015). While checkpoint dysfunction in some contexts decreases tumorigenesis, mutations of many other DNA damage checkpoint genes, such as *ATM*, *CHK2*, and *p53*, instead results in an elevated tumor incidence in both mice and humans due to an

increase in genomic instability (Bartkova et al., 2005; Jackson and Bartek, 2009b). Mice with partial *Atr* or *Chk1* impairment show modestly increased tumorigenesis in some settings (Blackford and Jackson, 2017), though hypomorphic *Hus1* mice are not predisposed to spontaneous malignancies, despite their increased genomic instability.

Here, we uncover a key role for the 9-1-1 component HUS1 in transformation and cancer development. *Hus1* loss in cultured cells reduced oncogene-induced proliferation and suppressed cell immortalization and malignant transformation. Furthermore, targeted *Hus1* inactivation in mice resulted in decreased tumor formation *in vivo*. Interestingly cancer cells were found to upregulate HUS1 through a mechanism involving alternative polyadenylation, which generates truncated *Hus1* transcripts that lack sequences for negative regulation of *Hus1* expression. In sum, the results shown here identify HUS1 as a new element of non-oncogene addiction and highlight the potential value of HUS1 as a target for cancer therapy.

5.3. MATERIALS & METHODS

Mice - $Hus1^{Flox}$, $Hus1^{+/\Delta 1}$, and $Hus1^{+/Neo}$ mice (Levitt et al., 2005; Levitt et al., 2007; Weiss et al., 2000a) were maintained on a 129S6 inbred genetic background. *LSL-*$Kras^{G12D}$ mice were maintained on an FVB inbred genetic background (Jackson et al., 2001). To generate experimental $Hus1^{Neo/\Delta 1}$ mice, as well as littermate controls, $Hus1^{+/\Delta 1}$ and $Hus1^{+/Neo}$ mice were bred, and first generation offspring were used for DMBA/TPA experiments. To generate $Hus1^{Neo/Neo}$ and control littermates, $Hus1^{+/Neo}$ mice were intercrossed. All animals were genotyped by PCR analysis of DNA extracted from tail tip biopsies. All animals used in this study were handled in

accordance with federal and institutional guidelines, under a protocol approved by the Cornell University Institutional Animal Care and Use Committee (IACUC).

Cell Culture - GM08399, HeLa, MDA-MB-231, MDA-MB-468, and WI-38 cells were cultured in DMEM supplemented with 10% Fetal Bovine Serum, 1.0 mM L-glutamine, 0.1 mM minimal essential medium amino acids, 100ug/mL Streptomycin sulfate, and 100U/mL penicillin. HME1 cells were cultured in human mammary epithelial cell growth media with addition of supplemental growth factors (epidermal growth factor, hydrocortisone, isoproterenol, transferrin, insulin, and bovine pituitary extract), 100ug/mL Streptomycin sulfate, and 100U/mL penicillin. For the production of mouse embryonic fibroblasts (MEFs), timed matings were performed by breeding $Hus1^{+/Flox}$ $Kras^{LSL\text{-}G12D}$ mice with $Hus1^{+/Flox}$ mice or by breeding $Hus1^{+/Neo}$ females with $Hus1^{Neo/\Delta 1}$ males. Embryos from pregnant females were harvested at 13.5dpc, as previously described (Levitt et al., 2007). After removal of the head, liver, and spleen, the remaining cells were plated in DMEM + 10% FBS, 1% non-essential amino acids, 1% L-glutamine, 1% penicillin streptomycin. Immortalized $Hus1^{-/-}$ and $Hus1^{+/+}$ MEFs on a $p21^{-/-}$ background were described previously (Weiss et al., 2003). All MEFs were maintained on a 3T3 passaging protocol (Todaro and Green, 1963).

Adeno-Cre infection of MEFs and metaphase spread preparation - Immortalized MEFs were seeded in 6-well plates and infected with Adeno-Cre virus in media containing heat inactivated serum and polybrene. Cells were passed after 48 hours and subsequently used for proliferation assays (Blasco et al., 1997), metaphase spread

preparation, and western blotting. Metaphase spreads were generated as described previously and evaluated using standard guidelines (Savage, 1976). Briefly, cells were treated with 0.15ug/ml colcemid for 1hr, harvested with trypsin, treated with hypotonization buffer (0.034M KCl/0.017M sodium citrate), fixed with methanol/acetic acid (3:1), and spotted onto microscope slides. Spreads were stained with 2% Giemsa in Gurr buffer and imaged at 100X magnification.

Virus production and infection - Ecotropic viruses were generated from Phoenix-Eco packaging cells following transfection using Fugene 6 (Roche) with plasmids pBabe-p-GFP, pBABE-p-HRas-V12 (Serrano et al., 1997), or pBABE-c-mycT58A+HRasG12V (Kendall et al., 2005), along with p(Psi)2 packaging vector. After collection of the virus-containing media from the transfected cells, 2 x 10^5 immortalized MEFs were seeded to a single well of a gelatinized 6-well plate and with virus in media containing heat inactivated serum and polybrene. Cells were passed after 48 hours and subsequently used for anchorage-independent growth assay.

Anchorage independent growth assays - Immortalized MEFs were infected with equal volumes of packaged retroviruses pBabe-p-GFP, pBABE-p-HRas-V12 (Serrano et al., 1997), or pBABE-c-mycT58A+HRasG12V (Addgene plasmid 11130) (Kendall et al., 2005). 48 hours after infection, 1 x10^5 cells were seeded in 0.4% top agar, plated over 0.6% base agar in 60mm dishes, and fed once a week with fresh top agar. Plates were imaged after two weeks of growth, and colony number and size were analyzed using ImageJ®. Statistical analysis of the data was by two-tailed Student's t-test.

Lung tumorigenesis and analysis - Mice were anesthetized with 2.5% Avertin and administered $6.67X10^8$ PFU of Adeno-Cre in 40 ul of MEM/CaCl2 directly into a catheter inserted in the trachea (DuPage et al., 2009). Mice were sacrificed at 8 or 20 weeks post-infection, and lungs were harvested, fixed, and processed for histopathological analysis. Lungs were serial sectioned, stained by Hematoxylin and Eosin, and scored for areas of hyperplasia, adenoma, or adenocarcinoma. Image quantification was performed using Aperio ImageScope software. Statistical analysis was performed with Prism 6 (GraphPad).

Two-step skin carcinogenesis - Mice were anesthetized with 2.5% Avertin and the dorsal trunk was shaved. Failure of hair regrowth after three days was used to confirm that the animals were not in anagen phase of the hair growth cycle (Muller-Rover et al., 2001). Mice treated with a single dose of 200nmol DMBA in acetone. One week following DMBA treatment, mice were treated twice weekly with 5μg TPA in acetone for twenty weeks. Papilloma development was monitored twice weekly, and tumor number and size were noted. Mice were euthanized 20 weeks post-DMBA application following intraperitoneal injection with 50μg of BrdU per gram of body weight at 6 hrs prior to euthanasia, and skin was harvested, fixed, and processed for histopathological analysis. Statistical analyses were performed with a random coefficient model with random slope and intercept. The fixed effects were the genotype, days, and their interaction term. Tumor latency was plotted using a Kaplan-Meier survival curve and analyzed by log rank survival analysis using SPSS software.

In vivo sensitivity to DMBA and TPA - For assessment of the acute sensitivity of skin cells to DMBA or TPA, mice were anesthetized with 2.5% Avertin, shaved, and given a single treatment of DMBA or TPA. Twenty hours after initial treatment, mice were injected intraperitoneally with 50μg of BrdU per gram of body weight. Four hours later, mice were euthanized and skin samples were harvested, fixed in formalin, paraffin embedded, and sectioned. Tissue sections were stained by TUNEL assay (ApopTag® Peroxidase In Situ Kit - Millipore) to assess apoptosis or with anti-BrdU antibody (Zymed-Invitrogen) to assess proliferation. Approximately 500 cells in at least three fields of view at 40X magnification from at least three mice were counted. Statistical analysis was by a random coefficient model with random slope and intercept. The fixed effects were the genotype, dose, and their interaction term.

Sensitivity to DMBA and TPA in cell culture - Primary MEFs were treated with a single dose of either DMBA or TPA dissolved in acetone or acetone alone added to cell culture media. The media was changed after 24 hours, and cell survival was determined after 48 hours using trypan blue exclusion staining to count viable cells.

Southern blotting - Genomic DNA for Southern blotting was isolated from infected cells or lung tissue using Proteinase K digestion and ethanol precipitation. DNA was digested with *Nhe*I, subjected to gel electrophoresis, transferred to a nylon membrane, and hybridized with a ^{32}P-labeled 190-base pair *Eag*I fragment from plasmid pCR2.1-5'UTR-Δ2,3, as previously described (Levitt et al., 2005). The extent of deletion of the conditional *Hus1* allele was quantified using a PhosphorImager (GE Healthcare).

Large-T antigen immortalization assay - Primary MEFs were prepared, grown in a low (3%) oxygen atmosphere, and transfected at passage 1 using Fugene 6 (Roche) with plasmids pSG5-Large-T (Zalvide and DeCaprio, 1995) or eGFP-C2 as a control for transfection efficiency. The transfected cells were passed after 48 hours, plated at low density, and fed every three days. After two weeks, immortalized colonies were harvested, pooled, and cultured further, or the plates were fixed with methanol, and stained overnight with 0.01% crystal violet in 95% ethanol. Colonies were counted for each plate, and statistical analysis was performed by T-test.

Luciferase assay: Human *HUS1* 3'UTR fragments were cloned from 293 genomic DNA by PCR (see Table 5.1 for primer sequences) and inserted downstream of Renilla luciferase in the pmirGLO plasmid (Promega). The resulting constructs were transfected into HME1 cells with FuGENE 6 transfection reagent (Promega). Following selection with 50 ug/mL G418, surviving colonies were pooled and replated for sequential measurement of Firefly and Renilla luciferase activity using the Dual-Glo Luciferase Assay system (Promega). For each well, the luminescence value for firefly luciferase were normalized against that for Renilla luciferase.

Immunoblotting - Standard immunoblotting procedures were performed using antibodies specific for HUS1 (Lyndaker et al., 2013b), MYC (Santa Cruz), HA (Covance), pCHK1 Ser345 (Cell Signaling), CHK2 (Cell Signaling), Histone 3 (Abcam), p53 (sigma), p-RPA32 (Bethyl), γH2Ax (Millipore) or β-actin (Sigma).

Table 5.1. Oligonucleotide sequences for qPCR and cloning

Human *HUS1* short isoform (qPCR)	Forward 5’ CACCCATGAGGACAGAAAC 3’ Reverse 5’ AGGCCTTTGTGGGATTTAC 3’
Human *HUS1* long isoform (qPCR)	Forward 5’ CCCAGTGACAGAAAGAACAG 3’ Reverse 5’ GTCCTCAGCAAGAGAGAGA 3’
Human *β-ACTIN* primers (qPCR)	Forward 5’ CCAACCGCGAGAAGATGA 3’ Reverse 5’ CCAGAGGCGTACAGGGATAG 3’
Human *HUS1* 3’ UTR short isoform (cloning)	Forward 5’ CTCGCTAGCCACCCTGTCGCT 3’ Reverse 5’ GAGGTCGACGAGCAACATGAAGTGATA TGTTTATCCA 3’
Human *HUS1* 3’ UTR long isoform (cloning)	Forward 5’ CTCGCTAGCCACCCTGTCGCT 3’ Reverse 5’ GAGGTCGACCTCAACTAAGGTTTCTTT AGCCACA 3’
RNAi – UPF1	5’-GAUGCAGUUCCGCUCCAUU-3’

RNA Isolation, RT-PCR and qPCR - Total RNA was isolated from various cell lines using RNA-STAT60 (Tel-Test 60) as per the manufacturer's instructions. DNAse-treated total RNA was revered transcribed using the qScript cDNA synthesis Kit (Quanta Biosciences). For qPCR analysis, RT reaction products were amplified with the Bio-Rad CFX96 Touch Real-Time PCR Detection System in triplicate using Sybr Green Select Master Mix (Life Technologies) along with isoform-specific primers (Table S1). The average fold change in gene expression was normalized to actin as an endogenous control for each sample.

Transfection - HEK293T cells were transfected with pCI-neo-FLAG-UPF1 R843C (Isken et al., 2008) plasmid that contained the dominant negative form of UPF1, using lipofectamine 2000 (Invitrogen). Cells were incubated in for 48 hours before RNA extraction. Using lipofectamine 2000, HEK293T cells were incubated with RNAi against UPF1 and incubated for 48 hours before RNA extraction.

5.4. RESULTS

Simultaneous conditional *Hus1* inactivation and *K-ras* activation result in slowed proliferation, increased chromosomal aberrations, and checkpoint activation.

DNA damage checkpoint proteins, and ATR pathway components in particular, have been associated with both tumor suppressor and promoter activities. In order to determine how loss of *Hus1*, an important ATR activator and protector of genomic integrity, affects cell transformation and tumorigenesis, we compared proliferation rates and chromosomal aberrations in mouse embryo fibroblasts (MEFs) with

inducible *K-ras* activation, with or without a *Hus1* defect. Mice carrying conditional alleles of *Hus1* (*Hus1*^{Flox}) and activated *K-ras* (*K-ras*$^{LSL-G12D}$) were intercrossed and embryos were harvested to generate *Hus1*$^{Flox/Flox}$ *K-ras*$^{LSL-G12D}$ and appropriate control MEFs (Levitt et al., 2005). Primary cultures were infected with an adenovirus (Adeno-Cre) that expresses CRE-recombinase, which inactivates *Hus1* by deleting exons 2 and 3 (Fig. 5.1A) and induces expression of *K-ras*^{G12D} by removing a lox-stop-lox cassette. While expression of K-RAS^{G12D} alone in cells which retained Hus1 expression (*Hus1*$^{+/Flox}$ *Kras*$^{+/LSL-G12D}$) resulted in increased proliferation as expected, simultaneous *Hus1* loss and *K-ras* activation resulted in decreased proliferative potential (Fig. 5.2A). *Hus1*$^{Flox/Flox}$ *Kras*^{G12D} MEFs demonstrated significantly reduced population doublings compared to cells that lost *Hus1* expression alone (*Hus1*$^{Flox/Flox}$ *Kras*$^{+/+}$).

To understand mechanistically which pathways were responsible for the decreased proliferation following *K-ras* activation in the context of *Hus1* dysfunction, Western blotting was performed on lysates prepared from MEFs at 3 or 6 days following Adeno-Cre infection (Fig. 5.2B, 5.1B). Combined *Hus1* loss and *K-ras* activation resulted in phosphorylation of the histone variant H2AX, phosphorylation of RPA, and activation of p53, indicating robust DNA damage response pathway activation. Consistent with this interpretation, *Hus1*$^{Flox/Flox}$-*Kras*^{G12D} MEFs showed an increase number of chromosomal abnormalities relative to cells with either *K-ras* activation or *Hus1* loss alone, at both three (Fig. 5.2C and D) and six days (Fig 5.1C) post-infection. Taken together these data indicate that oncogenic stresses in combination with loss of the DNA damage checkpoint protein HUS1 result in severe chromosomal damage and an overall growth disadvantage.

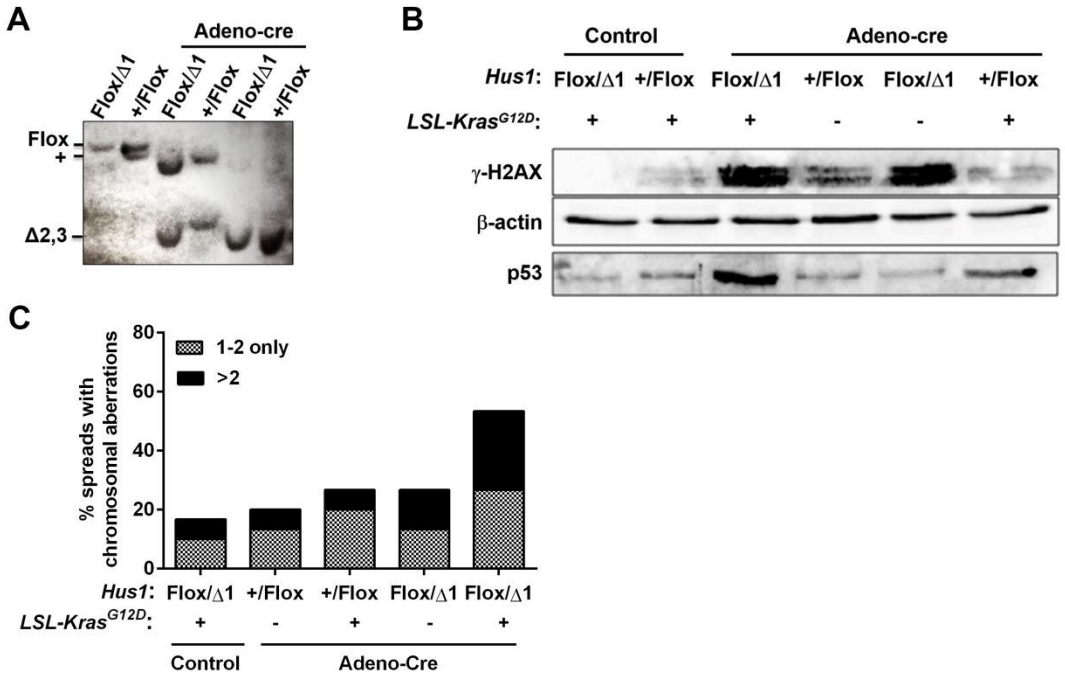

Figure 5.1: Enhanced oncogene-induced checkpoint activation and chromosomal aberrations following conditional *Hus1* inactivation. (A) Southern blot analysis of genomic DNA prepared from MEFs of the indicated genotype confirming recombination and deletion of floxed *Hus1* allele. The position of the bands for the conditional ($Hus1^{Flox}$), wild-type ($Hus1^{+}$), and recombined inactivated ($Hus1^{\Delta 2,3}$) *Hus1* alleles are indicated. (B) Western blot analysis of lysates from MEFs of the indicated genotype 6 days post Adeno-Cre infection. (C) Quantification of chromosomal aberrations in metaphase spreads prepared from MEFs of the indicated genotype 6 days post Adeno-Cre infection. 30 metaphase spreads were analyzed for each genotype.

Figure 5.2. Decreased proliferation, checkpoint activation, and chromosomal aberrations following simultaneous conditional *K-ras* activation and *Hus1* inactivation. (A) MEFs of the indicated genotype were infected with Adeno-Cre virus at day 0. Following recombination, cells undergo deletion of the floxed *Hus1* allele, leaving either one (in $Hus1^{+/Flox}$ cells) or no (in $Hus1^{Flox/\Delta 1}$cells) functional copies of *Hus1*. Cells containing the $LSL\text{-}K\text{-}ras^{G12D}$ express activated K-RAS following Adeno-Cre infection. Cells were counted and passed every three days and population doublings were calculated. (B) Western blot analysis of lysates from MEFs of the indicated genotypes 3 days post adeno-Cre infection. (C) Representative metaphase spreads prepared from MEFs of the indicated genotypes 3 days post adeno-Cre infection. Black arrowheads indicate chromosomal aberrations. (D) Quantification of chromosomal aberrations in metaphase spreads prepared from MEFs of the indicated genotype 3 days post adeno-Cre infection. 30 metaphase spreads were analyzed for each genotype.

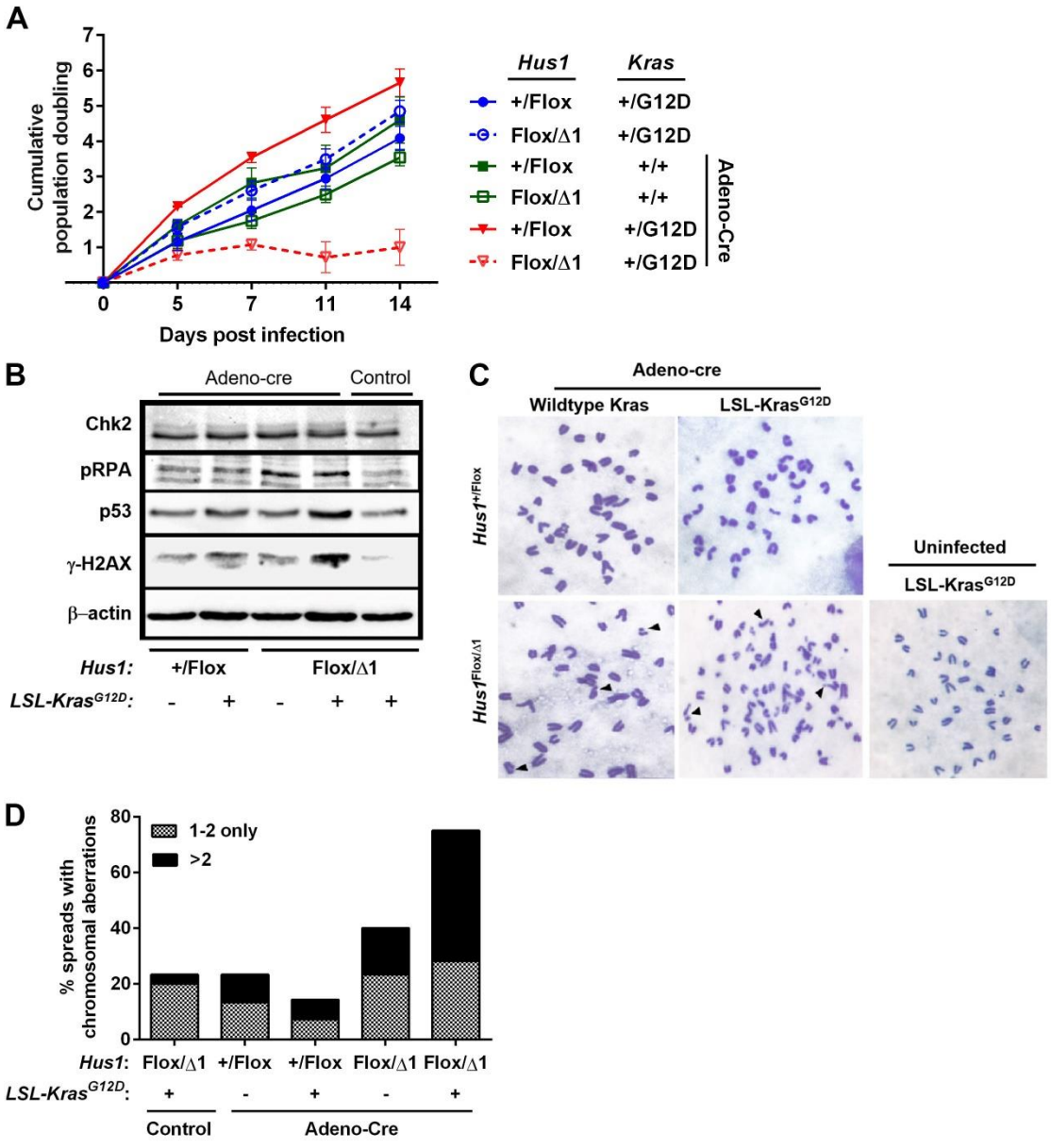
A
Cumulative population doubling
Days post infection
Hus1
Kras
+/Flox
+/G12D
Flox/Δ1
+/G12D
+/Flox
+/+
Flox/Δ1
+/+
+/Flox
+/G12D
Flox/Δ1
+/G12D
Adeno-Cre
B
Adeno-cre
Control
Chk2
pRPA
p53
γ-H2AX
β–actin
Hus1:
+/Flox
Flox/Δ1
LSL-KrasG12D:
C
Adeno-cre
Wildtype Kras
LSL-KrasG12D
Hus1+/Flox
Hus1Flox/Δ1
Uninfected
LSL-KrasG12D
D
% spreads with chromosomal aberrations
1-2 only
>2
Hus1: Flox/Δ1 +/Flox +/Flox Flox/Δ1 Flox/Δ1
LSL-KrasG12D: + - + - +
Control
Adeno-Cre

Complete *Hus1* loss impairs malignant transformation in cultured cells.

As conditional *Hus1* loss in combination with oncogene expression resulted in decreased proliferation, we next assessed whether *Hus1* deficiency impacts oncogene-induced transformation. A stringent assay of transformation, colony formation in soft agar following oncogenic *H-ras* expression, was used to compare *Hus1* wildtype (*Hus1*$^{+/+}$) and *Hus1*-null (*Hus1*$^{-/-}$) MEFs for the number and size of macrocolonies, reflecting the degree of transformation (Freedman and Shin, 1974). Littermate-matched immortalized *Hus1*$^{+/+}$ and *Hus1*$^{-/-}$ MEFs (Weiss et al., 2003) were transduced with a virus expressing activated *H-ras*, followed by selection of oncogene-expressing cells. *Hus1*$^{-/-}$ cells formed significantly fewer colonies in soft agar than *Hus1*$^{+/+}$ ($p<0.001$) following oncogenic *H-ras* expression (Fig. 5.3A and B). Furthermore, *Hus1*$^{-/-}$ cells expressing activated *H-ras* displayed increased DNA damage response activation as indicated by accumulation of γH2AX, p53, and phosphorylated RPA (Fig. 5.3C), similar to that observed with conditional *K-ras* activation with acute *Hus1* loss. By comparison, *Hus1*$^{+/+}$ MEFs exhibited relatively lower proteins levels of *H-ras*-induced p53 and phosphorylated RPA. Taken together, these data indicate that cells experiencing activated *Ras* signaling require HUS1 to prevent high levels of oncogene-induced DNA damage and to efficiently undergo malignant transformation.

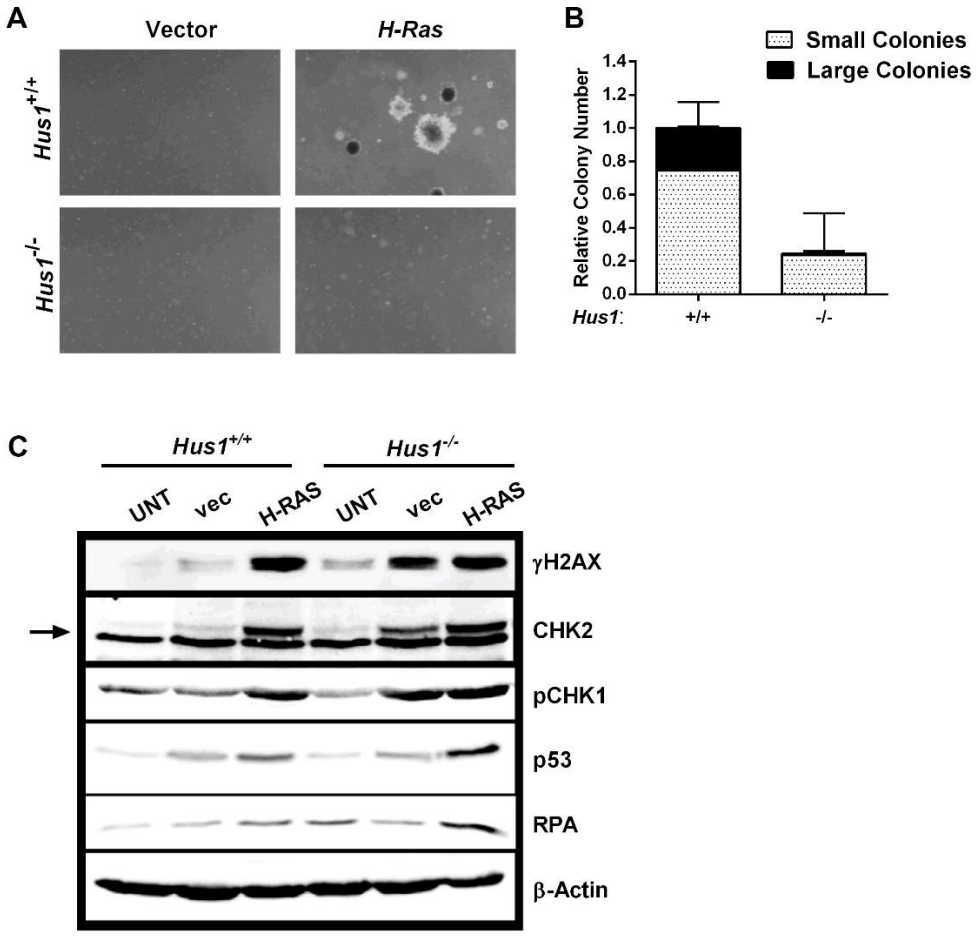

Figure 5.3. Decreased cell transformation associated with increased checkpoint activation following oncogene activation in *Hus1*-deficient cells. (A) Representative images from a soft agar growth assay using immortalized MEFs of the indicated genotype following transduction with a virus expressing activated *H-Ras*. (B) Quantification of the results shown in panel A. Three independent experiments were averaged. Data in each experiment were normalized to the total colony number for *Hus1*$^{+/+}$ cells to account for differences due to viral preparations. Small colony number: p=0.0007; Large colony number: p=0.0003; Total colony number: p<0.0001 (C) Western blot analysis of lysates from MEFs of the indicated genotypes 3 days post transduction with a virus expressing vector or activated *H-Ras.*

Conditional *Hus1* inactivation results in decreased tumor burden in a mouse model of lung cancer.

As absence of *Hus1* resulted in decreased activated *Ras*-induced transformation in cultured cells, we next sought to determine if *Hus1* loss would decrease tumorigenesis *in vivo* using a mouse model of non-small cell lung cancer. We employed the same *K-ras*$^{LSL\text{-}G12D}$ system described above in combination with Adeno-Cre infection of the lungs, which was previously demonstrated to result in lung hyperplasia, adenoma, and with extended incubation or additional genetic alterations, adenocarcinoma (Jackson et al., 2001). Along with control littermates, mice homozygous for the conditional *Hus1*^{Flox} and *K-ras*$^{LSL\text{-}G12D}$ alleles were administered Adeno-Cre intratracheally, and sacrificed at 8 or 20 weeks post-infection. At 8 weeks post-infection, *Hus1* expression had no apparent impact on the extent of hyperplasia or adenoma (Fig. 5.4A). However, at 20 weeks post oncogene activation, control *Hus1*$^{+/+}$ *K-ras*$^{LSL\text{-}G12D}$ and *Hus1*$^{+/Flox}$ *K-ras*$^{LSL\text{-}G12D}$ mice, which retained *Hus1* expression following Cre-mediated deletion, developed large areas of hyperplasia and adenoma in the lungs, as expected (Fig. 5.4B and C, 5.5). By contrast, *Hus1* deficiency in *Hus1*$^{Flox/Flox}$ *K-ras*^{G12D} mice resulted in reduced hyperplasia and adenoma compared to control mice, following expression of activated *K-ras* (Fig. 5.4B and C). The size of the largest adenoma per mouse also was significantly smaller in *Hus1*$^{Flox/Flox}$ *K-ras*^{G12D} mice as compared to *Hus1*$^{+/+}$ *K-ras*$^{LSL\text{-}G12D}$ and *Hus1*$^{+/Flox}$ *K-ras*$^{LSL\text{-}G12D}$ controls (Fig. 5.5). Taken together, the cell culture and animal model results suggest that *Hus1* deficiency interferes with oncogenic RAS-induced malignant transformation and tumorigenesis.

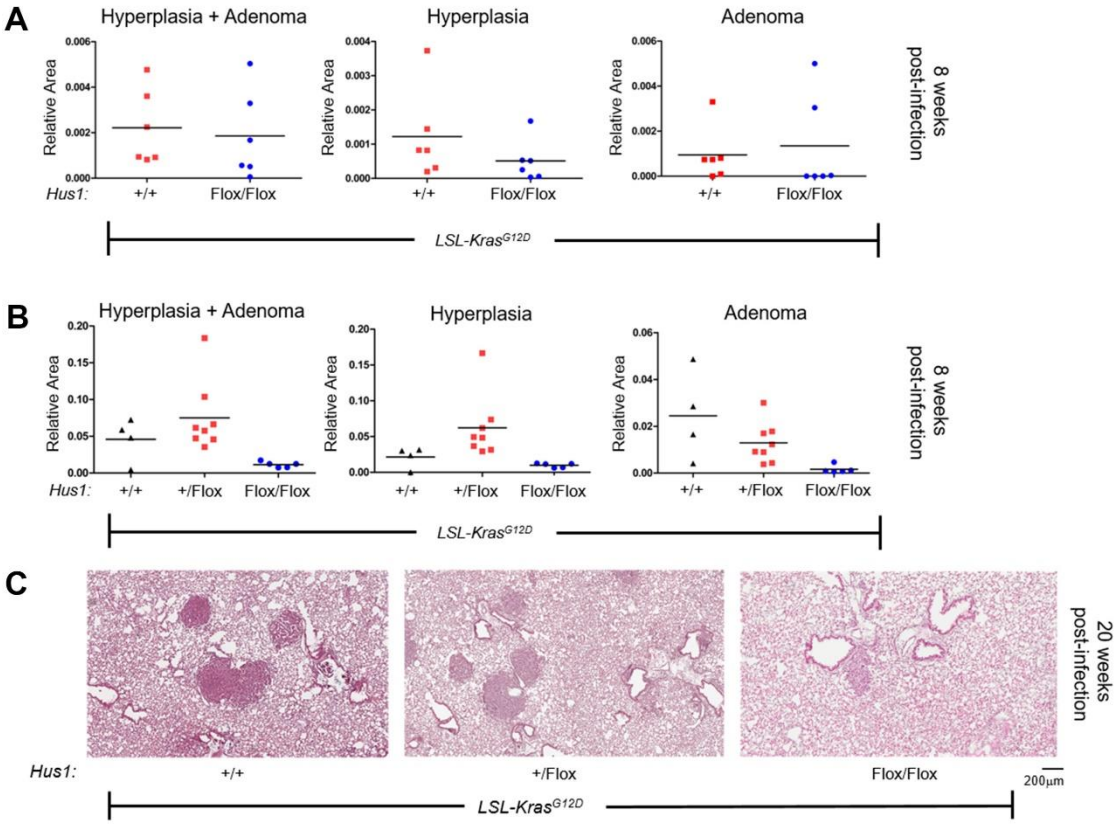

Figure 5.4. Suppression of *Kras*^{G12D}-driven lung tumorigenesis by conditional *Hus1* inactivation. (A) Mice were infected intratracheally with Adeno-cre virus and allowed to develop lesions for 8 weeks. H&E-stained lung tissue sections of were quantified to compare relative areas of hyperplasia and/or adenoma in *Hus1*$^{Flox/Flox}$ (n=6) and *Hus1*$^{+/Flox}$ (n=6) mice. (B) Mice were infected intratracheally with Adeno-Cre virus and allowed to develop lesions for 20 weeks, with subsequent quantification as in A for *Hus1*$^{Flox/Flox}$ (n=4) mice and *Hus1*$^{+/Flox}$ (n=5 mice). (C) Representative H&E-stained sections of lung at twenty weeks following Adeno-Cre infection. Scale bar is 200μm.

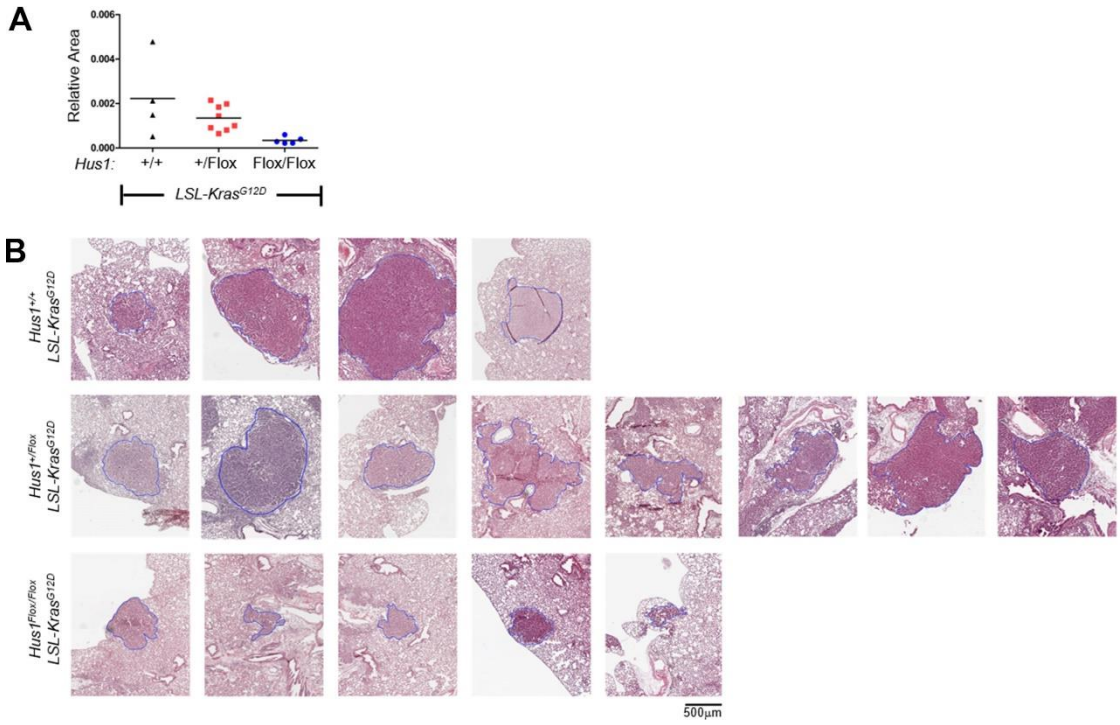

Figure 5.5: Effect of *Hus1* loss on *K-ras* induced lung tumors. (A) Quantification of the largest adenoma observed in each *Hus1*$^{+/+}$ *K-ras*$^{LSL\text{-}G12D}$ (n=4), *Hus1*$^{+/Flox}$ *K-ras*$^{LSL\text{-}G12D}$ (n=8), and *Hus1*$^{Flox/Flox}$ *K-ras*$^{LSL\text{-}G12D}$ (n=5) mouse at 20 weeks post intratracheal Adeno-Cre infection. Adenoma size is given relative to total lung volume. (B) Image of the largest adenoma measured in each mouse described in A. Sections were H&E stained, imaged and measured using Aperio software. Scale bar represents 500µm.

Partial *Hus1* impairment reduces oncogene-induced cell transformation in cultured cells.

Even in the absence of oncogenic events, complete *Hus1* loss results in genomic instability and decreased proliferative potential (Balmus et al., 2016; Lim et al., 2015; Weiss et al., 2003; Zhu and Weiss, 2007). Therefore, we next sought to determine if partially reduced *Hus1* levels that are compatible with normal development were sufficient to impair oncogene-induced transformation. For this purpose, we utilized a hypomorphic *Hus1* allele, $Hus1^{neo}$ that expresses wild-type *Hus1* at reduced levels (Levitt et al., 2007). Initial experiments assessed the ability of primary MEFs expressing incrementally reduced *Hus1* levels to undergo immortalization, the first step in transformation. $Hus1^{Neo/Neo}$ and $Hus1^{Neo/\Delta 1}$ MEFs, which express 40% or 20% of wild type *Hus1*, respectively, were compared to control $Hus1^{+}$ ($Hus1^{+/+}$, $Hus1^{+/Neo}$ and $Hus1^{+/\Delta 1}$) cells, which express *Hus1* at 50-100% of the wild-type level. Primary cultures were induced to undergo immortalization by the Large-T antigen oncogene, which is singly capable of immortalizing cells by targeting the retinoblastoma and p53 tumor suppressor proteins (Ali and DeCaprio, 2001). Primary $Hus1^{+}$ MEFs were more readily immortalized than $Hus1^{Neo/Neo}$ ($p=0.05$) or $Hus1^{Neo/\Delta 1}$ ($p < 0.001$), as quantified by colony formation (Fig. 5.6A and B). No immortalized colonies were formed when cells transduced with a virus expressing GFP were plated at the same density. Importantly, the early passage primary MEFs had similar growth rates prior to Large-T antigen expression and all cultures had nearly equivalent transduction efficiencies, as measured using the GFP-expressing virus (Fig. 5.7A).

Figure 5.6. Decreased immortalization and malignant transformation in MEFs with reduced *Hus1* expression. (A) Representative images of crystal violet-stained colonies formed by primary MEFs of the indicated genotypes following transduction with a virus expressing Large T antigen. (B) Quantification of colony forming assay described in A. Three independent assays were performed and averaged. Colony number in each experiment was normalized to results for $Hus1^{+/+}$ MEFs. Error bars denote standard deviation. The number of immortalized colonies was significantly higher for $Hus1^{+/+}$ MEFs as compared to $Hus1^{neo/neo}$ ($p=0.013$) or $Hus1^{neo/\Delta 1}$ ($p<0.0001$) cells. (C) Quantification of soft agar growth assay described in D. Anchorage-independent growth was significantly greater for $Hus1^{+}$ MEFs as compared to $Hus1^{Neo/Neo}$ or $Hus1^{Neo/\Delta 1}$ ($p=0.04$) cells. Colonies were imaged at 0.5X using stereoscope and counted using ImageJ software. Large colonies were identified as larger than 125 pixels, while small colonies were less than or equal to 125 pixels. Cell line numbers: $Hus1^{+}$: n=7, $Hus1^{Neo/Neo}$: n=3, $Hus1^{Neo/\Delta 1}$: n=8. Stats for total Colony Number: $Hus1^{+}$ versus $Hus1^{Neo/\Delta 1}$: p=0.04,+ versus $Hus1^{Neo/Neo}$: p=0.18, $Hus1^{Neo/Neo}$ versus $Hus1^{Neo/\Delta 1}$: p=0.78. (D) Representative images from a soft agar growth assay with immortalized MEFs of the indicated genotypes following transduction with a virus expressing activated *Ras* and *Myc*.

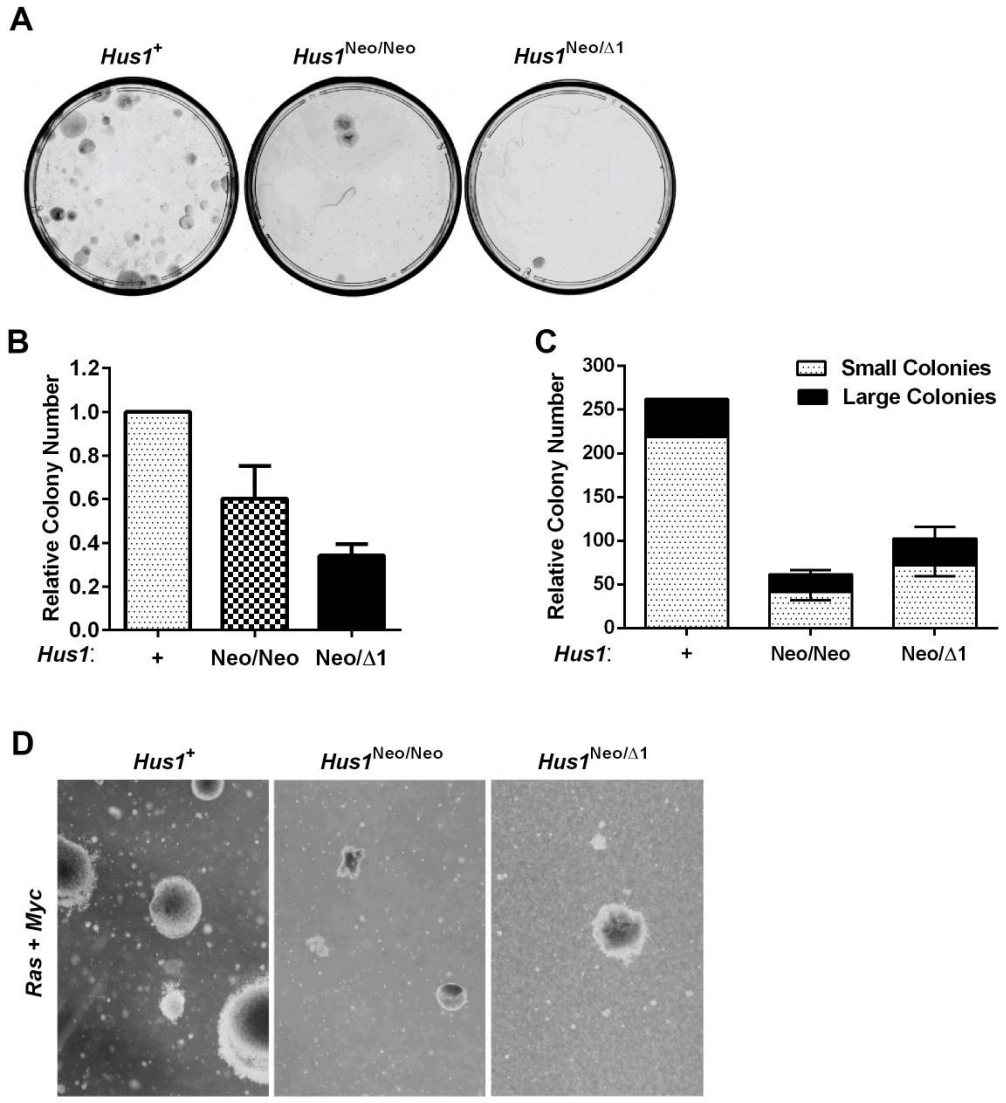
A
Hus1+
Hus1Neo/Neo
Hus1Neo/Δ1
B
Relative Colony Number
1.2
1.0
0.8
0.6
0.4
0.2
0.0
Hus1:
+
Neo/Neo
Neo/Δ1
C
Relative Colony Number
300
250
200
150
100
50
0
Small Colonies
Large Colonies
Hus1:
+
Neo/Neo
Neo/Δ1
D
Hus1+
Hus1Neo/Neo
Hus1Neo/Δ1
Ras + Myc

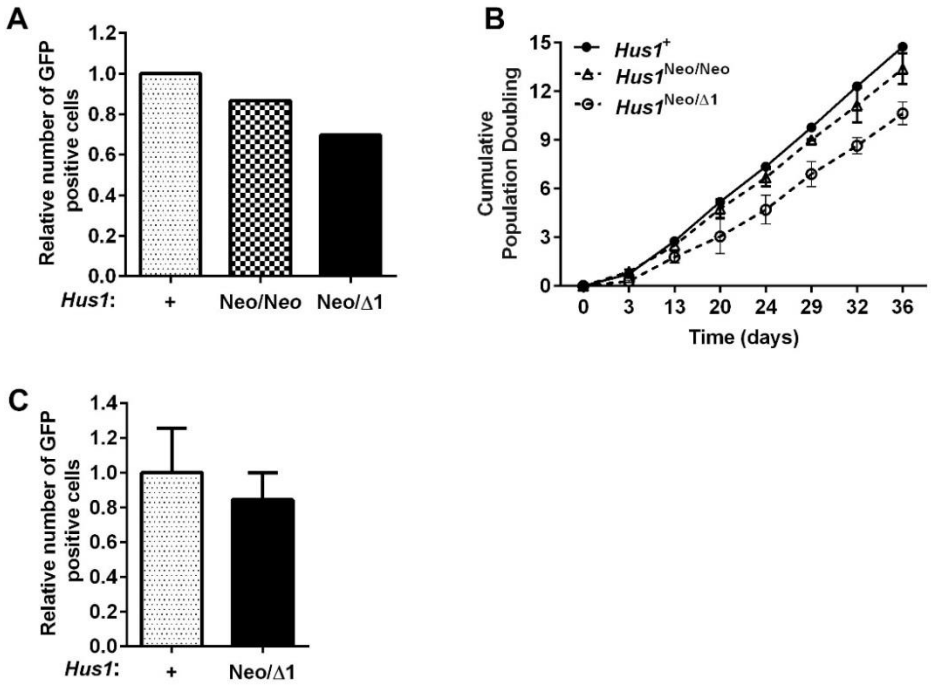

Figure 5.7. Effects of partial *Hus1* impairment on cell immortalization. Primary MEFs of the indicated genotypes following transduction with retroviruses expressing Large T antigen or GFP. (A) At 48 hrs post-infection, cells were analyzed by flow cytometry in order to quantify infection efficiency. $Hus1^{+}$ n=4, $Hus1^{Neo/Neo}$ n=3, $Hus1^{Neo/\Delta 1}$ n=5. $Hus1^{+}$ versus $Hus1^{Neo/\Delta 1}$, p=0.001; $Hus1^{+}$ versus $Hus1^{Neo/Neo}$, p=0.018; $Hus1^{Neo/Neo}$ versus $Hus1^{Neo/\Delta 1}$, p=0.063. Error bars represent SD. (B) After selection, immortalized colonies on each dish were harvested by trypsinization, pooled, and passaged on a 3T3 protocol. The proliferation rates were recorded and analyzed. (C) Large T-Antigen immortalized MEFs were transduced with a GFP-expressing retrovirus in parallel to transduction with a retrovirus expressing activated Ras and Myc. At 48 hr post-infection, cells were analyzed by flow cytometry in order to quantify infection efficiency, as in A. Plots show the relative number of GFP positive cells. $Hus1^{+}$ n=3, $Hus1^{Neo/\Delta 1}$ n=3, p=0.530. Error bars represent SD.

Interestingly, the number of immortalized colonies was reduced in *Hus1*$^{Neo/\Delta 1}$ MEFs, the immortalized colonies that did form despite partial *Hus1* impairment proliferated similarly to *Hus1*$^{+}$ cells (Fig. 5.7B). This enabled us to test the effect of incrementally reduced *Hus1* expression on oncogene-induced malignant transformation using anchorage-independent growth as the readout. Three independently derived, Large-T immortalized MEF cell lines were infected with retroviruses carrying GFP or activated *Ras* and *Myc*, and then grown in a suspension of soft agar. Similar infection efficiency was achieved in cells of each genotype, as determined by evaluating the percentage of cells 48 hours after infection (Fig. 5.7C). None of the cell lines transduced with the GFP-expressing vector formed colonies in soft agar, as expected. However, following expression of activated RAS *and* MYC, *Hus1*$^{+}$ cells formed several colonies in soft agar, in comparison *Hus1*$^{Neo/Neo}$ (p=0.06) and *Hus1*$^{Neo/\Delta 1}$ *(p=0.05)* cells formed fewer and smaller colonies (Fig. 5.6C and D). These results indicate that even reduced *Hus1* levels decrease the ability of cells to become transformed.

Mice with partial *Hus1* impairment are refractory to carcinogen-induced skin tumorigenesis.

Next, we assessed the effects of reduced *Hus1* levels in an *in vivo* model of skin tumorigenesis, using the well-characterized two-step chemical carcinogenesis skin papilloma mode (Hennings et al., 1993). *Hus1*$^{+}$, *Hus1*$^{Neo/Neo}$, and *Hus1*$^{Neo/\Delta 1}$ mice were treated with a single dose of 12-7-dimethylbenz(a)-anthracene (DMBA), followed by repeated applications of 12-O-tetradecanoylphorbol-13-acetate (TPA) over 20 weeks

to induce skin papillomas. DMBA induces A-T transversions at the second nucleotide of codon 61 of *H-Ras* resulting in *H-Ras* activation, and is a well-characterized tumor initiator (Quintanilla et al., 1986). TPA is potent tumor promoter that acts through activation of protein kinase C (Angel et al., 1987). Mice in anagen phase of the hair cycle were excluded from the assay, as stem cell proliferation and migration during anagen may result in altered papilloma development (Trempus et al., 2007). At each TPA application, tumor latency, size, and number were measured.

As reduced *Hus1* levels in cultured cells were linked with partial resistance to immortalization and transformation, we anticipated that fewer tumors would develop in $Hus1^{Neo/Neo}$ and $Hus1^{Neo/\Delta 1}$ mice as compared to $Hus1^{+}$ controls. Interestingly, a subset of $Hus1^{Neo/\Delta 1}$ mice developed papillomas with a slightly shorter latency than either $Hus1^{+}$ or $Hus1^{Neo/Neo}$ mice, though this difference in latency was not significant. Although overall tumor-free survival also was not significantly different between genotypes (Fig. 5.8C, 5.9C), $Hus1^{Neo/\Delta 1}$ mice had a reduced risk of papilloma development after 67 days as compared to $Hus1^{+}$ mice ($p < 0.05$ by Log Rank Hazard Analysis). Because the papillomas arise directly from clonal expansion of initially transformed cells, the number of papillomas directly reflects the transformation potential of the target cells (Yuspa, 1998). Although $Hus1^{Neo/\Delta 1}$ mice were the first to form papillomas, these mice ultimately developed the fewest and smallest papillomas ($p < 0.001$ when compared with $Hus1^{+}$). The average number of tumors and the size of the largest papilloma per mouse was greatest in $Hus1^{+}$ mice (Fig. 5.8 and 5.9), whereas $Hus1^{Neo/Neo}$ mice, with moderately reduced *Hus1* expression, showed an intermediate level of papilloma formation that was nevertheless significantly less than

that in *Hus1*$^{+}$ mice (p=0.004) (Fig. 5.9). Because these studies were conducted in a pure 129S6 strain background, which is associated with resistance for progression of papillomas to squamous cell carcinoma, we could not assess how *Hus1* impacted late stages of malignant progression (Hennings et al., 1993). Only a single papilloma from a *Hus1*$^{+}$ mouse underwent malignant conversion, and no papillomas from *Hus1*$^{Neo/\Delta 1}$ mice progressed to carcinoma. In combination with our cell culture data, these *in vivo* skin carcinogenesis data further support the conclusion that reduced *Hus1* expression impairs oncogene-driven proliferation and transformation.

Reduced *Hus1* levels do not cause acute hypersensitivity to DMBA or TPA

There are at least two possible explanations for the finding that reduced *Hus1* expression is associated with reduced carcinogen-induced papilloma number and size. First, impaired checkpoint function in *Hus1*$^{Neo/\Delta 1}$ cells may prevent transformation as these cells are unable to cope with the increased genomic stress associated with neoplastic proliferation. This possibility is supported by our cell culture data, demonstrating an increase in chromosomal aberrations and enhanced DNA damage checkpoint activation. An alternative explanation would be that impaired DNA damage responses may sensitize *Hus1*$^{Neo/\Delta 1}$ cells to DMBA or TPA, leading to cell death and fewer surviving cells capable of forming papillomas, as has been seen in other mouse models (Yan *et al*, 2004). To test whether cells with reduced *Hus1* expression were sensitive to DMBA or TPA, we treated primary MEFs with increasing doses of DMBA or TPA, and assessed for cell survival using a trypan blue exclusion assay (Fig. 5.10A and 5.11A). *Hus1*$^{Neo/\Delta 1}$ MEFs showed no increased

Figure 5.8. Decreased tumorigenesis following two-step chemical carcinogenesis in mice with partial *Hus1* impairment. *Hus1*$^{+}$ (n=18) and *Hus1*$^{Neo/\Delta 1}$ (n=18) mice were treated with a single DMBA dose followed by repeated TPA applications to induce papilloma formation. Tumor development was monitored for 20 weeks. *Hus1*$^{+}$ control animals include mice of *Hus1*$^{+/+}$ *Hus1*$^{+/Neo}$ and *Hus1*$^{+/\Delta 1}$ genotypes. (A) The average number of papillomas per mouse was plotted for each day. *Hus1*$^{Neo/\Delta 1}$ mice had significantly fewer papillomas as compared to control mice ($p<0.001$, determined by mixed model analysis: linear regression with covariant structure using SPSS software). (B) Fraction of tumor-free survival for *Hus1*$^{+}$ compared to *Hus1*$^{Neo/\Delta 1}$ mice over 20 weeks is not significantly different between genotypes ($p=0.420$, by Log Rank Comparison). *Hus1*$^{Neo/\Delta 1}$ mice were the first to develop papillomas, but showed a decreased risk for tumor development after 67 days ($p<0.05$ by Log Rank Hazard Analysis). (C) The average size of the largest papilloma per mouse was plotted for each day. *Hus1*$^{Neo/\Delta 1}$ mice had a significantly smaller average size for the largest papilloma per mouse as compared to control mice ($p < 0.001$). (D) Representative images of *Hus1*$^{+/+}$ (right) and *Hus1*$^{Neo/\Delta 1}$ (left) sex-matched littermates following DMBA/TPA treatment at 140 days after DMBA treatment.

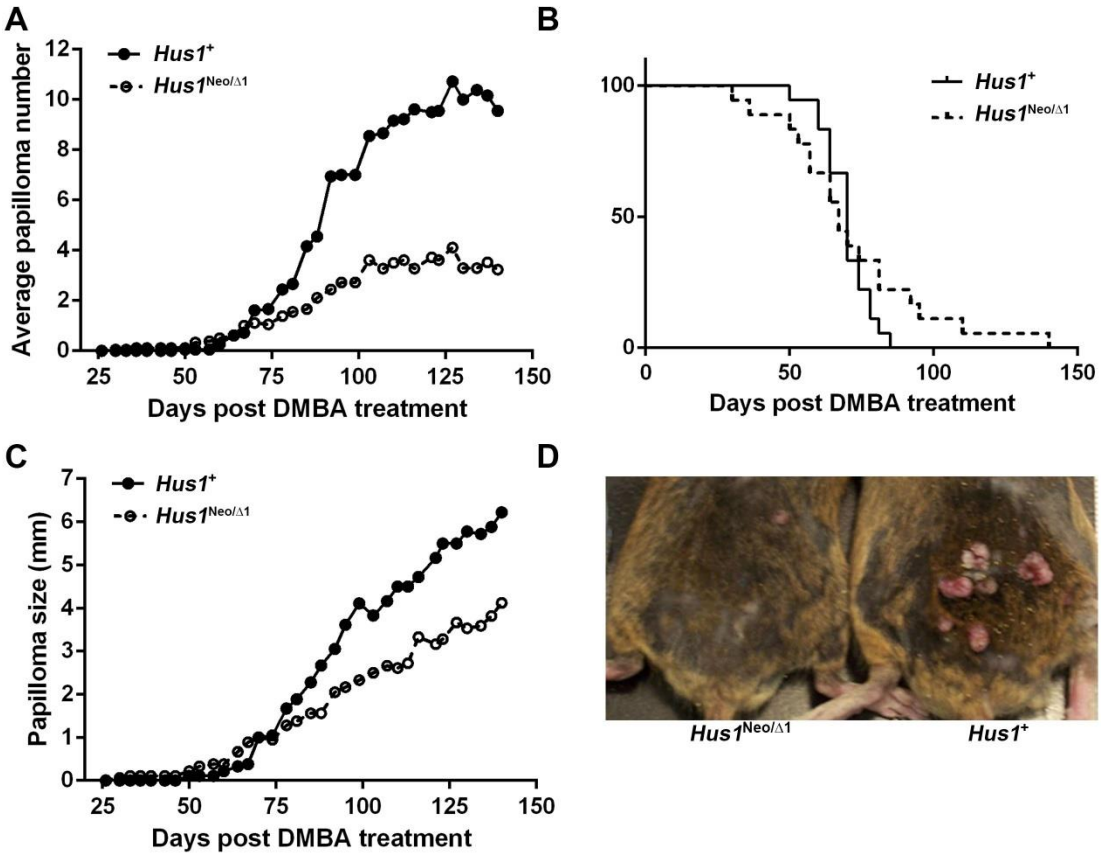
A
Average papilloma number
Hus1+
Hus1Neo/Δ1
Days post DMBA treatment
B
Hus1+
Hus1Neo/Δ1
Days post DMBA treatment
C
Papilloma size (mm)
Hus1+
Hus1Neo/Δ1
Days post DMBA treatment
D
Hus1Neo/Δ1
Hus1+

Figure 5.9: Decreased carcinogen-induced skin tumor development in mice with an intermediate degree of *Hus1* impairment. *Hus1*$^{+}$ (n=19) and *Hus1*$^{Neo/Neo}$ (n=16) mice were treated on their dorsal flank with a single DMBA dose and repeated TPA applications to induce papilloma formation. Tumor development was monitored for 20 weeks. (A) The average number of papillomas per mouse was plotted for each day. *Hus1*$^{Neo/Neo}$ mice had significantly fewer papillomas as compared to control mice (p=0.004, determined by mixed model analysis: linear regression with covariant structure using SPSS software). (B) Tumor free survival was not significantly different between *Hus1*$^{+}$ and *Hus1*$^{Neo/Neo}$ mice (p=0.077, by Log Rank Comparison). (C) The size of the largest papilloma per mouse was plotted for each day. The average size of the largest papilloma was reduced in *Hus1*$^{Neo/Neo}$ mice as compared to control mice, although this difference was not significant (p=0.605). (D) Representative images of DMBA/TPA-treated *Hus1*$^{+/Neo}$ (right) and *Hus1*$^{Neo/Neo}$ (left) sex-matched littermates at 140 days after DMBA treatment.

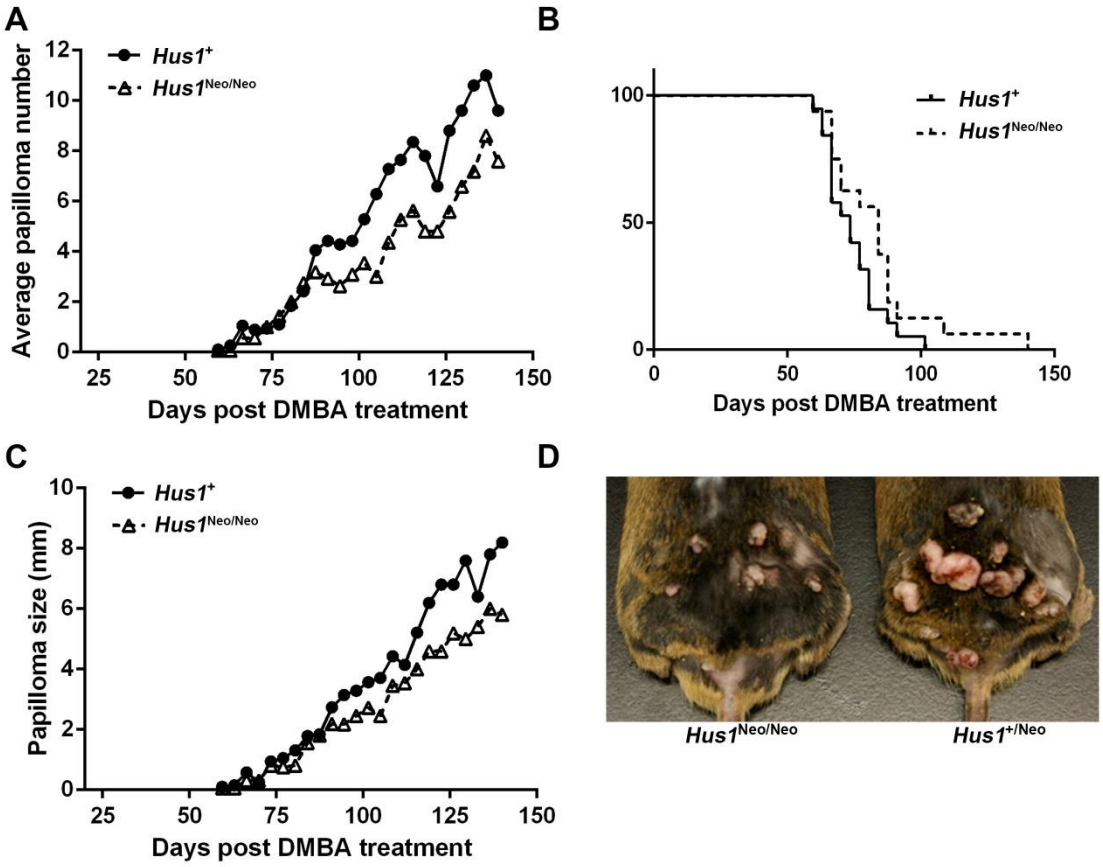
A
Average papilloma number
Hus1+
Hus1Neo/Neo
Days post DMBA treatment
B
Hus1+
Hus1Neo/Neo
Days post DMBA treatment
C
Papilloma size (mm)
Hus1+
Hus1Neo/Neo
Days post DMBA treatment
D
Hus1Neo/Neo
Hus1+/Neo

Figure 5.10: Lack of acute DMBA hypersensitivity in cells and mice with partial *Hus1* impairment. (A) Primary *Hus1*$^{+}$ or *Hus1*$^{Neo/\Delta 1}$ MEFs were treated with a single dose of DMBA (0μg/ml, 1 μg/ml, or 20μg/ml). 24 hours after treatment, cells were harvested, stained with trypan blue, and counted to assess cell survival relative to untreated cells. Each assay was done in triplicate using three independent primary cultures. (B-D) *Hus1*$^{+}$ and *Hus1*$^{Neo/\Delta 1}$ mice were shaved and treated with a single DMBA dose. Skin was harvested and stained to quantify apoptosis and proliferation. Quantification of (B) TUNEL- and (C) BrdU- positive cells in skin sections from mice of the indicated genotype treated with a single DMBA dose to determine the percentage of proliferating and apoptotic cells, respectively. There were no significant differences between genotypes in proliferation or cell death following DMBA treatment ($p=0.777$ and $p=0.908$, respectively). DMBA treatment at each dose was performed on three mice of each genotype and three fields of view were quantified per mouse. Error bars denote standard deviation. Statistical analysis was by a random coefficient model with random slope and intercept. The fixed effects were the genotype, dose, and their interaction term. (D) Representative images of skin sections from control and *Hus1*$^{Neo/\Delta 1}$ mice treated with 25nmol DMBA after staining by BrdU and TUNEL assays. Sections were counterstained with haematoxylin. Arrows point to brown, positive cells. Scale bar represents 100μm.

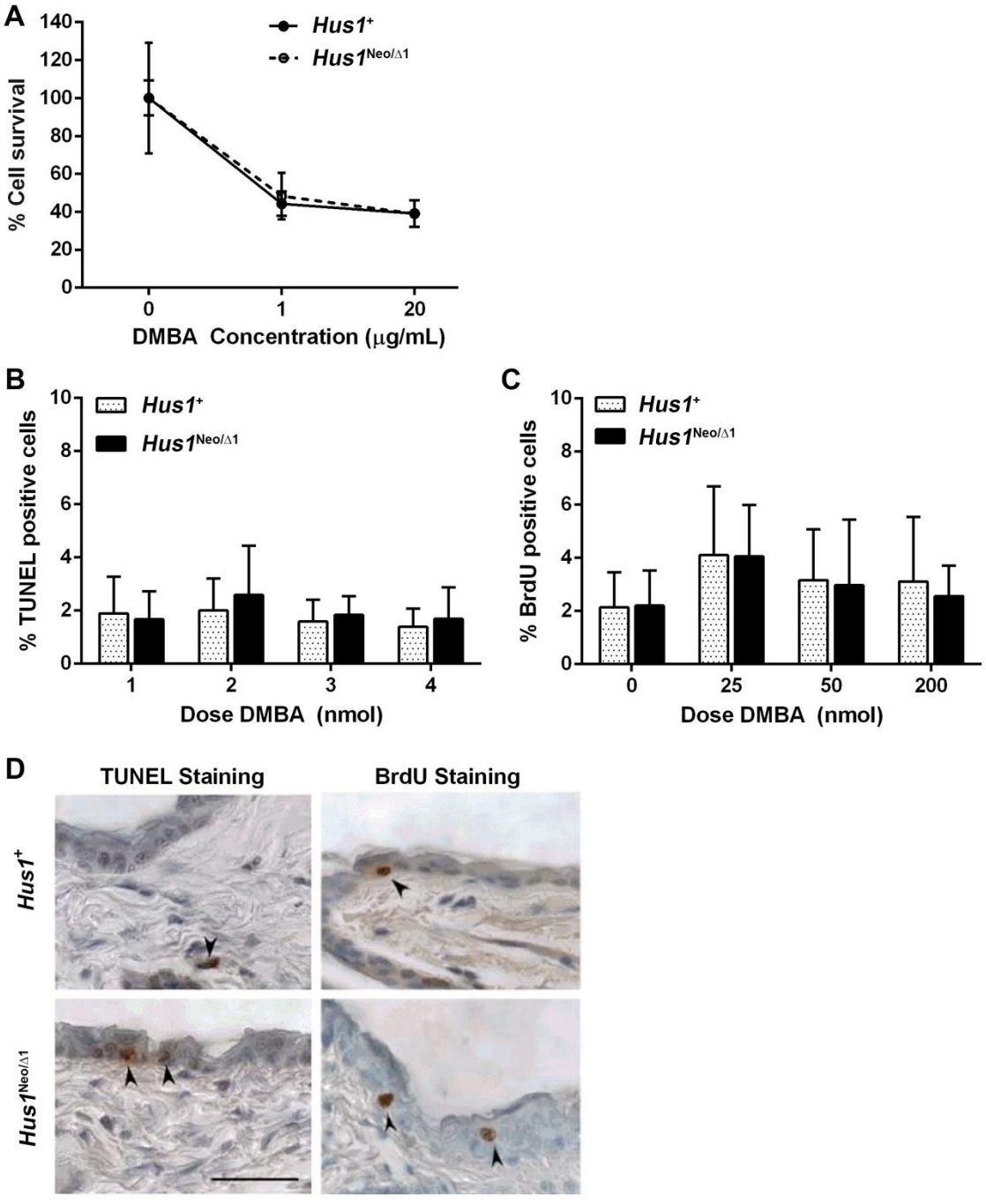
A
% Cell survival
140
120
100
80
60
40
20
0
Hus1+
Hus1Neo/Δ1
0
1
20
DMBA Concentration (μg/mL)
B
% TUNEL positive cells
10
8
6
4
2
0
Hus1+
Hus1Neo/Δ1
1
2
3
4
Dose DMBA (nmol)
C
% BrdU positive cells
10
8
6
4
2
0
Hus1+
Hus1Neo/Δ1
0
25
50
200
Dose DMBA (nmol)
D
TUNEL Staining
BrdU Staining
Hus1+
Hus1Neo/Δ1

Figure 5.11: Lack of acute TPA hypersensitivity in cells and mice with partial *Hus1* impairment. (A) Primary *Hus1*$^{+}$ or *Hus1*$^{Neo/\Delta 1}$ MEFs were treated with a single dose of TPA (0ng/ml, 100 ng/ml, or 1,000 ng/ml). 24 hours after treatment, cells were harvested, stained with trypan blue, and counted to assess cell survival relative to untreated cells. Each assay was done in triplicate using three different primary cultures. (B-D) *Hus1*$^{+}$ and *Hus1*$^{Neo/\Delta 1}$ mice were shaved and treated with a single TPA dose. Skin was harvested and stained to quantify apoptosis and proliferation. Quantification of (B) TUNEL- and (C) BrdU-positive cells in skin sections from mice of the indicated genotype treated with a single TPA dose to determine the percentage of proliferating and apoptotic cells, respectively. There were no significant differences between genotypes in proliferation or cell death following TPA treatment (p=0.352 and p=0.696, respectively). TPA treatment at each dose was performed on three mice of each genotype, and three fields of view were quantified per mouse. Error bars denote standard deviation. Statistical analysis was by a random coefficient model with random slope and intercept. The fixed effects were the genotype, dose, and their interaction term. (D) Representative images of skin sections from control and *Hus1*$^{Neo/\Delta 1}$ mice treated with 25ug/ml TPA after staining by BrdU and TUNEL assays. Sections were counterstained with haematoxylin. Arrows point to brown, positive cells. Scale bar represents 100μm.

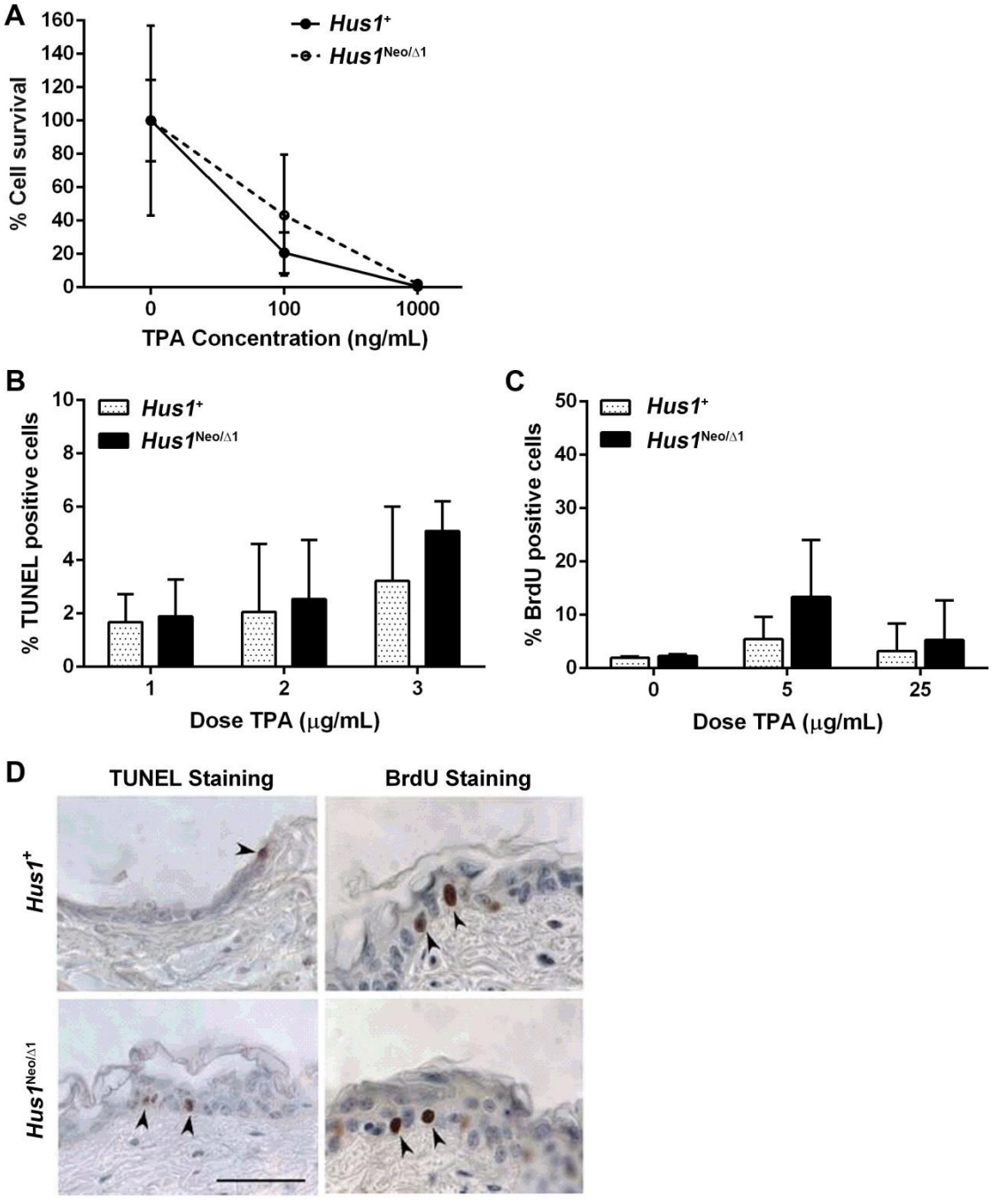
A
% Cell survival
160
140
120
100
80
60
40
20
0
Hus1+
Hus1Neo/Δ1
0
100
1000
TPA Concentration (ng/mL)
B
% TUNEL positive cells
10
8
6
4
2
0
Hus1+
Hus1Neo/Δ1
1
2
3
Dose TPA (μg/mL)
C
% BrdU positive cells
50
40
30
20
10
0
Hus1+
Hus1Neo/Δ1
0
5
25
Dose TPA (μg/mL)
D
TUNEL Staining
BrdU Staining
Hus1+
Hus1Neo/Δ1

sensitivity to either DMBA or TPA relative to *Hus1*$^{+}$ MEFs, as cells of either genotype showed similar survival at each tested dose.

While these results suggest that *Hus1*$^{Neo/\Delta 1}$cells are not hypersensitive to DMBA or TPA treatment, we additionally tested the *in vivo* DMBA or TPA sensitivity of the skin of mice expressing *Hus1* at reduced levels. A single DMBA or TPA dose was administered to the shaved dorsal flank, and the skin was harvested 24 hours later. The mice were not in the anagen phase of hair cycle, reducing the probability that cell proliferation would affect the results. TUNEL and BrdU staining were performed to assess the levels of apoptosis and proliferation, respectively, in the skin epithelium. Following either DMBA or TPA treatment at increasing doses, the percentage of cells undergoing apoptosis was similar to that of cells treated with acetone alone (Fig. 5.10B,D and 5.11B,D). Similarly, the cell proliferation following treatment was not significantly different between genotypes (Fig. 5.10C-D and 5.11C-D). Together, these results indicate that treatment of *Hus1*$^{Neo/\Delta 1}$ mice with DMBA or TPA at the doses used to induce papillomas does not trigger acute cell cycle arrest or cell death, arguing against early cell loss as the basis for alteration in tumorigenicity upon *Hus1* impairment.

HUS1 protein levels are upregulated in cancer cells.

The observation that *Hus1* impairment suppresses cell transformation implied that it is more likely that *Hus1* overexpression, rather than loss-of-function mutations, would occur in cancer. Using the Oncomine database, we evaluated the *HUS1*, *RAD9A*, and *RAD1* mRNA expression profiles in various human cancers relative to normal cells

(Fig. 5.12A). Consistent with case reports that 9-1-1 genes are upregulated in some cancers, RNA sequencing analysis of The Cancer Genome Atlas (TCGA) database also implicated increased *HUS1* expression in various cancer types in comparison to their normal tissues (Fig. 5.12B). We confirmed and extended these findings with *Hus1* RT-qPCR of human triple-negative breast cancer (MDA-MB-231 and MDA-MB-468) and cervical cancer (HeLa) cells. Non-transformed human fibroblasts (WI-38 and GM8399) and mammary epithelial cells (HMEI) were used as controls. Our data suggest that the transformed cells had significantly increased *HUS1* expression (Fig. 5.12C) and correspondingly higher HUS1 protein levels (Fig. 5.12F) compared to the non-transformed cells. Similarly, increased *Hus1* gene expression and HUS1 protein levels were observed in the primary tumors from Eu-myc and MMTV-PyMT mice as compared with the normal thymus and mammary tissues from WT mice, respectively (Fig. 5.12D, E; 5.12G, H). These findings are consistent with our findings that efficient cell transformation requires *Hus1*.

Cancer cells utilize alternative polyadenylation to increase *HUS1* expression.

As the number of cases with elevated cancer-associated *HUS1* mRNA levels was relatively small, it prompted our hypothesis that cancer cells might use other mechanisms to upregulate HUS1 protein abundance. It is now clear that APA, a RNA processing mechanism that generates distinct 3' termini on mRNAs, regulates many genes (Lianoglou *et al*, 2013; Di Giammartino *et al*, 2011), and *Hus1* in mice and humans exhibits several features characteristic of genes that undergo polyadenylation site switching. *Hus1* is a ubiquitously expressed gene with multiple mRNA transcript

Figure 5.12. *HUS1* expression is elevated in cancer cells. (A) Chart summarizing altered 9-1-1 complex gene expression in human cancers. Data were retrieved from the ONCOMINE cancer gene expression database (search done on 06/25/2018). Dark red, red, and pink boxes represent analyses in which the gene of interest is among the top 1%, 5% and 10% most overexpressed genes, respectively, in a given study. Dark blue, purple, and light purple boxes represent analyses in which the gene of interest is among the top 1%, 5% and 10% most underexpressed genes, respectively, in a given study. Unshaded boxes indicate that the gene of interest was not among the top overexpressed or underexpressed genes in the analyses. (B) RNA-sequencing analysis of *Hus1* gene expression across 22 tumor and normal tissues from TCGA. (C) RT-qPCR based quantification of total *HUS1* gene expression in non-transformed (WI-38, GM08399, HME1) or cancer (MDA-MB-468, MDA-MB-231, or HeLa) cells ($p<.001$, Student's T-test). Values are the average of triplicate samples, with error bars representing the standard deviation. (D) Quantification of total *Hus1* gene expression in primary mammary tumor derived from MMTV-PyMT mice along with normal mammary glands ($p<.001$, Student's T-test). Values are the average of triplicate samples, with error bars representing the standard deviation. (E) Quantification of total *Hus1* gene expression in primary lymphoma derived from Eu-myc mice along with normal thymus ($p<.001$, Student's T-test). Values are the average of triplicate samples, with error bars representing the standard deviation. Western blot of protein lysates prepared from (F) transformed and non-transformed cell lines; (G) MMTV-PyMT mice; (H) Eu-myc mice, using antibodies specific to HUS1 or β-ACTIN as a loading control.

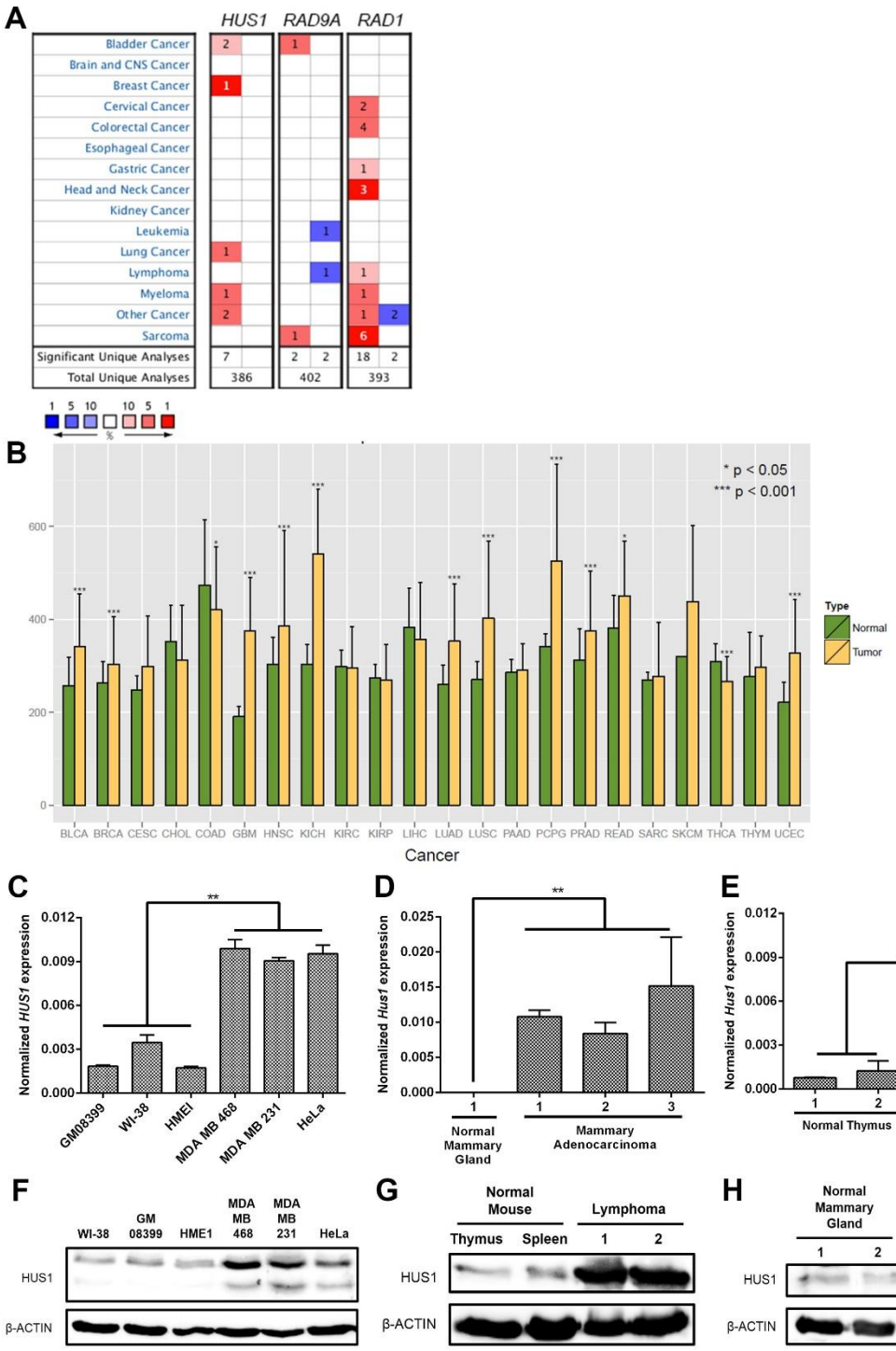
A
HUS1
RAD9A
RAD1
Bladder Cancer
Brain and CNS Cancer
Breast Cancer
Cervical Cancer
Colorectal Cancer
Esophageal Cancer
Gastric Cancer
Head and Neck Cancer
Kidney Cancer
Leukemia
Lung Cancer
Lymphoma
Myeloma
Other Cancer
Sarcoma
Significant Unique Analyses
Total Unique Analyses
1 5 10 10 5 1
%
B
* p < 0.05
*** p < 0.001
Type
Normal
Tumor
BLCA BRCA CESC CHOL COAD GBM HNSC KICH KIRC KIRP LIHC LUAD LUSC PAAD PCPG PRAD READ SARC SKCM THCA THYM UCEC
Cancer
C
Normalized HUS1 expression
GM08399
WI-38
HMEI
MDA MB 468
MDA MB 231
HeLa
D
Normalized Hus1 expression
Normal Mammary Gland
Mammary Adenocarcinoma
E
Normalized Hus1 expression
Normal Thymus
Lymphoma
F
WI-38
GM 08399
HME1
MDA MB 468
MDA MB 231
HeLa
HUS1
β-ACTIN
G
Normal Mouse
Thymus
Spleen
Lymphoma
HUS1
β-ACTIN
H
Normal Mammary Gland
Mammary Adenocarcinoma
HUS1
β-ACTIN

isoforms of varying length (Fig. 5.13A), with most normal tissues expressing the same long transcript isoform, although the testis expresses a distinct, shorter transcript (Weiss et al., 1999). The possibility that APA regulates *HUS1* was particularly intriguing given the studies reporting that rapidly proliferating cells and cancers upregulate oncogenes and other factors through APA to produce mRNA isoforms that lack 3′ untranslated region (3′UTR) sequences and thus avoid negative regulation by microRNAs (miRNAs) or other mechanisms (Mayr and Bartel, 2009; Sandberg et al., 2008).

By interrogating published datasets that mapped polyadenylation sites genome-wide (Lianoglou et al., 2013; Martin et al., 2012), we confirmed that human *HUS1* contains two major polyadenylation sites: a proximal site that produces a short transcript with a 204 nucleotide (nt) 3'UTR and a distal site that yields a long transcript with a 2,064 nt 3'UTR (Fig. 5.13A). Further analysis revealed that most normal tissues, except that in the testis, expressed higher levels of the long *HUS1* isoform, consistent with our published data showing that most normal mouse tissues express *Hus1* as a long transcript while a much shorter transcript is produced specifically in the testis (Weiss *et al*, 1999). Analysis of the genome-wide profiling of human polyadenylation sites also revealed that several cancer cell lines, including MCF-7 breast cancer and HeLa cells, expressed an increased ratio of short:long HUS1 transcripts (Fig. 5.13B) (Mayr, 2017). To validate these findings, we utilized the transformed and non-transformed cell lines to perform a *HUS1* isoform specific qPCR, and observed that the transformed cells produced a significantly greater amount of the short isoform relative to the long isoform (Fig. 5.13C) and expressed correspondingly

higher HUS1 protein levels (Fig. 5.13F) as compared to the non-transformed cells. Thus, expression of the short *HUS1* transcript correlates with greater protein abundance, suggesting that the long isoform 3'UTR sequence affects protein production negatively.

Next, to confirm that APA regulates *Hus1* expression in primary mouse tumors, we performed a *Hus1* isoform specific qPCR using primary tumors, as discussed earlier. Remarkably, there was a 4-fold and 2.5-fold increase in short *Hus1* transcript abundance in mammary tumors and lymphoma, respectively, as compared to the normal mammary gland and thymus tissue, respectively (Fig. 5.13C, D). We directly tested the impact of the HUS1 3'UTR length on gene expression using the pmir-GLO luciferase assay, in which the short and long *HUS1* 3′UTR fragments were cloned downstream of the *Renilla* luciferase open reading frame (Fig. 5.13F). Compared to the vector without the additional 3′UTR sequence, the relative expression of *Renilla* luciferase was significantly reduced when its mRNA species contained the long *HUS1* 3′UTR sequence (Fig. 5.13G). The short *HUS1* 3′UTR sequence did not alter *Renilla* luciferase expression (Fig. 5.13G), suggesting that it lacks the negative regulatory elements that suppress protein production from transcripts with the long 3′UTR sequence. Taken together, these results suggest that both murine and human cancer cells undergo a switch in *Hus1* polyadenylation site selection, increasing usage of a proximal site that produces short *Hus1* transcripts that have the same coding capacity but yield elevated HUS1 protein levels.

Figure 5.13. APA is responsible for upregulating *HUS1* expression in cancer cells. (A) Schematic depiction of the human HUS1 genomic locus and three major transcript isoforms. (B) 3'UTR RNA-seq data extract from (Mayr and Bartel, 2009), showing the ratios of short vs long *HUS1* isoforms in different tissues and cancers. (C) Quantification of the ratio of short versus long *HUS1* transcript isoforms from cells used in Fig 5.12C. RNA extracted cDNA were subjected to qPCR with primers that amplify both short and long isoforms and the long isoform alone. Values for the short isoform were calculated by subtracting long isoform-specific products from those generated with short isoform primers (which amplify both long and short transcripts) and then divided by values for the long isoform amplification, yielding a short:long isoform expression ratio ($p<.001$, Student's T-test). Values are the average of triplicate samples, with error bars representing the standard deviation. (D-E) Quantification of the ratio of short versus long *Hus1* transcript isoforms in primary mammary tumor derived from (D) MMTV-PYMT mice along with normal mammary gland and (E) Eu-Myc mice along with normal thymus. Values for the different isoforms were calculated as mentioned above. Values are the average of triplicate samples, with error bars representing the standard deviation. (F) The 3'UTR corresponding to the short or long HUS1 isoforms were cloned downstream of Firefly luciferase in the pmirGLO dual luciferase expression vector, which also contains Renilla luciferase for normalization. (G) Luciferase constructs mentioned in (F) were transfected into HME1 cells and stable cell pools were assayed sequentially for Firefly and Renilla luciferase activity. Average ratios are shown (N=6), with error bars representing SEM. ($p<.001$, Student's T-test).

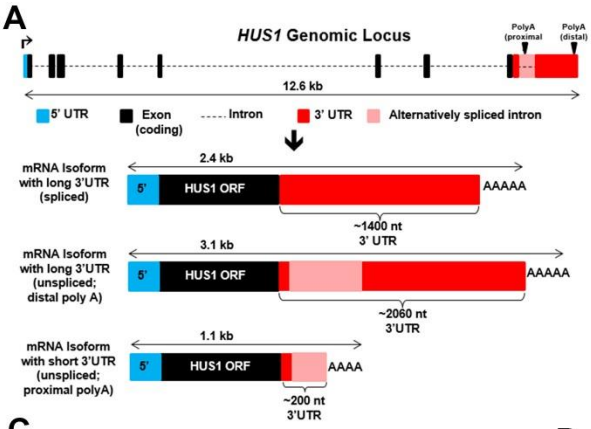

B

Cell Lines	3' UTR Abundance	Quantity Ratio (Short:Long) (Aligned Reads)
Non-transformed		
Brain	Long	1:2
Breast	Almost Equal	1
HEK 293	Almost Equal	1
Ovary	Long	2:1
Skeletal Muscle	Long	5:3
Testis	Short	5:2
Transformed		
HeLa	Short	5:1
MCF10a	Short	5:2
MCF10- HRAS	Short	2:1
MCF7	Short	3:1

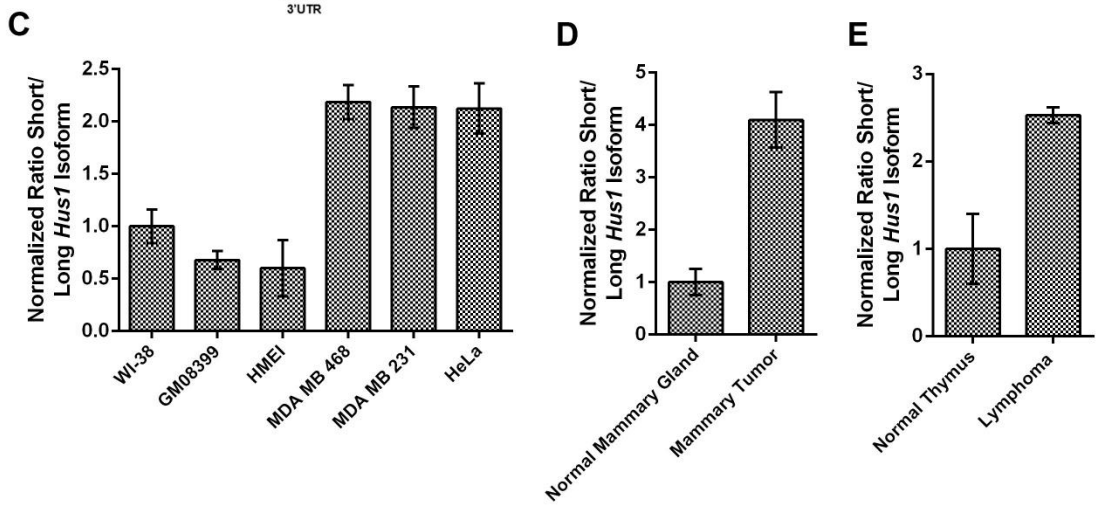

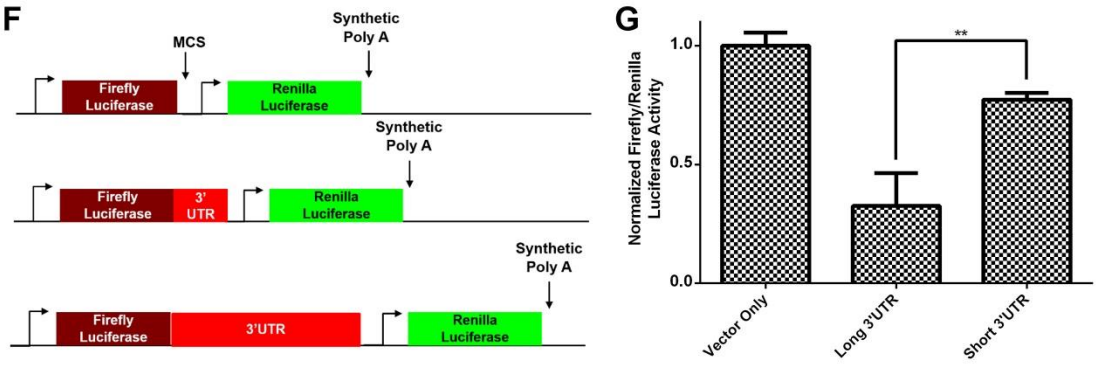

Nonsense-mediated mRNA decay (NMD) mechanisms regulate the 3'UTR of *Hus1*.

While analyzing the 3'UTR dataset from (Mayr et al., 2007), we observed a region within the *HUS1* 3'UTR containing a very low read count relative to the 3'UTR (Mayr and Bartel, 2009). Further analysis uncovered an intron within the 3'UTR of *HUS1* that may promote the expression of a spliced (intron-spliced) *HUS1* isoform. The presence of 3′UTR introns (3UI) is rare, and mRNA transcripts with excised 3UI are generally targeted for degradation via NMD (Bicknell et al., 2012). However, recent studies underscore the importance of 3UI in regulating mammalian gene expression (Chung et al., 2006; Sharangdhar et al., 2017). Hence, we performed isoform-specific RT-qPCR using our transformed and non-transformed cell lines to determine if the cells were actively generating a transcript with the spliced 3UI. Our results indicated the presence of three *HUS1* mRNA transcripts, which included the long, short, and spliced 3′UTR transcripts (Fig. 5.14A). The non-transformed cells maintained relatively lower expression of the spliced transcript compared to the other two transcripts (Fig. 5.14B). In contrast, the transformed cells had similar long and spliced *HUS1* transcript levels, with a significant increase in the short isoform, as reported earlier (Fig. 5.14B). Next, we tested the stability of the spliced transcript upon inhibit NMD pathway by a translational block. NMD is a mRNA surveillance pathway that is highly conserved among eukaryotes and it primarily reduces gene expression errors by degrading mRNA transcripts that contain a premature stop codon (Isken et al., 2008). Interestingly, a translational block upregulated the expression of the spliced transcripts significantly but had no effect on the long transcript levels, and modestly increased the

short transcript levels (Fig. 5.14C), suggesting that *HUS1* spliced transcript actively gets degraded through NMD. Next, we utilized a UPF1 (regulator of nonsense transcripts 1) dominant-negative mutant to test to directly validate if the spliced transcript underwent NMD. UPF1 is an RNA helicase and an integral EJC (exon junction complex) that promotes NMD. In the presence of the UPF1 dominant-negative mutant, there was a significant increase in the *HUS1* spliced mRNA transcript. On the contrary, *HUS1* short or long mRNA transcript abundance was not altered in presence or absence of the UPF1 mutant (Fig. 5.14D). The *HUS1* intron-spliced mRNA isoform was also stabilized upon *UPF1* knockdown (Fig. 5.14E). Together, these data argue for the presence of a third *HUS1* mRNA isoform that is targeted for degradation via the NMD pathway.

5.5. DISCUSSION

Genomic instability, DNA damage, and replication stress have emerged as hallmarks of cancer cells. Because defects in DNA damage checkpoints have been linked to both promotion and suppression of tumorigenesis, we set out to determine how dysfunction of HUS1, a component of the 9-1-1 complex, affects transformation in cultured cells and tumorigenesis *in vivo*. We previously reported that *Hus1* loss impedes cell proliferation and survival (Yazinski et al., 2009; Zhu and Weiss, 2007). The experiments described here indicate that *K-ras* expression worsens the effects of complete *Hus1* loss, resulting in decreased proliferation, an increase in chromosomal aberrations, and increased expression of several DNA damage markers. These data suggested that cells require *Hus1* to sustain *K-ras*-driven proliferation, a finding that

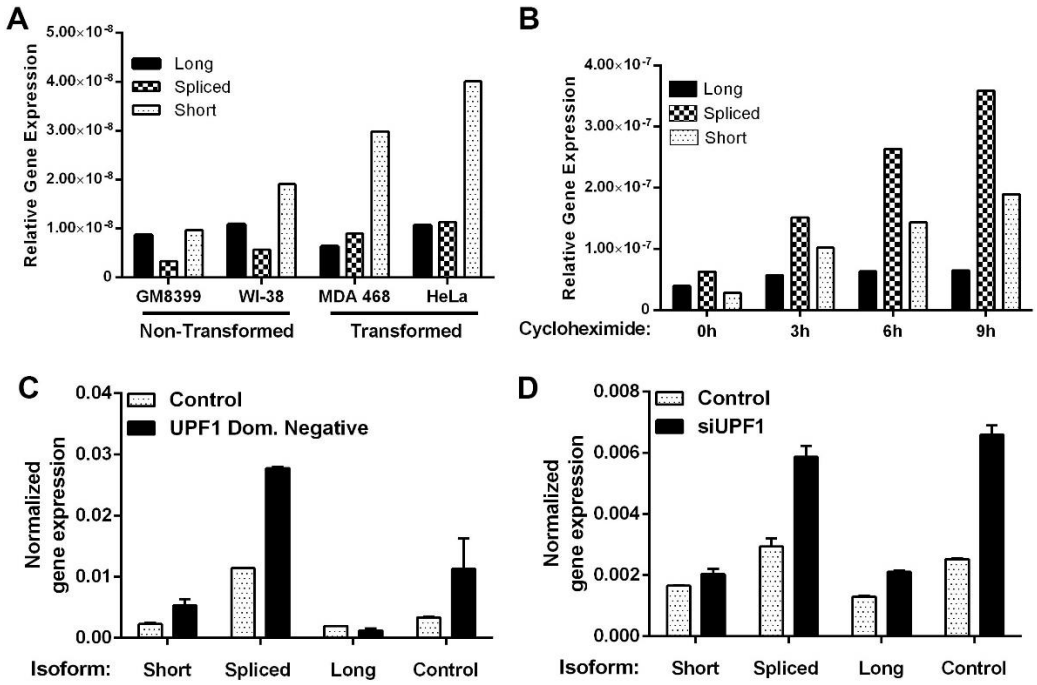

Figure 5.14. Non-mediated Decay (NMD) actively degrades intron-spliced *Hus1* mRNA transcript. (A) Total expression of all three *HUS1* isoforms (short, long and spliced) measured using RT-qPCR in cell lines used in Fig 5.12C. Values for the short and long isoform were calculated as described in Fig 5.13. 3'UI spanning primers were used to calculate values for intron-spliced *HUS1* isoform. (B) Total expression of all three isoforms of *HUS1* measured using RT-qPCR in HEK293T cells with or without the addition of cycloheximide at indicated time points. (C) Total expression of all three *HUS1* isoforms measured using RT-qPCR in HEK293T cells expressing UPF1 dominant negative mutant and WT-UPF1 (control). Values are the average of triplicate samples, with error bars representing the standard deviation. (D) Total expression of all three isoforms of *HUS1* (short, long and spliced) measured using RT-qPCR in HEK293T cells with siRNA against *UPF1* or scramble. Values are the average of triplicate samples, with error bars representing the standard deviation.

was confirmed *in vivo* using a mouse lung tumor model, in which lung-specific oncogenic *K-ras* expression resulted in fewer and smaller neoplasms when *Hus1* was completely deleted. Thus, the negative consequences of both acute and constitutive *Hus1* defects are exacerbated by activated *K-Ras*, resulting in decreased proliferation and impaired transformation.

Because complete *Hus1* knockout is embryonic lethal, we next determined how transformation was affected by partially reduced *Hus1* levels, which do not disrupt mouse development or survival (Levitt et al., 2007). Primary cells with decreasing levels of *Hus1* expression exhibited a decreased susceptibility to immortalization by large T antigen, and immortalized cell lines expressing reduced *Hus1* levels were found to have decreased transformation ability in soft agar assays. Finally, mice with incrementally reduced *Hus1* levels developed fewer and smaller tumors in a skin carcinogenesis model. Importantly, mice with the lowest expression of *Hus1* in our allelic series showed no increase in spontaneous tumor development, despite heightened genomic instability as evidenced by increased micronucleus formation in peripheral red blood cells (Levitt et al., 2007). This suggests that a 60-80% reduction in *Hus1* expression results in elevated genomic instability that has no overtly adverse effects in normal cells *in vivo*, but is incompatible with malignant transformation.

The data provided here are in contrast with other studies that made use of conditional *Rad9* knockout and *Rad1* heterozygote mice (Han et al., 2010; Hu et al., 2008). Because RAD9 and RAD1, along with HUS1, form the heterotrimeric 9-1-1 complex, a simple prediction would be that deficiencies in *Rad9* or *Rad1* would

phenocopy the reduced tumorigenicity reported here. However, complete *Rad9* inactivation in keratinocytes or germline *Rad1* heterozygosity result in increased tumorigenesis using the same two-step skin carcinogenesis procedure to induce papilloma formation. The distinct results associated with each 9-1-1 subunit may be due to the degree of checkpoint impairment, as well as the cell types affected, in the various models. In the data presented here, *Hus1* is reduced to 20%-40% of wild-type expression, whereas the *Rad1* and *Rad9* studies utilize heterozygous mice (Hu et al., 2008) or complete conditional knockout mice, respectively (Han et al., 2010). Unlike $Rad1^{+/-}$ mice, $Hus1^{+/-}$ and $Rad9^{+/-}$ mice do not show increased papilloma formation in the same skin carcinogenesis assay. In the previous work *Rad9* inactivation was targeted exclusively to keratinocytes, whereas $Hus1^{Neo/\Delta 1}$ mice express reduced *Hus1* globally in all cell types, raising the possibility of non-cell-autonomous effects in which surrounding cells with reduced *Hus1* expression may not be able to support transformation and tumor growth. In contrast to the effect of *Rad9* loss in the skin, we found that conditional *Hus1* inactivation in the lung results in a decrease in *Kras*-induced lung tumorigenesis. Consistent with this observation, complete *Hus1* inactivation in mammary epithelium results in extensive cell death with no increase in spontaneous tumorigenesis (Yazinski et al., 2009). One possible explanation for subunit-specific phenotypes is that individual 9-1-1 components have independent roles outside of the heterotrimeric complex, as suggested by our previous studies and those of others (Broustas and Lieberman, 2014b; Lyndaker et al., 2013a).

The reduced tumorigenesis following *Hus1* impairment observed in lung and skin is not universal to all tumor types and may depend on the initiating genetic event

or cell type of origin. For example, *Hus1*$^{Neo/\Delta 1}$ mice on a *p53*-null background develop thymic lymphoma and other neoplasms at the same rate as *Hus1*$^{+}$ *p53*-null mice (Levitt et al., 2007), suggesting that reduced *Hus1* levels do not effect tumorigenesis driven by *p53*-deficiency. Likewise, thymic lymphoma formation in *Atm*-deficient mice occurs with the same latency and penetrance in *Hus1*$^{Neo/Neo}$, *Atm*$^{-/-}$ mice with partial *Hus1* impairment (Balmus et al., 2012). This may be because cells undergoing transformation require *p53* and *Atm* to induce apoptosis or senescence in response to the damage caused by *Hus1* inhibition and thus prevent tumorigenesis. Alternatively, thymocytes have been shown to have a lower requirement for *Hus1* (Francia et al., 2006), and proliferation of tumors originating from this tissue may not be highly dependent on the 9-1-1 complex.

A requirement for HUS1 for optimal cell transformation and tumorigenesis raises the possibility of HUS1 being upregulated in cancers. Although increased *HUS1* transcript abundance is observed in some cancers ((Fig 5.13A-B); (Storcelova et al., 2013)), this does not appear to be a common event. Increased HUS1 protein levels also have been reported in cancers (de la Torre et al., 2008), and here we describe greater HUS1 levels in transformed cell lines and tumor tissue. Similarly, RAD9 expression is elevated in several cancers (Broustas and Lieberman, 2014b; Lieberman et al., 2011). In the case of *HUS1*, alternative polyadenylation plays a significant role in determining expression levels. In almost all normal tissues, *HUS1* is expressed in greatest abundance as a long isoform transcript, with an extensive 3'UTR of ~2,100 (human) or 3,200 (mouse) nucleotides (Hang et al., 2002; Weiss et al., 1999). The presence of the long 3'UTR correlated with lower HUS1 protein levels and also

suppressed expression of a heterologous reporter. We hypothesize that miRNA and RNA binding protein-binding sites in the 3'UTR are responsible for reduced translation efficiency and/or reduced stability of long *HUS1* isoform transcripts. Interestingly, one normal tissue, the testis, also predominantly expresses the short *Hus1* isoform (Hang et al., 2002; Weiss et al., 1999). This may reflect a greater requirement for *Hus1* in germ cells, where HUS1 has been established to be important for meiotic DSB repair and possibly other processes (Lyndaker et al., 2013c).

Cancer cells have usurped this mechanism to upregulate HUS1 and meet their increased need for genome maintenance by increasing usage of a proximal polyadenylation site that yields transcripts that lack most of the 3′UTR. Such APA is a common event in cancer and proliferating cells and leads to increased protein levels from genes such as *CCND1* (cyclin D1) and *IGF2BP1*/*IMP-1* (insulin-like growth factor 2 mRNA-binding protein 1). The mechanisms of polyadenylation site selection are still being resolved, but are thought to involve a complex set of protein factors that regulate mRNA precursor 3′ end maturation (Mayr, 2017). We therefore attempted to identify *Hus1*-specific regulatory factors via data-mining. starBase v2.0 (http://starbase.sysu.edu.cn), a protein–RNA interaction online database, detected numerous UPF1-binding hotspots on *HUS1* mRNA (crosslinking IP sequencing data) (Hurt et al., 2013; Zund and Muhlemann, 2013), and positive Pearson correlation analysis between *UPF1* and *HUS1* expression levels in 10 of 14 cancer cell types analyzed. *HUS1* mRNA was also identified as a NMD target in a high-throughput screen carried out to identify small-molecule NMD inhibitors (Nickless et al., 2014). Moreover, the NMD pathway is actively silenced in response to survival stress (ER

stress, hypoxia, starvation). Jointly, these data provide a possible explanation for the significant increase in the intron-spliced *Hus1* transcript when translation is blocked. To upregulate HUS1 expression, cells utilize APA mechanisms to generate short UTR versions of the *HUS1* transcript to bypass miRNA regulation, as well as intron-spliced *HUS1* transcripts, which would often be degraded by NMD. With NMD silenced during stress, intron-spliced *HUS1* transcripts remain stable and promote HUS1 accumulation, NMD pathway reactivation can degrade the spliced constructs, providing secondary regulation in case of excess *Hus1* expression.

Interestingly, a large family of mRNA cleavage and specificity factors can also regulate pre-mRNA 3'end cleavage and polyA tail synthesis. We examined the *HUS1* 3'UTR proximal and distal polyadenylation sites in a comprehensive CLIP-seq data set that details the binding hotspots of most cleavage and specificity factors (Martin et al., 2012). Interestingly, CFIm25, CFIm68, CSTF64 and CSTF64τ were enriched at the cleavage sites that give rise to both short and long *HUS1* transcript isoforms. Related factors such as CPSF30, 73, 100 and 160 were not detected at the *HUS1* 3'UTR (data not shown). It is thought that CFIm25 and CFIm68 expression levels impact the choice of proximal or distal cleaving by CPSF proteins (Martin et al., 2012). Interestingly, downregulation of CFIm25 in glioblastoma cells enhances their tumorigenic properties, and *Hus1* is among the CFIm25-regulated genes that show increased levels of short 3'UTR transcripts upon CFIm25 loss (Masamha et al., 2014).

Our findings that *Hus1* impairment suppresses tumorigenesis and transformation are consistent with the emerging picture of the relative roles of specific checkpoint mechanisms during tumorigenesis. While defects in both the ATR and

ATM pathways result in genomic instability, ATM appears to play a less critical role in responding to the stresses associated with oncogene-induced proliferation and malignant transformation. It is also worth noting that *Atm* is not essential for embryonic growth and development (Barlow et al., 1996), whereas the 9-1-1 complex and the ATR pathway are essentially for viability (Brown and Baltimore, 2000; Sancar et al., 2004). Although *ATR* and *CHK1* mutations cause a modest increase in cancer susceptibility (Bartek and Lukas, 2003; Chen et al., 2017), a prominent role for the ATR pathway appears to be enabling cancer cells to tolerate elevated levels of DNA damage and replication stress (Karnitz and Zou, 2015). That cancer cells similarly require intact and likely elevated HUS1 function further suggests that this dependency could be exploited therapeutically through inhibition of 9-1-1 complex formation or by disruption of effector protein binding to the checkpoint clamp.

5.6. ACKNOWLEDGMENTS

The 3'UTR story (Fig 5.12-5.14) was performed by Darshil Patel. The authors thank Scott Coonrod and John Schimenti for cell lines and reagents; Jeff Pleiss for advice and assistance with qPCR; Francoise Vermeylen from the Cornell Statistical Consulting Unit for assistance on statistical analyses; Yashira Negron for MMTV-PyMT mammary tumor tissue samples; Dr. Zhongsheng and Andrew Nickless for helpful discussion and suggestions; the staff of the Cornell Center for Animal Resources and Education and Laboratory Animal Services for excellent animal care. The authors are also grateful to Dr. Lynne Maquat for providing the UPF1 constructs. This work was supported by National Institutes of Health Grant R01 CA108773 (to

RSW). SAY was supported by a Department of Defense Breast Cancer Research Program predoctoral fellowship. GB was supported by a Cornell University College of Veterinary Medicine Graduate Research Assistantship. PXL was supported by funding from the Center for Vertebrate Genomics and the Comparative Cancer Biology Training Program. KH and NH were supported by Cornell University College of Veterinary Medicine Clinical Fellowships. SG was supported by the Biology Research Fellowships Program.

CHAPTER 6

SUMMARY AND FUTURE DIRECTIONS

The DDR genes are important for managing and repairing DNA alterations induced by exogenous or endogenous agents to maintain the genomic landscape. Among several DDR genes, those in the 9-1-1 complex also promote genome maintenance. The importance of the 9-1-1 complex in cells is striking, as its absence manifests severe phenotypes. In mice, the loss of *Hus1* causes severe genomic instability and embryonic lethality. Experiments using stable *Hus1*-null cells have reported similar results, including increased apoptosis and cellular proliferation defects. The 9-1-1 complex plays the separate roles of regulating ATR-mediated checkpoint signaling and DNA repair. Although the checkpoint function of the 9-1-1 complex is well-understood, its role in DNA repair largely remains unknown. To fully explore its role in DNA repair, we first identified functionally important residues of the 9-1-1 complex by applying a targeted mutagenesis approach using a 9-1-1 complex subunit, i.e., HUS1.

In the present study, we identified novel residues in HUS1 that mediate interaction with DNA, facilitate clamp formation, and affect protein–protein interaction with the 9-1-1 complex. Mutating the HUS1 residues that mediates the clamp formation and clamp-DNA interaction, abrogates both the ATR-mediated checkpoint activation as well as DNA repair functions of the 9-1-1 complex. This suggests that clamp formation integrity and clamp–DNA interaction is essential for its

role in protecting genome integrity. Interestingly, mutating the residues in the outer hydrophobic pockets of HUS1 only disrupted the ability of the 9-1-1 complex to mediate protein–protein interaction without affecting the checkpoint signaling function. However, this repair mutant (HUS1-PM4) form of HUS1 was only able to partially reduce the protein interaction with the repair proteins (MYH and FANCD2). In future studies, it would be ideal to further mutate the other surface residues of HUS1 to create a mutant that completely abrogates interaction with the repair proteins. Upon examining the HUS1 outer surface, we observed a series of conserved, positively charged residues adjacent to the (PCNA)-like hydrophobic pocket that may contribute to the stabilization of the protein interactions (Fig 6.1). Reversing the charge of these residues may cause additional disruption of HUS1 interaction with repair factors. It is also important to note that RAD9A and RAD1 can facilitate protein interaction with the 9-1-1 complex. So, without analyzing the RAD9A and RAD1 surfaces, it would be difficult to obtain a mutant that would completely disrupt interactions with all repair proteins. However, the HUS1-PM4 mutant analysis will allow for identification of specific interactions that require HUS1 subunit to mediate their interaction with the 9-1-1 complex. Given the evidence that HUS1-PM4 mutant is defective for recruiting HR protein, RAD51, using the DR-GFP reporter assay to measure homology-directed recombination repair in the HUS1 mutant cells would clarify the physiological relevance of the HUS1-mediated protein interactions with HR repair factors and its impact on HR. This technique is limited by low efficiency of transfecting MEFs. To overcome this problem, the HUS1-mAID system can be utilized in HCT116 cells to generate DR-GFP stable cells due to their higher

transfectability than MEFs.

Although independent studies have identified several repair proteins in the same and different repair pathways that interact with the 9-1-1 complex, a significant number of interactions remain unknown. So, we utilized a quantitative mass spectrometry based proteomic approach to identify novel interactions mediated by the 9-1-1 complex. The screen identified several novel 9-1-1 interactors along with the known 9-1-1–binding proteins, validating our system. Among the novel candidates, the most interesting find was the components of the neddylation pathway. Continued analysis revealed that several factors in the neddylation proteins not only interacted physically with the 9-1-1 complex, but were also dependent on HUS1 for their recruitment onto the chromatin. Overall, the data suggest that the 9-1-1 complex regulates the neddylation pathway; however, the mechanistic details have not been determined. As HUS1 affects the expression and localization of both neddylating (UBE2M) and deneddylating (COPS6) enzymes, it would be important to determine the global changes in the protein neddylation levels in the presence and absence of HUS1, clarifying the significance of the 9-1-1 complex in neddylation signaling.

A primary target of the neddylation pathway is the CRLs, which poly-ubiquitinate target proteins for proteasomal degradation and that we found interact with HUS1 (Lee and Zhou, 2010). Interestingly, PCNA has been implicated in promoting CRL-dependent protein degradation (Zhang et al., 2013). Several CRL target proteins utilize a PIP degron motif to facilitate their interactions with the PIP binding pocket on PCNA (Tsanov et al., 2014; Zhang et al., 2013). Recent studies have also implicated CRL-dependent, PCNA-independent destruction of the PIP

degron–containing protein, CHK1 (Huh and Piwnica-Worms, 2013). Given the structural similarity between PCNA and the 9-1-1 PIP motif–binding pocket and the physical association between CRLs and HUS1, it is likely that the 9-1-1 complex also interacts with PIP degron–containing proteins and promotes their degradation by CRLs. This hypothesis can be tested by measuring the protein stability of the known CRL targets, i.e., CHK1, p21, p27, and histones, in the absence of the 9-1-1 complex.

Besides the neddylation pathway proteins, our proteomic screen also identified several DDR proteins that interact with the 9-1-1 complex, which were previously unknown (Fig. 4.2B). Exploring other interactors and their physiological relevance to 9-1-1 interaction will also be essential for expanding the DDR network and for learning new mechanistic regulations. Furthermore, the HUS1-PM4 mutant can also be used to distinguish RAD9-RAD1-mediated protein interactions from HUS1-mediated protein interactions with the 9-1-1 complex. Using quantitative MS approach with the PM4 mutant cells will establish a HUS1 interactome separating the 9-1-1 interactions within each subunit that mediates it.

The 9-1-1 complex plays an important role in activating the ATR pathway via RAD9A C-terminal tail interaction with the ATR-activator TOPBP1 (Delacroix et al., 2007; Lee et al., 2007). While extensive research has been conducted to understand ATR signaling and its substrates, much remains unclear regarding the 9-1-1–dependent ATR-mediated phosphorylation events. For example, CHK1 is phosphorylated by ATR upon 9-1-1–mediated ATR activation; however, H2Ax phosphorylation by ATR occurs in a 9-1-1–independent manner. With the HUS1-mAID and the *Hus1*$^{+/+}$ and *Hus1*$^{-/-}$ MEFs systems established, it would make it

possible to conduct a comprehensive proteomic screen to understand the phosphoproteome changes induced by *Hus1* loss. The MS screen can be conducted by inducing MMC or HU damage in the cells, followed by phospho-protein enrichment and LC-MS/MS. We would expect two categories of differentially phosphorylated proteins in our MS screen; proteins that show decreased phosphorylation upon HUS1 depletion or absence would be 9-1-1–dependent and are likely to activate ATR. On the contrary, proteins that show increased phosphorylation may be proteins that are phosphorylated in a 9-1-1–independent manner, possibly as part of the DDR (e.g., ATM substrates). The phosphorylation status of the selected candidate proteins can be validated using immunoblotting. With absence of HUS1, cells may exhibit a secondary effect due to the additional loss of their checkpoint signaling independent DNA repair activity, resulting in alteration of the phosphoproteome. This issue can be resolved using RAD9A-SA mutants. RAD9A-SA mutant cells have a serine-to-alanine substitution in the RAD9A C-terminal tail that does not alter 9-1-1 clamp formation, DNA binding, or its repair protein recruitment activity; however, it is defective in ATR activation. The phosphoproteome screen can be refined by repeating the same experiment described above using *Rad9a*$^{+}$ and *Rad9a*$^{SA/SA}$ cells. This experiment will identify and characterize novel 9-1-1–mediated phosphorylation events that may occur to facilitate genotoxin-induced DNA damage repair in the absence of ATR activation without disrupting the 9-1-1 repair function. Additionally, we should acknowledge that ATM is hyperactive upon HUS1 depletion and this will likely result in hyperphosphorylation of some DDR proteins. This might obscure some of the effects of ATR dysfunction, particularly for substrates targeted by ATR and ATM. Overall,

this study will be able to identify novel phosphoproteins that will be altered in response to *Hus1* loss and ATR inactivation.

One major question remains regarding RAD51 chromatin loading defect in absence of *Hus1* upon DNA replication stress. The mechanism for loading RAD51 onto the DNA, along with its role in downstream HR repair, has been well characterized. Our study confirms the presence of ssDNA as well as RPA loading upon replication stress in *Hus1*-null cells, eliminating them as two possible reasons for the loss of RAD51 loading. However, the *Hus1*-null cells also exhibited RPA hyper-phosphorylation in response to replication stress, suggesting a possible mechanism for the RAD51 loading defects. The literature has shown that upon DNA damage, ATM and DNAPK can induce RPA hyperphosphorylation. Even though inhibitors of ATM and DNAPK partially reduced the phospho-RPA signal in our cells, they did not abrogate the signal completely. As PP4A dephosphorylates RPA32, overexpressing PP4A in combination with the inhibitors may result in complete dephosphorylation RPA and determine if that would rescue RAD51 loading. Another DDR protein that has been implicated in regulating RAD51 loading is PLK1 (polo-like kinase 1). PLK1 phosphorylates RAD51, which is important for its recruitment to the chromatin. Preliminary studies in our lab have suggested that PLK1 interacts with the 9-1-1 complex in a damage-specific manner. The chromatin recruitment of PLK1 was significantly decreased in the absence of *Hus1*, and other studies have identified PLK1 as a TOPBP1-interacting protein (Moudry et al., 2016). It is possible that excluding PLK1 in the absence of HUS1 from the damage site may reduce RAD51 phosphorylation, resulting in RAD51 loading defect. To test this hypothesis, the

phosphomimetic form of RAD51 can be exogenously overexpressed in *Hus1*$^{-/-}$ cells; subsequently, the mutant RAD51 loading onto the damaged DNA can be examined.

Accurate DNA resection of the double-strand break (DSB) is also critical for efficient RAD51 loading. Improper resection can promote faulty ssDNA formation. Excessive resection can prime the DNA ends for nuclease-dependent degradation and inhibit proper RAD51 loading (Kolinjivadi et al., 2017b{Schlacher, 2012 #290; Lemacon et al., 2017; Schlacher et al., 2011; Taglialatela et al., 2017)}. There is some evidence that suggest a function for the 9-1-1 complex in regulating activity of EXO1 and other nuclease (Karras et al., 2013; Ngo et al., 2014). It would be important to see *Hus1* loss results in resection defects that can account for the RAD51 loading defect. To address this issue, it would be ideal to observe the changes in ssDNA accumulation in the presence and absence of HUS1 upon replication stress, using DNA combing analysis. Along with ssDNA accumulation, BRCA2 and PALB2 (partner and localizer of BRCA2) are required for proper RAD51 recruitment and nucleofilament formation. In the absence of BRCA2, other proteins, RAD54, TONSL-MMS22L, and RAD52 can also recruit RAD51 to the chromatin (Burkovics et al., 2014; Higgs et al., 2015; Piwko et al., 2016); however, BRCA2 is required to stabilize the newly formed RAD51 nucleofilament. PALB2 interacts with both BRCA2 and RAD51 and aids RAD51 recruitment onto ssDNA. Based on the loss of RAD51 foci in the absence of *Hus1*, understanding the localization of BRCA2 and PALB2 is important in these cells. Our LUMIER screen also identified PALB2 as a potential interactor of RAD9A and HUS1, suggesting a possible role for the 9-1-1 complex in regulating PABL2 activity. Several FA proteins displayed interaction with the 9-1-1 complex subunits in

our LUMIER screen, further solidifying the idea that the 9-1-1 complex is a molecular scaffold that enables interactions with several proteins in the same pathway modulating DNA repair. Understanding the functional relevance for those interactions would provide novel insight on the mechanism for accurate ICL repair. Recently, a new BRCA2- and FANCD2-interacting protein was discovered: BOD1L (biorientation of chromosomes in cell division 1–like 1), which promotes RAD51 loading to protect stalled replication forks against MRE11-dependent fork degradation. Interestingly, BOD1L was identified in our proteomics screen as a potential HUS1-interacting protein, and our preliminary phosphoproteomic data suggest that BOD1L undergoes 9-1-1-medaited ATR-dependent phosphorylation in response to replication stress. These data prompted us to think that BOD1L might regulate RAD51 loading in a 9-1-1–dependent manner upon replication stress. Further studies will be required to identify the mechanistic details of the RAD51 loading defects. In conclusion, given that both RAD51 and the 9-1-1 complex play an important role in HR and replication fork stability, identifying the complex interaction patterns and the physiological relevance between these proteins will shed light on a new mechanism that promotes genome stability.

Interestingly, the 9-1-1 complex has been implicated in tumorigenesis. Like several other DDR proteins, it acts as a double-edged sword, protecting cells against mutation in precancerous lesions, but promoting DNA damage tolerance in cancer cells during the late stages of cancer progression. Expression of the 9-1-1 complex subunits is increased in several cancers, implying a role in promoting tumorigenesis. In accordance with the cancer databases, our results show increased HUS1 levels in

tumor cells compared to their non-transformed counterparts. It will also be interesting to see if the expression of other 9-1-1 complex subunits This increased protein expression of HUS1 results in parts from alternative polyadenylation (APA), a phenomenon where a short 3′ untranslated region (3′UTR) is generated within a protein-coding mRNA transcript to bypass negative microRNA regulation. We show increased expression of the shorter form of the *HUS1* mRNA transcript containing a truncated 3′UTR in cancer cells. It would be important to see how and when during tumorigenesis cells utilize the APA machinery and begin producing the short isoform of *HUS1* mRNA. Identifying the drivers for the switch in isoform production in cancer cells could be the focus of future studies to further clarify how they modulate *HUS1* expression. It would be important access if non-tumorigenic cells regulate HUS1 expression by similar mechanisms. Next, identifying the potential miRNAs that can interact with 3'UTR of *HUS1* and probing their expression in a cancer context may also shed light on the regulation of *Hus1* expression. Lastly, genetic manipulation of the *HUS1* 3'UTR will also provide novel insight regarding the mechanisms that govern the gene expression of *HUS1* in normal and cancer cells.

The relevance of the 3′UTR intron (3UI) in the genomic regions encoding *Hus1* in regulating HUS1 protein production is also unknown. Most of the mRNA transcripts containing 3UI undergo nonsense-mediated decay (NMD) and degradation; however, the NMD pathway is often inhibited during DNA damage. These observations prompt the question of whether cancer cells actively utilize NMD silencing to increase HUS1 protein production by explicitly expressing the 3UI-containing *HUS1* mRNA transcript, and, if so, to what advantage. It is important to

note that the NMD pathway is generally triggered upon encountering a "premature stop codon" within 55 nucleotides of the previous stop codon. Interestingly, *HUS1* has a premature stop codon 56 nucleotides into the 3'UTR. This suggests the interesting possibility that this premature stop codon activates the NMD pathway to regulate spliced transcript degradation, or DNA damage inhibit NMD pathway promoting spliced transcript stability.

Together, this study has begun to resolve the distinct roles for the 9-1-1 complex in regulating ATR-mediated checkpoint signaling as well as DNA repair. These studies reveal how HUS1 cooperates with different repair proteins to protect stalled replication forks, and coordinates ICL repair, and regulates protein neddylation, in the context of DNA repair. Overall, the 9-1-1 protects genomic integrity and cell viability, both in normal and cancer cells.

REFERENCES

Abmayr, S.M., Yao, T., Parmely, T., and Workman, J.L. (2001). Preparation of Nuclear and Cytoplasmic Extracts from Mammalian Cells. In Current Protocols in Molecular Biology (John Wiley & Sons, Inc), pp. 12.11.11-12.11.10.

Abraham, R.T. (2001). Cell cycle checkpoint signaling through the ATM and ATR kinases. Genes & development *15*, 2177-2196.

A. Adamo, S.J. Collis, C.A. Adelman, N. Silva, Z. Horejsi, J.D. Ward, E. Martinez-Perez, S.J.Boulton, A. La Volpe. (2010). Preventing nonhomologous end joining suppresses DNA repair defects of Fanconi anemia. Molecular Cell *39*, 25-35

Ahlskog, J.K., Larsen, B.D., Achanta, K., and Sorensen, C.S. (2016). ATM/ATR-mediated phosphorylation of PALB2 promotes RAD51 function. EMBO reports *17*, 671-681.

al-Khodairy, F., and Carr, A.M. (1992). DNA repair mutants defining G2 checkpoint pathways in Schizosaccharomyces pombe. Embo j *11*, 1343-1350.

al-Khodairy, F., Fotou, E., Sheldrick, K.S., Griffiths, D.J., Lehmann, A.R., and Carr, A.M. (1994). Identification and characterization of new elements involved in checkpoint and feedback controls in fission yeast. Molecular biology of the cell *5*, 147-160.

Ali, S.H., and DeCaprio, J.A. (2001). Cellular transformation by SV40 large T antigen: interaction with host proteins. Seminars in cancer biology *11*, 15-23.

Allen, J.B., Zhou, Z., Siede, W., Friedberg, E.C., and Elledge, S.J. (1994). The SAD1/RAD53 protein kinase controls multiple checkpoints and DNA damage-induced transcription in yeast. Genes & development *8*, 2401-2415.

Alver, R.C., Zhang, T., Josephrajan, A., Fultz, B.L., Hendrix, C.J., Das-Bradoo, S., and Bielinsky, A.K. (2014). The N-terminus of Mcm10 is important for interaction with the 9-1-1 clamp and in resistance to DNA damage. Nucleic Acids Res. *42*, 8389-8404.

Andreassen, P.R., D'Andrea, A.D., and Taniguchi, T. (2004). ATR couples FANCD2 monoubiquitination to the DNA-damage response. Genes & development *18*, 1958-1963.

Angel, P., Imagawa, M., Chiu, R., Stein, B., Imbra, R.J., Rahmsdorf, H.J., Jonat, C., Herrlich, P., and Karin, M. (1987). Phorbol ester-inducible genes contain a common cis element recognized by a TPA-modulated trans-acting factor. Cell *49*, 729-739.

Ashkenazy, H., Erez, E., Martz, E., Pupko, T., and Ben-Tal, N. (2010). ConSurf 2010: calculating evolutionary conservation in sequence and structure of proteins and nucleic acids. Nucleic Acids Res. *38*, W529-533.

Atkinson, J., and McGlynn, P. (2009). Replication fork reversal and the maintenance of genome stability. Nucleic acids research *37*, 3475-3492.

Auerbach, C., and Kilbey, B.J. (1971). Mutation in eukaryotes. Annual review of genetics *5*, 163-218.

Bai, H., Madabushi, A., Guan, X., and Lu, A.L. (2010). Interaction between human mismatch repair recognition proteins and checkpoint sensor Rad9-Rad1-Hus1. DNA Repair (Amst) *9*, 478-487.

Ball, H.L., Ehrhardt, M.R., Mordes, D.A., Glick, G.G., Chazin, W.J., and Cortez, D. (2007). Function of a conserved checkpoint recruitment domain in ATRIP proteins. Molecular and cellular biology *27*, 3367-3377.

Balmus, G., Lim, P.X., Oswald, A., Hume, K.R., Cassano, A., Pierre, J., Hill, A., Huang, W., August, A., Stokol, T., *et al.* (2016). HUS1 regulates in vivo responses to genotoxic chemotherapies. Oncogene *35*, 662-669.

Balmus, G., Zhu, M., Mukherjee, S., Lyndaker, A.M., Hume, K.R., Lee, J., Riccio, M.L., Reeves, A.P., Sutter, N.B., Noden, D.M., *et al.* (2012). Disease severity in a mouse model of ataxia telangiectasia is modulated by the DNA damage checkpoint gene Hus1. Human molecular genetics *21*, 3408-3420.

Bansbach, C.E., Betous, R., Lovejoy, C.A., Glick, G.G., and Cortez, D. (2009). The annealing helicase SMARCAL1 maintains genome integrity at stalled replication forks. Genes & development *23*, 2405-2414.

Barber, L.J., Youds, J.L., Ward, J.D., McIlwraith, M.J., O'Neil, N.J., Petalcorin, M.I.R., Martin, J.S., Collis, S.J., Cantor, S.B., Auclair, M., *et al.* (2008). SPAR1/RTEL1 maintains genomic stability by suppressing homologous recombination. Cell *135*, 261-271.

Barlow, C., Hirotsune, S., Paylor, R., Liyanage, M., Eckhaus, M., Collins, F., Shiloh, Y., Crawley, J.N., Ried, T., Tagle, D., *et al.* (1996). Atm-deficient mice: a paradigm of ataxia telangiectasia. Cell *86*, 159-171.

Barrios-Rodiles, M., Brown, K.R., Ozdamar, B., Bose, R., Liu, Z., Donovan, R.S., Shinjo, F., Liu, Y., Dembowy, J., Taylor, I.W., *et al.* (2005). High-Throughput Mapping of a Dynamic Signaling Network in Mammalian Cells. Science (New York, N.Y.) *307*, 1621-1625.

Bartek, J., Lukas, C., and Lukas, J. (2004). Checking on DNA damage in S phase. Nature reviews. Molecular cell biology *5*, 792-804.

Bartek, J., and Lukas, J. (2003). Chk1 and Chk2 kinases in checkpoint control and cancer. Cancer cell *3*, 421-429.

Bartkova, J., Horejsi, Z., Koed, K., Kramer, A., Tort, F., Zieger, K., Guldberg, P., Sehested, M., Nesland, J.M., Lukas, C., *et al.* (2005). DNA damage response as a candidate anti-cancer barrier in early human tumorigenesis. Nature *434*, 864-870.

Bass, T.E., Luzwick, J.W., Kavanaugh, G., Carroll, C., Dungrawala, H., Glick, G.G., Feldkamp, M.D., Putney, R., Chazin, W.J., and Cortez, D. (2016). ETAA1 acts at stalled replication forks to maintain genome integrity. Nature cell biology *18*, 1185-1195.

Beattie, T.R., and Bell, S.D. (2012). Coordination of multiple enzyme activities by a single PCNA in archaeal Okazaki fragment maturation. EMBO J. *31*, 1556-1567.

Bermudez, V.P., Lindsey-Boltz, L.A., Cesare, A.J., Maniwa, Y., Griffith, J.D., Hurwitz, J., and Sancar, A. (2003). Loading of the human 9-1-1 checkpoint complex onto DNA by the checkpoint clamp loader hRad17-replication factor C complex in vitro. Proc Natl Acad Sci U S A *100*, 1633-1638.

Bernstein, H., Byerly, H.C., Hopf, F.A., and Michod, R.E. (1985). Genetic damage, mutation, and the evolution of sex. Science (New York, N.Y.) *229*, 1277-1281.

Berti, M., Ray Chaudhuri, A., Thangavel, S., Gomathinayagam, S., Kenig, S., Vujanovic, M., Odreman, F., Glatter, T., Graziano, S., Mendoza-Maldonado, R., *et al.* (2013). Human RECQ1 promotes restart of replication forks reversed by DNA topoisomerase I inhibition. Nature structural & molecular biology *20*, 347-354.

Bhaskara, V., Dupre, A., Lengsfeld, B., Hopkins, B.B., Chan, A., Lee, J.H., Zhang, X., Gautier, J., Zakian, V., and Paull, T.T. (2007). Rad50 adenylate kinase activity regulates DNA tethering by Mre11/Rad50 complexes. Molecular cell *25*, 647-661.

Bi, X. (2015). Mechanism of DNA damage tolerance. World Journal of Biological Chemistry *6*, 48-56.

Bicknell, A.A., Cenik, C., Chua, H.N., Roth, F.P., and Moore, M.J. (2012). Introns in UTRs: why we should stop ignoring them. BioEssays : news and reviews in molecular, cellular and developmental biology *34*, 1025-1034.

Blackford, A.N., and Jackson, S.P. (2017). ATM, ATR, and DNA-PK: The Trinity at the Heart of the DNA Damage Response. Molecular cell *66*, 801-817.

Blackford, A.N., Nieminuszczy, J., Schwab, R.A., Galanty, Y., Jackson, S.P., and Niedzwiedz, W. (2015). TopBP1 interacts with BLM to maintain genome stability but is dispensable for preventing BLM degradation. Molecular cell *57*, 1133-1141.

Blaikley, E. J., Tinline-Purvis, H., Kasparek, T. R., Marguerat, S., Sarkar, S., Hulme, L., … Humphrey, T. C. (2014). The DNA damage checkpoint pathway promotes extensive resection and nucleotide synthesis to facilitate homologous recombination repair and genome stability in fission yeast. Nucleic Acids Research *42*, 5644–5656.

Blasco, M.A., Lee, H.W., Hande, M.P., Samper, E., Lansdorp, P.M., DePinho, R.A., and Greider, C.W. (1997). Telomere shortening and tumor formation by mouse cells lacking telomerase RNA. Cell *91*, 25-34.

Blasius, M., Forment, J.V., Thakkar, N., Wagner, S.A., Choudhary, C., and Jackson, S.P. (2011). A phospho-proteomic screen identifies substrates of the checkpoint kinase Chk1. Genome biology *12*, R78-R78.

Boerckel, J., Walker, D., and Ahmed, S. (2007). The Caenorhabditis elegans Rad17 homolog HPR-17 is required for telomere replication. Genetics *176*, 703-709.

Bracey, T.S., Williams, A.C., and Paraskeva, C. (1997). Inhibition of radiation-induced G2 delay potentiates cell death by apoptosis and/or the induction of giant cells in colorectal tumor cells with disrupted p53 function. Clinical cancer research : an official journal of the American Association for Cancer Research *3*, 1371-1381.

Braig, M., Lee, S., Loddenkemper, C., Rudolph, C., Peters, A.H., Schlegelberger, B., Stein, H., Dorken, B., Jenuwein, T., and Schmitt, C.A. (2005). Oncogene-induced senescence as an initial barrier in lymphoma development. Nature *436*, 660-665.

Branzei, D., and Foiani, M. (2010). Maintaining genome stability at the replication fork. Nature reviews. Molecular cell biology *11*, 208-219.

Broustas, C.G., and Lieberman, H.B. (2014a). DNA Damage Response Genes and the Development of Cancer Metastasis. Radiation research *181*, 111-130.

Broustas, C.G., and Lieberman, H.B. (2014b). DNA damage response genes and the development of cancer metastasis. Radiation research *181*, 111-130.

Broustas, C.G., Zhu, A., and Lieberman, H.B. (2012). Rad9 protein contributes to prostate tumor progression by promoting cell migration and anoikis resistance. The Journal of biological chemistry *287*, 41324-41333.

Brown, E.J., and Baltimore, D. (2000). ATR disruption leads to chromosomal fragmentation and early embryonic lethality. Genes & development *14*, 397-402.

Brown, J.S., and Jackson, S.P. (2015). Ubiquitylation, neddylation and the DNA damage response. Open biology *5*, 150018.

Brown, J.S., Lukashchuk, N., Sczaniecka-Clift, M., Britton, S., le Sage, C., Calsou, P., Beli, P., Galanty, Y., and Jackson, S.P. (2015). Neddylation promotes ubiquitylation and release of Ku from DNA-damage sites. Cell reports *11*, 704-714.

Bunting, K.A., Roe, M.S., and Pearl, L.H. (2003). Structural basis for recruitment of transletion DNA polymerase Pol IV/DinB to the beta-clamp. EMBO J. *22*, 5883-5892.

Bunting, S.F., Callén, E., Wong, N., Chen, H.-T., Polato, F., Gunn, A., Bothmer, A., Feldhahn, N., Fernandez-Capetillo, O., Cao, L., *et al.* (2010). 53BP1 inhibits homologous recombination in Brca1-deficient cells by blocking resection of DNA breaks. Cell *141*, 243-254.

Burkovics, P., Sebesta, M., Balogh, D., Haracska, L., and Krejci, L. (2014). Strand invasion by HLTF as a mechanism for template switch in fork rescue. Nucleic acids research *42*, 1711-1720.

Cabrera, G., Cabrejos, M.E., Morassutti, A.L., Cabezon, C., Orellana, J., Hellman, U., Zaha, A., and Galanti, N. (2008). DNA damage, RAD9 and fertility/infertility of Echinococcus granulosus hydatid cysts. Journal of cellular physiology *216*, 498-506.

Ceccaldi, R., Sarangi, P., and D'Andrea, A.D. (2016). The Fanconi anaemia pathway: new players and new functions. Nature reviews. Molecular cell biology *17*, 337-349.

Chang, D.Y., and Lu, A.L. (2005). Interaction of checkpoint proteins Hus1/Rad1/Rad9 with DNA base excision repair enzyme MutY homolog in fission yeast, Schizosaccharomyces pombe. J. Biol. Chem. *280*, 408-417.

Chang, H.H.Y., Pannunzio, N.R., Adachi, N., and Lieber, M.R. (2017). Non-homologous DNA end joining and alternative pathways to double-strand break repair. Nature reviews. Molecular cell biology *18*, 495-506.

Chapman, J.R., and Jackson, S.P. (2008). Phospho-dependent interactions between NBS1 and MDC1 mediate chromatin retention of the MRN complex at sites of DNA damage. EMBO reports *9*, 795-801.

Chen, C.F., Ruiz-Vega, R., Vasudeva, P., Espitia, F., Krasieva, T.B., de Feraudy, S., Tromberg, B.J., Huang, S., Garner, C.P., Wu, J., *et al.* (2017). ATR Mutations Promote the Growth of Melanoma Tumors by Modulating the Immune Microenvironment. Cell reports *18*, 2331-2342.

Chen, J.S., Lin, S.Y., Tso, W.L., Yeh, G.C., Lee, W.S., Tseng, H., Chen, L.C., and Ho, Y.S. (2006). Checkpoint kinase 1-mediated phosphorylation of Cdc25C and bad proteins are involved in antitumor effects of loratadine-induced G2/M phase cell-cycle arrest and apoptosis. Molecular carcinogenesis *45*, 461-478.

Cheng, C.K., Chow, L.W., Loo, W.T., Chan, T.K., and Chan, V. (2005). The cell cycle checkpoint gene Rad9 is a novel oncogene activated by 11q13 amplification and DNA methylation in breast cancer. Cancer research *65*, 8646-8654.

Cheung, R.S., and Taniguchi, T. (2017). Recent insights into the molecular basis of Fanconi anemia: genes, modifiers, and drivers. International journal of hematology.

Chung, B.Y.W., Simons, C., Firth, A.E., Brown, C.M., and Hellens, R.P. (2006). Effect of 5'UTR introns on gene expression in Arabidopsis thaliana. BMC genomics *7*, 120-120.

Ciccia, A., Bredemeyer, A.L., Sowa, M.E., Terret, M.E., Jallepalli, P.V., Harper, J.W., and Elledge, S.J. (2009). The SIOD disorder protein SMARCAL1 is an RPA-interacting protein involved in replication fork restart. Genes & development *23*, 2415-2425.

Ciccia, A., and Elledge, S.J. (2010). The DNA damage response: making it safe to play with knives. Molecular cell *40*, 179-204.

Ciccia, A., Nimonkar, A.V., Hu, Y., Hajdu, I., Achar, Y.J., Izhar, L., Petit, S.A., Adamson, B., Yoon, J.C., Kowalczykowski, S.C., *et al.* (2012). Polyubiquitinated

PCNA recruits the ZRANB3 translocase to maintain genomic integrity after replication stress. Molecular cell *47*, 396-409.

Cimprich, K.A., and Cortez, D. (2008). ATR: an essential regulator of genome integrity. Nature reviews. Molecular cell biology *9*, 616-627.

Collis, S.J., Ciccia, A., Deans, A.J., Horejsi, Z., Martin, J.S., Maslen, S.L., Skehel, J.M., Elledge, S.J., West, S.C., and Boulton, S.J. (2008). FANCM and FAAP24 function in ATR-mediated checkpoint signaling independently of the Fanconi anemia core complex. Molecular cell *32*, 313-324.

Constantin, N., Dzantiev, L., Kadyrov, F.A., and Modrich, P. (2005). Human mismatch repair: reconstitution of a nick-directed bidirectional reaction. The Journal of biological chemistry *280*, 39752-39761.

Coquel, F., Silva, M.J., Techer, H., Zadorozhny, K., Sharma, S., Nieminuszczy, J., Mettling, C., Dardillac, E., Barthe, A., Schmitz, A.L., *et al.* (2018). SAMHD1 acts at stalled replication forks to prevent interferon induction. Nature *557*, 57-61.

Cortez, D., Wang, Y., Qin, J., and Elledge, S.J. (1999). Requirement of ATM-dependent phosphorylation of brca1 in the DNA damage response to double-strand breaks. Science (New York, N.Y.) *286*, 1162-1166.

Couch, F.B., Bansbach, C.E., Driscoll, R., Luzwick, J.W., Glick, G.G., Betous, R., Carroll, C.M., Jung, S.Y., Qin, J., Cimprich, K.A., *et al.* (2013). ATR phosphorylates SMARCAL1 to prevent replication fork collapse. Genes & development *27*, 1610-1623.

Daley, J.M., and Sung, P. (2014). 53BP1, BRCA1, and the Choice between Recombination and End Joining at DNA Double-Strand Breaks. Molecular and cellular biology *34*, 1380-1388.

Damia, G., and Broggini, M. (2004). Cell cycle checkpoint proteins and cellular response to treatment by anticancer agents. Cell cycle (Georgetown, Tex.) *3*, 46-50.

David, S.S., O'Shea, V.L., and Kundu, S. (2007). Base-excision repair of oxidative DNA damage. Nature *447*, 941-950.

Davies, A.A., Masson, J.Y., McIlwraith, M.J., Stasiak, A.Z., Stasiak, A., Venkitaraman, A.R., and West, S.C. (2001). Role of BRCA2 in control of the RAD51 recombination and DNA repair protein. Molecular cell *7*, 273-282.

de Klein, A., Muijtjens, M., van Os, R., Verhoeven, Y., Smit, B., Carr, A.M., Lehmann, A.R., and Hoeijmakers, J.H. (2000). Targeted disruption of the cell-cycle checkpoint gene ATR leads to early embryonic lethality in mice. Current biology : CB *10*, 479-482.

de la Torre, J., Gil-Moreno, A., Garcia, A., Rojo, F., Xercavins, J., Salido, E., and Freire, R. (2008). Expression of DNA damage checkpoint protein Hus1 in epithelial ovarian tumors correlates with prognostic markers. International journal of gynecological pathology : official journal of the International Society of Gynecological Pathologists *27*, 24-32.

Delacroix, S., Wagner, J.M., Kobayashi, M., Yamamoto, K., and Karnitz, L.M. (2007). The Rad9-Hus1-Rad1 (9-1-1) clamp activates checkpoint signaling via TopBP1. Genes & development *21*, 1472-1477.

Dietlein, F., Thelen, L., and Reinhardt, H.C. (2014). Cancer-specific defects in DNA repair pathways as targets for personalized therapeutic approaches. Trends in genetics : TIG *30*, 326-339.

Dionne, I., Nookala, R.K., Jackson, S.P., Doherty, A.J., and Bell, S.D. (2003). A Heterotrimeric PCNA in the Hyperthermophilic Achaeon Sulfolobus solfatoricus. Mol. Cell *11*, 275-282.

Doerr, F., George, J., Schmitt, A., Beleggia, F., Rehkamper, T., Hermann, S., Walter, V., Weber, J.P., Thomas, R.K., Wittersheim, M., *et al.* (2017). Targeting a non-oncogene addiction to the ATR/CHK1 axis for the treatment of small cell lung cancer. Scientific reports *7*, 15511.

Donzelli, M., and Draetta, G.F. (2003). Regulating mammalian checkpoints through Cdc25 inactivation. EMBO reports *4*, 671-677.

Dore, A.S., Kilkenny, M.L., Rzechorzek, N.J., and Pearl, L.H. (2009). Crystal structure of the rad9-rad1-hus1 DNA damage checkpoint complex--implications for clamp loading and regulation. Molecular cell *34*, 735-745.

Dufault, V.M., Oestreich, A.J., Vroman, B.T., and Karnitz, L.M. (2003). Identification and characterization of RAD9B, a paralog of the RAD9 checkpoint gene. Genomics *82*, 644-651.

Dulbecco, R. (1949). Reactivation of ultra-violet-inactivated bacteriophage by visible light. Nature *163*, 949.

Dungrawala, H., Bhat, K.P., Le Meur, R., Chazin, W.J., Ding, X., Sharan, S.K., Wessel, S.R., Sathe, A.A., Zhao, R., and Cortez, D. (2017). RADX Promotes Genome Stability and Modulates Chemosensitivity by Regulating RAD51 at Replication Forks. Molecular cell *67*, 374-386.e375.

DuPage, M., Dooley, A.L., and Jacks, T. (2009). Conditional mouse lung cancer models using adenoviral or lentiviral delivery of Cre recombinase. Nature protocols *4*, 1064-1072.

Dupre, A., Boyer-Chatenet, L., and Gautier, J. (2006). Two-step activation of ATM by DNA and the Mre11-Rad50-Nbs1 complex. Nature structural & molecular biology *13*, 451-457.

Duursma, A.M., Driscoll, R., Elias, J.E., and Cimprich, K.A. (2013). A role for the MRN complex in ATR activation via TOPBP1 recruitment. Molecular cell *50*, 116-122.

Eichinger, C.S., and Jentsch, S. (2010). Synaptonemal complex formation and meiotic checkpoint signaling are linked to the lateral element protein Red1. Proc Natl Acad Sci U S A *107*, 11370-11375.

Eichinger, C.S., and Jentsch, S. (2011). 9-1-1: PCNA's specialized cousin. Trends in biochemical sciences *36*, 563-568.

Elizondo, L.I., Cho, K.S., Zhang, W., Yan, J., Huang, C., Huang, Y., Choi, K., Sloan, E.A., Deguchi, K., Lou, S., *et al.* (2009). Schimke immuno-osseous dysplasia: SMARCAL1 loss-of-function and phenotypic correlation. Journal of medical genetics *46*, 49-59.

Ellison, V., and Stillman, B. (2003). Biochemical characterization of DNA damage checkpoint complexes: clamp loader and clamp complexes with specificity for 5' recessed DNA. PLoS Biol. *1*, E33.

Enchev, R.I., Schulman, B.A., and Peter, M. (2015). Protein neddylation: beyond cullin-RING ligases. Nature reviews. Molecular cell biology *16*, 30-44.

Enoch, T., Carr, A.M., and Nurse, P. (1992). Fission yeast genes involved in coupling mitosis to completion of DNA replication. Genes & development *6*, 2035-2046.

Escribano-Díaz, C., Orthwein, A., Fradet-Turcotte, A., Xing, M., Young, Jordan T.F., Tkáč, J., Cook, Michael A., Rosebrock, Adam P., Munro, M., Canny, Marella D., *et al.* (2013). A Cell Cycle-Dependent Regulatory Circuit Composed of 53BP1-RIF1 and BRCA1-CtIP Controls DNA Repair Pathway Choice. Molecular cell *49*, 872-883.

Feng, L., Li, N., Li, Y., Wang, J., Gao, M., Wang, W., and Chen, J. (2015). Cell cycle-dependent inhibition of 53BP1 signaling by BRCA1. Cell Discovery *1*, 15019.

Feng, S., Zhao, Y., Xu, Y., Ning, S., Huo, W., Hou, M., Gao, G., Ji, J., Guo, R., and Xu, D. (2016). Ewing Tumor-associated Antigen 1 Interacts with Replication Protein A to Promote Restart of Stalled Replication Forks. The Journal of biological chemistry *291*, 21956-21962.

Feng, W., and Jasin, M. (2017). BRCA2 suppresses replication stress-induced mitotic and G1 abnormalities through homologous recombination. Nature communications *8*, 525.

Fong, P.C., Boss, D.S., Yap, T.A., Tutt, A., Wu, P., Mergui-Roelvink, M., Mortimer, P., Swaisland, H., Lau, A., O'Connor, M.J., *et al.* (2009). Inhibition of poly(ADP-ribose) polymerase in tumors from BRCA mutation carriers. The New England journal of medicine *361*, 123-134.

Ford, D., Easton, D.F., Stratton, M., Narod, S., Goldgar, D., Devilee, P., Bishop, D.T., Weber, B., Lenoir, G., Chang-Claude, J., *et al.* (1998). Genetic heterogeneity and penetrance analysis of the BRCA1 and BRCA2 genes in breast cancer families. The Breast Cancer Linkage Consortium. American journal of human genetics *62*, 676-689.

Forment, J.V., and Jackson, S.P. (2015). A flow cytometry-based method to simplify the analysis and quantification of protein association to chromatin in mammalian cells. Nature protocols *10*, 1297-1307.

Forment, J.V., and O'Connor, M.J. (2018). Targeting the replication stress response in cancer. Pharmacology & therapeutics.

Francia, S., Weiss, R.S., Hande, M.P., Freire, R., and d'Adda di Fagagna, F. (2006). Telomere and telomerase modulation by the mammalian Rad9/Rad1/Hus1 DNA-damage-checkpoint complex. Current biology : CB *16*, 1551-1558.

Freedman, V.H., and Shin, S.I. (1974). Cellular tumorigenicity in nude mice: correlation with cell growth in semi-solid medium. Cell *3*, 355-359.

Friedberg, E.C., McDaniel, L.D., and Schultz, R.A. (2004). The role of endogenous and exogenous DNA damage and mutagenesis. Current opinion in genetics & development *14*, 5-10.

Friedel, A.M., Pike, B.L., and Gasser, S.M. (2009). ATR/Mec1: coordinating fork stability and repair. Current opinion in cell biology *21*, 237-244.

Friedrich-Heineken, E., Toueille, M., Tannler, B., Burki, C., Ferrari, E., Hottiger, M.O., and Hubscher, U. (2005). The two DNA clamps Rad9/Rad1/Hus1 complex and proliferating cell nuclear antigen differentially regulate flap endonuclease 1 activity. J. Mol. Biol. *353*, 980-989.

Garcia, K., Blank, J.L., Bouck, D.C., Liu, X.J., Sappal, D.S., Hather, G., Cosmopoulos, K., Thomas, M.P., Kuranda, M., Pickard, M.D., *et al.* (2014). Nedd8-activating enzyme inhibitor MLN4924 provides synergy with mitomycin C through interactions with ATR, BRCA1/BRCA2, and chromatin dynamics pathways. Molecular cancer therapeutics *13*, 1625-1635.

Garfinkel, D.J., and Bailis, A.M. (2002). Nucleotide Excision Repair, Genome Stability, and Human Disease: New Insight from Model Systems. Journal of Biomedicine and Biotechnology *2*, 55-60.

Gembka, A., Toueille, M., Smirnova, E., Poltz, R., Ferrari, E., Villani, G., and Hubscher, U. (2007). The checkpoint clamp, Rad9-Rad1-Hus1 complex, preferentially stimulates the activity of apurinic/apyrimidinic endonuclease 1 and DNA polymerase beta in long patch base excision repair. Nucleic Acids Res. *35*, 2596-2608.

Gensler, H.L., and Bernstein, H. (1981). DNA damage as the primary cause of aging. The Quarterly review of biology *56*, 279-303.

Georgescu, R.E., Kim, S.S., Yurieva, O., Kuriyan, J., Kong, X.P., and O'Donnell, M. (2008). Structure of a sliding clamp on DNA. Cell *132*, 43-54.

Ghosal, G., and Chen, J. (2013). DNA damage tolerance: a double-edged sword guarding the genome. Translational cancer research *2*, 107-129.

Gilljam, K.M., Feyzi, E., Aas, P.A., Sousa, M.M., Muller, R., Vagbo, C.B., Catterall, T.C., Liabakk, N.B., Slupphaug, G., Drablos, F., *et al.* (2009). Identification of a novel, widespread, and functionally important PCNA-binding motif. The Journal of cell biology *186*, 645-654.

Gorgoulis, V.G., Vassiliou, L.-V.F., Karakaidos, P., Zacharatos, P., Kotsinas, A., Liloglou, T., Venere, M., DiTullio Jr, R.A., Kastrinakis, N.G., Levy, B., *et al.* (2005). Activation of the DNA damage checkpoint and genomic instability in human precancerous lesions. Nature *434*, 907.

Gu, Y., and Lu, A.-L. (2001). Differential DNA recognition and glycosylase activity of the native human MutY hmolog (hMYH) and recombinant hMYH expressed in bacteria. Nucleic Acids Res. *29*, 2666-2674.

Guan, X., Madabushi, A., Chang, D.Y., Fitzgerald, M.E., Shi, G., Drohat, A.C., and Lu, A.L. (2007). The human checkpoint sensor Rad9-Rad1-Hus1 interacts with and stimulates DNA repair enzyme TDG glycosylase. Nucleic Acids Res. *35*, 6207-6218.

Gulbis, J.M., Kelman, Z., Hurwitz, J., O'Donnell, M., and Kuriyan, J. (1996). Structure of the C-Terminal Region of p21WAF1/CIP1 Complexed with Human PCNA. Cell *87*, 297-306.

Guo, Z., Kozlov, S., Lavin, M.F., Person, M.D., and Paull, T.T. (2010). ATM activation by oxidative stress. Science (New York, N.Y.) *330*, 517-521.

Haahr, P., Hoffmann, S., Tollenaere, M.A., Ho, T., Toledo, L.I., Mann, M., Bekker-Jensen, S., Raschle, M., and Mailand, N. (2016). Activation of the ATR kinase by the RPA-binding protein ETAA1. Nature cell biology *18*, 1196-1207.

Haber, J.E. (2000). Partners and pathwaysrepairing a double-strand break. Trends in genetics : TIG *16*, 259-264.

Hakem, R. (2008). DNA-damage repair; the good, the bad, and the ugly. The EMBO Journal *27*, 589-605.

Halazonetis, T.D., Gorgoulis, V.G., and Bartek, J. (2008). An oncogene-induced DNA damage model for cancer development. Science (New York, N.Y.) *319*, 1352-1355.

Han, L., Hu, Z., Liu, Y., Wang, X., Hopkins, K.M., Lieberman, H.B., and Hang, H. (2010). Mouse Rad1 deletion enhances susceptibility for skin tumor development. Molecular cancer *9*, 67.

Hanahan, D., and Weinberg, R.A. (2011). Hallmarks of cancer: the next generation. Cell *144*, 646-674.

Hang, H., Zhang, Y., Dunbrack, R.L., Jr., Wang, C., and Lieberman, H.B. (2002). Identification and characterization of a paralog of human cell cycle checkpoint gene HUS1. Genomics *79*, 487-492.

Hanlon Newell, A. E., Hemphill, A., Akkari, Y. M. N., Hejna, J., Moses, R. E., & Olson, S. B. (2008). Loss of Homologous Recombination or Non-homologous End-joining Leads to Radial Formation Following DNA Interstrand Crosslink Damage. Cytogenetic and Genome Research, *121*, 174–180.

Harper, J.W., and Elledge, S.J. (2007). The DNA damage response: ten years after. Molecular cell *28*, 739-745.

Hartlerode, A.J., and Scully, R. (2009). Mechanisms of double-strand break repair in somatic mammalian cells. The Biochemical journal *423*, 157-168.

Hartwell, L.H., and Weinert, T.A. (1989). Checkpoints: controls that ensure the order of cell cycle events. Science (New York, N.Y.) *246*, 629-634.

Heikkinen, K., Mansikka, V., Karppinen, S.-M., Rapakko, K., and Winqvist, R. (2005). Mutation analysis of the ATR gene in breast and ovarian cancer families. Breast Cancer Research *7*, R495-R501.

Helleday, T., Petermann, E., Lundin, C., Hodgson, B., and Sharma, R.A. (2008). DNA repair pathways as targets for cancer therapy. Nature Reviews Cancer *8*, 193-204.

Helt, C.E., Wang, W., Keng, P.C., and Bambara, R.A. (2005). Evidence that DNA Damage Detection Machinery Participates in DNA Repair. Cell Cycle *4*, 529-532.

Hennings, H., Glick, A.B., Lowry, D.T., Krsmanovic, L.S., Sly, L.M., and Yuspa, S.H. (1993). FVB/N mice: an inbred strain sensitive to the chemical induction of squamous cell carcinomas in the skin. Carcinogenesis *14*, 2353-2358.

Heyer, W.D., Ehmsen, K.T., and Liu, J. (2010). Regulation of homologous recombination in eukaryotes. Annual review of genetics *44*, 113-139.

Higgs, M.R., Reynolds, J.J., Winczura, A., Blackford, A.N., Borel, V., Miller, E.S., Zlatanou, A., Nieminuszczy, J., Ryan, E.L., Davies, N.J., *et al.* (2015). BOD1L Is

Required to Suppress Deleterious Resection of Stressed Replication Forks. Molecular cell *59*, 462-477.

Hinds, P.W., Finlay, C.A., Quartin, R.S., Baker, S.J., R., F.E., Vogelstein, B., and Levine, A.J. (1990). Mutant p53 DNA Clones from Human Colon Carcinomas Cooperate with ras in Transforming Primary Rat Cells: A Comparison of the "Hot Spot" Mutant Phenotypes. Cell Growth Differ *1*, 571-580.

Ho, G.P., Margossian, S., Taniguchi, T., and D'Andrea, A.D. (2006). Phosphorylation of FANCD2 on two novel sites is required for mitomycin C resistance. Molecular and cellular biology *26*, 7005-7015.

Hoeijmakers, J. (2001). Genome maintenance mechanisms for preventing cancer. Nature *411*, 366-374.

Hoeijmakers, J.H. (2009). DNA damage, aging, and cancer. The New England journal of medicine *361*, 1475-1485.

Hollaender, A., and Duggar, B.M. (1938). The Effects of Sublethal Doses of Monochromatic Ultraviolet Radiation on the Growth Properties of Bacteria. Journal of Bacteriology *36*, 17-37.

Hopkins, K.M., Auerbach, W., Wang, X.Y., Hande, M.P., Hang, H., Wolgemuth, D.J., Joyner, A.L., and Lieberman, H.B. (2004). Deletion of mouse rad9 causes abnormal cellular responses to DNA damage, genomic instability, and embryonic lethality. Molecular and cellular biology *24*, 7235-7248.

Howlett, N. G., Harney, J. A., Rego, M. A., Kolling, F. W., & Glover, T. W. (2009). Functional Interaction between the Fanconi Anemia D2 Protein and Proliferating Cell Nuclear Antigen (PCNA) via a Conserved Putative PCNA Interaction Motif. *The Journal of Biological Chemistry 284*, 28935–28942.

Hsieh, P., and Yamane, K. (2008). DNA mismatch repair: Molecular mechanism, cancer, and ageing. Mechanisms of ageing and development *129*, 391-407.

Hu, Z., Liu, Y., Zhang, C., Zhao, Y., He, W., Han, L., Yang, L., Hopkins, K.M., Yang, X., Lieberman, H.B., *et al.* (2008). Targeted deletion of Rad9 in mouse skin keratinocytes enhances genotoxin-induced tumor development. Cancer research *68*, 5552-5561.

Huang, M., Kim, J.M., Shiotani, B., Yang, K., Zou, L., and D'Andrea, A.D. (2010). The FANCM/FAAP24 complex is required for the DNA interstrand crosslink-induced checkpoint response. Molecular cell *39*, 259-268.

Huertas, P. (2010). DNA resection in eukaryotes: deciding how to fix the break. Nature structural & molecular biology *17*, 11-16.

Huh, J., and Piwnica-Worms, H. (2013). CRL4(CDT2) targets CHK1 for PCNA-independent destruction. Molecular and cellular biology *33*, 213-226.

Hurt, J.A., Robertson, A.D., and Burge, C.B. (2013). Global analyses of UPF1 binding and function reveal expanded scope of nonsense-mediated mRNA decay. Genome research *23*, 1636-1650.

Hustedt, N., and Durocher, D. (2016). The control of DNA repair by the cell cycle. Nature cell biology *19*, 1-9.

Isken, O., Kim, Y.K., Hosoda, N., Mayeur, G.L., Hershey, J.W.B., and Maquat, L.E. (2008). Upf1 Phosphorylation Triggers Translational Repression during Nonsense-Mediated mRNA Decay. Cell *133*, 314-327.

Isono, M., Niimi, A., Oike, T., Hagiwara, Y., Sato, H., Sekine, R., Yoshida, Y., Isobe, S.-Y., Obuse, C., Nishi, R., *et al.* (2017). BRCA1 Directs the Repair Pathway to Homologous Recombination by Promoting 53BP1 Dephosphorylation. Cell reports *18*, 520-532.

Jackson, A.L., and Loeb, L.A. (2001). The contribution of endogenous sources of DNA damage to the multiple mutations in cancer. Mutation research *477*, 7-21.

Jackson, E.L., Willis, N., Mercer, K., Bronson, R.T., Crowley, D., Montoya, R., Jacks, T., and Tuveson, D.A. (2001). Analysis of lung tumor initiation and progression using conditional expression of oncogenic K-ras. Genes & development *15*, 3243-3248.

Jackson, S.P., and Bartek, J. (2009a). The DNA-damage response in human biology and disease. Nature *461*, 1071-1078.

Jackson, S.P., and Bartek, J. (2009b). The DNA-damage response in human biology and disease. Nature *461*, 1071-1078.

Jarrett, S.G., Carter, K.M., and D'Orazio, J.A. (2017). Paracrine regulation of melanocyte genomic stability: a focus on nucleotide excision repair. Pigment cell & melanoma research *30*, 284-293.

Jasin, M., and Rothstein, R. (2013). Repair of Strand Breaks by Homologous Recombination. Cold Spring Harbor Perspectives in Biology *5*, a012740.

Jette, N., and Lees-Miller, S.P. (2015). The DNA-dependent protein kinase: A multifunctional protein kinase with roles in DNA double strand break repair and mitosis. Progress in biophysics and molecular biology *117*, 194-205.

Jiang, X., Sun, Y., Chen, S., Roy, K., and Price, B.D. (2006). The FATC domains of PIKK proteins are functionally equivalent and participate in the Tip60-dependent activation of DNA-PKcs and ATM. The Journal of biological chemistry *281*, 15741-15746.

Jiang, Z., Kamath, R., Jin, S., Balasubramani, M., Pandita, T.K., and Rajasekaran, B. (2011). Tip60-mediated acetylation activates transcription independent apoptotic activity of Abl. Molecular cancer *10*, 88.

Jimeno, S., Fernandez-Avila, M.J., Cruz-Garcia, A., Cepeda-Garcia, C., Gomez-Cabello, D., and Huertas, P. (2015). Neddylation inhibits CtIP-mediated resection and regulates DNA double strand break repair pathway choice. Nucleic acids research *43*, 987-999.

Johnson, A., and O'Donnell, M. (2005). Cellular DNA replicases: components and dynamics at the replication fork. Annual review of biochemistry *74*, 283-315.

Julie D., T., Toby J., G., Frederic, P., Francois, J., and Desmond G., H. (1997). The CLUSTAL_X windows interface: flexible strategies for multiple sequence alignment aided by quality analysis tools. Nucleic Acids Res. *25*, 4876-4882.

Kadir, R., Bakhrat, A., Tokarsky, R., and Abdu, U. (2012). Localization of the Drosophila Rad9 protein to the nuclear membrane is regulated by the C-terminal region and is affected in the meiotic checkpoint. PloS one *7*, e38010.

Karnitz, L.M., and Zou, L. (2015). Molecular Pathways: Targeting ATR in Cancer Therapy. Clinical cancer research : an official journal of the American Association for Cancer Research *21*, 4780-4785.

Karras, G.I., Fumasoni, M., Sienski, G., Vanoli, F., Branzei, D., and Jentsch, S. (2013). Noncanonical role of the 9-1-1 clamp in the error-free DNA damage tolerance pathway. Molecular cell *49*, 536-546.

Kaur, R., Kostrub, C., and Enoch, T. (2001a). Structure-Function Analysis of Fission Yeast Hus1- Rad1-Rad9 Checkpoint Complex. Mol Biol Cell *12*, 3744-3758.

Kaur, R., Kostrub, C.F., and Enoch, T. (2001b). Structure-function analysis of fission yeast Hus1-Rad1-Rad9 checkpoint complex. Molecular biology of the cell *12*, 3744-3758.

Kelner, A. (1949). Effect of Visible Light on the Recovery of Streptomyces Griseus Conidia from Ultra-violet Irradiation Injury. Proceedings of the National Academy of Sciences of the United States of America *35*, 73-79.

Kendall, S.D., Linardic, C.M., Adam, S.J., and Counter, C.M. (2005). A network of genetic events sufficient to convert normal human cells to a tumorigenic state. Cancer research *65*, 9824-9828.

Kerzendorfer, C., and O'Driscoll, M. (2009). Human DNA damage response and repair deficiency syndromes: linking genomic instability and cell cycle checkpoint proficiency. DNA repair *8*, 1139-1152.

Khanna, K.K., and Jackson, S.P. (2001). DNA double-strand breaks: signaling, repair and the cancer connection. Nature genetics *27*, 247-254.

Kim, Y., Spitz, G.S., Veturi, U., Lach, F.P., Auerbach, A.D., and Smogorzewska, A. (2013). Regulation of multiple DNA repair pathways by the Fanconi anemia protein SLX4. Blood *121*, 54-63.

Knijnenburg, T.A., Wang, L., Zimmermann, M.T., Chambwe, N., Gao, G.F., Cherniack, A.D., Fan, H., Shen, H., Way, G.P., Greene, C.S., *et al.* (2018). Genomic and Molecular Landscape of DNA Damage Repair Deficiency across The Cancer Genome Atlas. Cell reports *23*, 239-254.e236.

Knipscheer, P., Raschle, M., Smogorzewska, A., Enoiu, M., Ho, T.V., Scharer, O.D., Elledge, S.J., and Walter, J.C. (2009). The Fanconi anemia pathway promotes replication-dependent DNA interstrand cross-link repair. Science (New York, N.Y.) *326*, 1698-1701.

Kolas, N.K., Chapman, J.R., Nakada, S., Ylanko, J., Chahwan, R., Sweeney, F.D., Panier, S., Mendez, M., Wildenhain, J., Thomson, T.M., *et al.* (2007). Orchestration of the DNA-damage response by the RNF8 ubiquitin ligase. Science (New York, N.Y.) *318*, 1637-1640.

Kolinjivadi, A.M., Sannino, V., de Antoni, A., Techer, H., Baldi, G., and Costanzo, V. (2017a). Moonlighting at replication forks - a new life for homologous recombination proteins BRCA1, BRCA2 and RAD51. FEBS Lett *591*, 1083-1100.

Kolinjivadi, A.M., Sannino, V., De Antoni, A., Zadorozhny, K., Kilkenny, M., Techer, H., Baldi, G., Shen, R., Ciccia, A., Pellegrini, L., *et al.* (2017b). Smarcal1-Mediated Fork Reversal Triggers Mre11-Dependent Degradation of Nascent DNA in the Absence of Brca2 and Stable Rad51 Nucleofilaments. Molecular cell *67*, 867-881.e867.

Kostrub, C.F., al-Khodairy, F., Ghazizadeh, H., Carr, A.M., and Enoch, T. (1997). Molecular analysis of hus1+, a fission yeast gene required for S-M and DNA damage checkpoints. Molecular & general genetics : MGG *254*, 389-399.

Kottemann, M.C., Conti, B.A., Lach, F.P., and Smogorzewska, A. (2018). Removal of RTF2 from Stalled Replisomes Promotes Maintenance of Genome Integrity. Molecular cell *69*, 24-35.e25.

Krejci, L., Altmannova, V., Spirek, M., and Zhao, X. (2012). Homologous recombination and its regulation. Nucleic acids research *40*, 5795-5818.

Krokan, H.E., and Bjørås, M. (2013). Base Excision Repair. Cold Spring Harbor Perspectives in Biology *5*, a012583.

Krokan, H.E., Standal, R., and Slupphaug, G. (1997). DNA glycosylases in the base excision repair of DNA. The Biochemical journal *325 (Pt 1)*, 1-16.

Kunkel, T.A., and Erie, D.A. (2005). DNA mismatch repair. Annual review of biochemistry *74*, 681-710.

Lamarche, B.J., Orazio, N.I., and Weitzman, M.D. (2010). The MRN complex in Double-Strand Break Repair and Telomere Maintenance. FEBS letters *584*, 3682-3695.

Lau, W.C., Li, Y., Liu, Z., Gao, Y., Zhang, Q., and Huen, M.S. (2016). Structure of the human dimeric ATM kinase. Cell cycle (Georgetown, Tex.) *15*, 1117-1124.

Lee, D.H., Pan, Y., Kanner, S., Sung, P., Borowiec, J.A., and Chowdhury, D. (2010). A PP4 phosphatase complex dephosphorylates RPA2 to facilitate DNA repair via homologous recombination. Nature structural & molecular biology *17*, 365-372.

Lee, J., Kumagai, A., and Dunphy, W.G. (2007). The Rad9-Hus1-Rad1 checkpoint clamp regulates interaction of TopBP1 with ATR. The Journal of biological chemistry *282*, 28036-28044.

Lee, J., and Zhou, P. (2010). Cullins and cancer. Genes & cancer *1*, 690-699.

Lee, J.H., and Paull, T.T. (2005). ATM activation by DNA double-strand breaks through the Mre11-Rad50-Nbs1 complex. Science (New York, N.Y.) *308*, 551-554.

Lees-Miller, S.P., and Meek, K. (2003). Repair of DNA double strand breaks by non-homologous end joining. Biochimie *85*, 1161-1173.

Lemacon, D., Jackson, J., Quinet, A., Brickner, J.R., Li, S., Yazinski, S., You, Z., Ira, G., Zou, L., Mosammaparast, N., *et al.* (2017). MRE11 and EXO1 nucleases degrade reversed forks and elicit MUS81-dependent fork rescue in BRCA2-deficient cells. Nature communications *8*, 860.

Levitt, P.S., Liu, H., Manning, C., and Weiss, R.S. (2005). Conditional inactivation of the mouse Hus1 cell cycle checkpoint gene. Genomics *86*, 212-224.

Levitt, P.S., Zhu, M., Cassano, A., Yazinski, S.A., Liu, H., Darfler, J., Peters, R.M., and Weiss, R.S. (2007). Genome maintenance defects in cultured cells and mice following partial inactivation of the essential cell cycle checkpoint gene Hus1. Molecular and cellular biology *27*, 2189-2201.

Li, G.-M. (2007). Mechanisms and functions of DNA mismatch repair. Cell research *18*, 85.

Li, T., Guan, J., Huang, Z., Hu, X., and Zheng, X. (2014). RNF168-mediated H2A neddylation antagonizes ubiquitylation of H2A and regulates DNA damage repair. Journal of cell science *127*, 2238-2248.

Li, T., Wang, Z., Zhao, Y., He, W., An, L., Liu, S., Liu, Y., Wang, H., and Hang, H. (2013). Checkpoint protein Rad9 plays an important role in nucleotide excision repair. DNA repair *12*, 284-292.

Liang, C.C., Li, Z., Lopez-Martinez, D., Nicholson, W.V., Venien-Bryan, C., and Cohn, M.A. (2016). The FANCD2-FANCI complex is recruited to DNA interstrand crosslinks before monoubiquitination of FANCD2. Nature communications *7*, 12124.

Lianoglou, S., Garg, V., Yang, J.L., Leslie, C.S., and Mayr, C. (2013). Ubiquitously transcribed genes use alternative polyadenylation to achieve tissue-specific expression. Genes & development *27*, 2380-2396.

Lieber, M.R. (2010). The Mechanism of Double-Strand DNA Break Repair by the Nonhomologous DNA End Joining Pathway. Annual review of biochemistry *79*, 181-211.

Lieberman, H.B., Bernstock, J.D., Broustas, C.G., Hopkins, K.M., Leloup, C., and Zhu, A. (2011). The role of RAD9 in tumorigenesis. Journal of molecular cell biology *3*, 39-43.

Lim, P.X., Patel, D.R., Poisson, K.E., Basuita, M., Tsai, C., Lyndaker, A.M., Hwang, B.J., Lu, A.L., and Weiss, R.S. (2015). Genome Protection by the 9-1-1 Complex Subunit HUS1 Requires Clamp Formation, DNA Contacts, and ATR Signaling-independent Effector Functions. The Journal of biological chemistry *290*, 14826-14840.

Lindahl, T. (1974). An N-glycosidase from Escherichia coli that releases free uracil from DNA containing deaminated cytosine residues. Proc Natl Acad Sci U S A *71*, 3649-3653.

Lindahl, T. (1993). Instability and decay of the primary structure of DNA. Nature *362*, 709.

Lindahl, T., and Wood, R.D. (1999). Quality control by DNA repair. Science (New York, N.Y.) *286*, 1897-1905.

Liu, S., Opiyo, S.O., Manthey, K., Glanzer, J.G., Ashley, A.K., Amerin, C., Troksa, K., Shrivastav, M., Nickoloff, J.A., and Oakley, G.G. (2012). Distinct roles for DNA-PK, ATM and ATR in RPA phosphorylation and checkpoint activation in response to replication stress. Nucleic acids research *40*, 10780-10794.

Liu, S., Shiotani, B., Lahiri, M., Marechal, A., Tse, A., Leung, C.C., Glover, J.N., Yang, X.H., and Zou, L. (2011). ATR autophosphorylation as a molecular switch for checkpoint activation. Molecular cell *43*, 192-202.

Liu, Y., Cussiol, J.R., Dibitetto, D., Sims, J.R., Twayana, S., Weiss, R.S., Freire, R., Marini, F., Pellicioli, A., and Smolka, M.B. (2017). TOPBP1(Dpb11) plays a conserved role in homologous recombination DNA repair through the coordinated recruitment of 53BP1(Rad9). The Journal of cell biology *216*, 623-639.

Loeb, L.A. (1998). Cancer cells exhibit a mutator phenotype. Advances in cancer research *72*, 25-56.

Long, D.T., Joukov, V., Budzowska, M., and Walter, J.C. (2014). BRCA1 promotes unloading of the CMG helicase from a stalled DNA replication fork. Molecular cell *56*, 174-185.

Long, D.T., Raschle, M., Joukov, V., and Walter, J.C. (2011). Mechanism of RAD51-dependent DNA interstrand cross-link repair. Science (New York, N.Y.) *333*, 84-87.

Longerich, S., Kwon, Y., Tsai, M.S., Hlaing, A.S., Kupfer, G.M., and Sung, P. (2014). Regulation of FANCD2 and FANCI monoubiquitination by their interaction and by DNA. Nucleic acids research *42*, 5657-5670.

Lopes, M., Cotta-Ramusino, C., Pellicioli, A., Liberi, G., Plevani, P., Muzi-Falconi, M., Newlon, C.S., and Foiani, M. (2001). The DNA replication checkpoint response stabilizes stalled replication forks. Nature *412*, 557-561.

Lopez-Martinez, D., Liang, C.-C., and Cohn, M.A. (2016). Cellular response to DNA interstrand crosslinks: the Fanconi anemia pathway. Cellular and Molecular Life Sciences *73*, 3097-3114.

Lord, C.J., and Ashworth, A. (2012). The DNA damage response and cancer therapy. Nature *481*, 287.

Luo, J., Solimini, N.L., and Elledge, S.J. (2009). Principles of cancer therapy: oncogene and non-oncogene addiction. Cell *136*, 823-837.

Lyndaker, A.M., Lim, P.X., Mleczko, J.M., Diggins, C.E., Holloway, J.K., Holmes, R.J., Kan, R., Schlafer, D.H., Freire, R., Cohen, P.E., *et al.* (2013a). Conditional inactivation of the DNA damage response gene Hus1 in mouse testis reveals separable roles for components of the RAD9-RAD1-HUS1 complex in meiotic chromosome maintenance. PLoS genetics *9*, e1003320.

Lyndaker, A.M., Lim, P.X., Mleczko, J.M., Diggins, C.E., Holloway, K.J., Holmes, R.J., Kan, R., Schlafer, D.H., Freire, R., Cohen, P.E., *et al.* (2013b). Conditional Inactivation of the DNA Damage Response Gene Hus1 in Mouse Testis Reveals Separable Roles for Components of the RAD9-RAD1-HUS1 Complex in Meiotic Chromosome Maintenance. PLoS Genet. *9*.

Lyndaker, A.M., Vasileva, A., Wolgemuth, D.J., Weiss, R.S., and Lieberman, H.B. (2013c). Clamping down on mammalian meiosis. Cell cycle (Georgetown, Tex.) *12*, 3135-3145.

Ma, T., Chen, Y., Zhang, F., Yang, C.Y., Wang, S., and Yu, X. (2013). RNF111-dependent neddylation activates DNA damage-induced ubiquitination. Molecular cell *49*, 897-907.

Madabushi, A., and Lu, A.-L. (2011). The novel role of cell cycle checkpoint clamp Rad9-Hus1-Rad1 (the 9-1-1 complex) in DNA repair. In Advances in Medicine and Biology, L.V. Berhardt, ed. (Hauppauge, NY: Nova Science Publishers), pp. 41-74.

Mailand, N., Gibbs-Seymour, I., and Bekker-Jensen, S. (2013). Regulation of PCNA-protein interactions for genome stability. Nature reviews. Molecular cell biology *14*, 269-282.

Majka, J., Binz, S.K., Wold, M.S., and Burgers, P.M. (2006a). Replication protein A directs loading of the DNA damage checkpoint clamp to 5'-DNA junctions. J. Biol. Chem. *281*, 27855-27861.

Majka, J., Niedziela-Majka, A., and Burgers, P.M. (2006b). The checkpoint clamp activates Mec1 kinase during initiation of the DNA damage checkpoint. Molecular cell *24*, 891-901.

Mao, Z., Bozzella, M., Seluanov, A., and Gorbunova, V. (2008). Comparison of nonhomologous end joining and homologous recombination in human cells. DNA repair *7*, 1765-1771.

Margalef, P., Kotsantis, P., Borel, V., Bellelli, R., Panier, S., and Boulton, S.J. (2018). Stabilization of Reversed Replication Forks by Telomerase Drives Telomere Catastrophe. Cell *172*, 439-453.e414.

Martin, G., Gruber, A.R., Keller, W., and Zavolan, M. (2012). Genome-wide analysis of pre-mRNA 3' end processing reveals a decisive role of human cleavage factor I in the regulation of 3' UTR length. Cell reports *1*, 753-763.

Masamha, C.P., Xia, Z., Yang, J., Albrecht, T.R., Li, M., Shyu, A.B., Li, W., and Wagner, E.J. (2014). CFIm25 links alternative polyadenylation to glioblastoma tumour suppression. Nature *510*, 412-416.

Matsuoka, S., Ballif, B.A., Smogorzewska, A., McDonald, E.R., 3rd, Hurov, K.E., Luo, J., Bakalarski, C.E., Zhao, Z., Solimini, N., Lerenthal, Y., *et al.* (2007). ATM and ATR substrate analysis reveals extensive protein networks responsive to DNA damage. Science (New York, N.Y.) *316*, 1160-1166.

Mayr, C. (2017). Regulation by 3'-Untranslated Regions. Annual review of genetics *51*, 171-194.

Mayr, C., and Bartel, D.P. (2009). Widespread shortening of 3'UTRs by alternative cleavage and polyadenylation activates oncogenes in cancer cells. Cell *138*, 673-684.

McNally, R., Bowman, G.D., Goedken, E.R., O'Donnell, M., and Kuriyan, J. (2010). Analysis of the role of PCNA-DNA contacts during clamp loading. BMC structural biology *10*, 3.

Meir, M., Galanty, Y., Kashani, L., Blank, M., Khosravi, R., Fernandez-Avila, M.J., Cruz-Garcia, A., Star, A., Shochot, L., Thomas, Y., *et al.* (2015). The COP9 signalosome is vital for timely repair of DNA double-strand breaks. Nucleic acids research *43*, 4517-4530.

Méndez, J., and Stillman, B. (2000). Chromatin Association of Human Origin Recognition Complex, Cdc6, and Minichromosome Maintenance Proteins during the Cell Cycle: Assembly of Prereplication Complexes in Late Mitosis. Molecular and cellular biology *20*, 8602-8612.

Michl, J., Zimmer, J., and Tarsounas, M. (2016). Interplay between Fanconi anemia and homologous recombination pathways in genome integrity. The EMBO journal *35*, 909-923.

Mijic, S., Zellweger, R., Chappidi, N., Berti, M., Jacobs, K., Mutreja, K., Ursich, S., Ray Chaudhuri, A., Nussenzweig, A., Janscak, P., *et al.* (2017). Replication fork reversal triggers fork degradation in BRCA2-defective cells. Nature communications *8*, 859.

Miki, Y., Swensen, J., Shattuck-Eidens, D., Futreal, P.A., Harshman, K., Tavtigian, S., Liu, Q., Cochran, C., Bennett, L.M., Ding, W., *et al.* (1994). A strong candidate for the breast and ovarian cancer susceptibility gene BRCA1. Science (New York, N.Y.) *266*, 66-71.

Moldovan, G.L., Pfander, B., and Jentsch, S. (2007). PCNA, the maestro of the replication fork. Cell *129*, 665-679.

Mordes, D.A., Glick, G.G., Zhao, R., and Cortez, D. (2008). TopBP1 activates ATR through ATRIP and a PIKK regulatory domain. Genes & development *22*, 1478-1489.

Moudry, P., Watanabe, K., Wolanin, K.M., Bartkova, J., Wassing, I.E., Watanabe, S., Strauss, R., Troelsgaard Pedersen, R., Oestergaard, V.H., Lisby, M., *et al.* (2016). TOPBP1 regulates RAD51 phosphorylation and chromatin loading and determines PARP inhibitor sensitivity. The Journal of cell biology *212*, 281-288.

Mukherjee, S., Ridgeway, A., and Lamb, D.J. (2010). DNA MISMATCH REPAIR AND INFERTILITY. Current opinion in urology *20*, 525-532.

Muller-Rover, S., Handjiski, B., van der Veen, C., Eichmuller, S., Foitzik, K., McKay, I.A., Stenn, K.S., and Paus, R. (2001). A comprehensive guide for the accurate

classification of murine hair follicles in distinct hair cycle stages. The Journal of investigative dermatology *117*, 3-15.

Murakami, H., and Keeney, S. (2008). Regulating the formation of DNA double-strand breaks in meiosis. Genes & development *22*, 286-292.

Nalepa, G., and Clapp, D.W. (2018). Fanconi anaemia and cancer: an intricate relationship. Nature reviews. Cancer *18*, 168-185.

Naryzhny, S.N. (2008). Proliferating cell nuclear antigen: a proteomics view. Cell. Mol. Life Sci. *65*, 3789-3808.

Natsume, T., Kiyomitsu, T., Saga, Y., and Kanemaki, M.T. (2016). Rapid Protein Depletion in Human Cells by Auxin-Inducible Degron Tagging with Short Homology Donors. Cell reports *15*, 210-218.

Neelsen, K.J., and Lopes, M. (2015). Replication fork reversal in eukaryotes: from dead end to dynamic response. Nature Reviews Molecular Cell Biology *16*, 207.

Ngo, G.H., Balakrishnan, L., Dubarry, M., Campbell, J.L., and Lydall, D. (2014). The 9-1-1 checkpoint clamp stimulates DNA resection by Dna2-Sgs1 and Exo1. Nucleic acids research *42*, 10516-10528.

Nickless, A., Jackson, E., Marasa, J., Nugent, P., Mercer, R.W., Piwnica-Worms, D., and You, Z. (2014). Intracellular calcium regulates nonsense-mediated mRNA decay. Nature medicine *20*, 961-966.

Nimonkar, A.V., Genschel, J., Kinoshita, E., Polaczek, P., Campbell, J.L., Wyman, C., Modrich, P., and Kowalczykowski, S.C. (2011). BLM–DNA2–RPA–MRN and EXO1–BLM–RPA–MRN constitute two DNA end resection machineries for human DNA break repair. Genes & development *25*, 350-362.

O'Connor, M.J. (2015). Targeting the DNA Damage Response in Cancer. Molecular cell *60*, 547-560.

Pandita, R.K., Sharma, G.G., Laszlo, A., Hopkins, K.M., Davey, S., Chakhparonian, M., Gupta, A., Wellinger, R.J., Zhang, J., Powell, S.N., *et al.* (2006). Mammalian

Rad9 plays a role in telomere stability, S- and G2-phase-specific cell survival, and homologous recombinational repair. Molecular and cellular biology *26*, 1850-1864.

Park, M.J., Park, J.H., Hahm, S.H., Ko, S.I., Lee, Y.R., Chung, J.H., Sohn, S.Y., Cho, Y., Kang, L.W., and Han, Y.S. (2009). Repair activities of human 8-oxoguanine DNA glycosylase are stimulated by the interaction with human checkpoint sensor Rad9-Rad1-Hus1 complex. DNA Repair (Amst) *8*, 1190-1200.

Parplys, A.C., Seelbach, J.I., Becker, S., Behr, M., Wrona, A., Jend, C., Mansour, W.Y., Joosse, S.A., Stuerzbecher, H.-W., Pospiech, H., *et al.* (2015). High levels of RAD51 perturb DNA replication elongation and cause unscheduled origin firing due to impaired CHK1 activation. Cell cycle (Georgetown, Tex.) *14*, 3190-3202.

Parrilla-Castellar, E.R., Arlander, S.J., and Karnitz, L. (2004). Dial 9-1-1 for DNA damage: the Rad9-Hus1-Rad1 (9-1-1) clamp complex. DNA repair *3*, 1009-1014.

Pasero, P., and Vindigni, A. (2017). Nucleases Acting at Stalled Forks: How to Reboot the Replication Program with a Few Shortcuts. Annual review of genetics *51*, 477-499.

Patel, D.S., Misenko, S.M., Her, J., and Bunting, S.F. (2017). BLM helicase regulates DNA repair by counteracting RAD51 loading at DNA double-strand break sites. The Journal of cell biology *216*, 3521-3534.

Paull, T.T. (2015). Mechanisms of ATM Activation. Annual review of biochemistry *84*, 711-738.

Paulovich, A.G., Toczyski, D.P., and Hartwell, L.H. (1997). When Checkpoints Fail. Cell *88*, 315-321.

Peltomaki, P., and Vasen, H. (2004). Mutations associated with HNPCC predisposition -- Update of ICG-HNPCC/INSiGHT mutation database. Disease markers *20*, 269-276.

Peretz, G., Arie, L.G., Bakhrat, A., and Abdu, U. (2009). The Drosophila hus1 gene is required for homologous recombination repair during meiosis. Mechanisms of development *126*, 677-686.

Perry, J., and Kleckner, N. (2003). The ATRs, ATMs, and TORs are giant HEAT repeat proteins. Cell *112*, 151-155.

Pick, E., Golan, A., Zimbler, J.Z., Guo, L., Sharaby, Y., Tsuge, T., Hofmann, K., and Wei, N. (2012). The minimal deneddylase core of the COP9 signalosome excludes the Csn6 MPN- domain. PloS one *7*, e43980.

Piwko, W., Mlejnkova, L.J., Mutreja, K., Ranjha, L., Stafa, D., Smirnov, A., Brodersen, M.M., Zellweger, R., Sturzenegger, A., Janscak, P., *et al.* (2016). The MMS22L-TONSL heterodimer directly promotes RAD51-dependent recombination upon replication stress. Embo j *35*, 2584-2601.

Poole, L.A., and Cortez, D. (2017). Functions of SMARCAL1, ZRANB3, and HLTF in maintaining genome stability. Critical Reviews in Biochemistry and Molecular Biology *52*, 696-714.

Popuri, V., Bachrati, C.Z., Muzzolini, L., Mosedale, G., Costantini, S., Giacomini, E., Hickson, I.D., and Vindigni, A. (2008). The Human RecQ helicases, BLM and RECQ1, display distinct DNA substrate specificities. The Journal of biological chemistry *283*, 17766-17776.

Querol-Audi, J., Yan, C., Xu, X., Tetsukawa, S.E., Tsai, M.-S., Tainer, J.A., Cooper, P.K., Nogales, E., and Ivanov, I. (2012). Repair complexes of FEN1 endonuclease, DNA, and Rad9-Hus1-Rad1 are distinguished from their PCNA counterparts by functionally important stability. Proc Natl Acad Sci U S A *109*, 8528-8533.

Quinet, A., Lemacon, D., and Vindigni, A. (2017). Replication Fork Reversal: Players and Guardians. Molecular cell *68*, 830-833.

Quintanilla, M., Brown, K., Ramsden, M., and Balmain, A. (1986). Carcinogen-specific mutation and amplification of Ha-ras during mouse skin carcinogenesis. Nature *322*, 78-80.

Rabut, G., and Peter, M. (2008). Function and regulation of protein neddylation. 'Protein modifications: beyond the usual suspects' review series. EMBO reports *9*, 969-976.

Randal Hofmann, E., Milstein, S., Boulton, S., Ye, M., J Hofmann, J., Stergiou, L., Gartner, A., Vidal, M., and Hengartner, M. (2002). Caenorhabditis elegans HUS-1 Is a DNA Damage Checkpoint Protein Required for Genome Stability and EGL-1-Mediated Apoptosis, Vol 12.

Rao, P.N., and Johnson, R.T. (1970). Mammalian Cell Fusion : Studies on the Regulation of DNA Synthesis and Mitosis. Nature *225*, 159.

Rao, Q., Liu, M., Tian, Y., Wu, Z., Hao, Y., Song, L., Qin, Z., Ding, C., Wang, H.-W., Wang, J., *et al.* (2017). Cryo-EM structure of human ATR-ATRIP complex. Cell research *28*, 143.

Raschle, M., Smeenk, G., Hansen, R.K., Temu, T., Oka, Y., Hein, M.Y., Nagaraj, N., Long, D.T., Walter, J.C., Hofmann, K., *et al.* (2015). DNA repair. Proteomics reveals dynamic assembly of repair complexes during bypass of DNA cross-links. Science *348*, 1253671.

Rass, U., Compton, S.A., Matos, J., Singleton, M.R., Ip, S.C.Y., Blanco, M.G., Griffith, J.D., and West, S.C. (2010). Mechanism of Holliday junction resolution by the human GEN1 protein. Genes & development *24*, 1559-1569.

Ray Chaudhuri, A., Callen, E., Ding, X., Gogola, E., Duarte, A.A., Lee, J.E., Wong, N., Lafarga, V., Calvo, J.A., Panzarino, N.J., *et al.* (2016). Replication fork stability confers chemoresistance in BRCA-deficient cells. Nature *535*, 382-387.

Rendtlew Danielsen, J.M., Larsen, D.H., Schou, K.B., Freire, R., Falck, J., Bartek, J., and Lukas, J. (2009). HCLK2 is required for activity of the DNA damage response kinase ATR. J. Biol. Chem. *284*, 4140-4147.

Richardson, C., and Jasin, M. (2000). Frequent chromosomal translocations induced by DNA double-strand breaks. Nature *405*, 697-700.

Rondinelli, B., Gogola, E., Yucel, H., Duarte, A.A., van de Ven, M., van der Sluijs, R., Konstantinopoulos, P.A., Jonkers, J., Ceccaldi, R., Rottenberg, S., *et al.* (2017). EZH2 promotes degradation of stalled replication forks by recruiting MUS81 through histone H3 trimethylation. Nature cell biology *19*, 1371-1378.

Ruzankina, Y., Pinzon-Guzman, C., Asare, A., Ong, T., Pontano, L., Cotsarelis, G., Zediak, V.P., Velez, M., Bhandoola, A., and Brown, E.J. (2007). Deletion of the developmentally essential gene ATR in adult mice leads to age-related phenotypes and stem cell loss. Cell stem cell *1*, 113-126.

Sakumi, K., Shiraishi, A., Shimizu, S., Tsuzuki, T., Ishikawa, T., and Sekiguchi, M. (1997). Methylnitrosourea-induced tumorigenesis in MGMT gene knockout mice. Cancer research *57*, 2415-2418.

Sakurai, S., Kitano, K., Yamaguchi, H., Hamada, K., Okada, K., Fukuda, K., Uchida, M., Ohtsuka, E., Morioka, H., and Hakoshima, T. (2005). Structural basis for recruitment of human flap endonuclease 1 to PCNA. EMBO J. *24*, 683-693.

Sancar, A., Lindsey-Boltz, L.A., Unsal-Kacmaz, K., and Linn, S. (2004). Molecular mechanisms of mammalian DNA repair and the DNA damage checkpoints. Annual review of biochemistry *73*, 39-85.

Sandberg, R., Neilson, J.R., Sarma, A., Sharp, P.A., and Burge, C.B. (2008). Proliferating cells express mRNAs with shortened 3' untranslated regions and fewer microRNA target sites. Science (New York, N.Y.) *320*, 1643-1647.

Sartori, A.A., Lukas, C., Coates, J., Mistrik, M., Fu, S., Bartek, J., Baer, R., Lukas, J., and Jackson, S.P. (2007). Human CtIP promotes DNA end resection. Nature *450*, 509-514.

Savage, J.R. (1976). Classification and relationships of induced chromosomal structual changes. Journal of medical genetics *13*, 103-122.

Savitsky, K., Bar-Shira, A., Gilad, S., Rotman, G., Ziv, Y., Vanagaite, L., Tagle, D.A., Smith, S., Uziel, T., Sfez, S., *et al.* (1995). A single ataxia telangiectasia gene with a product similar to PI-3 kinase. Science (New York, N.Y.) *268*, 1749-1753.

Schärer, O.D. (2013). Nucleotide Excision Repair in Eukaryotes. Cold Spring Harbor Perspectives in Biology *5*, a012609.

Schlacher, K., Christ, N., Siaud, N., Egashira, A., Wu, H., and Jasin, M. (2011). Double-strand break repair-independent role for BRCA2 in blocking stalled replication fork degradation by MRE11. Cell *145*, 529-542.

Schlacher, K., Wu, H., and Jasin, M. (2012). A distinct replication fork protection pathway connects Fanconi anemia tumor suppressors to RAD51-BRCA1/2. Cancer cell *22*, 106-116.

Schultz, N., Lopez, E., Saleh- Gohari, N., and Helleday, T. (2003). Poly(ADP-ribose) polymerase (PARP- 1) has a controlling role in homologous recombination. Nucleic acids research *31*, 4959-4964.

Serrano, M., Lin, A.W., McCurrach, M.E., Beach, D., and Lowe, S.W. (1997). Oncogenic ras provokes premature cell senescence associated with accumulation of p53 and p16INK4a. Cell *88*, 593-602.

Shafman, T., Khanna, K.K., Kedar, P., Spring, K., Kozlov, S., Yen, T., Hobson, K., Gatei, M., Zhang, N., Watters, D., *et al.* (1997). Interaction between ATM protein and c-Abl in response to DNA damage. Nature *387*, 520-523.

Sharangdhar, T., Sugimoto, Y., Heraud-Farlow, J., Fernandez-Moya, S.M., Ehses, J., Ruiz de Los Mozos, I., Ule, J., and Kiebler, M.A. (2017). A retained intron in the 3'-

UTR of Calm3 mRNA mediates its Staufen2- and activity-dependent localization to neuronal dendrites. EMBO reports *18*, 1762-1774.

Shi, G., Chang, D.Y., Cheng, C.C., Guan, X., Venclovas, C., and Lu, A.L. (2006). Physical and functional interactions between MutY glycosylase homologue (MYH) and checkpoint proteins Rad9-Rad1-Hus1. Biochem. J. *400*, 53-62.

Shinohara, A., Ogawa, H., and Ogawa, T. (1992). Rad51 protein involved in repair and recombination in S. cerevisiae is a RecA-like protein. Cell *69*, 457-470.

Sibanda, B.L., Chirgadze, D.Y., Ascher, D.B., and Blundell, T.L. (2017). DNA-PKcs structure suggests an allosteric mechanism modulating DNA double-strand break repair. Science (New York, N.Y.) *355*, 520.

Singh, R.K., Zerath, S., Kleifeld, O., Scheffner, M., Glickman, M.H., and Fushman, D. (2012). Recognition and cleavage of related to ubiquitin 1 (Rub1) and Rub1-ubiquitin chains by components of the ubiquitin-proteasome system. Molecular & cellular proteomics : MCP *11*, 1595-1611.

Sishc, B.J., and Davis, A.J. (2017). The Role of the Core Non-Homologous End Joining Factors in Carcinogenesis and Cancer. Cancers *9*.

Smirnova, E., Toueille, M., Markkanen, E., and Hubscher, U. (2005). The human checkpoint sensor and alternative DNA clamp Rad9–Rad1–Hus1 modulates the activity of DNA ligase I, a component of the long-patch base excision repair machinery. Biochem. J. *389*, 13-17.

Smogorzewska, A., Matsuoka, S., Vinciguerra, P., McDonald, E.R., 3rd, Hurov, K.E., Luo, J., Ballif, B.A., Gygi, S.P., Hofmann, K., D'Andrea, A.D., *et al.* (2007). Identification of the FANCI protein, a monoubiquitinated FANCD2 paralog required for DNA repair. Cell *129*, 289-301.

Sogo, J.M., Lopes, M., and Foiani, M. (2002). Fork reversal and ssDNA accumulation at stalled replication forks owing to checkpoint defects. Science (New York, N.Y.) *297*, 599-602.

Sohn, S.Y., and Cho, Y. (2009). Crystal structure of the human rad9-hus1-rad1 clamp. Journal of molecular biology *390*, 490-502.

Somyajit, K., Saxena, S., Babu, S., Mishra, A., and Nagaraju, G. (2015). Mammalian RAD51 paralogs protect nascent DNA at stalled forks and mediate replication restart. Nucleic acids research *43*, 9835-9855.

Sotiriou, S.K., Kamileri, I., Lugli, N., Evangelou, K., Da-Re, C., Huber, F., Padayachy, L., Tardy, S., Nicati, N.L., Barriot, S., *et al.* (2016). Mammalian RAD52 Functions in Break-Induced Replication Repair of Collapsed DNA Replication Forks. Molecular cell *64*, 1127-1134.

Soucy, T.A., Dick, L.R., Smith, P.G., Milhollen, M.A., and Brownell, J.E. (2010). The NEDD8 Conjugation Pathway and Its Relevance in Cancer Biology and Therapy. Genes & cancer *1*, 708-716.

Stergiou, L., Eberhard, R., Doukoumetzidis, K., and Hengartner, M.O. (2011). NER and HR pathways act sequentially to promote UV-C-induced germ cell apoptosis in Caenorhabditis elegans. Cell Death Differ *18*, 897-906.

Stocker, H., and Hafen, E. (2000). Genetic control of cell size. Current opinion in genetics & development *10*, 529-535.

Storcelova, M., Vician, M., Reis, R., Zeman, M., and Herichova, I. (2013). Expression of cell cycle regulatory factors hus1, gadd45a, rb1, cdkn2a and mre11a correlates with expression of clock gene per2 in human colorectal carcinoma tissue. Molecular biology reports *40*, 6351-6361.

Stucki, M., Clapperton, J.A., Mohammad, D., Yaffe, M.B., Smerdon, S.J., and Jackson, S.P. (2005). MDC1 directly binds phosphorylated histone H2AX to regulate cellular responses to DNA double-strand breaks. Cell *123*, 1213-1226.

Sy, S.M.H., Huen, M.S.Y., and Chen, J. (2009). PALB2 is an integral component of the BRCA complex required for homologous recombination repair. Proceedings of the National Academy of Sciences *106*, 7155.

Taglialatela, A., Alvarez, S., Leuzzi, G., Sannino, V., Ranjha, L., Huang, J.W., Madubata, C., Anand, R., Levy, B., Rabadan, R., *et al.* (2017). Restoration of Replication Fork Stability in BRCA1- and BRCA2-Deficient Cells by Inactivation of SNF2-Family Fork Remodelers. Molecular cell *68*, 414-430.e418.

Taipale, M., Krykbaeva, I., Koeva, M., Kayatekin, C., Westover, K.D., Karras, G.I., and Lindquist, S. (2012). Quantitative analysis of HSP90-client interactions reveals principles of substrate recognition. Cell *150*, 987-1001.

Takeishi, Y., Ohashi, E., Ogawa, K., Masai, H., Obuse, C., and Tsurimoto, T. (2010). Casein kinase 2-dependent phosphorylation of human Rad9 mediates the interaction between human Rad9-Hus1-Rad1 complex and TopBP1. Genes to cells : devoted to molecular & cellular mechanisms *15*, 761-771.

Taylor, A.M., Metcalfe, J.A., Oxford, J.M., and Harnden, D.G. (1976). Is chromatid-type damage in ataxia telangiectasia after irradiation at G0 a consequence of defective repair? Nature *260*, 441-443.

Thelen, M.P., Venclovas, C., and Fidelis, K. (1999). A sliding clamp model for the Rad1 family of cell cycle checkpoint proteins. Cell *96*, 769-770.

Tho, L.M., Libertini, S., Rampling, R., Sansom, O., and Gillespie, D.A. (2012). Chk1 is essential for chemical carcinogen-induced mouse skin tumorigenesis. Oncogene *31*, 1366-1375.

Tibbetts, R.S., Brumbaugh, K.M., Williams, J.M., Sarkaria, J.N., Cliby, W.A., Shieh, S.-Y., Taya, Y., Prives, C., and Abraham, R.T. (1999). A role for ATR in the DNA damage-induced phosphorylation of p53. Genes & development *13*, 152-157.

Todaro, G.J., and Green, H. (1963). Quantitative studies of the growth of mouse embryo cells in culture and their development into established lines. The Journal of cell biology *17*, 299-313.

Toledo, L., Neelsen, K.J., and Lukas, J. (2017). Replication Catastrophe: When a Checkpoint Fails because of Exhaustion. Molecular cell *66*, 735-749.

Tomida, J., Itaya, A., Shigechi, T., Unno, J., Uchida, E., Ikura, M., Masuda, Y., Matsuda, S., Adachi, J., Kobayashi, M., *et al.* (2013). A novel interplay between the Fanconi anemia core complex and ATR-ATRIP kinase during DNA cross-link repair. Nucleic acids research *41*, 6930-6941.

Trempus, C.S., Morris, R.J., Ehinger, M., Elmore, A., Bortner, C.D., Ito, M., Cotsarelis, G., Nijhof, J.G.W., Peckham, J., Flagler, N., *et al.* (2007). CD34 Expression by Hair Follicle Stem Cells Is Required for Skin Tumor Development in Mice. Cancer research *67*, 4173-4181.

Trenz, K., Smith, E., Smith, S., and Costanzo, V. (2006). ATM and ATR promote Mre11 dependent restart of collapsed replication forks and prevent accumulation of DNA breaks. The EMBO Journal *25*, 1764-1774.

Tsanov, N., Kermi, C., Coulombe, P., Van der Laan, S., Hodroj, D., and Maiorano, D. (2014). PIP degron proteins, substrates of CRL4Cdt2, and not PIP boxes, interfere with DNA polymerase eta and kappa focus formation on UV damage. Nucleic acids research *42*, 3692-3706.

Uckelmann, M., Densham, R.M., Baas, R., Winterwerp, H.H.K., Fish, A., Sixma, T.K., and Morris, J.R. (2018). USP48 restrains resection by site-specific cleavage of the BRCA1 ubiquitin mark from H2A. Nature communications *9*, 229.

Ueda, S., Takeishi, Y., Ohashi, E., and Tsurimoto, T. (2012). Two serine phosphorylation sites in the C-terminus of Rad9 are critical for 9-1-1 binding to TopBP1 and activation of the DNA damage checkpoint response in HeLa cells. Genes to cells : devoted to molecular & cellular mechanisms *17*, 807-816.

Vanderdys, V., Allak, A., Guessous, F., Benamar, M., Read, P.W., Jameson, M.J., and Abbas, T. (2018). The Neddylation Inhibitor Pevonedistat (MLN4924) Suppresses and Radiosensitizes Head and Neck Squamous Carcinoma Cells and Tumors. Molecular cancer therapeutics *17*, 368-380.

Vasileva, A., Hopkins, K.M., Wang, X., Weisbach, M.M., Friedman, R.A., Wolgemuth, D.J., and Lieberman, H.B. (2013). The DNA damage checkpoint protein RAD9A is essential for male meiosis in the mouse. J. Cell Sci. *126*, 3927-3938.

Venkitaraman, A.R. (2001). Functions of BRCA1 and BRCA2 in the biological response to DNA damage. Journal of cell science *114*, 3591-3598.

Verlinden, L., Vanden Bempt, I., Eelen, G., Drijkoningen, M., Verlinden, I., Marchal, K., De Wolf-Peeters, C., Christiaens, M.R., Michiels, L., Bouillon, R., *et al.* (2007). The E2F-regulated gene Chk1 is highly expressed in triple-negative estrogen receptor /progesterone receptor /HER-2 breast carcinomas. Cancer research *67*, 6574-6581.

Vindigni, A., and Lopes, M. (2017). Combining electron microscopy with single molecule DNA fiber approaches to study DNA replication dynamics. Biophysical chemistry *225*, 3-9.

Volkmer, E., and Karnitz, L.M. (1999). Human homologs of Schizosaccharomyces pombe rad1, hus1, and rad9 form a DNA damage-responsive protein complex. The Journal of biological chemistry *274*, 567-570.

Walker, A.I., Hunt, T., Jackson, R.J., and Anderson, C.W. (1985). Double-stranded DNA induces the phosphorylation of several proteins including the 90 000 mol. wt. heat-shock protein in animal cell extracts. Embo j *4*, 139-145.

Wang, A.T., Kim, T., Wagner, J.E., Conti, B.A., Lach, F.P., Huang, A.L., Molina, H., Sanborn, E.M., Zierhut, H., Cornes, B.K., *et al.* (2015). A Dominant Mutation in Human RAD51 Reveals Its Function in DNA Interstrand Crosslink Repair Independent of Homologous Recombination. Molecular cell *59*, 478-490.

Wang, H., Shi, L.Z., Wong, C.C., Han, X., Hwang, P.Y., Truong, L.N., Zhu, Q., Shao, Z., Chen, D.J., Berns, M.W., *et al.* (2013a). The interaction of CtIP and Nbs1 connects CDK and ATM to regulate HR-mediated double-strand break repair. PLoS genetics *9*, e1003277.

Wang, H., Shi, L.Z., Wong, C.C.L., Han, X., Hwang, P.Y.-H., Truong, L.N., Zhu, Q., Shao, Z., Chen, D.J., Berns, M.W., *et al.* (2013b). The Interaction of CtIP and Nbs1 Connects CDK and ATM to Regulate HR–Mediated Double-Strand Break Repair. PLoS genetics *9*, e1003277.

Wang, M., Wu, W., Wu, W., Rosidi, B., Zhang, L., Wang, H., and Iliakis, G. (2006a). PARP-1 and Ku compete for repair of DNA double strand breaks by distinct NHEJ pathways. Nucleic acids research *34*, 6170-6182.

Wang, X., Hu, B., Weiss, R.S., and Wang, Y. (2006b). The effect of Hus1 on ionizing radiation sensitivity is associated with homologous recombination repair but is independent of nonhomologous end-joining. Oncogene *25*, 1980-1983.

Wang, X., Ran, T., Zhang, X., Xin, J., Zhang, Z., Wu, T., Wang, W., and Cai, G. (2017). 3.9 A structure of the yeast Mec1-Ddc2 complex, a homolog of human ATR-ATRIP. Science (New York, N.Y.) *358*, 1206-1209.

Weinert, T.A., Kiser, G.L., and Hartwell, L.H. (1994). Mitotic checkpoint genes in budding yeast and the dependence of mitosis on DNA replication and repair. Genes & development *8*, 652-665.

Weiss, R.S., Enoch, T., and Leder, P. (2000a). Inactivation of mouse Hus1 results in genomic instability and impaired responses to genotoxic stress. Genes & development *14*, 1886-1898.

Weiss, R.S., Enoch, T., and Leder, P. (2000b). Inactivation of mouse Hus1 results in genomic instability and impaired responses to genotoxic stress. Genes Dev. *14*, 1886-1898.

Weiss, R.S., Kostrub, C.F., Enoch, T., and Leder, P. (1999). Mouse Hus1, a homolog of the Schizosaccharomyces pombe hus1+ cell cycle checkpoint gene. Genomics *59*, 32-39.

Weiss, R.S., Leder, P., and Enoch, T. (2000c). A conserved role for the Hus1 checkpoint protein in eukaryotic genome maintenance. Cold Spring Harbor symposia on quantitative biology *65*, 457-466.

Weiss, R.S., Leder, P., and Vaziri, C. (2003). Critical role for mouse Hus1 in an S-phase DNA damage cell cycle checkpoint. Molecular and cellular biology *23*, 791-803.

Weiss, R.S., Matsuoka, S., Elledge, S.J., and Leder, P. (2002). Hus1 Acts Upstream of Chk1 in a Mammalian DNA Damage Response Pathway. Curr. Biol. *12*, 73-77.

White, A.C., Tran, K., Khuu, J., Dang, C., Cui, Y., Binder, S.W., and Lowry, W.E. (2011). Defining the origins of Ras/p53-mediated squamous cell carcinoma. Proceedings of the National Academy of Sciences *108*, 7425-7430.

Wienholz, F., Vermeulen, W., and Marteijn, J.A. (2017). Amplification of unscheduled DNA synthesis signal enables fluorescence-based single cell quantification of transcription-coupled nucleotide excision repair. Nucleic acids research *45*, e68-e68.

Williams, R.S., Williams, J.S., and Tainer, J.A. (2007). Mre11-Rad50-Nbs1 is a keystone complex connecting DNA repair machinery, double-strand break signaling, and the chromatin template. Biochemistry and cell biology = Biochimie et biologie cellulaire *85*, 509-520.

Wu, C.S., Yu, C.L., Wu, C.S., Lan, C.C., and Yu, H.S. (2004). Narrow-band ultraviolet-B stimulates proliferation and migration of cultured melanocytes. Experimental dermatology *13*, 755-763.

Wu, L., Luo, K., Lou, Z., and Chen, J. (2008). MDC1 regulates intra-S-phase checkpoint by targeting NBS1 to DNA double-strand breaks. Proceedings of the National Academy of Sciences of the United States of America *105*, 11200-11205.

Wyatt, H.D., Sarbajna, S., Matos, J., and West, S.C. (2013). Coordinated actions of SLX1-SLX4 and MUS81-EME1 for Holliday junction resolution in human cells. Molecular cell *52*, 234-247.

Xing, G., Kirouac, K., Shin, Y.J., Bell, S.D., and Ling, H. (2009). Structural insight into recruitment of translesion DNA polymerase Dpo4 to sliding clamp PCNA. Mol. Microbiol. *71*, 678-691.

Xu, M., Bai, L., Gong, Y., Xie, W., Hang, H., and Jiang, T. (2009). Structure and functional implications of the human rad9-hus1-rad1 cell cycle checkpoint complex. The Journal of biological chemistry *284*, 20457-20461.

Xu, S., Wu, X., Wu, L., Castillo, A., Liu, J., Atkinson, E., Paul, A., Su, D., Schlacher, K., Komatsu, Y., *et al.* (2017). Abro1 maintains genome stability and limits replication stress by protecting replication fork stability. Genes & development *31*, 1469-1482.

Xu, X., Guardiani, C., Yan, C., and Ivanov, I. (2013). Opening pathways of the DNA clamps proliferating cell nuclear antigen and Rad9-Rad1-Hus1. Nucleic Acids Res. *41*, 10020-10031.

Yang, Y., He, S., Wang, Q., Li, F., Kwak, M.J., Chen, S., O'Connell, D., Zhang, T., Pirooz, S.D., Jeon, Y., *et al.* (2016). Autophagic UVRAG Promotes UV-Induced Photolesion Repair by Activation of the CRL4(DDB2) E3 Ligase. Molecular cell *62*, 507-519.

Yazinski, S.A., Westcott, P.M., Ong, K., Pinkas, J., Peters, R.M., and Weiss, R.S. (2009). Dual inactivation of Hus1 and p53 in the mouse mammary gland results in accumulation of damaged cells and impaired tissue regeneration. Proc Natl Acad Sci U S A *106*, 21282-21287.

Yoo, H.Y., Shevchenko, A., Shevchenko, A., and Dunphy, W.G. (2004). Mcm2 Is a Direct Substrate of ATM and ATR during DNA Damage and DNA Replication Checkpoint Responses. Journal of Biological Chemistry *279*, 53353-53364.

Yun, H., Shi, R., Yang, Q., Zhang, X., Wang, Y., Zhou, X., and Mu, K. (2014). Over expression of hRad9 protein correlates with reduced chemosensitivity in breast cancer with administration of neoadjuvant chemotherapy. Scientific reports *4*, 7548.

Yun, M.H., and Hiom, K. (2009). CtIP-BRCA1 modulates the choice of DNA double-strand break repair pathway throughout the cell cycle. Nature *459*, 460-463.

Yuspa, S.H. (1998). The pathogenesis of squamous cell cancer: lessons learned from studies of skin carcinogenesis. Journal of dermatological science *17*, 1-7.

Zafar, M.K., and Eoff, R.L. (2017). Translesion DNA Synthesis in Cancer: Molecular Mechanisms and Therapeutic Opportunities. Chemical research in toxicology *30*, 1942-1955.

Zalvide, J., and DeCaprio, J.A. (1995). Role of pRb-related proteins in simian virus 40 large-T-antigen-mediated transformation. Molecular and cellular biology *15*, 5800-5810.

Zellweger, R., Dalcher, D., Mutreja, K., Berti, M., Schmid, J.A., Herrador, R., Vindigni, A., and Lopes, M. (2015). Rad51-mediated replication fork reversal is a global response to genotoxic treatments in human cells. The Journal of cell biology *208*, 563-579.

Zhang, J., Dewar, J.M., Budzowska, M., Motnenko, A., Cohn, M.A., and Walter, J.C. (2015). DNA interstrand cross-link repair requires replication-fork convergence. Nature structural & molecular biology *22*, 242-247.

Zhang, J., and Walter, J.C. (2014). Mechanism and regulation of incisions during DNA interstrand cross-link repair. DNA Repair (Amst) *19*, 135-142.

Zhang, M., Behbod, F., Atkinson, R.L., Landis, M.D., Kittrell, F., Edwards, D., Medina, D., Tsimelzon, A., Hilsenbeck, S., Green, J.E., *et al.* (2008). Identification of tumor-initiating cells in a p53-null mouse model of breast cancer. Cancer research *68*, 4674-4682.

Zhang, S., Zhao, H., Darzynkiewicz, Z., Zhou, P., Zhang, Z., Lee, E.Y., and Lee, M.Y. (2013). A novel function of CRL4(Cdt2): regulation of the subunit structure of DNA polymerase delta in response to DNA damage and during the S phase. The Journal of biological chemistry *288*, 29550-29561.

Zhao, H., and Piwnica-Worms, H. (2001). ATR-Mediated Checkpoint Pathways Regulate Phosphorylation and Activation of Human Chk1. Molecular and cellular biology *21*, 4129-4139.

Zhao, W., Steinfeld, J.B., Liang, F., Chen, X., Maranon, D.G., Jian Ma, C., Kwon, Y., Rao, T., Wang, W., Sheng, C., *et al.* (2017). BRCA1–BARD1 promotes RAD51-mediated homologous DNA pairing. Nature *550*, 360.

Zhou, B.B., and Elledge, S.J. (2000). The DNA damage response: putting checkpoints in perspective. Nature *408*, 433-439.

Zhu, M., and Weiss, R.S. (2007). Increased common fragile site expression, cell proliferation defects, and apoptosis following conditional inactivation of mouse Hus1 in primary cultured cells. Molecular biology of the cell *18*, 1044-1055.

Zhu, W., and Dutta, A. (2006). An ATR- and BRCA1-mediated Fanconi anemia pathway is required for activating the G2/M checkpoint and DNA damage repair upon rereplication. Molecular and cellular biology *26*, 4601-4611.

Zou, L. (2017). DNA Replication Checkpoint: New ATR Activator Identified. Current biology : CB *1*, 33-35.

Zou, L., Cortez, D., and Elledge, S.J. (2002). Regulation of ATR substrate selection by Rad17-dependent loading of Rad9 complexes onto chromatin. Genes & development *16*, 198-208.

Zou, L., and Elledge, S.J. (2003). Sensing DNA damage through ATRIP recognition of RPA-ssDNA complexes. Science (New York, N.Y.) *300*, 1542-1548.

Zuazua-Villar, P., Ganesh, A., Gagou, ME., Meuth, M. (2015). Extesive RPA2 hyperphosphorylation promotes apoptosis in resposne to DNA replication stress in CHK1 inhibited cells. Nucleic Acid Research.:43(20);9776-9787.

Zund, D., and Muhlemann, O. (2013). Recent transcriptome-wide mapping of UPF1 binding sites reveals evidence for its recruitment to mRNA before translation. Translation (Austin, Tex.) *1*, e26977.